BISSETT-BERMAN
APOLLO GUIDANCE AND
NAVIGATION NOTEBOOK

Volume XII

395-427

(NASA-CR-145603) APOLLO GUIDANCE AND NAVIGATION NOTEBOOK, VOLUME 12 (Bissett-Berman Corp.) 380 P

N75-77180

Unclas
00/98 39940

RECEIVED
JAN 1972
NASA STI FACILITY

The Bissett-Berman Corporation 2941 Nebraska Avenue, Santa Monica, California EXbrook 4-3270

Contract NAS 9-4435

398-427
complete
USM 7/19/66

Volume XII

APOLLO GUIDANCE AND NAVIGATION NOTES

TABLE OF CONTENTS

Note No.	Title	Author(s)
398	The Status of Ionospheric Scale Height Representations in Precision S-band Space Vehicle Tracking Models . .	H. R. Wright
399	Estimates of Linear Regression Parameters.	E. Pugh
400	Modification to OEA Program to Simulate Effects of Real Time Orbit Data Processing Scheme	H. Engel
401	Checkout of the Principal Axis Determination Program	J. W. Childress, III
402	Method for Evaluating Effect of Random Noise Components on Errors in Estimated Orbit Parameters	L. Lustick
403	Checkout of Weighting Function Program	L. Lustick/ G. Hempstead
404	Checkout of Multiple Station Program	L. Lustick
405	Accuracy Achieved by Employing an Optimum Filter for Processing Tracking Data During Apollo Lunar Missions	L. Bonin
406	High Frequency Characteristics of Mariner IV Doppler Residuals	H. Epstein
407	Visibility and Master Measurable Changes	L. Lustick
408	Effect of Uncertainty in Refraction Parameters on an Earth Orbit	L. Lustick
409	The Az-El Program	B. Murphy
410	Checkout of Visibility Addition to OEA	L. Lustick/ G. Hempstead
411	Checkout of Change to Range-Rate Information Matrix Calculations	L. Lustick/ G. Hempstead

Note No.	Title	Author(s)
412	The Effects of Bias Updating in the Presence of Station and Clock Errors During a Translunar Trajectory . . .	J. Childress, III
413	Effects of Gravitational Harmonics on Earth Parking Orbit Prediction	C. P. Siska
414	Using the OEAP to Calculate the Covariance of the First Corrective Boost After the Ascent Burn	C. H. Dale
415	Long Period Station-Keeping for a Lunar Orbit	J. Childress, III
416	Techniques for Estimation of Parameters Associated with Statistical Type Noise	H. Epstein
417	Effect of Ionosphere on Determination of Orbit Parameters	J. B. Murphy
418	Effects of Gravitational Harmonics on Lunar Parking Orbit Prediction	C. P. Siska
419	Techniques for Estimation of Parameters Associated with Statistical Type Error Sources	H. Epstein
420	A Technique for the RTCC to Correct Measurement Data for the Effect of the Troposphere	H. Epstein
421	Clock Errors in Orbit Determination	H. Engel
422	Techniques for Estimation of Parameters Associated with Statistical Type Error Sources.	H. Epstein
423	Moon Position Parameter	C. Siska
424	Stepwise Estimation	E. Pugh
425	The Effect of Sampling Rate on the Uncertainty in State Vectors.	H. Epstein/ C. H. Dale
426	Error Characteristics of Rubidium Atomic Frequency Standards	H. Epstein
427	Check of the Boost at T_2 and T_3 in the LEM G and N Study.	C. H. Dale

The Bissett-Berman Corporation 2941 Nebraska Avenue, Santa Monica, California EXbrook 4-3270

APOLLO NOTE NO. 398
(Task I, Item IB)

H. R. Wright
4 January 1966

THE STATUS OF IONOSPHERIC SCALE HEIGHT REPRESENTATIONS IN PRECISION S-BAND SPACE VEHICLE TRACKING MODELS

INTRODUCTION

Discussions showing the need for a realistic global scale height model to correct S-band tracking measurements made through the ionosphere have been given in previous Apollo notes (Apollo Notes 317 and 376). Since this parameter measures, first of all, the thickness of the ionosphere, its representation in functional form would make possible the improvement of even a simple slab, such as that derived in Apollo Note 317. If computations now in progress (Apollo Note 377) demonstrate that the use of the latter as an S-band ionospheric tracking model is inadequate, the scale height could become a central problem in this program unless another basic procedure is found that also avoids its explicit use. Beyond this, if computations indicate the need to incorporate a variable profile, the one derived in Apollo Note 317 could serve as a first approximation but modification almost certainly would be required as work proceeded and this would involve the scale height. Because the scale height also scales the ionospheric height profile (see Apollo Note 303), this involvement will appear in an important way. As will become clear later, presently available scale height data are not entirely adequate for our purposes.

Only in recent years has it been recognized generally that this parameter is not quite as simple to interpret as it is in classical Chapman theory. The complications, arising principally from the fact that the ionosphere is not at thermal equilibrium in a classical sense, are discussed in Apollo Note 376 and will not be repeated. The object of this note is to describe the often conflicting experimental evidence and propose a preliminary model. These data were obtained by means

of several more or less independent observational techniques. Each method has its advantages and shortcomings as a data source for correcting space vehicle tracking measurements at S-band, but no single method is entirely adequate.

It cannot be claimed that the papers reviewed in the preparation of this note were evaluated without bias, intentional or otherwise. This is evident from the preceding discussion because, depending on the outcome of the computations now in progress, a very simple representation will undoubtedly be of value in the near future. Accordingly, the simplest possible model having a reasonable degree of plausibility was sought and which, with its shortcomings at least does not do violence to the majority of observations even though examples where there is conflict are not uncommon. Additional bias was introduced by a self imposed requirement that the primary dependence should be on a routinely measured parameter for which real time data could be made available. Here this was chosen to be maximum usable frequency data. The procedure suggested as a result of this analysis is given on pp. 36 - 38. Since it is more or less arbitrary, the model can only be considered an interim measure. An alternate analytical form for use when station observations are not available but which has no potential for extension to real time inputs, is given on p. 33. The notation is summarized in an appendix.

When evaluating the data presented here, the different demands of tracking models and those of satisfying theoretical constructions must be kept in mind. If it were not for these differences, the task would appear as hopeless as that of deducing a simple theoretical method for predicting the weather on a moment-to-moment basis. Most authors in the field of upper atmospheric physics are primarily concerned with fundamentals while we are free to use theory if it can aid and ignore it if not. Ionospheric observations can be manipulated without regard to physical niceties provided only that the results empirically reduce phase path errors. The point of view usually adopted in the literature is even more strikingly at variance with ours in the matter of data interpretation. With few exceptions, observers report mean values, usually on a monthly or annual basis, while ultimately we must either obtain data on a real time basis or predict it. This may not prove as difficult as it appears, although in all probability

those techniques that emphasize the direct use of data will remain most attractive with the function of prediction models being limited to providing guidance and establishing bounds. While real time ionospheric observations may prove to be the only practical way to correct the phase path distortions, it must be remembered that this is a problem of great simplicity when measured in terms of the complexities involved in those to which most authors address themselves; that is, to describe the state of the ionosphere in fundamental terms. The latter has resulted in an almost chaotic flood of periodical literature and from this we seek aid in devising procedures in what is basically a specialized engineering investigation.

CHAPMAN SCALE HEIGHT GENERAL CHARACTERISTICS FROM BOTTOMSIDE OBSERVATIONS

Concerning general scale height morphology based on electron density height profile determinations obtained from ground-based sounder data, Wright[38] has discussed daytime seasonal Scat ("scale height at the F2 maximum") variations which exhibit maxima in the summer and minima in the winter. In contrast to the sudden seasonal changes that occur in the peak electron density, daytime Scat varies almost sinusoidally during the year. The amplitude increases with latitude and often exceeds a factor of two from summer to winter. At night, on the other hand, there is little seasonal Scat variation except at low latitudes. In addition, when a few high latitude stations such as Thule, are excluded, values are nearly the same over wide areas of the darkened hemisphere. Scat data at Thule are far from typical being systematically 25% to 50% higher than those at lower latitudes.

In high latitudes, the F2 layer thickness is greatest at night with a maximum in the early morning hours. Moderate and low latitude Scat variations follow a different diurnal pattern which is characterized in summer by an increase at sunrise that reaches a maximum before noon. During summer afternoons there is a decrease until sunset, after which Scat remains constant through the night. Winter diurnal variations are small except for a brief sunrise enhancement at mid and low latitudes.

In summary, the diurnal Scat variations are most marked in the high latitude summer. This was illustrated by Wright[39] by the diurnal and seasonal Scat variations shown in Figure 1 for five mid latitude stations.

With regard to the assessment of scale height determinations made from bottomside sounder data, recall that most of the ionization is topside. According to Chapman theory, the topside to bottomside electron content ratio, n_a/n_b, should be about 2.15, but most observers report higher ratios. As one example, Roger[20] in the years 1959-1960 observed afternoon n_a/n_b values that always exceeded 3 and, at times, approached 5 (see Apollo Note 303, Figure 61). Now in principle H_m, the Chapman scale height, is determined by measuring n_t, the total electron content and N_m, the electron density at the F2 peak and applying the relation

$$H_m = n_t/(4.133\ N_m),$$

Then it is clear that bottomside experiments will be subject to considerable fluctuation due to the basic problem of estimating n_t when only a small fraction may be observable. This problem is compounded by the fact that h_m not only is the most difficult parameter to measure, but perhaps also the most variable. Thus, the sensitivity of n_b to h_m variations, which of course varies the bottomside thickness measurement where the electron density is greatest, has a significant influence on the result finally obtained for H_m. Somewhat compensating for these deficiencies, ground-based soundings may be made continuously above a fixed location so that diurnal, seasonal and solar cycle variations are discernible.

Another critical matter is judging the relevance of reported scale height data to the real time tracking problem when it must be emphasized that most published observations are for monthly means. The day-to-day variability, which can be quite large, is obscured by this method of reporting data. Wright has investigated the matter and finds that the variability shows definite diurnal and latitudinal dependencies when averaged on an annual basis. Figure 2 illustrates his results for the standard deviation expressed as a percentage of the mean Scat value.

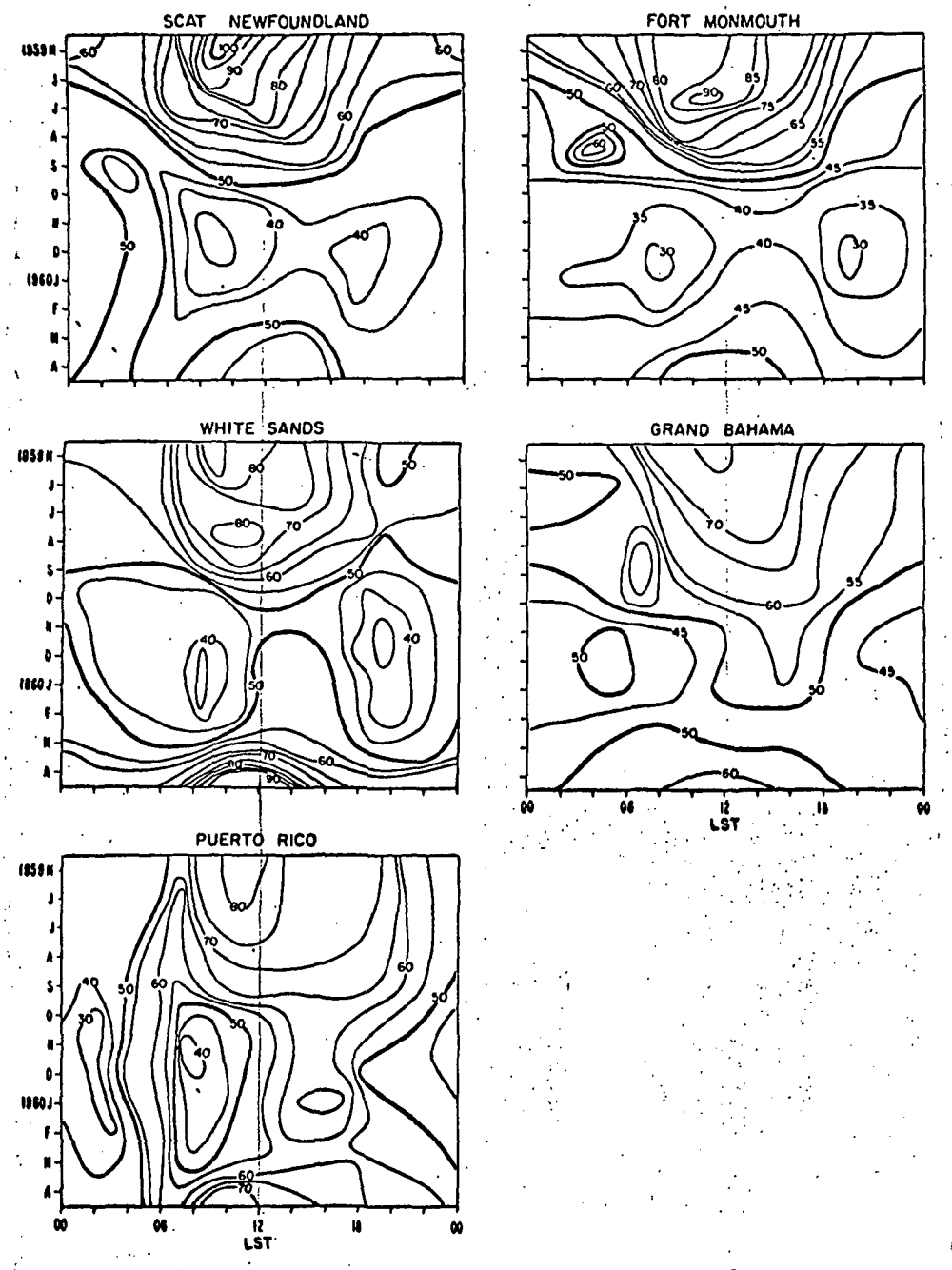

Figure 1. Diurnal and Seasonal Variations of Scat at Mid Latitude Stations With Contours Given in km. (Ref. 39)

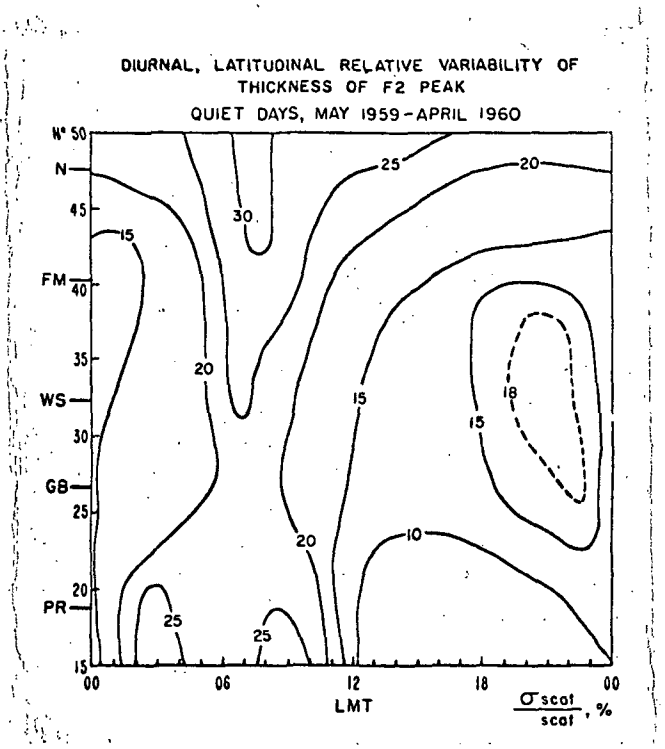

Figure 2. Diurnal Relative Scat Variability As a Function of Latitude Averaged Over May 1959 Through April 1960. (Ref. 39)

SOME DETAILED RESULTS OF SCAT AND H OBSERVATIONS: HEIGHT GRADIENTS AND LAYER MOVEMENTS

For some time it was customary to apply approximate Chapman theory and compute the scale height by finding the parabola

$$N(h) = N_m \left\{ 1 - \left[(h - h_m)/Y_m \right]^2 \right\}$$

that best fitted the observed bottomside N(h) profiles where h is the height, h_m is the F2 layer height, N is the electron density, and Y_m, the parabolic layer half thickness, was considered to be approximately double H_m, the neutral scale height at the peak ionization level. Then the prevalent interpretation of theory was uncomplicated with the ionospheric molecular weight assumed to be known and that Y_m could be taken as simply proportional to the temperature throughout the isothermal layer. Subsequently, Berning[3] published results of a rocket sounding experiment indicating this simple model needed modification. It was deduced that a neutral scale height gradient dH/dh existed in the topside ionosphere above Wallops Island, Virginia, at 0700 EST, November 10, 1959, with a value of about 0.22 ($\cong$ 0.45 for ions). The latter is not to be confused with dH_m/dh_m, the Chapman scale height variation with F2 layer height changes. At that time, Wright[37] suggested the Chapman model be modified to include a scale height gradient, pointing out that it was unreasonable to account for observations, as some workers did, with an H that changed abruptly from say 50 km below h_m to 100 km above. He presented data for March, April and May, 1959, from the Puerto Rico Observatory indicating that, in general, the NBS parameter "Scat" ($\cong Y_m/2$) varied linearly with the layer height for the three-hour period centered on midnight. The latter observation is used prominently in the derivation of the proposed interim scale height model.

Berning reached his conclusions regarding the scale height gradient based on the N(h) profile derived from dispersive doppler effects observed during a rocket flight at altitudes extending to 1500 km. His data were reduced using Nicolet's[16] earlier conclusion that if a constant scale height gradient, $\beta = dH/dh$, exists, then the altitude variation of any atmospheric constituent follows a distribution that can be described by

$$n/n_o = (g_o/g)\,(H/H_o)^{-(1+\beta)/\beta}$$

where H is the given constituent scale height, n its number density, g the acceleration of gravity and the subscript o, refers to an arbitrary base level. Assuming atomic oxygen ions to be dominant the results shown in Table 1 were obtained, where the third column was inferred from the author's data on the basis that, as discussed in Apollo Note 376, above 350 km it is probable that $H \cong 2\,H_i$.

h (km)	H_i (km)	H (km)
262	30	30
362	75	37.5
462	120	60
562	165	82.5
662	210	105
762	255	127

Table 1. Scale Heights at 0700 EST, November 10, 1959 Above Wallops Island, with $h_m \cong 260$ km. (Ref. 3)

Further evidence supporting a positive scale height gradient dH/dh, has been given by Evans[6] who used a completely independent technique based on incoherent backscattering by ionospheric electrons in the beam of the Millstone radar. While data interpretation is not

simple, the technique enjoys the advantage of a capability for continuous ground-based ionospheric observations, including the region above h_m. It was found[6] that all day winter and summer average gradients during 1960-1961 were 0.16 km/km and 0.13 km/km, respectively, where, as above, it here is assumed that $H_i = 2H$. In winter there was little or no daytime variation, but in summer H decreased steadily during daylight hours. The steepest gradient, 0.28 km/km, was observed in summer and the shallowest, about 0.12 km/km, occurred during midday in winter. This is similar to the trend observed in the summer of 1960 by Roger[20] at DeBilt based on staellite beacon data.

These findings were confirmed substantially by Lawrence, et al,[14] using a third independent technique based on radio frequency satellite beacon observations. A reasonable inference drawn from their data is that during the period September 1958 - December 1959, the Chapman scale height increased with the layer height at a rate dH_m/dh_m of about 0.25 km/km over the regions surrounding Boulder, Colorado, and Stanford, California. A related theoretical study was made by Garriott and Rishbeth[9] and discussed in Apollo Note 317. The trend in dH_m/dh_m is what would be expected if h_m always occurs at the same pressure level in an isothermal ionosphere supported by a more or less static lower atmosphere. Then heating increases not only H and the height at which a given pressure occurs, but in the case of the latter, the entire height is not subject to expansion so dH_m/dh_m is positive and less than unity. An important requirement in the foregoing argument is that the atmosphere be in thermal equilibrium. As discussed in Apollo Note 376, it is not always reasonable to assume these conditions are satisfied.

Anticipating results of another study conducted in order to describe ionospheric vertical movements in analytical form, a brief digression will be made to illustrate the last point. Consider the situation after the onset of heating near dawn in the upper atmosphere. Then the darkened lower levels are still contracting and fixed pressure

levels near the altitude of sunrise will be driven lower, but above this level the atmosphere is expanding. Furthermore, it now appears the electron temperature, T_e, reaches its diurnal maximum in the early morning hours preceding ground level sunrise[5]. This maximum is approached at a rate of about 1000°K/hour, beginning at ionospheric dawn[23]. Within two hours the effective plasma temperature, $(T_e + T_i)/2$, exceeds that of the midday maximum reported for the ions and neutrals, T_i. Vertical movement of a constant plasma pressure level in a non-uniformly heated atmosphere is a complicated problem. Qualitatively it can be argued, however, that contraction of the nearly equilibrium lower levels in darkness cannot compensate for the plasma expansion in the sunlit upper levels. Because of this, the altitude of a given plasma pressure must rise. Then it is conceivable that for such a model, h_m would have both an early morning and an afternoon maximum corresponding to the T_e and T_i diurnal maxima, respectively. Although this is not in conflict with the general pattern of the F2 layer movements, the subject of an isothermal ionosphere supported by a realistic lower atmosphere does not appear to have received attention. Considering the utility of a better analytical description of vertical movements in refractive index calculations using even very simplified models, the study made of this matter will be described in a detailed future Apollo note.

SCAT AND H OBSERVATIONS: DIURNAL AND SEASONAL VARIATIONS

The technique used by Lawrence, et al,[14] was Faraday fading of satellite radio signals. It has been more widely used than incoherent backscatter studies and, like rocket probe experiments, yields data over relatively localized areas. While the topside measurements are not as straightforward in some respects as those made by rockets or radars, the results are not completely biased by bottomside conditions as are the ground-based ionsonde data which Wright, for example, based his conclusions described above. Satellite beacon methods share with rocket

probe experiments the shortcoming that observations are relatively brief, but they have the advantage that as the orbit precesses, combined diurnal and seasonal variations eventually are obtained. An example of this seasonal and diurnal pattern of variations observed near the peak of the solar cycle by the Boulder and Stanford groups is shown in Figure 3. Seasonal effects were eliminated by the authors with the results shown in Figure 4 where a diurnal pattern is indicated with an early morning maximum and an evening minimum. This diurnal variation was estimated to range between about 115 km - 85 km. Notice the sharp scale height increase amounting to about 80 km beginning shortly after 01 LMT and continuing through the dawn period. Data variability does not allow definite statements regarding the changes at dawn, but it appears the layer thickness decreases precipitously at sunrise. While this is consistent with the sharp effective pre-dawn temperature maximum noted above, only slight changes occur during the rest of the day. The midday maximum demanded by simple theory is hardly evident and, in fact, the data are not much at variance with a steady decrease of, say, 1.5 km/hr from dawn until after midnight.

Qualitatively, the last results can be "explained" by arguing that h_m rises during the night to levels where the mean molecular weight, M, is much lower than it is during the day. This is quite plausible because Alouette data have been interpreted by King, et. al.[10] as indicating a drop in M from about 0.016 kg/mole in the evening at 600 km to less than 0.004 kg/mole at dawn. Plausibility arguments are treacherous in this field, however as can be illustrated by pointing out that with equal plausibility a line of reasoning can be based on the fact that when the layer reaches its greatest height it is about 200 km below the level where the transition to species of low atomic mass occurs. Then, in the absence of definite experimental evidence, a case could be made for an increase in M preceding the onset of ionization production at dawn. The reason is simply that the recombination rate at h_m is much

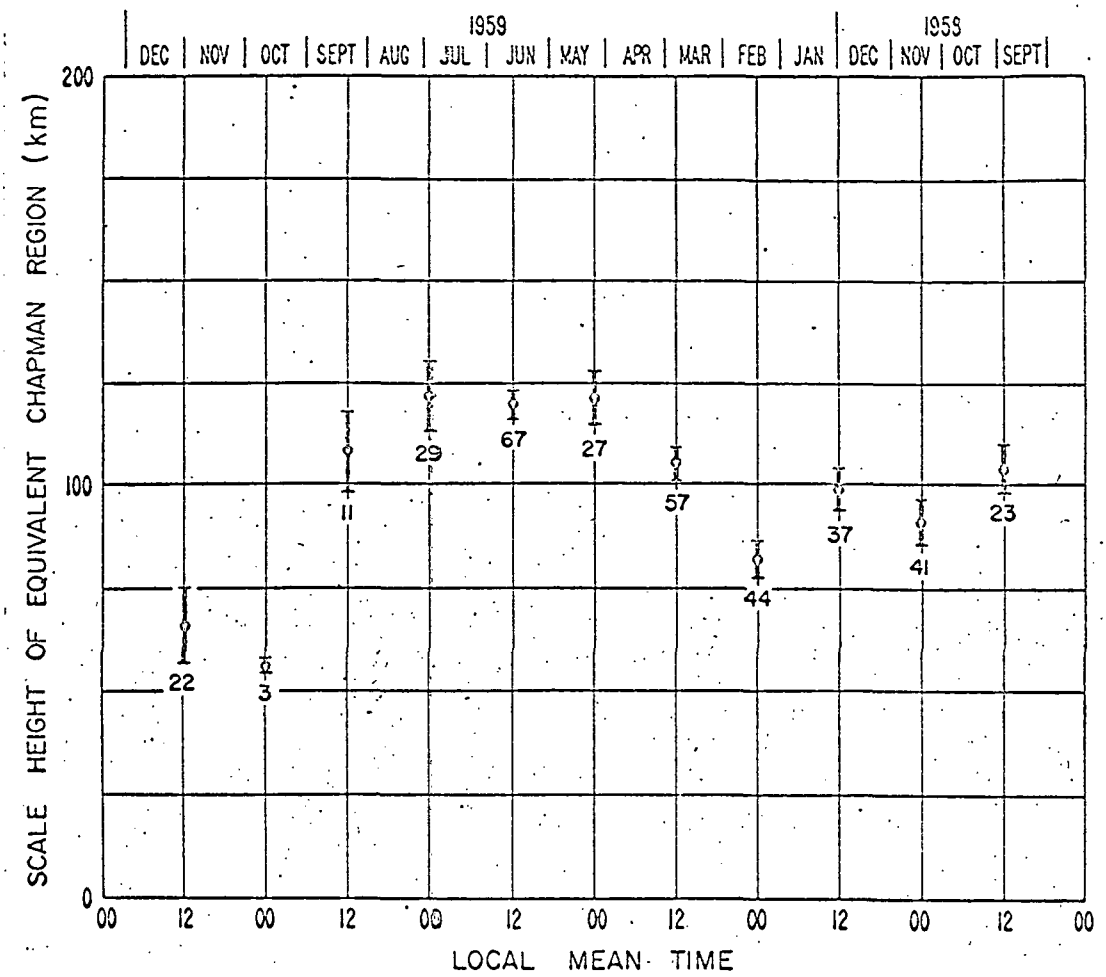

Figure 3. The Seasonal Variation of the Twelve-Hour Average Values of the Scale Height of the Equivalent Chapman Region. The Bars Indicate the Standard Deviation of the Mean, Above and Below the Mean Value; the Numbers Below them Indicate the Number of Observations. (Ref. 14)

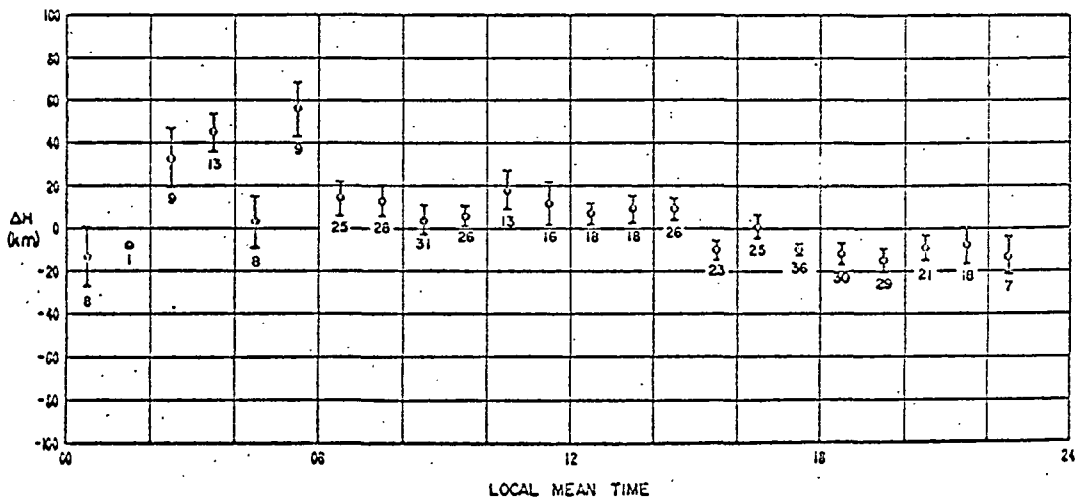

Figure 4. Approximate Diurnal Scale Height Variation Estimated by Eliminating Seasonal Effects in Figure 3 above. (Ref. 14)

greater than at 600 km; the NO^+ population increases at the expense of O^+[17]. This could flatten the predawn rise in H_m that would otherwise be attributed to the effective plasma temperature maximum. On this basis, the scale height should reach a minimum at ionospheric dawn and a maximum at about 1400 LT. Experiments will be described below indicating there are large parts of the world where, at certain periods, the observations have been interpreted so they follow these qualitative conclusions. At the present, unfortunately, any agreement appears to be fortuitous.

Yet another example is furnished by observations of the multiple frequency navigation satellite, 1961 Omicron I, which led Arendt and Soicher[1] to conclude that during November-December 1961, there was a secondary post-midnight maximum in the electron content below 1000 km at Fort Monmouth. The increase amounted to about 5×10^{12} electrons/sq. cm. They ascribe the enhancement to a downward ionization drift from higher levels, but recognize that horizontal drift from low latitudes also is a possible mechanism. Data are not cited for N_m, but since the electron content to 1000 km is nearly proportional to $N_m H$, the increase could also be attributed to an increase in H. Thus, although the enhancement peaked before 02 EST, the observations could also be explained as evidence of the predawn effective temperature peak.

SCALE HEIGHT OBSERVATIONS: SOME COMPARITIVE RESULTS DEDUCED FROM ELECTRON CONTENT MEASUREMENTS

Vanguard I daytime radio transmissions were recorded by Roger[20] at Jodrell Bank for Faraday rotation measurements. From these data, together with N_m values measured at De Bilt, Holland, equivalent slab thicknesses were deduced. The author compared his results with those of other observational programs and found fairly close agreement with the work of Ross and Anderson[22] for November 1959 (see Figure 63 in Apollo Note 303). In February 1960 there was

also agreement with the Ross and Anderson measurements of February 1959, but in the summer of 1960, Roger found the scale height decreased from about 80 km in the morning to about 65 km in the late afternoon, while Ross and Anderson observed an increase during the day.

In their observations, Ross and Anderson[22] applied the differential Doppler technique to harmonically related Sputnik III radio signals received during the day at the Pennsylvania State University to obtain n_t. The implied Chapman scale height in November 1959 was about 54 km and essentially constant from 08-18 LMT. In February 1959, it increased monotonically from about 50 km at 0800 LMT to about 65 km at 1800 LMT. Summer scale heights in that year appeared to increase from about 85 km in the morning to about 95 km in the late afternoon.

Accurate n_t determinations derived from Faraday rotation of moon reflected radio signals transmitted and received at Jodrell Bank combined with N_m measurements at De Bilt, in a geometry similar to that used later by Rogers, were published by Evans and Taylor[7] providing yet another independent means for determing the Chapman scale height. During the winter of 1960, their measurements implied H underwent a diurnal variation which was essentially out of phase with the patterns just discussed, exhibiting a daytime minimum of about 60 km and an early morning maximum of 98 km. Later, the results of similar experiments were given by Taylor[28] which implied the phase of the diurnal variation reversed near the summer Solstice in both 1960 and 1961 (see Figure 37 in Apollo Note 303) with a midday maximum of about 90 km and an early morning minimum of about 50 km. The summer daytime values appeared to be somewhat smaller in 1961 than in 1960, a period of decreasing solar activity, but the data scatter was such that the author could not assert that the effect is real.

When evaluating the sometimes conflicting evidence obtained by these different observational techniques, remember that since the moon moves slowly across the sky, diurnal patterns should be more evident

in lunar reflection data than in those obtained with artificial satellites. The principal reason for this is that continuous measurements may be made over appreciable time periods at essentially constant magnetic activity levels. Further, the complete diurnal pattern may be observed in as short a time as three weeks so that seasonal changes do not seriously obscure the results. A final and very important feature is that moon reflection experiments determine the total electron content. By contrast, since most beacon satellites orbit at 1000 km or less, the question arises: How serious are the effects of the neglected ionization in satellite observations? At 1000 km, Thomas and Sader[30] frequently observed electron densities as high as 3×10^4/cu. cm. and, since daytime N_m as low as 3×10^5/cu. cm. are not unusual, it is seen this question is not trivial. For our purposes, the lunar reflection technique is thus quite attractive.

SCALE HEIGHTS OBSERVED TOPSIDE WITH SATELLITE SOUNDERS

When compared with the vast body of published bottomside sounder data, available topside information is very scanty indeed. It was for this reason, rather than the quality of topside observations, that the suggested model is heavily weighted by conclusions based on ground-based observational data. Actually, most topside soundings are more reliable than those made bottomside. The reason, first of all, is that N may be measured accurately at the satellite thus removing the uncertainty present in all bottomside N(h) data reductions. Secondly, satellites make very rapid and nearly continuous latitude scans which simplifies the separation of geographical and temporal effects. Finally, there is a high N(h) profile determination rate (typically about four per minute) showing ionospheric conditions at closely adjacent geographical positions which gives considerable assurance that the measured profiles are representative. To illustrate, Figure 5 was constructed from topside satellite sounder data given by King, et al,[11] as an example of the latitude dependence of the equivalent Chapman scale height obtainable with essentially continuous latitude scans.

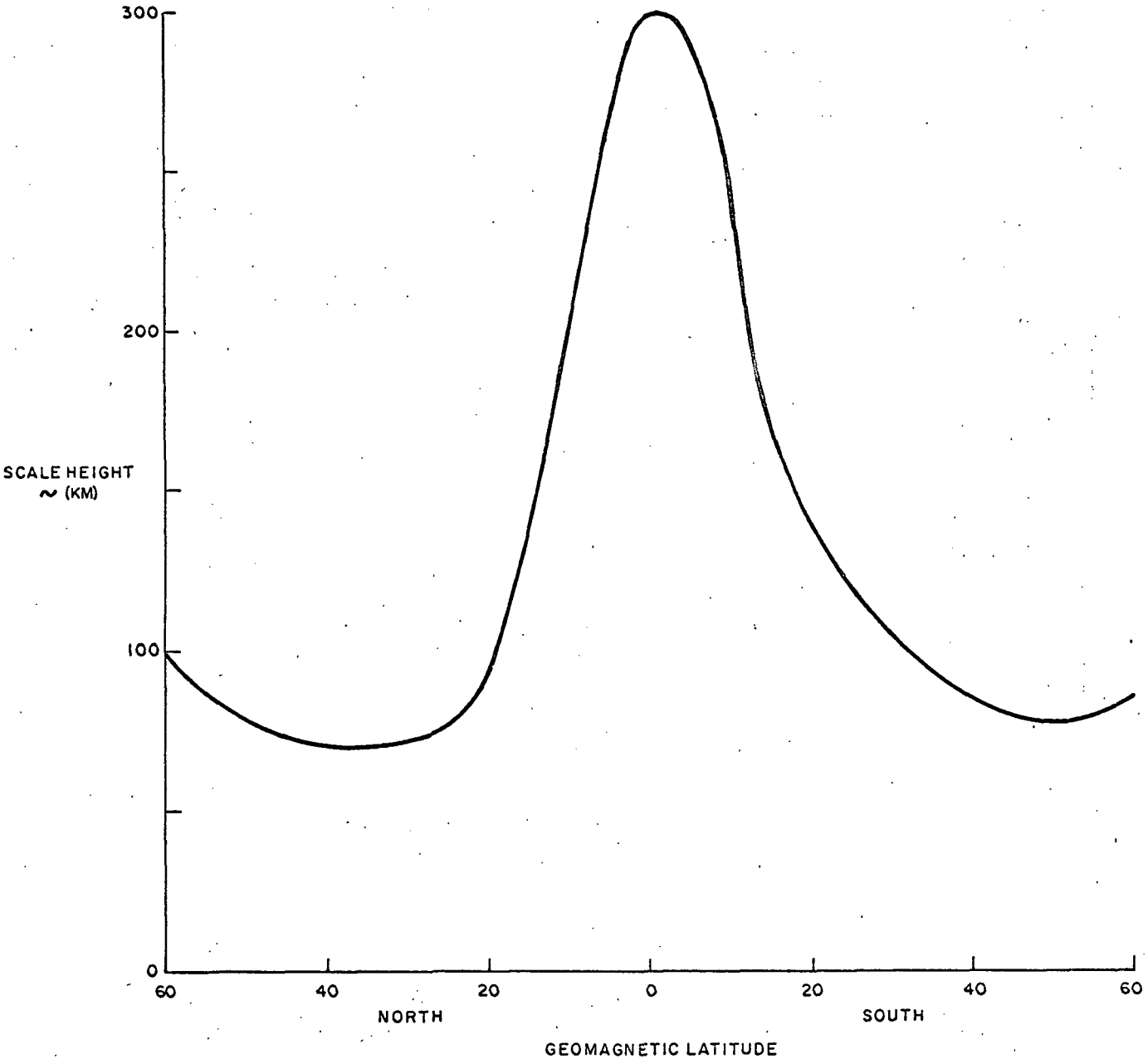

Figure 5. Chapman Scale Height Latitude Variation, October 1962 During Morning As Derived from Alouette Topside Scale Height Contours Given by King, et. al.[10], Assuming $H_i = 2H$ And That the Lowest Contour Corresponded to the Level h_m.

Daytime height gradients have been observed to be relatively small at high latitudes. One example is the midday profile deduced by Barrington, et. al., [2] for September 17, 1963 over northern Labrador which is shown in Figure 6. There the scale height could be considered constant for the present application. Another example is the midnight profile on September 1, 1963, over the Arctic Ocean north of Alaska, also shown in Figure 10, where there was a slight gradient with $dH/dh = 0.07$ km/km but again this could be ignored for our purposes. Nelms, [15] on the other hand, has shown that on at least one pass made one year earlier between 17°N and 68°N, the scale height at the 800 km level was double that at the 400 km level. This is illustrated in Figure 7 for a point in the orbit shortly after sunset over northern Afghanistan on October 3, 1962.

Another important conclusion of the topside sounder analysis reported by Nelms is that there are altitude ranges in which the scale height is relatively constant for a given geographical location. At the time the data was taken it appeared a transition region existed between those regions of the differing scale heights and this tended to broaden and move downward with latitude. This suggested model is illustrated in Figure 8, where it will be noted that scale heights tend to increase slightly at high latitudes. King, et. al., [11] also concluded from topside sounder studies that the electron scale height tended to increase with latitude. For example, an irregular increase from about 100 km at 32°N geographic to about 180 km at 60°N geographic was observed during the midmorning of October 1, 1962 at heights corresponding approximately to h_m. Referring again to Figure 8, note also that at the lowest levels, presumably near h_m, the scale height, although constant over a considerable altitude range, fluctuates with latitude but that no regular pattern is apparent beyond the general tendency to increase slightly with latitude.

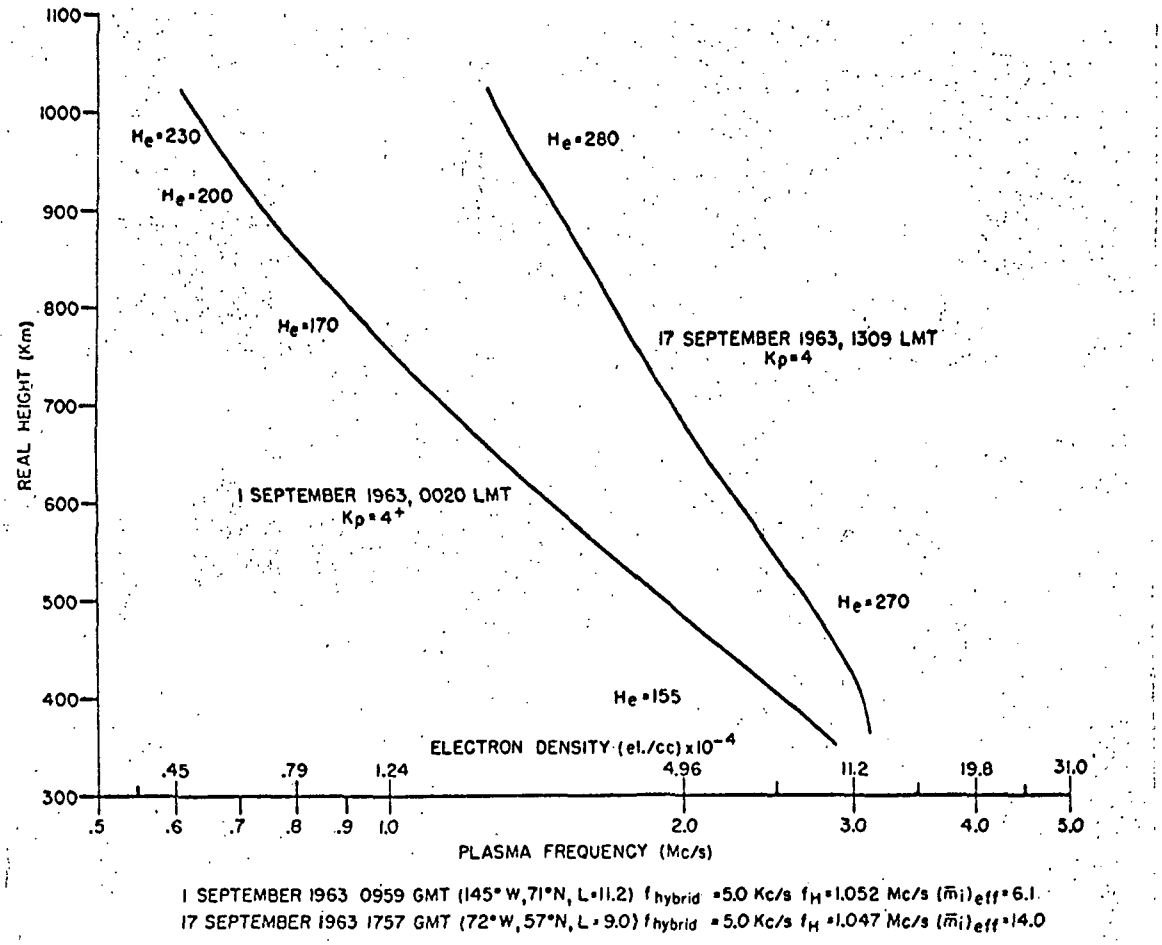

Figure 6. Topside Ionosphere Profiles for Midnight and Midday Near the Arctic Circle in September, 1963, After Barrington, et.al. (Ref. 2)

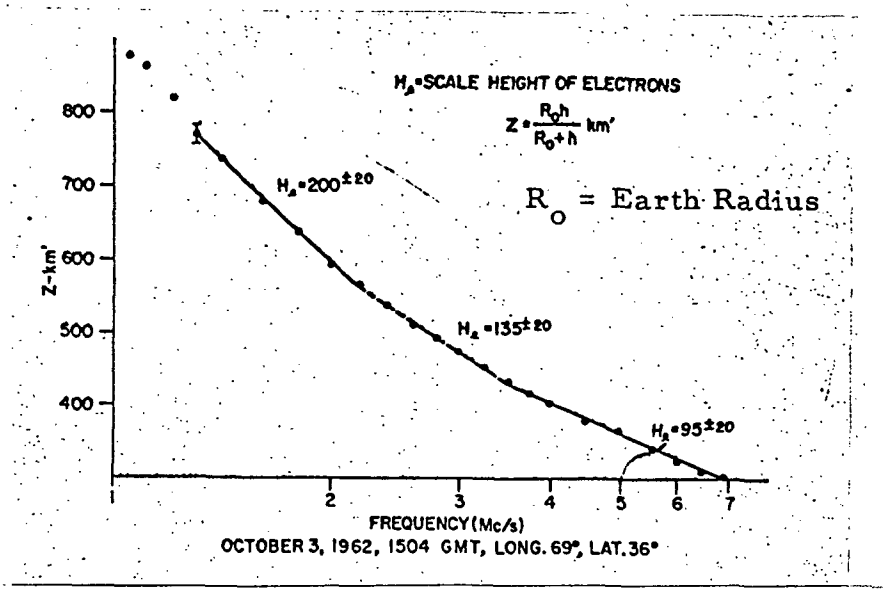

Figure 7. "Reduced Height" Topside Electron Scale Height Profile. If T_e and T_i Are Nearly Equal Below the Satellite Sounder, Then $H \cong H_e^1/2$. (Ref. 10)

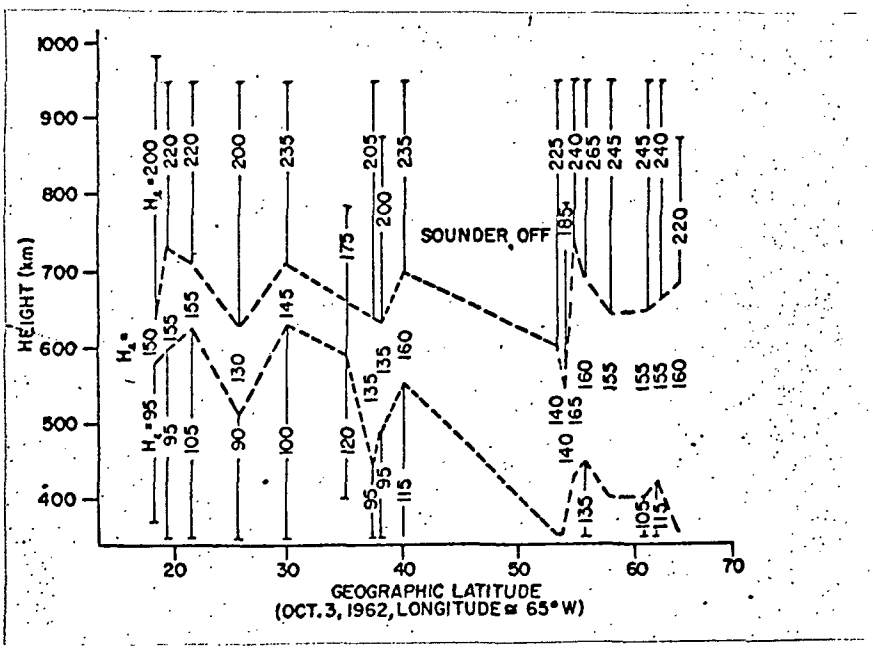

Figure 8. Electron Scale Height Dependence On Height and Latitude As Determined by Topside Soundings. The Lines Indicate Altitude Intervals Over Which the Scale Height Was Constant. Times of day at which observations were made were not specified. (Ref. 10)

DIURNAL H VARIATIONS: THE CASE FOR A LINEAR TIME DEPENDENCE

Inferred Chapman scale heights were among the results of an observational program based on Faraday fading of a satellite beacon that was conducted at Delhi, India by Somayajulu, et. al.,[26] Their results are summarized in Table 2.

Date	Time IST	n_t per sq. m x 10^{17}	H Above h_m (km)	H Average in F (km)
3	1408	3.46	144	107.4
8.9	1306	3.10	70	60.5
9.10	1030	3.50	94	74.3
10.10	0942	2.80	120	93.0
13.10	0854	2.50	66	54.1
20.10	0615	0.43	42	41.7
25.10	0500	0.56	163	124.4
26.10	0408	0.36	76	66.7

Table 2. Chapman Scale Heights and Total Electron Content, n_t, Over Delhi (Magnetic Dip = $42^{o}4$ N) in 1962. (Ref. 26)

Despite the scattered data points, which were as great as 50-75 km near dawn, these authors believed they detected a scale height increase that was linear with time between 03 and 15 LT. Based on the Faraday fading measured during passes of Transit 4A satellite over Columbus, Ohio, at about 1000 km altitude, Potts[19] also concluded the neutral scale height has a midday maximum. Undismayed by the great data variability shown in Figure 9, he made an interpretation similar to that reported in the earlier paper by Somayajulu, et al,[26] deciding that this midday maximum during the period August-October, 1962, was approached linearly in time during the morning and, in addition, underwent a symmetrical decrease during the afternoon that could be described roughly by

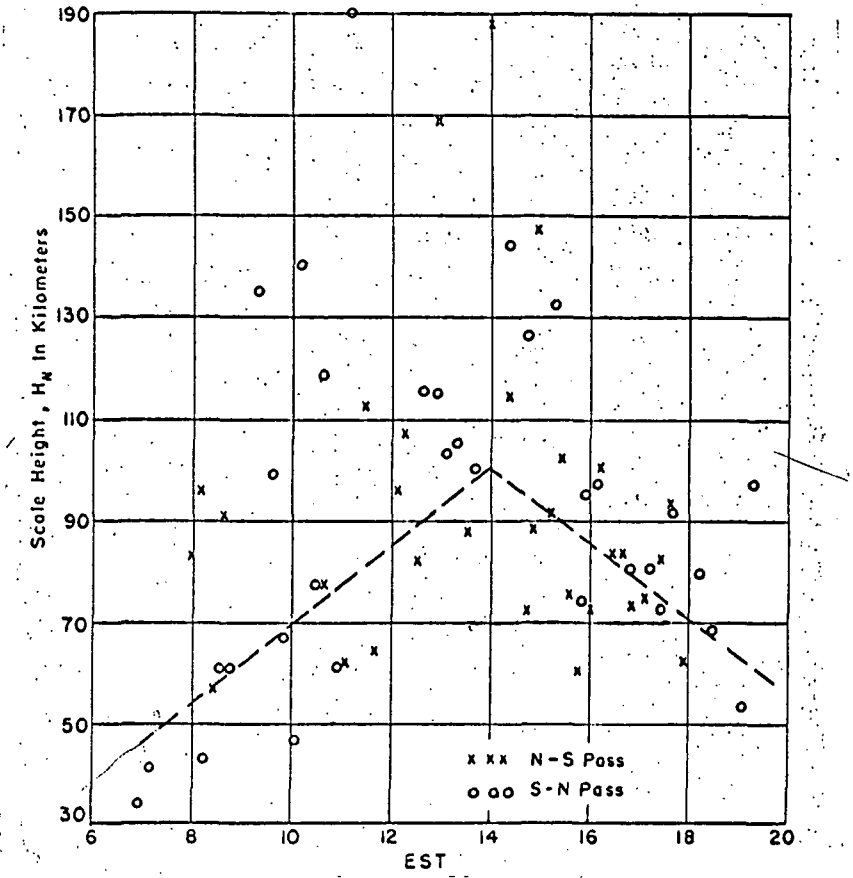

Figure 9. Daytime Neutral Scale Heights, After Potts (1965), As Determined by the Faraday Rotation Rate of Signals From Transit 4A Satellite as Received at Columbus, Ohio During the Period August-October, 1962. (Ref. 19)

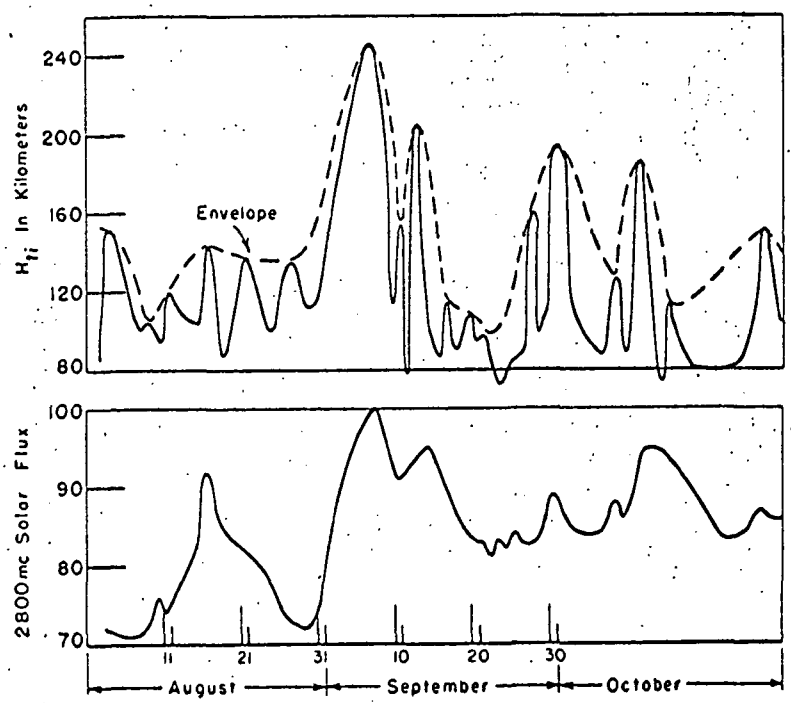

Figure 10. Correlation of the Midday Neutral Scale Height With the 2800 Mc/s Solar Flux, After Potts (1965) (Ref. 19)

$$H = H_a(1 - 0.075\,|14 - t|)$$

in which H_a correlates with the 2800 Mc/s solar flux, as shown in Figure 10, but is otherwise time independent. This interpretation of course has the appeal that then H is in phase with the diurnal temperature pattern as demanded by simple theory.

Equivalent slab thickness determinations deduced earlier from Faraday rotation measurements of Transit 4A by Blumle[4] during the period September 1961-January 1962 imply the scale height at the magnetic equator follows a somewhat similar diurnal pattern with a maximum of about 110 km at 14 LMT and a minimum of 30 km at 02 LMT. His data (see Figure 80, Apollo Note 303 and divide the slab thickness by 4.13) indicate an anomalous scale height which has a nearly constant value of about 55 km for nearly two hours centered between the times of sunrise at the F2 layer and sunrise at the ground. While Blumle drew a smooth curve somewhat resembling a sinusoid through his data points, the measurements are so scattered that the possibility the pattern he observed is as linear as that inferred by Potts, cannot be excluded.

Other observations that also indicated a more or less linear time dependence have been described by Shirke[25] who finds bottomside ionograms indicate pronounced diurnal variations at Ahmedabad (magnetic dip = 34°N) with a maximum near noon and a minimum near midnight during high sunspot years as illustrated in Figure 11. His data also indicate near equality between the slab thickness parameter n_t/N_m and the scale height that is implied by an exponential distribution. Remembering that in an alpha-Chapman layer the equivalent slab thickness, $n_t/N_m = 4.133\,H$, it is probable the author tacitly has made the indicated division and Figure 12 was so interpreted to illustrate the seasonal variation of the diurnal patterns for high and low sunspot years. Not evident in the latter figures are the large predawn variations evident in the Lawrence, et al,[14] data nor the "dramatic"

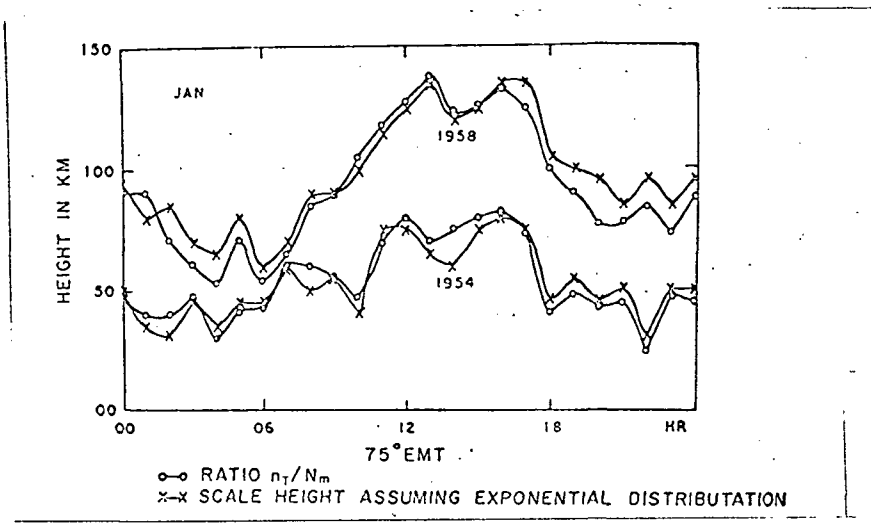

Figure 11. Diurnal Variation of the Slab Thickness Parameter n_T/N_m Compared With That of the Scale Height Near h_m for a Low Solar Activity Year, 1954, and a High Solar Activity Year, 1958, over Ahmedabad (23°01 N; 72°36 E; 34° N dip) in January. (Ref. 25)

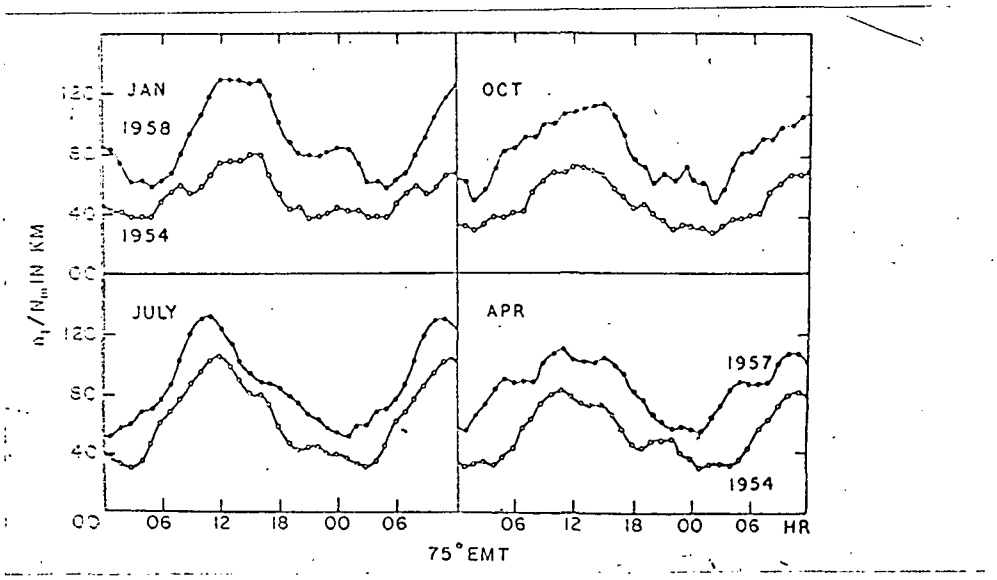

Figure 12. Diurnal Variation of the Slab Thickness Parameter for the Seasons of High and Low Sunspot Years Over Ahmedabad. (Ref. 25)

scale height changes reported by King, et al[11] when the dawn solar zenith angle reaches 100°. Fortunately, these changes occur when N_m is near its diurnal minimum so that large relative changes are not as serious as at other times.

With regard to the work of the latter two authors, it should be noted that Delhi is one of the lowest latitude stations at which topside scale heights are not strongly effected by horizontal diffusion of ionization along magnetic field lines. These effects may be so important in fact, that King, et al[12] suggest that below 45° dip angle it is not possible to use N(h) distributions to make useful deductions regarding ionospheric temperature and composition. This does not imply that the indirectly derived low latitutde scale height data will not be useful for refractive index calculations. On the contrary, since the electron content is measured, the effects should be of second order involving only profile distortion effects. Furthermore, at dip angle greater than 45° it appears the assumption may be made with confidence that the vertical electron distributions have the same scale heights as those along field lines.

SCALE HEIGHT DEPENDENCE ON THE SOLAR CYCLE

The serious variability of scale height measurements, notwithstanding, when averages are taken a strong and relatively simple dependence on the sunspot number R has been recognized for years. Titheridge,[29] for example, reports that Explorer 7 elevation angle data at Auckland, New Zealand indicated the scale height at the peak ionization level in winter varied about 20% from day to day but had no diurnal variation. This variability did not obscure a sunspot dependence which could be represented by

$$H_m = 54(1 + 0.0023\,\bar{R}) \text{ (kilometers) (winter)} \qquad (1)$$

where $\overline{R}$ is the mean sunspot number. In summer, H_m was about 25% higher than in winter with a diurnal variation of about $\pm$ 4 km which will be taken to be given by

$$H = 67(1 + 0.0023\overline{R}) \text{ km} \quad \text{(summer)} \tag{2}$$

These results will be compared with those of other authors on the basis that seasonal variation is sinusoidal and that statistically R, the daily Zürich sunspot number, may be substituted for $\overline{R} = 1.75R$. When this is done the extrapolation takes the form

$$H_m = 6.5\,(9.3 + \sin\theta_o)(1 + 0.0013\,R) \tag{3}$$

where to compare these data with those obtained in the northern hemisphere, use

$$\theta_o = 2\pi\,(d - 80)/365$$

with d being the number of day of the year.

An investigation of the Y_m sunspot dependence has also been made by Stubbe.[27] For Lindau, West Germany, he deduced that on magnetically quiet December days the noon parabolic layer half thickness is represented by

$$Y_m = 51.99 + 0.316R - 0.327R^2 \times 10^{-3} \text{ (kilometers)} \tag{4}$$

where again R is the Zürich sunspot number and it will be remembered that $H_m \cong Y_m/2$ only for equilibrium (see Apollo Note No. 376). In conflict with the findings both of Titheridge and of Wright, that the winter scale height has little or no diurnal variation; and not in agreement with the observations that showed a winter diurnal midday

maximum; Stubbe concluded that at midnight the layer half-thickness was greater than at noon and followed

$$Y_m = 88.1 + 0.207R \text{ (kilometers)} \qquad (5)$$

Plots of these relations and the data on which they were derived are displayed as Figures 13 and 14. The number of significant figures quoted by the author is somewhat surprising, even for a monthly mean, considering the large unexplained day-to-day variations so strikingly illustrated there. At noon, in fact, the correlation coefficient of the Y_m equation with sunspot number is only 0.85; at midnight it drops to 0.79. For comparison purpose, at least, writing these results in the form given by Titheridge assuming a linear dependence on R is justified. Equations (4) and (5) become, respectively,

$$H = 26\left[\, 1 + 0.0068\ R \,\right] \text{ km}, \quad \text{(noon)} \qquad (4a)$$

$$H = 44\left[\, 1 + 0.0024\ R \,\right] \text{ km}, \quad \text{(midnight)} \qquad (4b)$$

Explicit sunspot number dependence was not given by Shirke,[25] but for comparison purposes, his data for the January midday maximum which was discussed above will be scaled later according to

$$H = 75\left[\, 1 + 0.0025R \,\right] \text{ km}, \quad \text{(midday maximum)} \qquad (6)$$

and the early morning minimum according to

$$H = 27\left[\, 1 + 0.0011R \,\right] \quad \text{(early morning minimum)} \qquad (7)$$

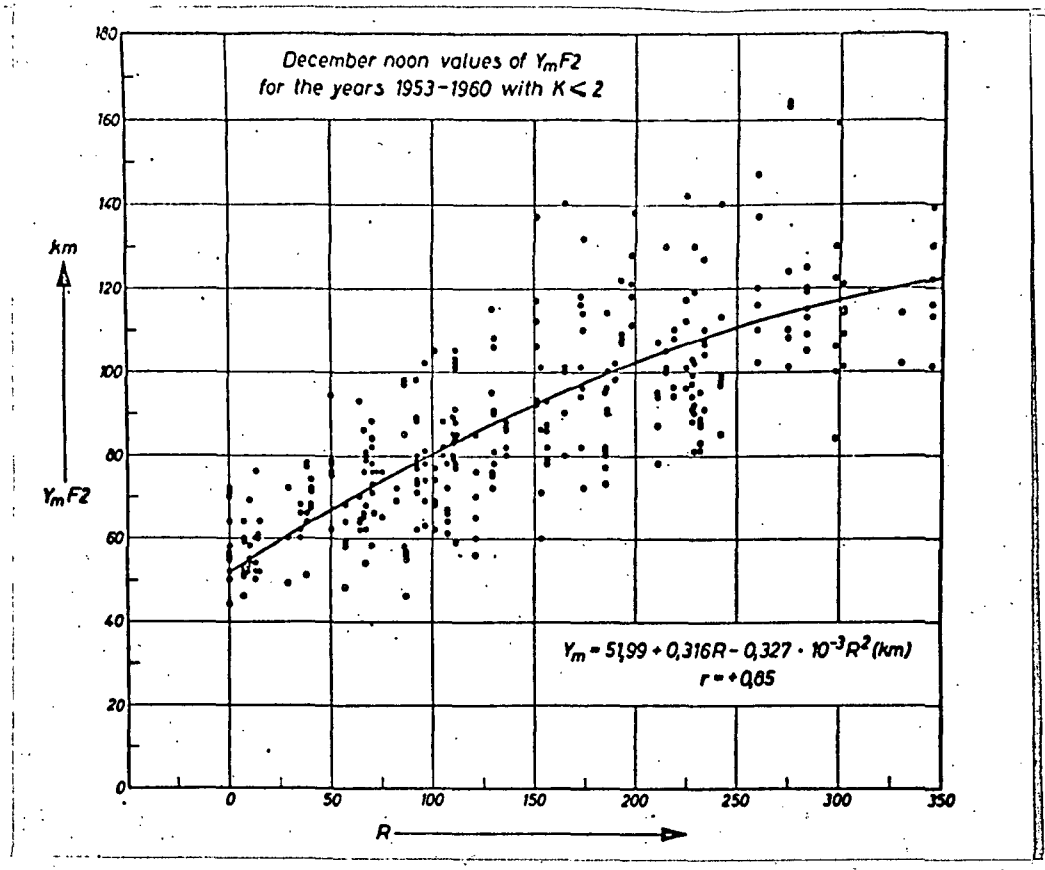

Figure 13. Noon Mean Y_m Values Plotted Against Daily Zurich Sunspot Number R for Magnetically Quiet December Days From 1953 to 1960 As Deduced By Stubbe From Ionograms Taken at Lindau/Harz. (Ref. 27)

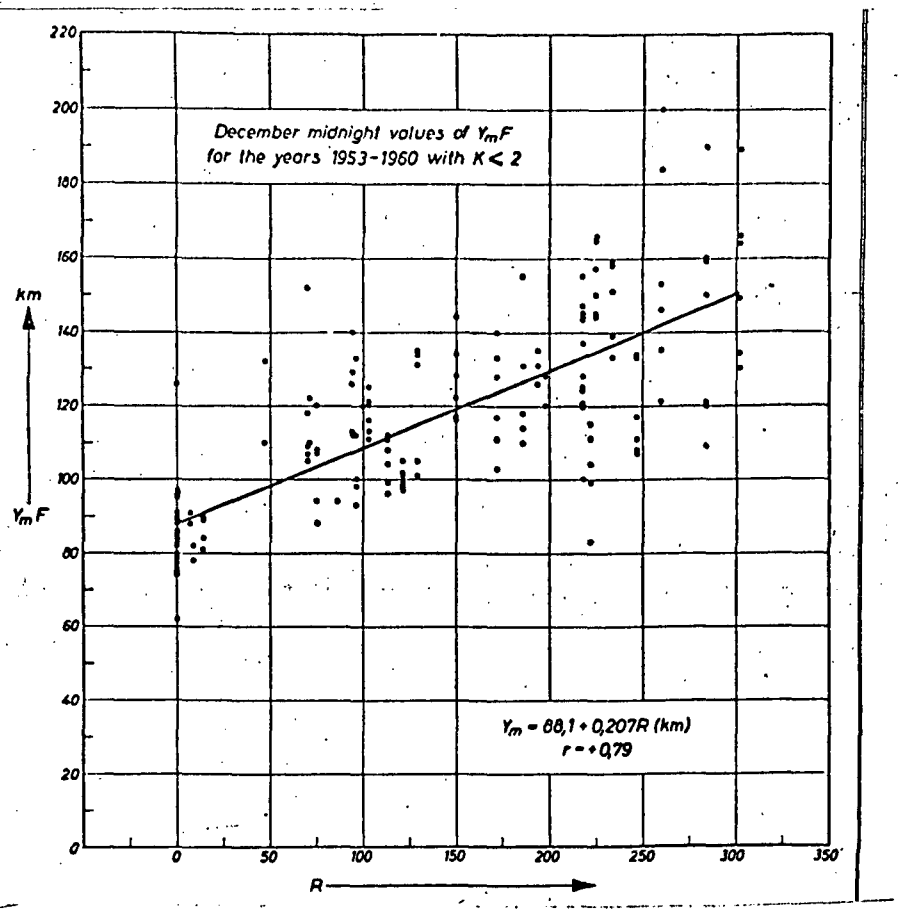

Figure 14. Midnight Mean Y_m Values Plotted Against Daily Zurich Sunspot Number R for Magnetically Quiet December Nights From 1953 to 1960 As Deduced By Stubbe From Ionograms Taken at Lindau/Harz. (Ref. 27)

SUMMARY

An attempt has been made to summarize the measurements published by a number of investigators in Table 3. Although proposed "standard" model atmospheres have been completely arbitrary, it is nonetheless of interest to compare results with the neutral scale height at the F2 peak, say at 300 km altitude, from the profile reported by Norton, et al[18] and often cited as a standard. The latter, which was calculated based on the widely accepted 1959 ARDC model atmosphere, is given in Table 4. Near h_m it agrees with some observations. Above h_m the gradient is about 0.1 km/km, again in agreement with some observations, but differs from most others. Although arbitrary steps must be taken to derive any H_m model, those taken for reference atmospheres result in such inflexibility that none proposed to date appear suitable for our application.

No serious attempt was made to rank these experiments. Each method has its advantages and drawbacks. None may be considered better than 10-25% accurate as far as absolute values are concerned. About the most that may be said is that, in addition to the easily measured N_m, the total electron content is the most important single quantity determining H. Thus bottomside data provide the poorest ionospheric sampling and lunar reflections the best.

Considering both the diversity of the reported data and the fact that no one observational technique is without serious limitations as a data source for refractive index calculations, a summary by almost any reviewer will be biased. As indicated in the introduction, the summary given here is biased by the fact that this study has sought a simple empirical relation for the scale height variations that has some potential for extention to real time predictions. It was for this reason that it was decided to compare those data sets for which a symmetrical diurnal pattern, to be expected on the basis of elementary theory, is at least plausible even if the respective authors may not have chosen that representation. In this, the simplest possible

Table 3. Scale Height (km) Estimates

	Source	Period	Day	Night	
#	Ross (1960)	Sept. '58- Dec. '59	100 55	59 41	Summer Winter, U. of Pa.
#	Yeh and Swenson (1961)	Sept. '58- May '59	98	70	12 hr. average, Urbana
#	Blumle (1963)	Sept. '61- Jan. '62	110	30	Magnetic equator
ϕ	Jackson and Bauer (1961)	April '61	57		Wallops Island flight at 5 EST
ϕ	Hanson and McKibbin(1961)	Nov. '60		43	Wallops Island
#	Somayajulu, et al	Sept. '62- Oct. '62	100 120	50 70	(Entire F above h_m) over Delhi
✓	King, et al	Sept. '62	75	-	(H_i = 150 km at h_m) (20-50° Geomag. Lat.)
	Goldbey, et al (1964)	Oct. '62	70	-	
ϕ	Knecht, et al (Sept. 1961)	June '61	75	-	(Flight at 1817LT 400-600 km) Wallops Island
ϕϕ	Evans (July 1962)	'60-'61 '61	50 70 65	- - -	Winter, Millstone Summer Summer morning
ϕϕ	Evans(p. 266 in Thrane)	Summer '61	58	49	Midday and all night averages
ϕ	Berning (1960)	Nov. '59	30	-	At h_m, Wallops Island 0700 LT
##	Shirke (1963)	Jan. '58- Jan. '54	140 75	45	Afternoon max. and early morning min. over Ahmedabad
	Norton, et al (1962)	-	60.28	-	ARDC 1959 Model Atmosphere at 300 km
✓	Barrington, et. al (1965)	1 Sept. '63 17 Sept. '63	 135	77	Near Arctic Circle

Table 3. Scale Height (km) Estimates (continued)

	Source	Period	Day	Night	
#	Titheridge	≅ Jan. '54	54	54	Zero sunspot, Auckland, N. Z.
		Winter '61	60		
		Summer '61	77		
#	Lawrence, et al (April 1963)	May '59	120	-	Boulder and Stanford 12 hr. averages centered at 00 LT and 12 LT
		June '59		120	
		Sept. '58	100		
		Dec. '59	65		
		Oct. '59	-	57	
		'58-'59	115	85	Average diurnal range
##	Stubbe	≅ Dec. '59	60	75	Peak of solar cycle-Lindau (≅ 67° dip)
		Zero Sunspot	26	44	
##					
##	Wright (May, June 1962)	Dec. '59	40	50	Noon and midnight at St. Johns, Newfoundland (≅ 72° dip)
		≅ Dec. '57	50	95	Scaled to solar cycle peak by Stubbe's results
#	Potts	Aug. -Oct. '62	100	45	14 and 07 EST, Columbus, Ohio
**	Taylor (1964)	May-June, '60 & '61	97	55	De Bilt, Holland
**	Evans and Taylor	Winter, '60	60	98	
#	Ross and Anderson	Nov. '59	54		Pa. State U. (08-18 LMT)
		Feb. '59	50		08 LMT
			65		18 LMT
		Summer '59	85		08 LMT
			95		18 LMT
#	Roger	Nov. '59	54		De Bilt 08-18 LMT
		Feb. '59	50	75	*10 and 22 LMT
		Summer '59	80		08 LMT
			65		18 LMT
**	Taylor (Reported by Roger)	Feb. '60	40	90	DeBilt 10 LT and 22 LT
#	Schmelovsky and Cumme (1965)	'58-'59 Equinox		140	Means at Kuhlangsborn (54°N Geomag.)
		'63 Autumn		70	
✓✓	Galperin and Temny (1965)	'62 Summer		60	At ~300 km in Brazilian Anomaly

Table 3. Scale Height (km) Estimates (continued)

*On basis of straight line through his data point for 1500 LMT and that of Ross and Anderson for 1200 LMT (see Figure 63, Apollo Note 303) and that the diurnal minimum and maximum coincide with those of Taylor, as reported by Roger. (Ref. 20)

#	Beacon satellite
##	Bottomside ionosonde
**	Lunar reflection
ϕ	Sounding rocket
ϕϕ	Incoherent backscatter
✓	Satellite ionosonde
✓✓	Height dependence of hard trapped protons with satellite probe

Table 4. Neutral Scale Height Altitude Dependence Based on the 1959 ARDC Model Atmosphere. (Ref. 18)

Altitude (km)	Scale Height (km)
0	8.43
10	6.55
20	6.39
30	6.83
40	7.73
50	8.42
60	7.61
70	6.34
80	4.98
90	5.00
100	6.05
120	14.62
140	26.46
160	38.35
180	44.93
200	48.12
300	60.28
400	72.48
500	85.04
600	101.6
700	113.0

relation, namely that proposed by Potts, was used. Data sets were selected if a daily maximum could be estimated with at least half an assumed 24-hour diurnal period indicated. The interval of pre-dawn anomalies was ignored in those cases where the irregular deviations at that time were so conspicuous that a linear relation became untenable. Table 5 shows the examples picked with the corresponding estimated linear coefficients. Observe that the largest coefficient is that given by Potts, but even here the evidence for a pronounced diurnal pattern is inconclusive. In fact, referring to Figure 9, from which Potts made his derivation, a case could be made for a constant mean scale height - say 80 km from 8-20 EST.

Another interesting data comparison is obtained by scaling the measurements to zero sunspot and the same season. There is no method for doing this that could be considered free from criticism. That adopted here was first to assume a sinusoidal variation with the seasons. Next, and quite arbitrarily, the sunspot number dependence was taken to be that given by Titheridge. There is little to recommend this comparison technique beyond the perhaps fortuitous fact that agreement is then found with the work of Lawrence, et al,[14] for the essentially same dip angle in the opposite hemisphere. A less satisfying justification for this procedure follows from the fact that data variability is such that other observations, those of Potts for example, do not deviate greatly from the results of this scaling procedure.

An empirical relation reflecting the general trends described above was used to estimate H values that would correspond to late summer 1962. Derivation proceeded by trial and the result adopted takes the form

$$H = 6.5 \left[9.3 + \sin(2\pi/365)(t\text{-March } 21)\right] \left[1 + 0.0023 \bar{R}\right] \quad \text{(km)}$$

Figure 15 shows the linear coefficients calculated after making these extrapolations. The general increase with latitude sometimes found in topside satellite sounder experiments is not evident. Further, the data point scatter appears to be about as great as when the influence of solar activity, seasons and geomagnetic latitude are ignored.

Table 5. Coefficients for Fitting Several Workers' Scale Height Data to the Relation $H/H_a = 1 - a|t_o - t|$ Suggested by Potts When it is assumed the Variations Follow a 24-Hour Period.

		a^{-1} (hours)	t_o (hrs)	H_a (km)	Dip
Blumle	Sept. '61 - Jan. '62	0.060	14	110	0
Shirke	Jan. '58	0.044	15	140	
	Jan. '54	0.050	15	80	
	April '57	0.046	12	120	34°N
	April '54	0.052	12	85	
	July '57	0.055	10	140	
	July '54	0.060	12	85	
	Oct. '56	0.044	15	120	
	Oct. '54	0.054	12	75	
Somayajulu, et al	Sept. - Oct. '62	0.041	15	100	42°N
	Aug. - Oct. '62	0.035	15	120	
Lawrence,# et al	Sept. '58 - Dec. '59	≅0.022	10	115	64N
Potts	Aug. - Oct. '62	0.075	14	120	67°N
Taylor	May - June '60 & '61	0.033	12	90	70°N
Roger*	Nov. '59	0	12**	49	70°N
	Feb. '60	0.027	>17	>70	
	April-May '60	0.029	<07	<90	
	July-Aug. '60	0	14**	75	
	Sept.-Oct. '60	0	--	65	
Wright	Dec. '59	0.025	09	50	72°N

* Based on daytime observations

**Time at which deviation above average is greatest

\# Outside an approximately 4-hour pre-dawn interval

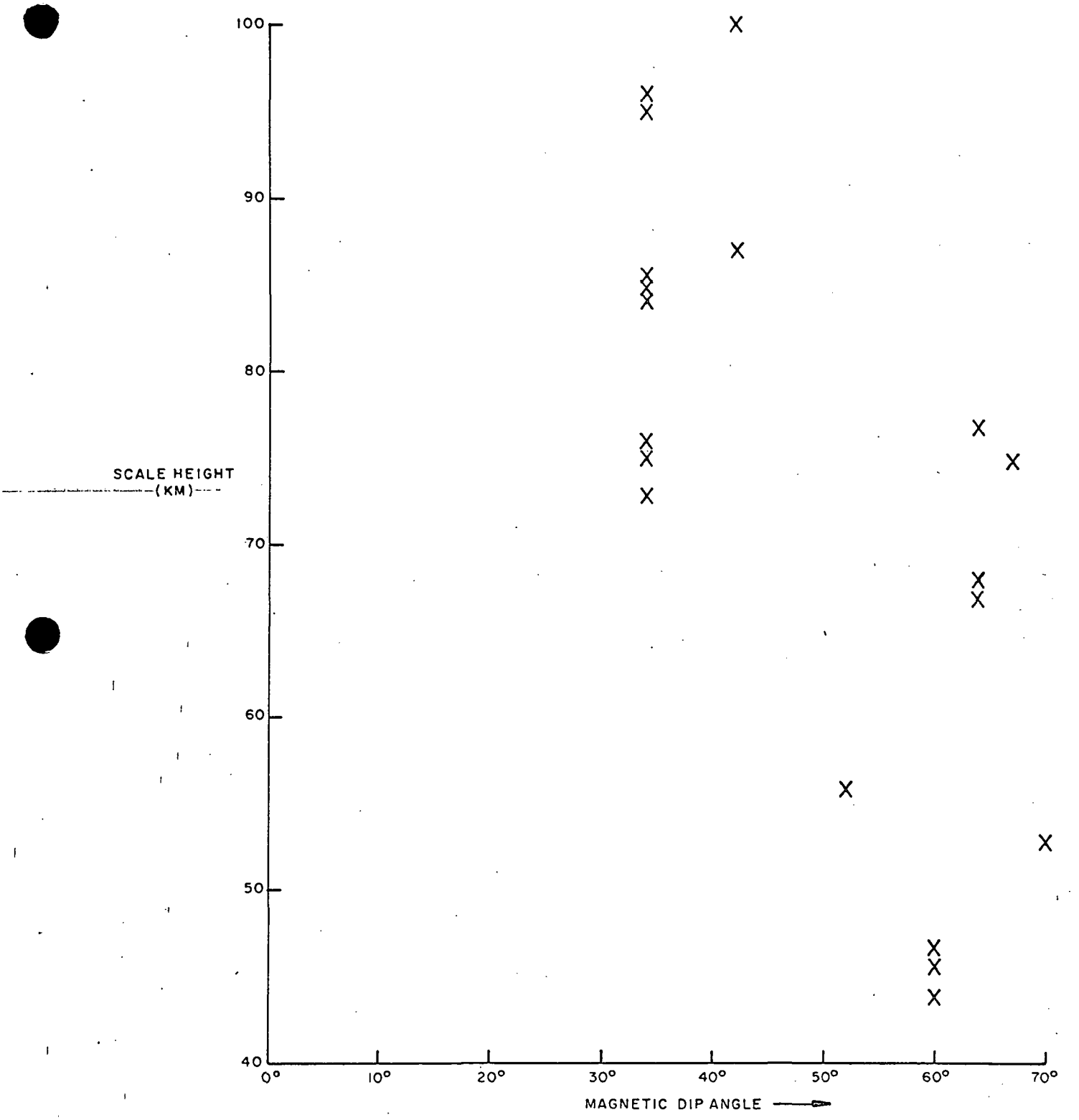

Figure 15. Scale Height Daily Maxima as Given By a Number of Authors After Being Scaled to Zero Sunspot in Summer

AN INTERIM MODEL SCALE HEIGHT

This discussion was intended to give some background concerning the scale height problem and to indicate why additional work is needed to provide H_m predictions reflecting real time variations rather than mean values. From these considerations it was decided that great detail is not warranted in current models and that only general trends in H_m may be incorporated with any realism. Even this program poses serious problems primarily because the diurnal variations based on mean observations do not seem to follow a definite pattern. In addition, while the nocturnal ionosphere may be considered to be at equilibrium for our purposes, this assumption is doubtful during the day and untenable at dawn. As pointed out in Apollo Note No. 376, this complicates scale height interpretations. Thus there would appear little justification for inferring H_m characteristics by extrapolating to daytime periods the observation by Wright that Scat varied linearly with h_m in the middle of the night. Nonetheless, arbitrary steps must be taken if <u>any</u> model is to be derived and since all observations show H increases with h, the assumption will be made that the variation is linear and that it also applies to H_m and h_m. Although this procedure is somewhat questionable for the daytime ionosphere, there is little evidence to indicate it would not prove adequate for our rather specialized purpose. At any rate it was adapted in preference to other equally arbitrary measures that might suggest themselves. The principal attractive feature is that h_m enjoys the practical advantage that real time inputs then could be realized. Recognizing the shortcomings and basic arbitrariness of this procedure, it nonetheless is proposed as the basis of an interim model until results of the computational program indicate additional work is required.

As discussed above, Berning and Wright found gradients such that $dH/dh = 0.22$ and $dH_m/dh_m = 0.20$, respectively, while the work of Lawrence, et al, indicates $dH_m/d_m = 0.25$ near the peak of the solar cycle. An examination of Stubbe's Y_m and h_m data indicates

a mean over the solar cycle was $dH_m/dh_m = 0.17$. While dH_m/dh_m undoubtedly undergoes diurnal changes and further depends both on solar activity and or the seasons, the work of Evans and of Roger furnishing examples, it was decided the simplest model would be obtained if these dependencies were reflected in the base scale height rather than in dH_m/dh_m. Accordingly, Wright's result was adopted for use with this model. Over most of the earth, 250 km is an acceptable reference layer height, h_{mo} (see Apollo Note No. 378), but the assignment of a corresponding reference scale height, H_{mo}, is not so straightforward. To illustrate, at Millstone, a representative winter day scale height was 50 km during a period of low solar activity. Over Wallops Island, the scale height was only 30 km at 0700 EST, November 10, 1959, a period of moderate solar activity. Based on the Scat data reported by Wright,[36] H_m ranged from 30-80 km near Midnight during the Spring months of 1959. A clear pattern is not discernable but quite arbitrarily it was decided to use a factor $(1 - \sin\delta \sin^2\lambda)$ to reflect the winter seasonal maximum that increases with latitude, λ, where δ, the solar declination, is positive to the north. To account for the sunspot dependence, the factor $(1 + 0.004R)$ was used and the reference scale height taken to be

$$H_{mo} = 3 \times 10^4 (1 + 0.004R)(1 - \sin\delta \sin^2\lambda) \qquad \text{(meters)}$$

If now it is assumed that the H_m variations can be ascribed to the changes that occur as the layer moves up or down, the scale height becomes

$$H_m = H_{mo} + (h_m - h_{mo})\, dH_m/dh_m$$

and it is suggested that $dH_m/dh_m = 0.2$ be used, and that h_m be determined from the reported M(3000) F2 values by the method described in Apollo Note No. 378.

Neither geographical variability, such as that illustrated by Figure 8, nor the irregular day to day fluctuations, evident in Figures 14 and 15, for example, can be expected to find description through this model. On the other hand, the tendency for h_m to form a dome over the magnetic equator will cause the predicted H_m to increase slightly toward the poles, in general agreement with observation. Further, since h_m usually is highest at night, the model will exhibit a diurnal pattern following the usual tendency for H_m to have small nocturnal values.

NOTATION

Units are meters and hours unless noted.

a coefficient if H has a linear time variation

d = number of the day of the year

g = acceleration of gravity (meters/sec^2)

g_o = acceleration of gravity at a reference altitude (meters/sec^2)

h = height above earth surface

h_m = height of the F2 peak

h_{mo} = base height if the H_m height gradient is linear

H = neutral scale height as a function of h

H_a = Diurnal minimum H_m if scale height changes are linear in time

H_e = electron scale height

H_i = ion scale height

H_o = scale height at a reference altitude

H_m = scale height near the F2 peak

H_{mo} = base scale height if the H_m height gradient is linear

K_p = three hour geomagnetic index

$(m_i)_{eff}$ = effective plasma atomic mass number

n = electron content in a vertical column

n_a = electron content above the F2 peak

n_b = electron content below the F2 peak

n_t = electron content through entire ionosphere

N_o = electron density at a reference altitude

N = electron density

N_m = electron density at the F2 peak

R_o = earth radius

R = daily Zurich sunspot number

$\overline{R}$ = monthly mean Zurich sunspot number

"Scat" = NBS "scale height at F2 maximum"

t = time

t_o = time H reaches its diurnal minimum

L = magnetic shell coordinate (distance in earth radii at which the magnetic shell crosses the magnetic equator)

Y_m = parabolic F2 layer half thickness

Z = "reduced height" = $R_o h/(R_o + h)$

β = scale height altitude gradient (dH/dh)

δ = solar declination

λ = latitude

θ_o = 2π (d-80)/365 (northern hemisphere)

σ = standard deviation

σ_{Scat} = "Scat" standard deviation of the average diurnal variability (see figure 2).

BIBLIOGRAPHY

1. Arendt, P. R., and Soicher, H., "Downward Flux at 1,000 km Altitude From Electron Content Measurement at Mid-latitudes", Nature, 204, No. 4962, pp 983-984, 5 December 1964

2. Barrington, R. E., Belrose, J. S., and Nelms, G. L., "Ion Composition and Temperatures at 1000 km as Deduced from Simultaneous Observations of a VLF Plasma Resonance and Topside Sounding Data from the Alouette 1 Satellite", Journal of Geophysical Research, Vol. 70, No. 7, April 1, 1965, pp 1647-1664

3. Berning, W. W., "A Sounding Rocket Measurement of Electron Densities to 1500 Kilometers", J. Geophys. Res. 65, No. 9, September 1960, pp 2589-2594

4. Blumle, L. J., "Satellite Observations of the Equatorial Ionosphere", J. Geophys. Res. 67, pp 4601-05, 1962; see also "Satellite Observation of the Equatorial Ionosphere", NASA Technical Note D-1756, June 1963

5. Bourdeau, R. E., "The Temperature of Charged Particles in the Upper Atmosphere", Space Research V, North Holland Publishing Co., pp 77-90, 1965

6. Evans, J. V., "Incoherent Backscatter Studies of the Ionosphere At Millstone Hill", pp 266-304, entitled, Electron Density Distribution in Ionosphere and Exosphere", E. Thrane, ed., North Holland Publishing Co., 1964

7. Evans, J. V. and Taylor, G. N., "The Electron Content of the Ionosphere in Winter", Proc. Royal Soc. A, Vol. 263, October 10, 1961, pp 189-211

8. Galperin, Yu I. and Temny, V. V., "Atmospheric Scale Height in the 200-400 km Range According to Radiation Belt Data", Space Res. V, 1965, North Holland Publishing Co., pp 769-778

9. Garriott, O. K. and Rishbeth, H., "Effects of Temperature Changes on the Electron Density Profile in the F2 Layer", Planetary and Space Science, 1963, Vol. 11, pp 587-590

10. King, J. W., Smith, P. A., Eccles, D., Fooks, G. F., and Helm, H., "Preliminary Investigation of the Structure of the Upper Ionosphere as Observed by the Topside Sounder Satellite, Alouette", J. Geophys. Res., 1963, Vol. 68, pp 464-487

11. King, J. W., Smith, P. A., Helm, H., Eccles, D., and Fooks, G. F., "The Structure of the Upper Ionosphere as Observed by the Topside Sounder Alouette", Space Res. IV, 1963, Warsaw Proceedings John Wiley and Sons, Inc., (1964), pp 449-451

12. King, J. W., Legg, A. J., and Smith, P. A., "Studies of the Composition and Temperature of the Upper Ionosphere as Deduced from Electron Distribution Observed by the Topside Sounder Satellite", Space Res. IV, 1965, North Holland Publishing Co., pp 639-640

13. Knecht, R. W., Van Zandt, T. E., and Russell, S., "First Pulsed Radio Soundings of the Topside Ionosphere", J. Geophys. Res., Sept. 1961, Vol. 66 No. 9, pp 3078-3081

14. Lawrence, R. S., Posakony, D. J., Garriott, O. K., and Hall, S. C., "The Total Electron Content of the Ionosphere at Middle Latitudes Near the Peak of the Solar Cycle", J. Geophys. Res., April 1, 1963, Vo. 68, No. 7, pp 1889-1898

15. Nelms, G. L., "Scale Heights of the Upper Atmosphere From Topside Soundings", Canadian J. Phys., 1963, Vol. 41, pp 202-206

16. Nicolet, M., "Constitution of the Atmosphere at Ionospheric Levels", J. Geophys. Res., 1959, Vol. 64, pp 2092-2101

17. Nicolet, M., "The Structure of the Upper Atmosphere", Research in Geophysics, 1964, H. Odishaw, ed., MIT Press pp 243-275

18. Norton, R. B., Van Zandt, T. E., and Danison, J. S., "A Model of the Atmosphere and Ionosphere in the E and F1 Regions", Proc. Int. Conf. on the Ionosphere, Inst. Phys., Phys. Soc., London, 1962

19. Potts, B. C., "Mean Ionospheric Scale Heights Deduced from Faraday Rotation Measurements", J. Geophys. Res., June 1, 1965, Vol. 70, No. 11, pp 2651-2663

20. Roger, R. S., "Measurements of Equivalent Slab Thickness of the Daytime Ionosphere", Journal of Atmospheric and Terrestrial Physics, 1964, Vol. 26, pp 475-497

21. Ross, W. J., "The Determination of Ionospheric Electron Content from Satellite Doppler Measurements: 1) Method of Analysis, 2) Experimental Results", J. Geophys. Res., Sept. 1960, Vol. 65, No. 9, p 2601

22. Ross, W. J., and Anderson, D. S., "Symposium on Electron Density Profiles in the Ionosphere and Exosphere, B. Maehlum, editor, 1962, Pergamon Press

23. Sagalyn, R. C. and Smiddy, M., and Bhargava, Y. N., "Satellite Measurements of the Diurnal Variation of the Electron Temperatures in the F Region", Space Res. V, 1965, North Holland Publishing Co., pp 189-206

24. Schmelovsky, K. H., and Cumme, G., "The Variations of Ionospheric Electron Content from Sunspot Maximum to Minimum as Measured at Kuhlengsborn", Space Res. V, 1965, North Holland Publ. Co., pp 702-703

25. Shirke, J. S., "A Comparison of Electron Density Profiles Over Ahmedabad in Years of Low and High Solar Activity", JATP 25, August 1963, No. 8, pp 429-440

26. Somayajulu, Y. V., Yyagi, T. R., and Bhatnagar, V. P., "Ionospheric Electron Content and its Variations From Faraday Fading of Satellite Radio Transmissions", Space Res. IV, 1963 Warsaw Proceedings, John Wiley and Sons, Inc., 1964, pp 498-507

27. Stubbe, P., "Temperature Variation at the F-Layer Maximum During a Sunspot Cycle", JATP, Nov. 1964, Vol. 26, No. 11, pp 1055-1068

28. Taylor, G. N., "The Electron Content of the Ionosphere at Middle Latitudes in Summer", Proc. Royal Soc., June 16, 1964, Vol. 279A pp 497-509

29. Titheridge, J. E., "The Refraction of Satellite Signals - I Theoretical Calculations", JATP, Feb. 1964, Vol. 26, No. 2, pp 159-175; see also "The Refraction of Satellite Signals - II Experimental Results", JATP, Feb. 1964, Vol. 26 No. 2, pp 177-191

30. Thomas, J. O., and Sader, A. Y., "Electron Density at the Alouette Orbit", J. Geophys. Res., Nov. 1, 1964, Vol. 69, No. 21, pp 4561-81

31. Wright, H. R., "The Quiet Ionosphere as it Relates to Precision Tracking at S-Band", Apollo Note 303, January 25, 1965

32. Wright, H. R., "A Simple Time Dependent World-Wide Ionospheric Refractive Index Model", Apollo Note 317, April 6, 1965

33. Wright, H. R., "Some Comments Concerning Equivalent Slab Thickness and Scale Height Interpretations in Relation to the Question of Thermal Equilibrium", Apollo Note 376, October 25, 1965

34. Wright, H. R., "Computational Procedure for Refractive Index Estimates Based on a Global Time Dependent Slab Model Ionosphere", Apollo Note 377, October 25, 1965

35. Wright, H. R., "Peak Ionization Level Height Anomalies", Apollo Note 378, October 27, 1965

36. Wright, J. W., "A Model of the F Region Above h max F-2", J. Geophys. Res., Jan. 1960, Vol. 65, pp 185-191

37. Wright, J. W., "Comment on Models of the Ionosphere Above h max F2", J. Geophys. Res., September 1960, Vol. 65, No. 9, pp 2595-2596

38. Wright, J. W., "Temperature Control of the Structure and Variations of the Quiet Ionosphere", Proc. Int. Conf. on the Ionosphere, London, 1962, pp 19-25, Chapman and Hall, Ltd., London, 1963

39. Wright, J. W., "Diurnal and Seasonal Changes in Structure of the Mid-latitude Quiet Ionosphere", NBS J. Res., May-June 1962, Vol. 66D, No. 3, pp 297-310

40. Yeh, K. C., and Swenson, Jr., G. W., "Ionospheric Electron Content and its Variations Deduced from Satellite Observations", J. Geophys. Res., April 1961, Vol. 66, No. 4, pp 1061-1067

APOLLO NOTE NO. 399
(Task 2, Item II)

E. Pugh
5 January 1966

ESTIMATES OF LINEAR REGRESSION PARAMETERS

INTRODUCTION

Assume that 2N values of a measurable, m_i, are taken at times $t_1, \ldots, t_{2N}$ respectively, where m_i may be written in the form:

$$m_i = a + bt_i + n_i, \quad i = 1, \ldots, 2N \tag{1}$$

The n_i are independent noise samples with zero mean and known variance σ_n^2. In this note we consider ways of estimating the parameters a and b and give a numerical comparison of the estimates.

LEAST SQUARES ESTIMATES

The least squares estimates a^* and b^* are the values of a and b which minimize the sum of squares:

$$Q = \sum_{i=1}^{2N} (m_i - a - bt_i)^2 \tag{2}$$

Thus:

$$\frac{\partial Q}{\partial a} = -2 \sum_{i=1}^{2N} (m_i - a^* - b^* t_i) = 0 \tag{3}$$

$$\frac{\partial Q}{\partial b} = -2 \sum_{i=1}^{2N} (m_i - a^* - b^* t_i)\, t_i = 0 \tag{4}$$

Solving (3) and (4) for a^* and b^* gives:

$$a^* = \bar{m} - b^* \bar{t} \tag{5}$$

$$b^* = \frac{\sum_{i=1}^{2N} (m_i - \bar{m})(t_i - \bar{t})}{\sum_{i=1}^{2N} (t_i - \bar{t})^2} \tag{6}$$

where:

$$\bar{m} = \frac{1}{2N} \sum_{i=1}^{2N} m_i, \quad \bar{t} = \frac{1}{2N} \sum_{i=1}^{2N} t_i \tag{7}$$

Substituting $m_i = a + bt_i + n_i$, $\bar{m} = a + b\bar{t} + \bar{n}$ gives:

$$b^* = b + \frac{\sum_{i=1}^{2N} n_i (t_i - \bar{t})}{\sum_{i=1}^{2N} (t_i - \bar{t})^2} \tag{8}$$

$$a^* = a + \bar{n} - \frac{\bar{t} \sum_{i=1}^{2N} (t_i - \bar{t}) n_i}{\sum_{i=1}^{2N} (t_i - \bar{t})^2} \tag{9}$$

so that both a^* and b^* are unbiased. The variance may therefore be

found as:

$$\text{Var } b^* = E\left\{ \frac{\sum_{i=1}^{2N} n_i (t_i - \bar{t})}{\sum_{i=1}^{2N} (t_i - \bar{t})^2} \right\}^2 = \frac{\sigma_n^2}{\sum_{i=1}^{2N} (t_i - \bar{t})^2} \tag{10}$$

$$\text{Var } a^* = E\left\{ \bar{n} - \frac{\bar{t} \sum_{i=1}^{2N} (t_i - \bar{t})\, n_i}{\sum_{i=1}^{2N} (t_i - \bar{t})^2} \right\}^2$$

$$= E\left\{ \sum_{i=1}^{2N} \left[\frac{1}{2N} - \frac{\bar{t}\,(t_i - \bar{t})}{\sum_{i=1}^{2N} (t_i - \bar{t})^2} \right] n_i \right\}^2 \tag{11}$$

$$= \frac{\sigma_n^2 \sum_{i=1}^{2N} t_i^2}{2N \sum_{i=1}^{2N} (t_i - \bar{t})^2}$$

Also:

$$\text{Cov}(a^*, b^*) = -\frac{\sigma_n^2\, \bar{t}}{\sum_{i=1}^{2N} (t_i - \bar{t})^2} \tag{12}$$

"AVERAGE" ESTIMATES

The "average" estimates $\hat{a}$ and $\hat{b}$ are the solutions to:

$$\overline{m}_1 = \hat{a} + \hat{b}\,\overline{t}_1 \tag{13}$$

$$\overline{m}_2 = \hat{a} + \hat{b}\,\overline{t}_2 \tag{14}$$

where:

$$\overline{m}_1 = \frac{1}{N} \sum_{i=1}^{N} m_i\,, \quad \overline{m}_2 = \frac{1}{N} \sum_{i=N+1}^{2N} m_i \tag{15}$$

$$\overline{t}_1 = \frac{1}{N} \sum_{i=1}^{N} t_i, \quad \overline{t}_2 = \frac{1}{N} \sum_{i=N+1}^{2N} t_i \tag{16}$$

Thus:

$$\hat{b} = \frac{\overline{m}_2 - \overline{m}_1}{\overline{t}_2 - \overline{t}_1} \tag{17}$$

$$\hat{a} = \overline{m}_1 - \left(\frac{\overline{m}_2 - \overline{m}_1}{\overline{t}_2 - \overline{t}_1}\right) \overline{t}_1 \tag{18}$$

Substituting $\overline{m}_1 = a + b\,\overline{t}_1 + \overline{n}_1$, $\overline{m}_2 = a + b\,\overline{t}_2 + \overline{n}_2$, we have:

$$\hat{b} = b + \frac{\overline{n}_1 - \overline{n}_2}{\overline{t}_1 - \overline{t}_2} \tag{19}$$

$$\hat{a} = a + \left(\frac{\overline{t}_1}{\overline{t}_1 - \overline{t}_2}\right) \overline{n}_2 - \left(\frac{\overline{t}_2}{\overline{t}_1 - \overline{t}_2}\right) \overline{n}_1 \tag{20}$$

Thus $\hat{a}$ and $\hat{b}$ are unbiased and:

$$\text{Var } \hat{b} = E\left[\frac{\bar{n}_1 - \bar{n}_2}{\bar{t}_1 - \bar{t}_2}\right]^2 = \frac{2\sigma_n^2}{N(\bar{t}_1 - \bar{t}_2)^2} \tag{21}$$

$$\text{Var } \hat{a} = E\left[\left(\frac{\bar{t}_1}{\bar{t}_1 - \bar{t}_2}\right)\bar{n}_2 - \left(\frac{\bar{t}_2}{\bar{t}_1 - \bar{t}_2}\right)\bar{n}_1\right]^2 \tag{22}$$

$$= \left[\frac{\bar{t}_1^2 + \bar{t}_2^2}{(\bar{t}_1 - \bar{t}_2)^2}\right] \frac{\sigma_n^2}{N}$$

$$\text{Cov}(\hat{a}, \hat{b}) = E\left[\left(\frac{\bar{t}_1}{\bar{t}_1 - \bar{t}_2}\right)\bar{n}_2 - \left(\frac{\bar{t}_2}{\bar{t}_1 - \bar{t}_2}\right)\bar{n}_1\right]\left[\left(\frac{\bar{n}_1}{\bar{t}_1 - \bar{t}_2}\right) - \left(\frac{\bar{n}_2}{\bar{t}_1 - \bar{t}_2}\right)\right] \tag{23}$$

$$= -\frac{(\bar{t}_1 + \bar{t}_2)}{(\bar{t}_1 - \bar{t}_2)^2} \quad \frac{\sigma_n^2}{N}$$

END POINT ESTIMATES

The end point estimates are defined as:

$$\tilde{a} = m_1 \tag{24}$$

$$\tilde{b} = \left(\frac{m_{2N} - m_1}{t_{2N} - t_1}\right) \tag{25}$$

If we set $t_1 = 0$ then:

$$E\tilde{a} = E\left[a + bt_1 + n_1 \right] = a \tag{26}$$

$$\text{Var } \tilde{a} = \sigma_n^2 \tag{27}$$

$$\tilde{b} = b + \frac{n_{2N} - n_1}{t_{2N} - t_1} \tag{28}$$

$$E\tilde{b} = b \tag{29}$$

$$\text{Var } \tilde{b} = E\left[\frac{n_{2N} - n_1}{t_{2N} - t_1} \right]^2 = \frac{2\sigma_n^2}{(t_{2N} - t_1)^2} \tag{30}$$

NUMERICAL COMPARISON

To obtain a numerical comparison of the variances of these unbiased estimates of a and b, we set $t_i = (i-1)$, $i = 1, \ldots, 2N$. This gives:

$$\bar{t}_1 = \frac{1}{N} \sum_{j=o}^{N-1} j = (N-1)/2 \tag{31}$$

$$\bar{t}_2 = \frac{1}{N} \sum_{j=N}^{2N-1} j = (2N-1) - (N-1)/2 \tag{32}$$

$$\bar{t} = \frac{1}{2N} \sum_{j=o}^{2N-1} j = N - 1/2 \tag{33}$$

The variance ratios of the estimates reduce to:

$$\text{Var } a^*/\sigma_n^2 = \frac{\sum_{i=1}^{2N} t_i^2}{2N \sum_{i=1}^{2N} (t_i - \bar{t})^2} = \frac{\sum_{j=0}^{2N-1} j^2}{2N \sum_{j=0}^{2N-1} (j - \bar{t})^2} \tag{34}$$

$$= \frac{4 - (1/N)}{2N+1}$$

$$\text{Var } \hat{a}/\sigma_n^2 = \frac{1}{N} \left[\frac{\bar{t}_1^2 + \bar{t}_2^2}{(\bar{t}_1 - \bar{t}_2)^2} \right] \tag{35}$$

$$= \frac{(N-1)^2 + (3N-1)^2}{4N^3}$$

$$\text{Var } \tilde{a}/\sigma_n^2 = 1 \tag{36}$$

$$\text{Var } b^*/\sigma_n^2 = \frac{1}{\sum_{i=1}^{2N} (t_i - \bar{t})^2} = \frac{1}{\sum_{j=0}^{2N-1} (j - \bar{t})^2} \tag{37}$$

$$= \frac{6}{4N^3 - N}$$

$$\text{Var } \hat{b}/\sigma_n^2 = \frac{2}{N(\bar{t}_1 - \bar{t}_2)^2} = \frac{2}{N^3} \tag{38}$$

$$\text{Var } \tilde{b}/\sigma_n^2 = \frac{2}{(t_{2N} - t_1)^2} = \frac{2}{(2N-1)^2} \tag{39}$$

The graphical comparison of these variance ratios is given in Figure 1.

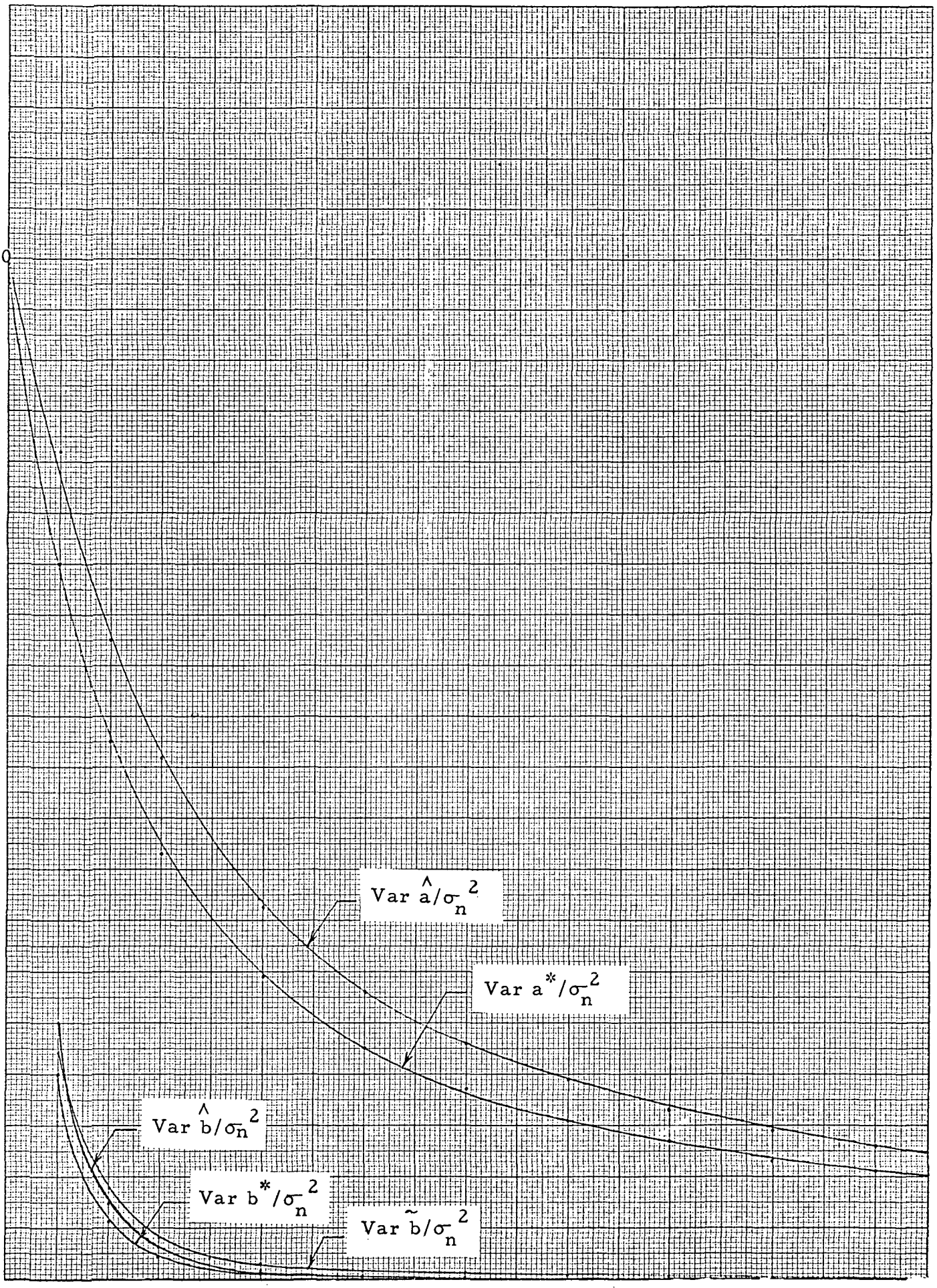

Figure 1.

10 X 10 TO THE CENTIMETER 46 1510
18 X 25 CM. MADE IN U.S.A.
KEUFFEL & ESSER CO.

The Bissett-Berman Corporation 2941 Nebraska Avenue, Santa Monica, California EXbrook 4-3270

APOLLO NOTE NO. 400
Task II, Item II

H. Engel
10 January 1966

MODIFICATION TO OEA PROGRAM TO SIMULATE EFFECTS OF REAL TIME ORBIT DATA PROCESSING SCHEME

We use quantities with bars (- or =) over them to denote the estimates that the Real Time Orbit Determination Program (RTODP) is thought to be calculating. We use quantities with carets ($\wedge$ or $\hat{\hat{}}$) to denote the estimates the RTODP is actually calculating. There is a difference between the estimates the RTODP is thought to be calculating and the estimates it is actually calculating for several reasons. These include the RTODP assumption that the only biases are biases on the measurables, and the assumption that the errors resulting from errors in the dynamic biases are uncorrelated from batch to batch.

We begin with our interpretation of the procedure to be followed in the RTODP. We let $\bar{x}_p(i)$ be the estimate of the state vector at the time of the end of the ith batch of data based on all data obtained up to the end of the i-1st batch. We break $\bar{x}_p(i)$ into two parts

$$\bar{x}_p(i) = \begin{bmatrix} \bar{\bar{x}}_p(i) \\ 0 \end{bmatrix}$$

$\bar{\bar{x}}_p(i)$ being the estimate of the three components of position and three components of velocity, and o being the new a priori estimates of the biases on the measurables in the ith batch of data. When we have completed the algorithm for one iteration it will be seen how $\bar{\bar{x}}_p(i)$ is obtained. We have

$$\operatorname{cov} \bar{x}_p(i) = \begin{bmatrix} \operatorname{cov} \bar{\bar{x}}_p(i) & 0 \\ 0 & B(i) \end{bmatrix}$$

in which $\operatorname{cov} \bar{\bar{x}}_p(i)$ is obtained by the algorithm we are outlining and

B(i), the a priori covariance of the measurement biases in the ith batch, is an arbitrarily determined input. The form of $\bar{x}_p(i)$ and of cov $\bar{x}_p(i)$ are according to assumptions made in the RTODP.

The data obtained in the ith batch of measurements results in an estimate $\hat{x}_q(i)$ of the state vector at the end of the ith batch. Letting $G_{11}(i)$, $G_{12}(i)$ and $G_{1\mu}(i)$ be the matrices with elements

$$G_{11,jk}(i) = \sum_{\ell=1}^{N_i} \frac{1}{\sigma_\ell^2} \frac{\partial M_\ell}{\partial x_j(i)} \frac{\partial M_\ell}{\partial x_k(i)}$$

$$G_{12,jk}(i) = \sum_{\ell=1}^{N_i} \frac{1}{\sigma_\ell^2} \frac{\partial M_\ell}{\partial x_j(i)} \frac{\partial M_\ell}{\partial b_k}$$

$$G_{1\mu,j}(i) = \sum_{\ell=1}^{N_i} \frac{1}{\sigma_\ell^2} \frac{\partial M_\ell}{\partial x_j(i)} \frac{\partial M_\ell}{\partial \mu}$$

where M_ℓ is the ℓth measurement in the ith batch and σ_ℓ^2 is its variance. We have

$$\bar{x}_q(i) = G_{11}^{-1}(i)\, e_1(i) - G_{11}^{-1}(i)\, G_{1\mu}(i) \Delta\hat{\mu}$$

in which b is the vector of non-estimated parameters, of which μ is one, $\Delta\hat{\mu}$ is the a priori error in the estimate of μ and $e_1(i)$ is the vector with elements

$$e_{1,j}(i) = \sum_{\ell=1}^{N_i} \frac{1}{\sigma_\ell^2} \frac{\partial M_\ell}{\partial x_j(i)} n_\ell(i)$$

where $n_\ell(i)$ is the zero mean random noise on the measurement M_ℓ.

The RTODP obtains its "best estimate" * of x(i) as a weighted sum of $\bar{x}_p(i)$ and $\bar{x}_q(i)$

$$\bar{x}(i) = W_p(i)\,\bar{x}_p(i) + W_q(i)\,\bar{x}_q(i)$$

in which

$$W_p(i) = W^{-1}(i)\ \ \mathrm{cov}^{-1}\bar{x}_p(i)$$

$$W_q(i) = W^{-1}(i)\ G_{11}(i)$$

and

$$W(i) = G_{11}(i) + \ \mathrm{cov}^{-1}\bar{x}_p(i)$$

The expected values of $\bar{x}_p(i)$, $\bar{x}_q(i)$ and $\bar{x}(i)$ are all zero, so

$$E\left[\bar{x}(i)\bar{x}^T(i)\right] = W_p(i)\ \mathrm{cov}\,\bar{x}_p(i)\,W_p^T(i) + W_q(i)\,E\left[\bar{x}_q(i)\bar{x}_q^T(i)\right]W_q^T(i)$$
$$+\left\{W_p(i)\,E\left[\bar{x}_p(i)\bar{x}_q^T(i)\right]W_q^T(i)\right\} + \left\{W_p(i)\,E\left[\bar{x}_p(i)\bar{x}_q^T(i)\right]W_q^T(i)\right\}^T$$

The RTODP assumes, contrary to fact, that $E\left[\bar{x}_p(i)\,\bar{x}_q^T(i)\right]$ is zero, so it finds

$$\mathrm{cov}\,\bar{x}(i) = E\left[\bar{x}(i)\,\bar{x}^T(i)\right]$$
$$= W_p(i)\ \mathrm{cov}\,\bar{x}_p(i)\,W_p^T(i)$$
$$+ W_q(i)\left\{G_{11}^{-1}(i)G_{11}(i)G_{11}^{-1}(i) + \left(G_{11}^{-1}(i)G_{1\mu}(i)\right)\mathrm{cov}\,\Delta\mu\left(G_{11}^{-1}(i)G_{1\mu}(i)\right)^T\right\}W_q^T(i)$$

---

* "Formulas for Apollo Bayes D. C. Program" MSC Internal Note 65-FM4-214, Nov. 15, 1965, Laurel A. Phillips

By substitution, then,

$$\text{cov}\ \bar{x}(i) = \left[W^{-1}(i)\ \text{cov}^{-1}\bar{x}_p(i)\right]\ \text{cov}\ \bar{x}_p(i)\left[\ \text{cov}^{-1}\bar{x}_p(i)\,W^{-1}(i)\right]$$

$$+\left[W^{-1}(i)G_{11}(i)\right]\left\{G_{11}^{-1}(i) + G_{11}^{-1}(i)G_{1\mu}(i)\ \text{cov}\,\hat{\Delta\mu}\,G_{1\mu}^{T}(i)G_{11}^{-1}(i)\right\}\left[G_{11}(i)W^{-1}(i)\right]$$

$$= W^{-1}(i)\ \text{cov}^{-1}\bar{x}_p(i)W^{-1}(i)+W^{-1}(i)G_{11}(i)W^{-1}(i)$$

$$+W^{-1}(i)G_{1\mu}(i)\,\text{cov}\,\hat{\Delta\mu}G_{1\mu}^{T}(i)W^{-1}(i)$$

$$= W^{-1}(i) +\left[W^{-1}(i)G_{1\mu}(i)\right]\ \text{cov}\ \hat{\Delta\mu}\left[W^{-1}(i)\,G_{1\mu}(i)\right]^{T}$$

Now, $\bar{\bar{x}}(i)$ is the first six elements of $\bar{x}(i)$, corresponding to *the three components of position and the three components of velocity.* The covariance of $\bar{\bar{x}}(i)$ is the upper left 6 x 6 submatrix of $\text{cov}\ \bar{x}(i)$. The RTODP obtains $\bar{\bar{x}}_p(i+1)$ by projecting ahead $\bar{\bar{x}}(i)$ with a Q matrix. We let $Q_{oo}(i+1/i)$ be the matrix of partial derivatives of position and velocity at the time of the end of the i+1st batch with respect to position and velocity at the time of the end of the ith batch. We also let $Q_{o\mu}(i+1/i)$ be the partial derivatives of position and velocity at the time of the end of the i+1st batch with respect to the dynamic biases at the time of the end of the ith batch. In the RTODP, $\bar{\bar{x}}_p(i+1)$ is computed as

$$\bar{\bar{x}}_p(i+1) = Q_{oo}\ (i+1/i)\ \bar{\bar{x}}(i)$$

but it is recognized that the uncertainty in the dynamic biases will increase the covariance of $\bar{\bar{x}}(i)$, for actually

$$\begin{bmatrix}\bar{\bar{x}}_p(i+1)\\ \hat{\Delta\mu}\end{bmatrix} = \begin{bmatrix}Q_{oo}(i+1/i) & Q_{o\mu}(i+1/i)\\ 0 & I\end{bmatrix}\begin{bmatrix}\bar{\bar{x}}(i)\\ \hat{\Delta\mu}\end{bmatrix}$$

leading to

$$\text{cov}\ \bar{\bar{x}}_p(i+1) = \text{upper left } 6 \times 6 \text{ of cov} \left\{ \begin{bmatrix} \bar{\bar{x}}_p(i+1) \\ \mu \end{bmatrix} \right\}$$

$$= Q_{oo}(i+1/i)\ \text{cov}\ \bar{\bar{x}}(i) Q_{oo}^T(i+1/i) + Q_{o\mu}(i+1/i)\ \text{cov}\,\Delta\hat{\mu}\, Q_{o\mu}^T\ (i+1/i)$$

$$+ \left[Q_{oo}(i+1/i)\ \ E\left[\bar{\bar{x}}(i)\,\Delta\hat{\mu}^T\right]\ Q_{o\mu}^T\ (i+1/i) \right]$$

$$+ \left[Q_{oo}(i+1/i)\cdot E\left[\bar{\bar{x}}(i)\,\Delta\hat{\mu}^T\right]\ Q_{o\mu}^T\ (i+1/i) \right]^T$$

where $E\left[\bar{\bar{x}}(i)\,\Delta\hat{\mu}^T\right]$ is the first six rows of $E\left[\bar{x}(i)\,\Delta\hat{\mu}^T\right]$. Now,

$$E\left[\bar{x}(i)\,\Delta\hat{\mu}^T\right] = W_p(i)\ E\left[\bar{x}_p(i)\Delta\hat{\mu}^T\right] + W_q(i)\ E\left[\bar{x}_q(i)\Delta\hat{\mu}^T\right]$$

but in the RTODP it is assumed that $E\left[\bar{x}_p(i)\Delta\hat{\mu}^T\right]$ is zero, so

$$E\left[\bar{x}(i)\Delta\hat{\mu}^T\right] = W^{-1}(i)G_{11}(i)\ E\left[\bar{x}_q(i)\Delta\hat{\mu}^T\right]$$

$$= W^{-1}(i)G_{11}(i)\left\{ -G_{11}^{-1}(i)\,G_{1\mu}(i)\ \ \text{cov}\,\Delta\hat{\mu} \right\}$$

$$= -W^{-1}(i)\,G_{1\mu}(i)\ \ \text{cov}\,\Delta\hat{\mu}$$

In order to determine the actual covariances of the estimates, we trace this process through again, starting with

$$\hat{x}_p(i) = \begin{bmatrix} \hat{\bar{x}}_p(i) \\ 0 \end{bmatrix}$$

and

$$\text{cov}\ \hat{x}_p(i) = \begin{bmatrix} \text{cov}\ \hat{\bar{x}}_p(i) & 0 \\ 0 & B(i) \end{bmatrix}$$

Then

$$\hat{x}(i) = W_p(i)\,\hat{x}_p(i) + W_q(i)\,\hat{x}_q(i)$$

The expected values of $\hat{x}_p(i)$, $\hat{x}_q(i)$ and $\hat{x}(i)$ are all zero, so the covariance of $\hat{x}(i)$ is

$$\begin{aligned}\text{cov}\,\hat{x}(i) &= E\left[\hat{x}(i)\hat{x}^T(i)\right] \\ &= W_p(i)\ \text{cov}\,\hat{x}_p(i)\,W_p^T(i) + W_q(i)\ \text{cov}\,\hat{x}_q(i)\,W_q^T(i) \\ &= \left\{W_p(i)\ E\left[\hat{x}_p(i)\hat{x}_q^T(i)\right] W_q^T(i)\right\} + \left\{W_p(i)\ E\left[\hat{x}_p(i)\hat{x}_q^T(i)\right] W_q^T(i)\right\}^T\end{aligned}$$

Now we have that

$$\hat{x}_q(i) = G_{11}^{-1}(i)\,e_1(i) - G_{11}^{-1}(i)\,G_{12}(i)\Delta\hat{b}$$

so

$$\text{cov}\,\hat{x}_q(i) = G_{11}^{-1}(i) + \left[G_{11}^{-1}(i)\,G_{12}(i)\right]\ \text{cov}\,\Delta\hat{b}\left[G_{11}^{-1}(i)\,G_{12}(i)\right]$$

Also, we have that

$$\hat{x}_p(i) = \begin{bmatrix}\hat{\hat{x}}_p(i) \\ 0\end{bmatrix}$$

$$\text{cov}\,\hat{x}_p(i) = \begin{bmatrix}\text{cov}\,\hat{\hat{x}}_p(i) & 0 \\ 0 & B(i)\end{bmatrix}$$

and

$$E\left[\hat{x}_p(i)\hat{x}_q^T(i)\right] = E\left\{\begin{bmatrix}\hat{\hat{x}}_p(i) \\ 0\end{bmatrix}\left[G_{11}^{-1}(i)\,e_1(i) - G_{11}^{-1}(i)G_{12}(i)\Delta\hat{b}\right]^T\right\}$$

$$= \begin{bmatrix}-E\left[\hat{\hat{x}}_p(i)\,\Delta\hat{b}^T\right]G_{12}^T(i)G_{11}^{-1}(i) \\ 0\end{bmatrix}$$

We shall leave evaluation of $E\left[\hat{\hat{x}}_p(i)\Delta\hat{b}^T\right]$ until a little later. Now $\hat{\hat{x}}(i)$ is the first six elements of $\hat{x}(i)$. Then

$$\begin{bmatrix} \hat{\hat{x}}_p(i+1) \\ \Delta\hat{\mu} \end{bmatrix} = \begin{bmatrix} Q_{11}(i+1/i) & Q_{o\mu}(i+1/i) \\ 0 & I \end{bmatrix} \begin{bmatrix} \hat{\hat{x}}(i) \\ \Delta\hat{\mu} \end{bmatrix}$$

so

$$\text{cov}\ \hat{\hat{x}}_p(i+1) = Q_{oo}(i+1/i)\ \text{cov}\ \hat{\hat{x}}(i)\, Q_{oo}^T(i+1/i) + Q_{o\mu}(i+1/i)\ \text{cov}\ \Delta\hat{\mu}\, Q_{o\mu}^T(i+1/i)$$
$$+ \left[Q_{oo}(i+1/i)\ E\left[\hat{\hat{x}}(i)\Delta\hat{\mu}^T\right] Q_{o\mu}^T(i+1/i)\right]$$
$$+ \left[Q_{oo}(i+1/i)\ E\left[\hat{\hat{x}}(i)\Delta\hat{\mu}^T\right] Q_{o\mu}^T(i+1/i)\right]^T$$

in which cov $\hat{\hat{x}}(i)$ is the upper left 6 x 6 submatrix of cov $\hat{x}(i)$, and

$$E\left[\hat{\hat{x}}_p(i)\,\Delta\hat{b}^T\right] = Q_{oo}(i+1/i)\,E\left[\hat{\hat{x}}(i)\Delta\hat{b}^T\right] + Q_{o\mu}(i+1/i)\,E\left[\Delta\hat{\mu}\,\Delta\hat{b}^T\right]$$

In turn, we have that $E\left[\hat{\hat{x}}(i)\Delta\hat{b}^T\right]$ is the first six rows of $E\left[\hat{x}(i)\Delta\hat{b}^T\right]$ and $E\left[\hat{\hat{x}}(i)\Delta\hat{\mu}^T\right]$ is one column of $E\left[\hat{\hat{x}}(i)\Delta\hat{b}^T\right]$. Now

$$E\left[\hat{x}(i)\,\Delta\hat{b}^T\right] = W_p(i)E\left[\hat{x}_p(i)\,\Delta\hat{b}^T\right] + W_q(i)\,E\left[\hat{x}_q(i\ \Delta\hat{b}^T\right]$$

where

$$E\left[\hat{x}_p(i+1)\Delta\hat{b}^T\right] = \begin{bmatrix} E\left[\hat{\hat{x}}_p(i)\Delta\hat{b}^T\right] \\ 0 \end{bmatrix}$$

and

$$E\left[\hat{x}_p(i+1)\,\Delta\hat{b}^T\right] = -\,G_{11}^{-1}(i)G_{12}(i)\ \text{cov}\ \Delta\hat{b}$$

The quantities $G_{11}(i)$, $G_{12}(i)$, $G_{1\mu}(i)$, $Q_{oo}(i+1/i)$ and $Q_{o\mu}(i+1/i)$ are not directly available from the Bissett-Berman OEA Program. Instead, the quantities C(i) and Q(i) are available, where

$$C_{j,k}(i) = \sum_{\ell=1}^{N_i} \frac{1}{\sigma_\ell^2} \frac{\partial M_\ell}{\partial a_j} \frac{\partial M_\ell}{\partial a_k}$$

The measurements being those of the ith batch, and Q(i) is the matrix of partial derivatives of position, velocity and all nuisance parameters at the time of the end of the ith batch with respect to similar quantities at the (fixed) time at which the orbit parameters are specified in the OEA Program. Then $G_{11}(i)$, $G_{12}(i)$ and $G_{1\mu}(i)$ are all submatrices of the matrix G(i)

$$G(i) = Q^{-T}(i)\, C(i)\, Q^{-1}(i)$$

and $Q_{oo}(i+1/i)$ and $Q_{o\mu}(i+1/i)$ are submatrices of the matrix Q(i+1/i)

$$Q(i+1/i) = Q(i+1)\, Q^{-1}(i)$$

The Bissett-Berman Corporation 2941 Nebraska Avenue, Santa Monica, California EXbrook 4-3270

APOLLO NOTE NO. 401
(Task II, Item II)

J. W. Childress, III
2 February 1966

CHECKOUT OF THE PRINCIPAL AXIS DETERMINATION PROGRAM

INTRODUCTION

Part B of the OEAP now includes a principal axis routine that finds the principal axes of the position and velocity covaraiance ellipsoids and the Euler angles that describe the orientation of these principle axes with respect to the coordinate system in which the covariance matrix is given. This routine is described in Apollo Notes 328 and 367. The present note describes the checkout of this routine.

CHECKOUT PROCEDURE

The eigenvalues of the position or velocity covariance submatrix are determined in two ways. In the first, they are found as part of the calculations necessary to determine the Euler angles referred to above. In the second, they are computed using the derived Euler angles. If the eigenvalues determined in these two ways differ by more than some pre-assigned amount, then an error message is printed instead of the principal axis values.

In this checkout, the eigenvalues found by the two methods have been compared, using several examples, one of which is reported here.

ACTUAL TEST CASE

The position covariance submatrix for one test case is:

512,154	-61,591.3	160,623
-61,591.3	255,684	79,415.3
160,623	79,415.3	93,056.3

Denoting the element in the ith row and jth column of this matrix by V_{ij}, the equation for the eigenvalues is:

$$\lambda^3 + B_2\lambda^2 + B_1\lambda + B_o = \begin{vmatrix} V_{11}-\lambda & V_{12} & V_{13} \\ V_{21} & V_{22}-\lambda & V_{23} \\ V_{31} & V_{32} & V_{33}-\lambda \end{vmatrix} = 0$$

The computed values of B corresponding to the position matrix above are

$$B_2 = -1186110 \ , \quad B_1 = 325101 \ , \quad B_o = -1202.96$$

This equation is solved in the computer using the subroutine cubic which solves cubic monic polynomial equations. The eigenvalues are:

$$\lambda_1 = 570,252 \ , \quad \lambda_2 = 287,995 \ , \quad \lambda_3 = 2,647.14$$

The direction cosines that are computed next are:

0.947414	-0.109597	0.300658
0.0100162	-0.928910	-0.370171
0.319854	0.353717	-0.878964

The corresponding Euler angles are found to be:

$$\phi = -42.1220^\circ \ , \quad x = -151.518^\circ \ , \quad \psi = -39.0840^\circ$$

As a first check, the direction cosines computed from these angles are found to be:

0.947414	-0.109597	0.300658
0.0100162	-0.928910	-0.370171
0.319854	0.353717	-0.878964

and agrees in all figures printed to the previous matrix of direction cosines.

Next, the Euler angles are used to compute a rotated covariance matrix that should be the covariance matrix related to the principal axis directions. Its main diagonal elements should be λ_1 , λ_2 and λ_3, and its off-diagonal elements should be zero. We find

570, 252.	-0.0029	0.12
-0.0022	287, 995.	0.052
0.12	0.052	2647.13

It is found that the off-diagonal elements are very small compared to the diagonal elements and that the e diagonal elements agree to within five significant figures with the eigenvalues computed via the cubic subroutine.

Similar computations starting with the velocity covariance submatrix

17.2466	-1.83399	5.23217
-1.83399	7.98074	2.44806
5.23217	2.44806	2.85387

leads to the coefficients

$$B_2 = -0.200927 \ , \ B_1 = 10.02541 \ , \ B_o = 6.76183$$

the eigenvalues

$$\lambda_1 = 19.0396 \ , \quad \lambda_2 = 8.95718 \ , \quad \lambda_3 = 0.0843851$$

the direction cosines

0.951437	-0.0928091	0.293522
0.0193403	-0.933568	-0.357877
0.307237	0.346174	-0.886436

and the Euler angles

$$\phi = -41.5891^{\circ} \ , \quad x = -152.429^{\circ} \ , \quad \psi = -39.3577^{\circ}$$

The corresponding direction cosines matrix computed from ϕ, x, and ψ is:

0.951437	-0.0928091	0.293522
0.0193403	-0.933568	-0.357877
0.307237	0.346174	-0.886436

and the covariance matrix rotated by the angles ϕ, x, and ψ is:

19.0396	-0.0000008	-0.0000031
-0.0000009	8.95718	0.0000027
-0.0000031	0.0000027	0.0843846

This test procedure was applied to several cases, and good agreement was found in all cases.

The Bissett-Berman Corporation 2941 Nebraska Avenue, Santa Monica, California EXbrook 4-3270

APOLLO NOTE NO. 402
(Task II, Item II)

L. Lustick
21 January 1966

METHOD FOR EVALUATING EFFECT OF RANDOM NOISE COMPONENTS ON ERRORS IN ESTIMATED ORBIT PARAMETERS

PURPOSE

The purpose of this note is to describe the procedure for evaluating the uncertainty in the estimated orbit parameters for a realistic model for the noise sources in all the MSFN measurables.

INTRODUCTION

Given a filter for the estimated orbit parameters, previous error analyses have neglected any self-correlation and cross-correlation that may exist in the actual MSFN measurables. This note describes both a procedure for taking this into account as well as how the correlation functions of the errors in the measurables can be generated.

METHOD

Appendix A generates a general expression for the noise in the estimated parameters for a specified filter given any arbitrary self-correlation and cross-correlation noise matrix of the measurables.

The purpose of the remainder of this note is to indicate how any term in the noise correlation matrix can be generated consistent with our most current knowledge of MSFN noise sources.

GENERIC GENERATION OF NOISE MATRIX ELEMENTS

In this report, we will restrict ourselves to tracking in range-rate mode using a master and two slaves. The transit time will be assumed constant. This is the approximate situation for tracking a vehicle orbiting the Moon. The results generated, however, can be

generalized to other tracking situations. A non-destruct mode is assumed.

For the problem outlined, the following components of the noise matrix are required:

1. Self-correlation in Master.
2. Self-correlation in Slave.
3. Cross-correlation between Master and Slave.
4. Cross-correlation between Slaves.

Let

$\eta(t)$ = rate noise (due to clock)

$N(t)$ = range noise (quantization and equipment)

s = transit time

T = sampling interval

1. Self-Correlation in Master

$$\Delta\dot{R}_m(i) = \frac{1}{2T}\left\{\int_o^{(i+1)T}\left[\eta(t+s) - \eta(t)\right]dt - \int_o^{iT}\left[\eta(t+s) - \eta(t)\right]dt + (N_{i+1} - N_i)\right\}$$

since

$$\overline{\eta N} = 0$$

we can treat these two noise sources separately. Let us first concern ourself with the rate noise, η.

$$\Delta\dot{R}_m(i) = \frac{1}{2T}\int_{iT}^{(i+1)T}\left[\eta(t+s) - \eta(t)\right]\,dt$$

let

$$t_1 = t - iT$$

$$\Delta\dot{R}_m(i) = \frac{1}{2T}\int_{o}^{T}\left[\eta(t_1+iT+s) - \eta(t_1+iT)\right]\,dt_1$$

$$\Delta\dot{R}_m(j) = \frac{1}{2T}\int_{o}^{T}\left[\eta(t_2+jT+s) - \eta(t_2+jT)\right]\,dt_2$$

$$\overline{\Delta\dot{R}_m(i)\ \Delta\dot{R}_m(j)} = \frac{1}{4T^2}\left\{\int_o^T\int_o^T \overline{\eta(t_1+iT+s)\ \eta(t_2+jT+s)}\right.$$

$$- \overline{\eta(t_1+iT+s)\ \eta(t_2+jT)}$$

$$- \overline{\eta(t_1+iT)\ \eta(t_2+jT+s)}$$

$$\left. + \overline{\eta(t_1+iT)\ \eta(t_2+jT)}\quad dt_1\,dt_2\right\}$$

let

$$R_\eta = \overline{\eta(t)\ \eta(t+\tau)}$$

$$\overline{\Delta\dot{R}_m(i)\ \Delta\dot{R}_m(j)} = \frac{1}{4T^2}\int_o^T\int_o^T 2R_\eta\left[(t_1-t_2)+(i-j)\,T\right] - R_\eta\left[(t_1-t_2)+(i-j)\,T+s\right]$$

$$- R_\eta\left[(t_1-t_2)+(i-j)\,T-s\right]\,dt_1\,dt_2$$

let

$$u = (t_1 - t_2)$$

$$v = t_2$$

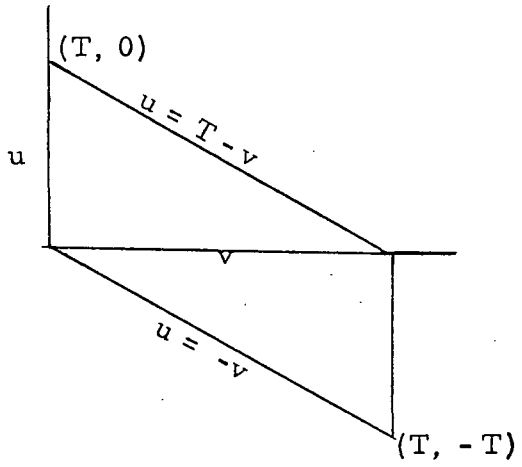

The preceding integral can be rewritten as

$$\frac{1}{4T^2}\left\{\int_{-T}^{o} du \int_{-\mu}^{T} 2\,R_\eta\left[u+(i-j)\,T\right] - R_\eta\left[u+(i-j)\,T+s\right]\right.$$

$$- R_\eta\left[u+(i-j)\,T-s\right]\,dv$$

$$+ \int_{o}^{T} du \int_{o}^{T-u} 2\,R_\eta\left[u+(i-j)\,T\right] - R_\eta\left[u+(i-j)\,T+s\right]$$

$$\left. - R_\eta\left[u+(i-j)\,T-s\right]\,dv\right\}$$

We can now perform integration with respect to v giving after simplification

$$\Delta\dot{R}_m(i)\ \dot{R}_m(j) = \frac{1}{4T^2}\int_0^T (T-w)\left\{2\left[R_\eta\left|w-(i-j)T\right| + R_\eta\left|w+(i-j)T\right|\right]\right.$$

$$- R_\eta\left|w-(i-j)T+s\right| - R_\eta\left|w+(i-j)T+s\right|$$

$$\left. - R_\eta\left|w-(i-j)T-s\right| - R_\eta\left|w+(i-j)T-s\right|\right\} dw$$

Now suppose $s > T$ as it would be during rendezvous where T = 1 sec and s = 2 + seconds. Since all terms are symmetric in i and j, we set

$$i \geqslant j$$

and let

$$R_\eta = K\,\delta(o)$$

For this case,

$w + (i-j)T + s$ is not greater than or equal to zero or less than or equal to T

$w - (i-j)T - s$ is not greater than or equal to zero or less than or equal to T

$$\therefore\ \overline{\Delta\dot{R}_m(i)\,\Delta\dot{R}_m(j)} = \frac{1}{4T^2}\int_0^T (T-w)\left\{2\left[R_\eta\left|w-(i-j)T\right| + R_\eta\left|w+(i-j)T\right|\right]\right.$$

$$- R_\eta\left|w-(i-j)T+s\right|$$

$$\left. - R_\eta\left|w+(i-j)T-s\right|\right\} dw$$

for $i = j$

$$\overline{\Delta\dot{R}_m(i)\,\Delta\dot{R}_m(j)} = \frac{K}{2T}$$

for $i > j$

$$\Delta\dot{R}_m(i)\,\Delta\dot{R}_m(j) = \frac{-1}{4T^2}\int_0^T (T-w)\left\{R_\eta\left|w-(i-j)\,T+s\right| + R_\eta\left|w-(i-j)\,T-s\right|\right\}dw$$

let

$$f(z) = K \qquad 0<z<T$$
$$= \frac{K}{2} \qquad z = 0 = T$$
$$= 0 \qquad \text{for all other } z$$

then

$$\Delta\dot{R}_m(i)\Delta\dot{R}_m(j) = \frac{-1}{4T^2}\left\{\left[T-\left|(i-j)\,T-s\right|\right] f\left|(i-j)\,T-s\right| + \left[T-\left|s-(i-j)\,T\right|\right] f\left|s-(i-j)\,T\right|\right\}$$

when

$$(i-j)\,T-s = 0$$

$$\overline{\Delta\dot{R}_m(i)\,\Delta\dot{R}_m(j)} = \frac{-1}{4T^2}\left\{T \times \left|\frac{K}{2}+\frac{K}{2}\right|\right\} = \frac{-K}{4T}$$

let

$$(i-j)\,T-s = \mathcal{E}$$

then

$$\overline{\Delta\dot{R}_m(i)\,\Delta\dot{R}_m(j)} = \frac{-K}{4T^2}\,(T - |\mathcal{E}|) \qquad 0 < |\mathcal{E}| < T$$

Summary for Self-Correlation in Master

$s > T$

$$\left.\begin{aligned}
\overline{\Delta\dot{R}_m(i)\,\Delta\dot{R}_m(j)} &= \frac{K}{2T} && i = j \\
&= -\frac{K}{4T} && (i-j)\,T - s = 0 \\
&= \frac{-K}{4T^2}\,(T - |\mathcal{E}|) \\
& && 0 < |(i-j)\,T - s| \leq T
\end{aligned}\right\} \qquad (1)$$

Let us now put in the Range Noise

The Range Noise is considered as independent of the rate noise, therefore, its correlation function can be added to that of the rate noise (it is further assumed that tne range noise is "receiver equipment oriented", then let

σ^2 = variance of range noise = variance in N

$$\left.\begin{aligned}
\overline{\Delta\dot{R}_m(i)\,\Delta\dot{R}_m(j)} &= \frac{1}{4T^2}\,\overline{(N_{i+1} - N_i)\,(N_{(j+1)} - N_j)} \\
&= \frac{\sigma^2}{2T^2} \quad \text{for } i = j \\
&= -\frac{\sigma^2}{4T^2} \quad \text{for } |i-j| = 1 \\
&= 0 \quad \text{for all other, } |i-j|
\end{aligned}\right\} \qquad (2)$$

The total correlation function for a Master can be obtained by adding the results of equations (1) and (2).

2. Self-Correlation in Slave

At $i \neq j$, there is no effect of rate noise. However, if I assume range noise is receiver oriented, then

$$\left.\begin{aligned} \overline{\Delta\dot{R}_s(i)\,\Delta\dot{R}_s(j)} &= \frac{2K}{T} + \frac{2\sigma^2}{T^2} \qquad i = j \\ &= \frac{-\sigma^2}{T^2} \text{ for } |i-j| = 1 \\ &= 0 \text{ for all other } |i-j| \end{aligned}\right\} \tag{3}$$

3. Cross-Correlation between Master and Slave

Since Range Noise is assumed receiver oriented, there is only a cross-correlation due to the rate noise.

$$\Delta\dot{R}_m(i) = \frac{1}{2T}\int_{iT}^{(i+1)T}\left[\eta_m(t+s) - \eta_m(t)\right]\,dt$$

$$\Delta\dot{R}_s(j) = \frac{1}{T}\int_{jT}^{(j+1)T}\left[\eta_s(t+s) - \eta_m(t)\right]\,dt$$

$$t_1 = t - iT$$

$$t_2 = t - jT$$

$$\Delta\dot{R}_m(i) = \frac{1}{T}\int_{o}^{T}\left[\eta_m(t_1+iT+s) - \eta_m(t_1+iT)\right]\,dt_1$$

$$\Delta\dot{R}_s(j) = \frac{1}{T} \int_0^T \left[\eta_s (t_2 + jT + s) - \eta_m (t_2 + jT) \right] dt_2$$

$$\overline{\Delta\dot{R}_m(i)\, \Delta\dot{R}_s(j)} = \frac{1}{2T^2} \int_0^T \int_0^T - R_m \left(t_1 - t_2 + (i-j)\, T + s \right)$$

$$+ R_m \left(t_1 - t_2 + (i-j)\, T \right) dt_1\, dt_2$$

let

$$u = t_1 - t_2$$

$$v = t_2$$

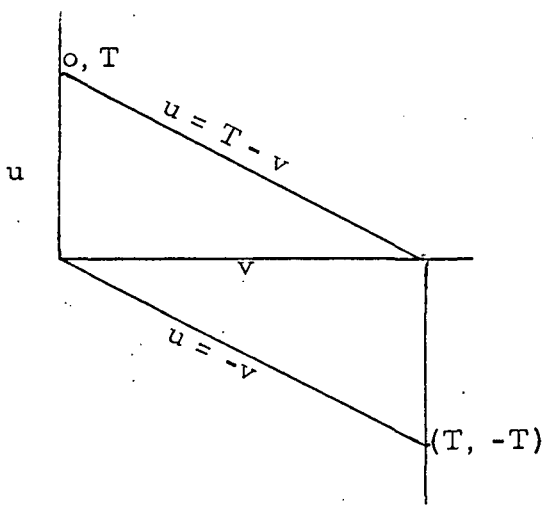

$$\overline{\Delta\dot{R}_m(i)\,\Delta\dot{R}_s(j)} = \frac{1}{2T^2}\left\{\int_{-T}^{o} du \int_{-u}^{T}\left[-R_\eta\left|u+(i-j)\,T+s\right| + R_\eta\left|u+(i-j)\,T\right|\right] dv \right.$$

$$\left. + \int_{o}^{T} du \int_{o}^{T-u}\left[-R_\eta\left|u+(i-j)\,T+s\right| + R_\eta\left|u+(i-j)\,T\right|\right] dv\right\}$$

$$= \frac{1}{2T^2}\left\{-\int_{o}^{-T}(T+u)\left[-R_\eta\left|u+(i-j)\,T+s\right| + R_\eta\left|u+(i-j)\,T\right|\right] du \right.$$

$$\left. + \int_{o}^{T}(T-u)\left[-R_\eta\left|u+(i-j)\,T+s\right| + R_\eta\left|u+(i-j)\,T\right|\right] du\right\}$$

$$= \frac{1}{2T^2}\left\{\int_{o}^{T}(T-w)\left[-R_\eta\left|-w+(i-j)\,T+s\right| + R_\eta\left|-w+(i-j)\,T\right|\right] dw \right.$$

$$\left. + \int_{o}^{T}(T-w)\left[-R_\eta\left|w+(i-j)\,T+s\right| + R_\eta\left|w+(i-j)\,T\right|\right] dw\right\}$$

$$= \frac{1}{2T^2}\left\{\int_{o}^{T}(T-w)\left[-R_\eta\left|w-(i-j)\,T-s\right| + R_\eta\left|w-(i-j)\,T\right| \right.\right.$$

$$\left.\left. - R_\eta\left|w+(i-j)\,T+s\right| + R_\eta\left|w+(i-j)\,T\right|\right] dw\right\}$$

Summary for Cross-Correlation between Slave and Master ($s > T$)

$$\overline{\Delta\dot{R}_m(i)\,\Delta\dot{R}_s(j)} = 0 \qquad i > j$$

$$= \frac{T}{2T^2}\left[K\left(\frac{1}{2}+\frac{1}{2}\right)\right] = \frac{K}{2T} \qquad i = j$$

$$\overline{\Delta\dot{R}_m(i)\,\Delta\dot{R}_s(j)} = \frac{-K\,(T-|\varepsilon|)}{2T^2} \qquad |\varepsilon| = |s-(j-i)\,T|$$

$$0 \leqslant |\varepsilon| \leqslant T$$

4. Cross-Correlation Between Two Slaves

Since the range noise, N is assumed receiver oriented, there is only a cross-correlation due to the rate noise.

$$\Delta\dot{R}_{s_1}(i) = \frac{1}{T}\int_0^T \left[\eta_{s_1}(t_1+iT+s) - \eta_m(t_1+iT)\right] dt_1$$

$$\Delta R_{s_2}(j) = \frac{1}{T}\int_0^T \left[\eta_{s_2}(t_2+jT+s) - \eta_m(t_2+jT)\right] dt_2$$

$$\overline{\Delta\dot{R}_{s_1}(i)\,\Delta\dot{R}_{s_2}(j)} = \frac{1}{T^2}\int_0^T\int_0^T + R_\eta\left(t_1 - t_2 + (i-j)\,T\right) dt_1\, dt_2$$

$$= \frac{1}{T^2}\left\{ -\int_0^{-T} du \int_{-u}^{T} R_\eta\left(u + (i-j)\,T\right) dv \right.$$

$$\left. + \int_0^T du \int_0^{T-u} R_\eta\left(u + (i-j)\,T\right) dv \right\}$$

$$= \frac{1}{T^2}\left\{ -\int_0^{-T} (T+u)\, R_\eta\left(u + (i-j)\,T\right) du \right.$$

$$\left. + \int_0^T (T-u)\, R_\eta\left(u + (i-j)\,T\right) du \right\}$$

$$\overline{\Delta\dot{R}_{s_1}(i)\,\Delta\dot{R}_{s_2}(j)} = \frac{1}{T^2}\int_0^T (T-w)\left[R_\eta\left(w - (i-j)\,T\right)\right.$$

$$\left. + R_\eta\left(w + (i-j)\,T\right)\right] dw$$

$$\overline{\Delta\dot{R}_{s_1}(i)\,\Delta\dot{R}_{s_2}(j)} = \frac{K}{T} \qquad i = j$$

$$= 0 \qquad |i-j| \neq 0$$

In closing let me say that evaluating the errors is simpler than it appears from the above analysis. If we consider that the weighting functions are consistent with the estimate of the state vector at some time of interest, it is only required to evaluate the mean square error in each of the state vector components , the cross-correlation in the estimate of the parameters is not required. For example, suppose ${}_{\ell}w(k)$ is the weighting function for ℓ th measurable at the k th time for the parameter $a_1(t)$, then,

$$\Delta a_1 = \sum_k {}_1w(k)\ {}_1\eta(k) + \sum_k {}_2w(k)\ {}_2\eta(k) + \sum_k {}_3w(k)\ {}_3\eta(k)$$

and $\overline{\Delta a_1^2}$ can be generated from this form. Likewise, the mean square error in the other components of the state vector can be determined. A saving in machine time can be had if all the mean square error components of the state vector are calculated simultaneously. For example, when calculating

$${}_1w(k)\ {}_2w(\ell)\ {}_1\eta(k)\ {}_2\eta(\ell)$$

it can be done for each component of state vector.

However, this simultaneous calculation technique will either require more tape to core manipulation or limit the size of the problem that can be undertaken.

APPENDIX A

Consider the problem of self-correlated and cross-correlated noise in the measurable for a specified filter.

Let

M_i^j = ith measurement of the jth measurable

η_i^j = ith noise in the jth measurable

Δa = $\hat{a} - a_{ap}$ = column vector of change in updated parameter

C_m = information matrix from measurables only

C_a = apriori information matrix

Now, for a weighted least square filter, we have

$$(\hat{a} - a_{ap}) = C^{-1} \left\{ \sum_j^m \frac{1}{\sigma_j^2} \begin{bmatrix} \sum_{i=1}^{N_j} \frac{\partial M_i^j}{\partial a_1} (M_i^j - M_{c_i}^j) \\ \vdots \\ \sum_{i=1}^{N_j} \frac{\partial M_i^j}{\partial a_k} (M_i^j - M_{c_i}^j) \end{bmatrix} \right\} \tag{A1}$$

$a_{ap} = a_\tau + (a_{ap} - a_\tau)$ $\qquad$ a_τ = true value of parameter

then

$$(\hat{a} - a_\tau) = (a_{ap} - a_\tau) + (\hat{a} - a_{ap})$$

$$(\hat{a} - a_\tau) = C^{-1} C (a_{ap} - a_\tau) + (\hat{a} - a_{ap}) \qquad \text{(A2)}$$

Substitution of equation (A1) in (A2) and using the following equation, yields equation (A3)

$$M_i^j - M_{ci} = \eta_i^j - \sum_k \frac{\partial M_i^j}{\partial a_k} \left[a_{ap}(k) - a_\tau(k) \right]$$

$$(\hat{a} - a_\tau) = C^{-1} C (a_{ap} - a_\tau) + C^{-1} \left\{ \sum_j \frac{1}{\sigma_j^2} \begin{bmatrix} \sum_i^{N_j} \frac{\partial M_i^j}{\partial a_1} \eta_i^j \\ \vdots \\ \sum_i^{N_j} \frac{\partial M_i^j}{\partial a_k} \eta_i^j \end{bmatrix} - C_m (a_{ap} - a_\tau) \right\} \qquad \text{(A3)}$$

$$\therefore (\hat{a} - a_\tau) = C^{-1} \left\{ (C - C_m)(a_{ap} - a_\tau) + \sum_j^m \frac{1}{\sigma_j^2} \begin{bmatrix} \sum_i^{N_j} \frac{\partial M_i^j}{\partial a_1} \eta_i^j \\ \vdots \\ \sum_i^{N_j} \frac{\partial M_i^j}{\partial a_k} \eta_i^j \end{bmatrix} \right\}$$

or since $(C - C_m) = C_a$

$$(\hat{a} - a_\tau) = C^{-1}\left\{ C_a\,(a_{ap} - a_\tau) + \sum_j^m \frac{1}{\sigma_j^2} \begin{bmatrix} \sum_i^{N_j} \frac{\partial M_i^j}{\partial a_1}\,\eta_i^j \\ \vdots \\ \sum_i^{N_j} \frac{\partial M_i^j}{\partial a_k}\,\eta_i^j \end{bmatrix} \right\} \tag{A4}$$

For the moment, assume that $\overline{(a_{ap} - a_\tau)\,\eta_i^j} = 0$, then, of course, the effect of the apriori is as in equation (A5)

$$\overline{(\hat{a} - a_\tau)\,(\hat{a} - a_\tau)^T} = C^{-1}\,C_{ap}\,C^{-1} \tag{A5}$$

Let us now work on the effect of the measurables. Let us rewrite equation (A4) in matrix notations.

$$(\hat{a} - a_\tau) = C^{-1}\left[\begin{pmatrix} \frac{\partial M_1^1}{\partial a_1} & \cdots & \frac{\partial M_{N_1}^1}{\partial a_1} \\ \frac{\partial M_1^1}{\partial a_k} & \cdots & \frac{\partial M_{N_1}^1}{\partial a_k} \end{pmatrix} \frac{1}{\sigma_1^2} \begin{pmatrix} \frac{\partial M_1^2}{\partial a_1} & \cdots & \frac{\partial M_{N_2}^2}{\partial a_1} \\ \frac{\partial M_1}{\partial a_k} & & \frac{\partial M_{N_2}^2}{\partial a_k} \end{pmatrix} \frac{1}{\sigma_2^2} \right| \cdots$$

$$\cdots \left[\left(\begin{array}{ccc} \frac{\partial M_1^m}{\partial a_1} & \cdots & \frac{\partial M_{N_m}^m}{\partial a_1} \\ \cdot & & \\ \frac{\partial M_1^m}{\partial a_k} & \cdots & \frac{\partial M_{N_m}^m}{\partial a_k} \end{array} \right) \frac{1}{\sigma_m^2} \right] \left[\begin{array}{c} \eta_1^1 \\ \cdot \\ \cdot \\ \cdot \\ \eta_{N_1}^1 \\ \hline \eta_1^2 \\ \cdot \\ \cdot \\ \cdot \\ \eta_{N_2}^2 \\ \hline \cdot \\ \cdot \\ \cdot \\ \cdot \\ \hline \eta_1^m \\ \cdot \\ \cdot \\ \cdot \\ \eta_{N_m}^m \end{array} \right]$$

Now

$$C^{-1} \left[\frac{1}{\sigma_j^2} \left(\begin{array}{ccc} \frac{\partial M_1^j}{\partial a_1} & \cdots & \frac{\partial M_{N_1}^j}{\partial a_1} \\ & & \\ \frac{\partial M_1^j}{\partial a_k} & \cdots & \frac{\partial M_{N_1}^1}{\partial a_k} \end{array} \right) \right] = W_i^j$$

where: W_i^j is the weighting function that is already calculated in the weighting function analysis program.

In terms of W_i^j $a - a_T$ can be rewritten as

$$(\hat{a} - a_T) = \left[W_i^1 \mid W_i^2 \mid \ldots \mid W_i^m \right] \times \begin{bmatrix} \eta_1^1 \\ \vdots \\ \eta_{N_1}^1 \\ \hline \eta_1^2 \\ \vdots \\ \eta_{N_2}^2 \\ \hline \vdots \\ \hline \eta_1^m \\ \vdots \\ \eta_{N_m}^m \end{bmatrix}$$

$$\overline{(\hat{a} - a_T)(\hat{a} - a_T)^T} = \left[W_i^1 \mid \ldots \mid W_i^m \right] \times \begin{bmatrix} \overline{\eta_i^1 \eta_i^{1T}} & \ldots & \overline{\eta_i^1 \eta^{jT}} & \overline{\eta_i^1 \eta_i^{mT}} \\ & \overline{\eta_i^2 \eta_i^{2T}} & \overline{\eta_i^2 \eta_i^{jT}} & \\ & & \ddots & \\ & & & \overline{\eta_i^m \eta_i^{mT}} \end{bmatrix} \begin{bmatrix} W_i^{1T} \\ \vdots \\ W_i^{mT} \end{bmatrix}$$

The difficulty in performing this calculation on the computer is associated with being able to generate generically the self- and cross-correlation matrix of the noises.

The Bissett-Berman Corporation 2941 Nebraska Avenue, Santa Monica, California EXbrook 4-3270

APOLLO NOTE NO. 403
(Task II, Item II)

CHECKOUT OF WEIGHTING FUNCTION PROGRAM

L. Lustick/
G. Hempstead
25 January 1966

PURPOSE

The purpose of this note is to indicate recent changes that have been added to the Bissett-Berman "Weighting Function Program" and the manner in which they were checked out.

INTRODUCTION

The weighting function program previously calculated the functions of time that each measurable is multiplied by consistent with a filter that only updates the six orbit parameters. The errors in each component of the state vector are then given by the following expression.

$$\Delta a_{j=1-6} = \sum_{\ell} \sum_{k} {}_{\ell}W^{j}(k) \; {}_{\ell}M(k) - {}_{\ell}M_{c}(k)$$

where

${}_{\ell}W^{j}(k)$ = weighting function at the kth time for the ℓth measurable

${}_{\ell}M(k) - {}_{\ell}M_{c}(k)$ = error in measurable.

The weighting function approach is particularly useful for evaluating the effect of errors that are conveniently represented in the time domain. It also has utility in evaluating errors in the state vector when the measurable errors are statistical, but complicated by the fact that there may be cross-correlation between measurables as well as self-correlation within a measurable.

The weighting function program has been recently modified so that the filter consistent with any number of parameters (up to 40) being updated can be determined.

METHOD

The weighting function program is a spur off the Orbit Error Analysis Program. In Program A, the $\frac{\partial_\ell M(k)}{\partial a_j}$ are calculated and saved on tape to be used later in the weighting function program.

The modified Part B (The Weighting Function Program) then calculates the following for each value of (k)

$$ {}_\ell W_{j=1-m} = C^{-1} \frac{1}{\sigma_\ell^2} \begin{pmatrix} \frac{\partial_\ell M(k)}{\partial a_1} \\ \vdots \\ \frac{\partial_\ell M(k)}{\partial a_6} \\ \vdots \\ \frac{\partial_\ell M(k)}{\partial a_m} \end{pmatrix} $$

where: C^{-1} is the total covariance matrix of the updated parameters

$\frac{\partial_\ell M(k)}{\partial a_j}$ = partial derivative of the ℓ measurable at the kth time and is non-zero for all parameters on which the ℓth measurable depends and is equal to zero for all parameters being updated on which the particular measurable does not depend.

If the state vector is being estimated at some future time, t, the formula for the weighting function is as follows:

$$ {}_{\ell}W^{(t)}_{j=1-m} = Q(t)\, C^{-1}\, \frac{1}{\sigma_{\ell}^{2}} \begin{pmatrix} \frac{\partial_{\ell} M(k)}{\partial a_1} \\ \vdots \\ \frac{\partial_{\ell} M(k)}{\partial a_6} \\ \vdots \\ \frac{\partial_{\ell} M(k)}{\partial a_m} \end{pmatrix} $$

CHECKOUT PROCEDURE

The multiple station program was used on an Earth parking with tracking from four stations with vector range as the measurable from each station.

A bias with no apriori was assumed for each of the measurables (a total of 18 updated parameters). The multiple station version of the OEA Program gave the contribution to each of the non-updated parameters to the uncertainty in the future state vector components. The error in the same state vector was calculated using the weighting function approach. The nuisance parameter was $N_o H$ the zenith range error of one of the stations.

The following table compares the two results for the state vector components at some future time and their agreement constitute the check.

	Multiple Station Program	Weighting Function Approach
$\overline{\Delta x^2}(t)$	1.235928 E-04	1.2359177 E-04
$\overline{\Delta \dot{y}^2}(t)$	8.695090 E-11	8.6950155 E-11
$\overline{\Delta a_7^2}$	6.305648 E-06	6.30559 E-06

The Bissett-Berman Corporation 2941 Nebraska Avenue, Santa Monica, California EXbrook 4-3270

APOLLO NOTE NO. 404
(Task 2, Item II)

L. Lustick
27 January 1966

CHECKOUT OF MULTIPLE STATION PROGRAM

PURPOSE

The purpose of this note is to indicate the manner in which the multiple station version of the Orbit Error Analysis Program has been checked out.

METHOD OF CHECKOUT

The method of checkout was to compare the answers obtained with the multiple station version of the OEA Program with the already existing OEA Program on a problem which they both can handle. The use of the multiple station program is described in Apollo Note 389. This note is primarily concerned with the checkout of the program but the example used does provide a good illustration of the use of the program. The ability of the multiple station OEA to present the contribution of each group of nuisance parameters as well as the total should allow the user to determine which set of nuisance parameters are contributing most to the total error.

DEFINITION OF CHECKOUT PROBLEM

The orbit was a typical LEM rendezvous orbit as depicted in Figure 1. The orientation of the station and the Earth-Moon plane are shown in Figure 2. The measurables were range-rate from the three master stations shown in Figure 2. The measurements were made every 6 seconds for 14 minutes of total tracking time. There was no a priori knowledge assumed for the orbit parameters. The a priori standard deviations for all stations was taken as 20 meters in the up direction and 50 meters in the east and north directions.

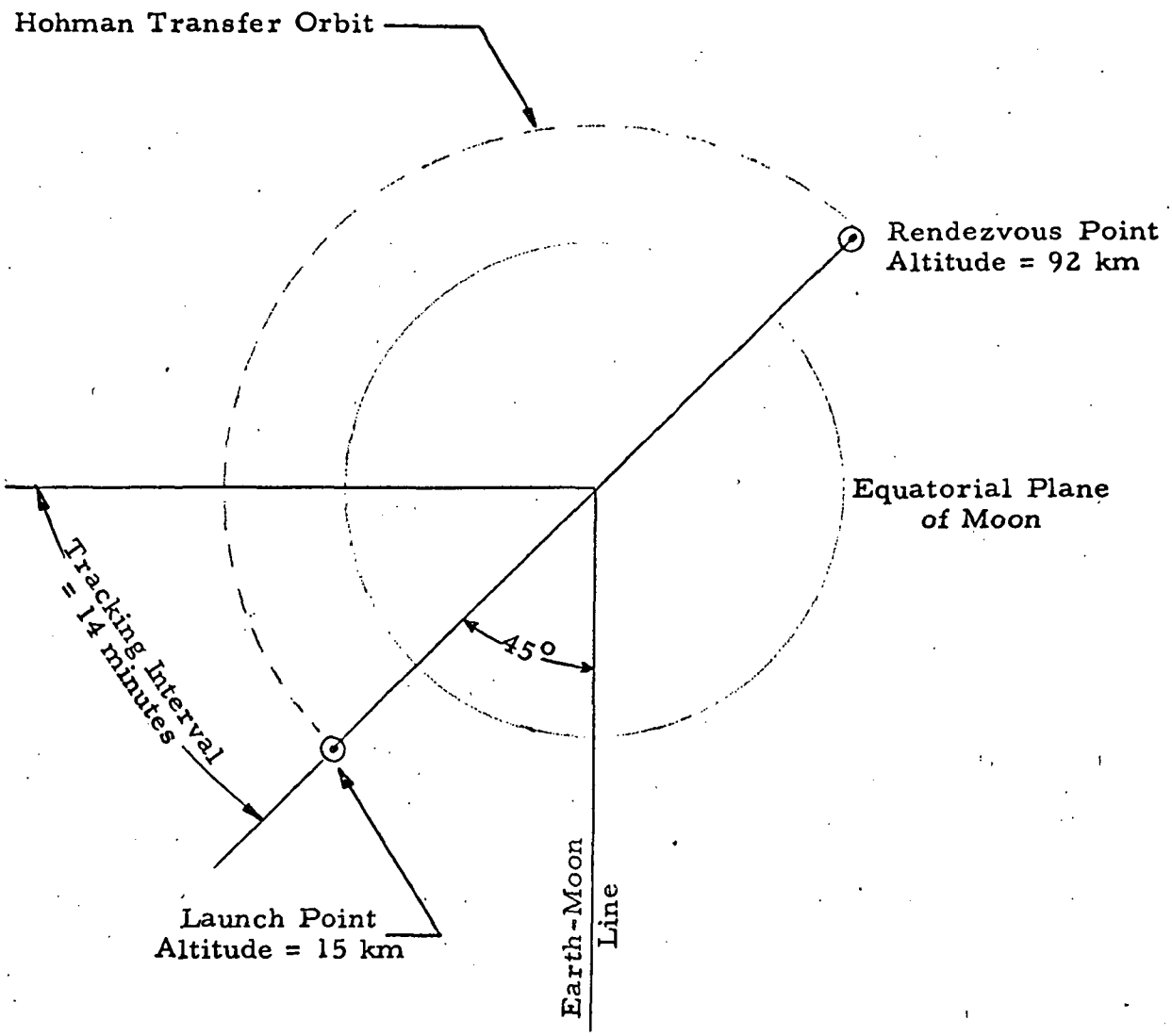

Figure 1. Orbit Geometry

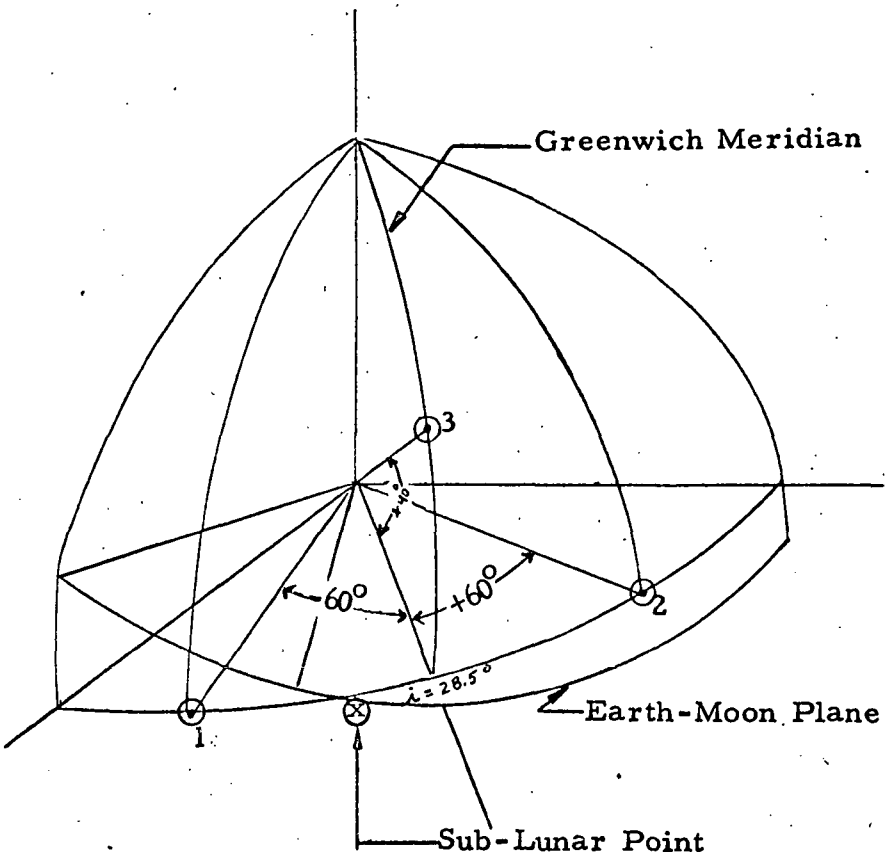

Figure 2. Station Geometry

The a priori uncertainty in the lunar gravitational constant was taken as approximately 0.01% of its expected value. The a priori covariance matrix and the Part A data sheets for each of the stations are shown in Figures (3 - 6).

DISCUSSION

The 6 orbit parameters were the only parameters updated. To show the flexibility of the multiple station program the effect of each nuisance parameter on the rendezvous miss was calculated separately. The Part B data sheet for running this problem with the multiple station version of the program is shown in Figure 7. The function of each group is listed below:

		Effect Of
1st Group	-	Up station location error Data Set 101.
2nd Group	-	East station location error Data Set 101.
3rd Group	-	North station location error Data Set 101.
4th Group	-	Same as 1 for Data Set 102.
5th Group	-	Same as 2 for Data Set 102.
6th Group	-	Same as 3 for Data Set 102.
7th Group	-	Same as 1 for Data Set 103.
8th Group	-	Same as 2 for Data Set 103.
9th Group	-	Same as 3 for Data Set 103.
10th Group	-	Effect of error in gravitational constant, μ.

The outputs of the multiple station OEA covariance at rendezvous are shown in Figures 8 - 19.

Figure 8 - Total white noise effect.

Figure 9 - 18 - Effect of Group 1 - 10 respectively.

Figure 19 - Total error at rendezvous.

Figure 19 is the normal output that is given with the regular OEA Program. Figure 20 shows the results obtained with the regular OEA for the same problem. Comparison of Figure 20 with Figure 19 constitutes the check.

A PRIORI 100

A(9, 9)	=	3.24900000E 17
A(11,11)	=	4.00000000E 02
A(12,12)	=	2.50000000E 03
A(13,13)	=	2.50000000E 03
A(14,14)	=	4.00000000E 02
A(15,15)	=	2.50000000E 03
A(16,16)	=	2.50000000E 03
A(17,17)	=	4.00000000E 02
A(18,18)	=	2.50000000E 03
A(19,19)	=	2.50000000E 03

FIGURE 3.

INPUT DATA

01	1.7528160E 06	A1
02	0	A4
03	1.69050300E 03	A5
04	1.00000000E 00	GAM ID
05	2.85000000E 01	BETA
06	9.00000000E 01	XI
07	1.75960000E 02	ETA
08	3.25000000E 02	ZETA
09	4.04666700E 01	LAMBDA
10	-3.66666700E 00	ALPHA
11	7.29116000E-05	OMEGAE
12	2.66900000E-06	OMEGAM
13	6.37816500E 06	RHOE
14	3.84402000E 08	RHOM
15	4.90277800E 12	MU
16	7.00000000E 00	D TIME
16	1.40000000E 01	D TIME
16	5.67100000E 01	D TIME
17	0	REENTRY RAD
18	-2.00000000E 00	BIG L
19	-2.15260000E 01	SMA L
20	1.00000000E 00	RRATE IND
21	0	RANGE IND
22	0	Q IND
23	5.67100000E 01	QF IND
24	0	ANG 1 IND
25	0	ANG 2 IND
26	0	PVW IND
27	1.00000000E-01	T INIT
28	1.00000000E-01	T INCR
29	1.20000000E 01	DIMENS
30	0	LAMBDA2
31	0	ALPHA2
32	1.00000000E 00	M-S IND
33	0	E-M IND

FIGURE 4.

INPUT DATA

01	1.7528160E 06	A1
02	0	A4
03	1.6905030E 03	A5
04	1.0000000E 00	GAM ID
05	2.8500000E 01	BETA
06	9.0000000E 01	XI
07	1.7596000E 02	ETA
08	3.2500000E 02	ZETA
09	-0	LAMBDA
10	6.0000000E 01	ALPHA
11	7.2911600E-05	OMEGAE
12	2.6690000E-06	OMEGAM
13	6.3781650E 06	RHOE
14	3.8440200E 08	RHOM
15	4.9027780E 12	MU
16	7.0000000E 00	D TIME
16	1.4000000E 01	D TIME
17	0	REENTRY RAD
18	-2.0000000E 00	BIG L
19	-2.1526000E 01	SMA L
20	1.0000000E 00	RRATE IND
21	0	RANGE IND
22	0	Q IND
23	0	QF IND
24	0	ANG 1 IND
25	0	ANG 2 IND
26	0	PVW IND
27	1.0000000E-01	T INIT
28	1.0000000E-01	T INCR
29	1.2000000E 01	DIMENS
30	0	LAMBDA2
31	0	ALPHA2
32	1.0000000E 00	M-S IND
33	-0	F-M IND

FIGURE 5.

INPUT DATA

01	1.7528160E 06	A1
02	0	A4
03	1.6905030E 03	A5
04	1.0000000E 00	GAM ID
05	2.8500000E 01	BETA
06	9.0000000E 01	XI
07	1.7596000E 02	ETA
08	3.2500000E 02	ZETA
09	-0	LAMBDA
10	-6.0000000E 01	ALPHA
11	7.2911600E-05	OMEGAE
12	2.6690000E-06	OMEGAM
13	6.3781650E 06	RHOE
14	3.8440200E 08	RHOM
15	4.9027780E 12	MU
16	7.0000000E 00	D TIME
16	1.4000000E 01	D TIME
17	0	REENTRY RAD
18	-2.0000000E 00	BIG L
19	-2.1526000E 01	SMA L
20	1.0000000E 00	RRATE IND
21	0	RANGE IND
22	0	Q IND
23	0	QF IND
24	0	ANG 1 IND
25	0	ANG 2 IND
26	0	PVW IND
27	1.0000000E-01	T INIT
28	1.0000000E-01	T INCR
29	1.2000000E 01	DIMENS
30	0	LAMBDA2
31	0	ALPHA2
32	1.0000000E 00	M-S IND
33	-0	F-M IND

FIGURE 6.

```
DS 100      A    T=       -0   SG=1.00000E 00        0 0 0 0 7 0 0 0 0 0 0 0 0 0 0 0 0 0 0 0 0 0 0 0 0 0
DS 101      Q    T=    56.71   SG=1.00000E 00  *
DS 101      RD   T=    14.00   SG=1.22470E-02        0 7 0 0 0 0 0 0 0 0 0 0 0 0 0 0 0 0 0 0 0 0 0 0 0 0

DS 100      A    T=       -0   SG=1.00000E 00        0 0 0 0 0 7 0 0 0 0 0 0 0 0 0 0 0 0 0 0 0 0 0 0 0 0
DS 101      Q    T=    56.71   SG=1.00000E 00  *
DS 101      RD   T=    14.00   SG=1.22470E-02        0 0 7 0 0 0 0 0 0 0 0 0 0 0 0 0 0 0 0 0 0 0 0 0 0 0

DS 100      A    T=       -0   SG=1.00000E 00        0 0 0 0 0 0 7 0 0 0 0 0 0 0 0 0 0 0 0 0 0 0 0 0 0 0
DS 101      Q    T=    56.71   SG=1.00000E 00  *
DS 101      RD   T=    14.00   SG=1.22470E-02        0 0 0 7 0 0 0 0 0 0 0 0 0 0 0 0 0 0 0 0 0 0 0 0 0 0

DS 100      A    T=       -0   SG=1.00000E 00        0 0 0 0 0 0 0 7 0 0 0 0 0 0 0 0 0 0 0 0 0 0 0 0 0 0
DS 101      Q    T=    56.71   SG=1.00000E 00  *
DS 102      RD   T=    14.00   SG=1.22470E-02        0 7 0 0 0 0 0 0 0 0 0 0 0 0 0 0 0 0 0 0 0 0 0 0 0 0

DS 100      A    T=       -0   SG=1.00000E 00        0 0 0 0 0 0 0 0 7 0 0 0 0 0 0 0 0 0 0 0 0 0 0 0 0 0
DS 101      Q    T=    56.71   SG=1.00000E 00  *
DS 102      RD   T=    14.00   SG=1.22470E-02        0 0 7 0 0 0 0 0 0 0 0 0 0 0 0 0 0 0 0 0 0 0 0 0 0 0

DS 100      A    T=       -0   SG=1.00000E 00        0 0 0 0 0 0 0 0 0 7 0 0 0 0 0 0 0 0 0 0 0 0 0 0 0 0
DS 101      Q    T=    56.71   SG=1.00000E 00  *
DS 102      RD   T=    14.00   SG=1.22470E-02        0 0 0 7 0 0 0 0 0 0 0 0 0 0 0 0 0 0 0 0 0 0 0 0 0 0

DS 100      A    T=       -0   SG=1.00000E 00        0 0 0 0 0 0 0 0 0 0 7 0 0 0 0 0 0 0 0 0 0 0 0 0 0 0
DS 101      Q    T=    56.71   SG=1.00000E 00  *
DS 103      RD   T=    14.00   SG=1.22470E-02        0 7 0 0 0 0 0 0 0 0 0 0 0 0 0 0 0 0 0 0 0 0 0 0 0 0

DS 100      A    T=       -0   SG=1.00000E 00        0 0 0 0 0 0 0 0 0 0 0 7 0 0 0 0 0 0 0 0 0 0 0 0 0 0
DS 101      Q    T=    56.71   SG=1.00000E 00  *
DS 103      RD   T=    14.00   SG=1.22470E-02        0 0 7 0 0 0 0 0 0 0 0 0 0 0 0 0 0 0 0 0 0 0 0 0 0 0

DS 100      A    T=       -0   SG=1.00000E 00        0 0 0 0 0 0 0 0 0 0 0 0 7 0 0 0 0 0 0 0 0 0 0 0 0 0
DS 101      Q    T=    56.71   SG=1.00000E 00  *
DS 103      RD   T=    14.00   SG=1.22470E-02        0 0 0 7 0 0 0 0 0 0 0 0 0 0 0 0 0 0 0 0 0 0 0 0 0 0

DS 100      A    T=       -0   SG=1.00000E 00        0 0 7 0 0 0 0 0 0 0 0 0 0 0 0 0 0 0 0 0 0 0 0 0 0 0
DS 101      Q    T=    56.71   SG=1.00000E 00        0 0 0 0 0 7 0 0 0 0 0 0 0 0 0 0 0 0 0 0 0 0 0 0 0 0
DS 101      RD   T=    14.00   SG=1.22470E-02        0 0 0 0 0 7 0 0 0 0 0 0 0 0 0 0 0 0 0 0 0 0 0 0 0 0
DS 102      RD   T=    14.00   SG=1.22470E-02        0 0 0 0 0 7 0 0 0 0 0 0 0 0 0 0 0 0 0 0 0 0 0 0 0 0
DS 103      RD   T=    14.00   SG=1.22470E-02        0 0 0 0 0 7 0 0 0 0 0 0 0 0 0 0 0 0 0 0 0 0 0 0 0 0
```

FIGURE 7.

(Q)(COV)(QT) - LOCAL COORDINATE SYSTEM

7.493762E 03	-2.793096E 04	4.901441E 03	2.249564E 01	-5.119996E 00	1.181535E 00
-2.793096E 04	1.089393E 05	-2.399678E 04	-8.670574E 01	1.921920E 01	-5.025026E-01
4.901441E 03	-2.399678E 04	1.239427E 05	1.580798E 01	-3.567114E 00	4.707982E 01
2.249564E 01	-8.670574E 01	1.580798E 01	6.928906E-02	-1.543949E-02	1.520467E-05
-5.119996E 00	1.921920E 01	-3.567114E 00	-1.543949E-02	3.506248E-03	-8.114946E-04
1.181535E 00	-5.025026E-01	4.707982E 01	1.520468E-05	-8.114946E-04	2.800845E-02

SQRT((1,1)+(2,2)+(3,3)) = 4.902812 4E 02
SQRT((4,4)+(5,5)+(6,6)) = 3.174960 8E-01

SQRT(1, 1) =	8.656651 8E 01
SQRT(2, 2) =	3.300594 7E 02
SQRT(3, 3) =	3.520549 4E 02
SQRT(4, 4) =	2.632281 6E-01
SQRT(5, 5) =	5.921358 0E-02
SQRT(6, 6) =	1.673572 5E-01

PRINCIPAL POSITION UNCERTAINTIES

1ST AXIS = 3.805390E 02 PHI =-7.545460E 01
2ND AXIS = 3.086527E 02 CHI =-8.940577E 01
3RD AXIS = 1.729812E 01 PSI =-4.954988E 01

PRINCIPAL VELOCITY UNCERTAINTIES

1ST AXIS = 2.696912E-01 PHI =-1.256861E 01
2ND AXIS = 1.674212E-01 CHI =-8.838459E 01
3RD AXIS = 6.367550E-03 PSI =-2.454516E-01

FIGURE 8.

GROUP 1

					6X6	07 BI	08 US	09 ES	10 NS	11 VL	12 MU	13 CL	14 VA	15 UM	16 EM	17 NM	18 ED	19 ND	20 RM	21 AM	22 BS	23 RS	24 AS	25 L1	26 L2	27 L3	28 L4	29 L5	30 L6
DS 100	A	T=	-0	SG=1.00000E 00		0	0	0	0	7	0	0	0	0	0	0	0	0	0	0	0	0	0	0	0	0	0	0	0
DS 101	0	T=	56.71	SG=1.00000E 00	*																								
DS 101	RD	T=	14.00	SG=1.22470E-02		0	7	0	0	0	0	0	0	0	0	0	0	0	0	0	0	0	0	0	0	0	0	0	0

(Q)(COV)(QT) - LOCAL COORDINATE SYSTEM

3.570458E 01	-2.139080E 02	-2.943600E 01	1.605802E-01	-2.549399E-02	-1.608097E-01
-2.139080E 02	1.281534E 03	1.763526E 02	-9.620441E-01	1.527358E-01	9.634189E-01
-2.943600E 01	1.763526E 02	2.426798E 01	-1.323875E-01	2.101806E-02	1.325766E-01
1.605802E-01	-9.620441E-01	-1.323875E-01	7.222042E-04	-1.146584E-04	-7.232362E-04
-2.549399E-02	1.527358E-01	2.101806E-02	-1.146584E-04	1.820337E-05	1.148222E-04
-1.608097E-01	9.634189E-01	1.325766E-01	-7.232362E-04	1.148222E-04	7.242697E-04

SQRT((1,1)+(2,2)+(3,3)) =	3.662657 7E 01
SQRT((4,4)+(5,5)+(6,6)) =	3.827110 1E-02
SQRT(1, 1) =	5.975331 2E 00
SQRT(2, 2) =	3.579851 4E 01
SQRT(3, 3) =	4.926254 4E 00
SQRT(4, 4) =	2.687385 6E-02
SQRT(5, 5) =	4.266540 7E-03
SQRT(6, 6) =	2.691225 9E-02

FIGURE 9.

GROUP 2

					6X6	07 BI	08 US	09 ES	10 NS	11 VL	12 MU	13 CL	14 VA	15 UM	16 EM	17 NM	18 ED	19 ND	20 RM	21 AM	22 BS	23 RS	24 AS	25 L1	26 L2	27 L3	28 L4	29 L5	30 L6
DS 100	A	T=	-0	SG=1.00000E 00		0	0	0	0	0	7	0	0	0	0	0	0	0	0	0	0	0	0	0	0	0	0	0	0
DS 101	Q	T=	56.71	SG=1.00000E 00	*																								
DS 101	RD	T=	14.00	SG=1.22470E-02		0	0	7	0	0	0	0	0	0	0	0	0	0	0	0	0	0	0	0	0	0	0	0	0

(Q)(COV)(QT) - LOCAL COORDINATE SYSTEM

2.646616E 03	-1.593855E 04	-3.260254E 03	1.197676E 01	-1.890084E 00	-1.255008E 01
-1.593855E 04	9.598570E 04	1.963402E 04	-7.212687E 01	1.138253E 01	7.557957E 01
-3.260254E 03	1.963402E 04	4.016169E 03	-1.475366E 01	2.328315E 00	1.545992E 01
1.197676E 01	-7.212687E 01	-1.475366E 01	5.419855E-02	-8.553218E-03	-5.679302E-02
-1.890084E 00	1.138253E 01	2.328315E 00	-8.553218E-03	1.349806E-03	8.962659E-03
-1.255008E 01	7.557957E 01	1.545992E 01	-5.679302E-02	8.962659E-03	5.951170E-02

SQRT((1,1)+(2,2)+(3,3)) =	3.203882E 02
SQRT((4,4)+(5,5)+(6,6)) =	3.392053E-01
SQRT(1, 1) =	5.144527E 01
SQRT(2, 2) =	3.098155E 02
SQRT(3, 3) =	6.337325E 01
SQRT(4, 4) =	2.328058E-01
SQRT(5, 5) =	3.673970E-02
SQRT(6, 6) =	2.439501E-01

FIGURE 10.

GROUP 3

					6X6	07 BI	08 US	09 ES	10 NS	11 VL	12 MU	13 CL	14 VA	15 UM	16 EM	17 NM	18 ED	19 ND	20 RM	21 AM	22 BS	23 RS	24 AS	25 L1	26 L2	27 L3	28 L4	29 L5	30 L6
DS 100	A	T=	-0	SG=1.00000E 00		0	0	0	0	0	0	7	0	0	0	0	0	0	0	0	0	0	0	0	0	0	0	0	0
DS 101	Q	T=	56.71	SG=1.00000E 00	*																								
DS 101	RD	T=	14.00	SG=1.22470E-02		0	0	0	7	0	0	0	0	0	0	0	0	0	0	0	0	0	0	0	0	0	0	0	0

(Q)(COV)(QT) - LOCAL COORDINATE SYSTEM

1.339310E 02	-7.971211E 02	-3.344598E 01	5.974768E-01	-9.562385E-02	-5.591577E-01
-7.971211E 02	4.744250E 03	1.990615E 02	-3.556020E 00	5.691273E-01	3.327956E 00
-3.344598E 01	1.990615E 02	8.352315E 00	-1.492052E-01	2.387971E-02	1.396359E-01
5.974768E-01	-3.556020E 00	-1.492052E-01	2.665391E-03	-4.265855E-04	-2.494447E-03
-9.562385E-02	5.691273E-01	2.387971E-02	-4.265855E-04	6.827337E-05	3.992266E-04
-5.591577E-01	3.327956E 00	1.396359E-01	-2.494447E-03	3.992266E-04	2.334466E-03

SQRT((1,1)+(2,2)+(3,3)) = 6.990374E 01
SQRT((4,4)+(5,5)+(6,6)) = 7.119080 3E-02

SQRT(1, 1) =	1.1572856E 01
SQRT(2, 2) =	6.887851 3E 01
SQRT(3, 3) =	2.890037 2E 00
SQRT(4, 4) =	5.162742 5E-02
SQRT(5, 5) =	8.262769 9E-03
SQRT(6, 6) =	4.831631 2E-02

FIG 11

FIGURE 11.

GROUP 4

						6X6	07 BJ	08 US	09 ES	10 NS	11 VL	12 MU	13 CL	14 VA	15 UM	16 EM	17 NM	18 ED	19 ND	20 RM	21 AM	22 BS	23 RS	24 AS	25 L1	26 L2	27 L3	28 L4	29 L5	30 L6
DS 100	A	T=	=0	SG=1.00000E 00			0	0	0	0	0	0	0	7	0	0	0	0	0	0	0	0	0	0	0	0	0	0	0	0
DS 101	Q	T=	56.71	SG=1.00000E 00	*																									
DS 102	RD	T=	14.00	SG=1.22470E-02			0	7	0	0	0	0	0	0	0	0	0	0	0	0	0	0	0	0	0	0	0	0	0	0

(Q)(COV)(QT) - LOCAL COORDINATE SYSTEM

3.489458E 03	-1.316612E 04	-5.187831E 03	1.067669E 01	-2.404859E 00	-2.183495E 00
-1.316612E 04	4.967724E 04	1.957427E 04	-4.028437E 01	9.073803E 00	8.238573E 00
-5.187831E 03	1.957427E 04	7.712829E 03	-1.587321E 01	3.575341E 00	3.246236E 00
1.067669E 01	-4.028437E 01	-1.587321E 01	3.266749E-02	-7.358147E-03	-6.680840E-03
-2.404859E 00	9.073803E 00	3.575341E 00	-7.358147E-03	1.657376E-03	1.504817E-03
-2.183495E 00	8.238573E 00	3.246236E 00	-6.680840E-03	1.504817E-03	1.366301E-03

SQRT((1,1)+(2,2)+(3,3)) = 2.4673778E 02
SQRT((4,4)+(5,5)+(6,6)) = 1.889210 5E-01
SQRT(1, 1) = 5.907163 3E 01
SQRT(2, 2) = 2.228839 3E 02
SQRT(3, 3) = 8.782271 5E 01
SQRT(4, 4) = 1.807414 9E-01
SQRT(5, 5) = 4.071088 9E-02
SQRT(6, 6) = 3.696351 3E-02

FIGURE 12

GROUP 5

					6X6	07 BI	08 US	09 ES	10 NS	11 VL	12 MU	13 CL	14 VA	15 UM	16 EM	17 NM	18 ED	19 ND	20 RM	21 AM	22 BS	23 RS	24 AS	25 L1	26 L2	27 L3	28 L4	29 L5	30 L6
DS 100	A	T=	-0	SG=1.00000E 00		0	0	0	0	0	0	0	0	7	0	0	0	0	0	0	0	0	0	0	0	0	0	0	0
DS 101	Q	T=	56.71	SG=1.00000E 00	*																								
DS 102	RD	T=	14.00	SG=1.22470E-02		0	0	7	0	0	0	0	0	0	0	0	0	0	0	0	0	0	0	0	0	0	0	0	0

(Q)(COV)(QT) = LOCAL COORDINATE SYSTEM

2.371568E 02	-8.952928E 02	-2.891172E 02	7.248149E-01	-1.635601E-01	-1.201451E-01
-8.952928E 02	3.379827E 03	1.091449E 03	-2.736255E 00	6.174572E-01	4.535609E-01
-2.891172E 02	1.091449E 03	3.524619E 02	-8.836196E-01	1.993957E-01	1.464686E-01
7.248149E-01	-2.736255E 00	-8.836196E-01	2.215228E-03	-4.998836E-04	-3.671958E-04
-1.635601E-01	6.174572E-01	1.993957E-01	-4.998836E-04	1.128026E-04	8.286059E-05
-1.201451E-01	4.535609E-01	1.464686E-01	-3.671958E-04	8.286059E-05	6.086628E-05

SQRT((1,1)+(2,2)+(3,3)) = 6.300353 8E 01
SQRT((4,4)+(5,5)+(6,6)) = 4.887634 8E-02
SQRT(1, 1) = 1.539989 7E 01
SQRT(2, 2) = 5.813628 0E 01
SQRT(3, 3) = 1.877396 8E 01
SQRT(4, 4) = 4.706621 4E-02
SQRT(5, 5) = 1.062085 9E-02
SQRT(6, 6) = 7.801684 8E-03

FIGURE 13.

GROUP 6

					6X6	07 BI	08 US	09 ES	10 NS	11 VL	12 MU	13 CL	14 VA	15 UM	16 EM	17 NM	18 ED	19 ND	20 RM	21 AM	22 BS	23 RS	24 AS	25 L1	26 L2	27 L3	28 L4	29 L5	30 L6
DS 100	A	T=	=0	SG=1.00000E 00		0	0	0	0	0	0	0	0	0	7	0	0	0	0	0	0	0	0	0	0	0	0	0	0
DS 101	Q	T=	56.71	SG=1.00000E 00	*																								
DS 102	RD	T=	14.00	SG=1.22470E-02		0	0	0	7	0	0	0	0	0	0	0	0	0	0	0	0	0	0	0	0	0	0	0	0

(Q)(COV)(QT) = LOCAL COORDINATE SYSTEM

8.541141E 00	-3.227297E 01	-7.638017E 00	2.607178E-02	-5.896948E-03	-3.079946E-03
-3.227297E 01	1.219445E 02	2.886049E 01	-9.851306E-02	2.228181E-02	1.163767E-02
-7.638017E 00	2.886049E 01	6.833888E 00	-2.331500E-02	5.273416E-03	2.754278E-03
2.607178E-02	-9.851306E-02	-2.331500E-02	7.958395E-05	-1.800040E-05	-9.401515E-06
-5.896948E-03	2.228181E-02	5.273416E-03	-1.800040E-05	4.071352E-06	2.126447E-06
-3.079946E-03	1.163767E-02	2.754278E-03	-9.401515E-06	2.126447E-06	1.110632E-06

SQRT((1,1)+(2,2)+(3,3)) = 1.171819E 01
SQRT((4,4)+(5,5)+(6,6)) = 9.206841E-03

SQRT(1, 1) = 2.922523E 00
SQRT(2, 2) = 1.042847E 01
SQRT(3, 3) = 2.613511E 00
SQRT(4, 4) = 8.920983E-03
SQRT(5, 5) = 2.017759E-03
SQRT(6, 6) = 1.053865E-03

FIGURE 14.

GROUP 7

					6X6	07 BI	08 US	09 ES	10 NS	11 VL	12 MU	13 CL	14 VA	15 UM	16 EM	17 NM	18 ED	19 ND	20 RM	21 AM	22 BS	23 RS	24 AS	25 L_1	26 L2	27 L3	28 L4	29 L5	30 L6
DS 100	A	T=	=0	SG=1,00000E 00		0	0	0	0	0	0	0	0	0	0	7	0	0	0	0	0	0	0	0	0	0	0	0	0
DS 101	Q	T=	56.71	SG=1,00000E 00	*																								
DS 103	RD	T=	14.00	SG=1,22470E-02		0	7	0	0	0	0	0	0	0	0	0	0	0	0	0	0	0	0	0	0	0	0	0	0

(Q)(COV)(QT) = LOCAL COORDINATE SYSTEM

7.730166E 02	-1.846245E 03	-9.228180E 02	1.669742E 00	-5.184089E-01	1.170499E 00
-1.846245E 03	4.409504E 03	2.204025E 03	-3.987951E 00	1.238149E 00	-2.795578E 00
-9.228180E 02	2.204025E 03	1.101649E 03	-1.993318E 00	6.188703E-01	-1.397328E 00
1.669742E 00	-3.987951E 00	-1.993318E 00	3.606699E-03	-1.119781E-03	2.528318E-03
-5.184089E-01	1.238149E 00	6.188703E-01	-1.119781E-03	3.476611E-04	-7.849731E-04
1.170499E 00	-2.795578E 00	-1.397328E 00	2.528318E-03	-7.849731E-04	1.772366E-03

SQRT((1,1)+(2,2)+(3,3)) = 7.9272754E 01
SQRT((4,4)+(5,5)+(6,6)) = 7.567513 6E-02
SQRT(1, 1) = 2.780317 6E 01
SQRT(2, 2) = 6.640409 6E 01
SQRT(3, 3) = 3.319109 9E 01
SQRT(4, 4) = 6.005579 7E-02
SQRT(5, 5) = 1.864567 1E-02
SQRT(6, 6) = 4.209948 2E-02

FIGURE 15

GROUP 8

					6X6	07 BI	08 US	09 ES	10 NS	11 VL	12 MU	13 CL	14 VA	15 UM	16 EM	17 NM	18 ED	19 ND	20 RM	21 AM	22 BS	23 RS	24 AS	25 L1	26 L2	27 L3	28 L4	29 L5	30 L6
DS 100	A	T=	-0	SG=1.00000E 00		0	0	0	0	0	0	0	0	0	0	0	7	0	0	0	0	0	0	0	0	0	0	0	0
DS 101	Q	T=	56.71	SG=1.00000E 00	*																								
DS 103	RD	T=	14.00	SG=1.22470E-02		0	0	7	0	0	0	0	0	0	0	0	0	0	0	0	0	0	0	0	0	0	0	0	0

(Q)(COV)(QT) - LOCAL COORDINATE SYSTEM

8.108778E 03	-1.924515E 04	-1.189862E 04	1.748916E 01	-5.433209E 00	1.142467E 01
-1.924515E 04	4.567592E 04	2.823986E 04	-4.150829E 01	1.289503E 01	-2.711500E 01
-1.189862E 04	2.823986E 04	1.745974E 04	-2.566316E 01	7.972557E 00	-1.676428E 01
1.748916E 01	-4.150829E 01	-2.566316E 01	3.772093E-02	-1.171844E-02	2.464093E-02
-5.433209E 00	1.289503E 01	7.972557E 00	-1.171844E-02	3.644706E-03	-7.654991E-03
1.142467E 01	-2.711500E 01	-1.676428E 01	2.464093E-02	-7.654991E-03	1.609652E-02

SQRT((1,1)+(2,2)+(3,3)) =	2.669165E 02
SQRT((4,4)+(5,5)+(6,6)) =	2.397038E-01
SQRT(1, 1) =	9.004875E 01
SQRT(2, 2) =	2.137192E 02
SQRT(3, 3) =	1.321353E 02
SQRT(4, 4) =	1.942187E-01
SQRT(5, 5) =	6.033630E-02
SQRT(6, 6) =	1.268720E-01

FIGURE 16.

GROUP 9

					6X6	07 BI	08 US	09 ES	10 NS	11 VL	12 MU	13 CL	14 VA	15 UM	16 EM	17 NM	18 ED	19 ND	20 RM	21 AM	22 BS	23 RS	24 AS	25 L1	26 L2	27 L3	28 L4	29 L5	30 L6
DS 100	A	T=	=0	SG=1.00000E 00		0	0	0	0	0	0	0	0	0	0	0	0	7	0	0	0	0	0	0	0	0	0	0	0
DS 101	Q	T=	56.71	SG=1.00000E 00	*																								
DS 103	RD	T=	14.00	SG=1.22470E=02		0	0	0	7	0	0	0	0	0	0	0	0	0	0	0	0	0	0	0	0	0	0	0	0

(Q)(COV)(QT) = LOCAL COORDINATE SYSTEM

6.357286E 00	-1.603258E 01	7.359728E 00	1.392935E-02	-4.295057E-03	1.531171E-02
-1.603258E 01	4.043292E 01	-1.856066E 01	-3.512875E-02	1.083180E-02	-3.861495E-02
7.359728E 00	-1.856066E 01	8.520239E 00	1.612579E-02	-4.972318E-03	1.772612E-02
1.392935E-02	-3.512875E-02	1.612579E-02	3.052040E-05	-9.410834E-06	3.354926E-05
-4.295057E-03	1.083180E-02	-4.972318E-03	-9.410834E-06	2.901790E-06	-1.034477E-05
1.531171E-02	-3.861495E-02	1.772612E-02	3.354926E-05	-1.034477E-05	3.687871E-05

SQRT((1,1)+(2,2)+(3,3)) = 7.437095E 00
SQRT((4,4)+(5,5)+(6,6)) = 8.384563E-03

SQRT(1, 1) = 2.521366E 00
SQRT(2, 2) = 6.3586889E 00
SQRT(3, 3) = 2.989448E 00
SQRT(4, 4) = 5.524527E-03
SQRT(5, 5) = 1.703464 2E-03
SQRT(6, 6) = 6.072784 2E-03

FIGURE 17.

GROUP 10

					6X6	07 BI	08 US	09 ES	10 NS	11 VL	12 MU	13 CL	14 VA	15 UM	16 EM	17 NM	18 ED	19 ND	20 RM	21 AM	22 BS	23 RS	24 AS	25 L1	26 L2	27 L3	28 L4	29 L5	30 L6
DS 100	A	T=	=0	SG=1.00000E 00		0	0	7	0	0	0	0	0	0	0	0	0	0	0	0	0	0	0	0	0	0	0	0	0
DS 101	Q	T=	56.71	SG=1.00000E 00		0	0	0	0	0	7	0	0	0	0	0	0	0	0	0	0	0	0	0	0	0	0	0	0
DS 101	RD	T=	14.00	SG=1.22470E-02		0	0	0	0	0	7	0	0	0	0	0	0	0	0	0	0	0	0	0	0	0	0	0	0
DS 102	RD	T=	14.00	SG=1.22470E-02		0	0	0	0	0	7	0	0	0	0	0	0	0	0	0	0	0	0	0	0	0	0	0	0
DS 103	RD	T=	14.00	SG=1.22470E-02		0	0	0	0	0	7	0	0	0	0	0	0	0	0	0	0	0	0	0	0	0	0	0	0

(Q)(COV)(QT) - LOCAL COORDINATE SYSTEM

4.126331E 04	-9.672739E 04	1.699389E 04	9.703086E 01	-4.967601E 01	4.587674E 00
-9.672739E 04	2.267435E 05	-3.983625E 04	-2.274549E 02	1.164480E 02	-1.075420E 01
1.699389E 04	-3.983625E 04	6.998765E 03	3.996122E 01	-2.045858E 01	1.889389E 00
9.703086E 01	-2.274549E 02	3.996122E 01	2.281685E-01	-1.168134E-01	1.078794E-02
-4.967601E 01	1.164480E 02	-2.045858E 01	-1.168134E-01	5.980387E-02	-5.523002E-03
4.587674E 00	-1.075420E 01	1.889389E 00	1.078794E-02	-5.523002E-03	5.100601E-04

SQRT((1,1)+(2,2)+(3,3)) =	5.244097 8E 02
SQRT((4,4)+(5,5)+(6,6)) =	5.371056 1E-01
SQRT(1, 1) =	2.031337 2E 02
SQRT(2, 2) =	4.761759 5E 02
SQRT(3, 3) =	8.365862 3E 01
SQRT(4, 4) =	4.776698 7E-01
SQRT(5, 5) =	2.445482 9E-01
SQRT(6, 6) =	2.258450 9E-02

FIGURE 18

TOTAL

PARAMETERS IN COLUMNS 1- 6 UPDATED -- OTHER PARAMETERS NOT UPDATED

(Q)(COV)(QT) - LOCAL COORDINATE SYSTEM

6.419663E 04	-1.768090E 05	2.735336E 02	1.628617E 02	-6.533743E 01	2.802917E 00
-1.768090E 05	5.409992E 05	7.296315E 03	-4.794561E 02	1.716292E 02	4.736883E 01
2.735336E 02	7.296315E 03	1.616323E 05	-3.686548E 00	-9.286016E 00	4.995291E 01
1.628617E 02	-4.794561E 02	-3.686548E 00	4.313642E-01	-1.620710E-01	-2.906220E-02
-6.533743E 01	1.716292E 02	-9.286016E 00	-1.620710E-01	7.051168E-02	-3.718293E-03
2.802917E 00	4.736883E 01	4.995291E 01	-2.906220E-02	-3.718293E-03	1.104230E-01

SQRT((1,1)+(2,2)+(3,3)) = 8.756871 9E 02
SQRT((4,4)+(5,5)+(6,6)) = 7.824952 6E-01

SQRT(1, 1) =	2.533705 4E 02
SQRT(2, 2) =	7.355264 5E 02
SQRT(3, 3) =	4.020351 6E 02
SQRT(4, 4) =	6.567832 0E-01
SQRT(5, 5) =	2.655403 6E-01
SQRT(6, 6) =	3.322995 3E-01

PRINCIPAL POSITION UNCERTAINTIES		PRINCIPAL VELOCITY UNCERTAINTIES	
1ST AXIS = 7.742839E 02	PHI = 1.082919E 02	1ST AXIS = 7.037047E-01	PHI = 1.586230E 02
2ND AXIS = 4.019540E 02	CHI = -8.906294E 01	2ND AXIS = 3.325161E-01	CHI = -9.770491E 01
3RD AXIS = 7.579904E 01	PSI = 1.791046E 02	3RD AXIS = 8.081820E-02	PSI = 1.761239E 02

FIGURE 19.

(Q)(COV)(QT) - LOCAL COORDINATE SYSTEM

6.419663E 04	-1.768090E 05	2.735336E 02	1.628617E 02	-6.533743E 01	2.802917E 00
-1.768090E 05	5.409992E 05	7.296315E 03	-4.794561E 02	1.716292E 02	4.736883E 01
2.735336E 02	7.296315E 03	1.616323E 05	-3.686548E 00	-9.286016E 00	4.995291E 01
1.628617E 02	-4.794561E 02	-3.686548E 00	4.313642E-01	-1.620710E-01	-2.906220E-02
-6.533743E 01	1.716292E 02	-9.286016E 00	-1.620710E-01	7.051168E-02	-3.718293E-03
2.802917E 00	4.736883E 01	4.995291E 01	-2.906220E-02	-3.718293E-03	1.104230E-01

MISS TIME = 2.476520E 01 MINIMUM MISS = 4.752145E 02 REND MISS = 8.756871E 02

SQRT((2,2)+(3,3)) =	8.382311E 02
SQRT((4,4)+(5,5)+(6,6)) =	7.824952E-01
SQRT(1, 1) =	2.533705E 02
SQRT(2, 2) =	7.355264E 02
SQRT(3, 3) =	4.020351E 02
SQRT(4, 4) =	6.567832E-01
SQRT(5, 5) =	2.655403E-01
SQRT(6, 6) =	3.322995E-01

PRINCIPAL POSITION UNCERTAINTIES			PRINCIPAL VELOCITY UNCERTAINTIES		
1ST AXIS = 7.742839E 02	PHI = 1.082919E 02		1ST AXIS = 7.037047E-01	PHI = 1.586230E 02	
2ND AXIS = 4.019540E 02	CHI = -8.906294E 01		2ND AXIS = 3.325161E-01	CHI = -9.770491E 01	
3RD AXIS = 7.579904E 01	PSI = 1.791046E 02		3RD AXIS = 8.081820E-02	PSI = 1.761239E 02	

FIGURE 20.

The Bissett-Berman Corporation 2941 Nebraska Avenue, Santa Monica, California EXbrook 4-3270

APOLLO NOTE NO. 405

(Task III)

L. Bonin
25 March 1966

ACCURACY ACHIEVED BY EMPLOYING AN OPTIMUM FILTER FOR PROCESSING TRACKING DATA DURING APOLLO LUNAR MISSIONS

During lunar missions, the Unified S-band Systems (USBS) provide tracking information for determining the ephemeris of the Apollo spacecraft. The real time orbit determination program presently being planned by MSC for use during these missions will utilize the tracking data to estimate the orbit parameters and an artificial bias in the measurables. While this filter provides more accurate results than one in which only the orbit parameters are estimated, it is not the optimum filter. For an optimum filter, the tracking data is used to estimate all parameters that have an appreciable effect on the spacecraft's ephemeris. This Note presents the accuracy obtained with an optimum filter during the translunar and circular lunar orbit phases of the Apollo mission.

After the Apollo spacecraft is injected into the translunar orbit, Doppler tracking data are obtained from USBS stations. While the spacecraft is in a low altitude earth orbit, it is usually visible to only one station at a time and only for a short period of time. In order to obtain a good estimate of the spacecraft's orbit at the time of translunar injection, range and angle tracking data are obtained from C-band radar sites.

During the earth orbit phase, the spacecraft is assumed to be in a 100 n. mi. circular orbit, inclined 30° to the equator. The spacecraft is initially located at a latitude of 28.5°N and a longitude of 80.6°N. For the first 6 minutes of flight, it is visible to the Bermuda tracking station. From 48 to 52 minutes, it is visible to the Carnarvon station; and, from 94 to 99 minutes, it is again visible to the Bermuda station. Range and angle tracking data obtained at one

minute sample rates are used to predict the spacecraft's ephemeris at the end of 2 1/2 orbits when translunar injection is initiated.

The C-band tracking data are assumed to be corrupted by noise with an uncertainty of 45 feet in range and of 0.25 milliradians in each angle. The nuisance parameters included in this study are biases on the range and angle measurables, station location uncertainties, clock rate uncertainties, and clock acceleration uncertainties. The assumed a priori uncertainties are:

Station Location	180 ft each axis
Clock Rate	10^{-10} sec/sec
Clock Acceleration	10^{-10} parts/part/hr

No a priori knowledge is assumed on either the orbit parameters or the measurable biases.

Table 1 shows the RMS position and velocity uncertainties that result when the tracking data are used to predict the ephemeris of the spacecraft at the end of 2 1/2 orbits. Two data processing schemes are illustrated. In the first case, the tracking information is used to estimate only the orbit parameters and the measurable biases. In the second case, all parameters are estimated. The accuracies obtained when all parameters are estimated are used as the a priori uncertainties at initiation of translunar injection.

During Apollo translunar flight, tracking data are obtained from the USBS stations at Antigua, Bermuda, Ascension and Madrid. Both three-way Doppler and range data are processed. At large distances from either the Earth or the Moon, range-rate data provide a good estimate of only the velocity of the spacecraft; range data are required to obtain position estimates. For the Doppler data, tracking was switched from Bermuda to Madrid and back to Bermuda to improve the station to spacecraft geometry. Range data from Antigua, Bermuda, and Ascension are included to improve the

estimate of the spacecraft's position as it traveled away from the Earth. A sample rate of 1 minute and 1 hour is used for the Doppler and range measurements, respectively.

The flight time of the cislunar trajectory used in this analysis is approximately 64 hours. The Apollo spacecraft is injected into orbit at a latitude of 28° N and a longitude of 133° W. In the Earth's sphere of influence, the orbit is inclined 32° to the equator.

Table 2 shows the predicted Apollo RMS position and velocity uncertainties from 2 hours after translunar injection until pericynthion. For these results, the tracking data are processed to estimate all appreciable nuisance parameters. The nuisance parameters, and their assumed a priori knowledge, applicable to both the range and range-rate measurements are:

Station Location	100 ft each axis
Earth Gravitation Constant	10^{11} ft^3/sec^2
Moon Gravitational Constant	3×10^{9} ft^3/sec^2
Clock Offset	10^{-3} sec
Clock Rate	10^{-10} sec/sec

In addition, a bias uncertainty of 30 feet was assumed for the range measurements. No bias is assumed for the range-rate measurable, but the clock rate parameter is very similar. The estimated noise on the range and range-rate measurements is 15 feet and 0.006 feet per second, respectively.

Tracking data on the Apollo spacecraft are obtained during the first 8 hours of flight in the Earth's sphere of influence and throughout the flight phase in the Lunar sphere of influence. The sample rate is 1 minute for the Doppler data and 1 hour for the range data.

When the stay on the lunar surface is completed, the LEM vehicle ascends to a low altitude lunar orbit. Rendezvous with the Apollo Command Module occurs after the LEM completes approximately one revolution in the parking orbit. An analysis was conducted to determine the accuracy provided by USBS tracking when an optimum data processing filter is employed. The parking orbit for the LEM vehicle is circular at an altitude of 60 n. mi. and at an inclination of 180° to the lunar equator. At insertion into the parking orbit, the LEM is located on the earth-moon line.

Table 3 shows the LEM RMS position and velocity accuracy achieved during the first revolution in the parking orbit. These accuracies are obtained by optimumly processing the USBS Doppler tracking data. The tracking stations employed are Madrid, Ascension, and Carnarvon. No tracking information is obtained from 30 to 90 minutes after insertation because of occultation by the Moon. The a priori uncertainties of the parameters considered in this study are:

LEM Position	0.5 n. mi. each axis
LEM Velocity	3 fps each axis
Station Location	100 ft. each axis
Moon Gravitational Constant	3×10^{9} ft^3/sec^2
Clock Offset	10^{-3} sec
Clock Rate	10^{-10} sec/sec

No bias was considered for the Doppler measurements, but clock rate uncertainties have a similar effect. The Doppler noise is assumed to be 0.006 fps for 1 minute sample.

While the accuracies presented here are based on an optimum processing of tracking data, they are somewhat pessimistic because they ignore the negative correlation inherent in the noise of Doppler

data. Even though these results are better than estimates that do not include the important nuisance parameters, including the effect of correlated noise will provide a substantial improvement.

TABLE I

Apollo RMS Uncertainty After 2 1/2 Earth Orbits

	Position (ft)	Velocity (fps)
Orbit parameters and measurable bias updated	900	1.5
All parameters updated	600	1.2

TABLE 2

Apollo RMS Uncertainty During Translunar Flight

(All parameters updated)

Time From Initiation of Translunar Boost (hr)	Position (ft)	Velocity (fps)
2	1,020	0.12
8	1,060	0.026
LSOI	2,940	0.008
1 Hour before Perilune	1,412	0.044
Perilune	1,043	0.007

TABLE 3

LEM RMS Uncertainty in Lunar Orbit

(All parameters updated)

Time From LEM Ascent Burnout (min)	Position (ft)	Velocity (fps)
15	1,370	2.4
30	1,310	0.87
90	1,310	0.98
105	832	0.54
120	232	0.83

The Bissett-Berman Corporation 2941 Nebraska Avenue, Santa Monica, California EXbrook 4-3270

APOLLO NOTE NO. 406
(Task I, Item II)

H. Epstein
14 February 1966

HIGH FREQUENCY CHARACTERISTICS OF MARINER IV DOPPLER RESIDUALS

A theoretical model for error sources with correlation time less than about 100 seconds has been established from prior doppler measurement data. A number of sets of Mariner IV doppler measurement data has been employed to verify the validity of this model. This model accounts for three error sources. The nature of these error sources for doppler counting intervals equal to or greater than one second will be indicated.

The measurable will be treated here as the difference in successive doppler counts divided by the count time. This quantity most correctly represents the average doppler frequency but will be referred to as the doppler frequency for simplicity. The analysis treats the residuals in counts per second or cycles per second (cps) for convenience in analysis.

One error source is associated with the quantization error present in doppler counting techniques. This error may be treated as a random count error in accumulated doppler for each counter reading. The analysis for this type of quantization error and more sophisticated model are indicated in Apollo Notes 203 and 225. This error source may be considered as a random count error, a random phase error, or a random range error. These representations involve only simple scale factors for conversion.

The variance and correlation function for the frequency error is given below as:

$$\phi_q(o) = 2\left(\frac{K_q}{MT}\right)^2 \qquad (1)$$

$$\rho_q(rT) = 1 \qquad r = o \qquad (2a)$$

$$= -1/2 \qquad |r| = 1 \qquad (2b)$$

$$= 0 \qquad |r| > 1 \qquad (2c)$$

where

$\phi_q(o) = \sigma_q^2$ = variance - $(cps)^2$

$K_q = \frac{1}{\sqrt{12}}$ = standard deviation of the counter error - (counts)

m = quantization error reduction factor

T = count time - (seconds)

$\rho(rT)$ = normalized autocorrelation function

r = any integer including zero

The second error source to be considered is a random count component. The nature of this error is similar to random quantization error and is given as:

$$\phi_1(o) = 2\left(\frac{K_1}{T}\right)^2 \tag{3}$$

$$\rho_1(rT) = 1 \qquad r = o \tag{4a}$$

$$= -1/2 \qquad |r| = 1 \tag{4b}$$

$$= o \qquad |r| \geq 1 \tag{4c}$$

where

$\phi_1(o)$ = variance - $(cps)^2$

K_1 = standard deviation of the error - (counts)

$\rho_1(rT)$ = normalized autocorrelation function

The final source of errors to be considered is associated with portions of the Earth-based equipment which generate critical frequencies and are common to both the transmitter and receiver in a two-way

doppler mode. The primary units involved are the atomic frequency standard, the frequency synthesizer, and appropriate isolation amplifiers. This error source is considered to arise from white frequency noise on the critical frequencies. The associated two-way and three-way errors must be represented in different fashions. The nature of the associated three-way frequency error will be given first.

$$\phi_3(o) = \frac{K_3^2}{T} = \frac{K_{3-T}^2 + K_{3-R}^2}{T} \tag{5}$$

$$\rho_3(rT) = 1 \qquad r = o \tag{6a}$$

$$= o \qquad |r| \geq 1 \tag{6b}$$

where

$\phi_3(o)$ = variance - $(cps)^2$

K_{3-T} = quality factor related to the transmitter stability - $(cycles/\sqrt{sec})$

K_{3-R} = quality factor related to the receiver stability - $(cycles/\sqrt{sec})$

$K_3 = \sqrt{K_{3-T}^2 + K_{3-R}^2}$ = equivalent quality factor - $(cycles/\sqrt{sec})$

The two-way performance must be indicated by a more complex model since the transmitter noise is a time delayed version of the received noise for this component. The delay is given by the round-trip transit time. The variance can be shown to be of the following form:

$$\phi_2(o) = \frac{K_2^2 \tau_d}{T^2} \qquad o \leq \tau_d \leq T \tag{7a}$$

$$= \frac{K_2^2}{T} \qquad \tau_d \geq T \tag{7b}$$

where

$\phi_2(o)$ = variance - $(cps)^2$

K_2 = quality factor - $(cycles/\sqrt{sec})$

τ_d = round-trip transit time - (seconds)

For the sake of simplicity, the normalized autocorrelation function $\left|\rho_2(rT)\right|$ will be indicated only for the transit time equal to or less than the count time and for the transit time an integer multiple of the count time

$$\text{for } \tau_d \leqslant T, \quad \rho_2(rT) = -1/2 \qquad |r| = 1 \tag{8a}$$

$$= o \qquad |r| \geqslant 1 \tag{8b}$$

$$\text{for } \tau_d > T, \quad \rho_2(rT) = -1/2 \qquad |r| = \frac{\tau_d}{T} \tag{9a}$$

$$= o \qquad |r| \neq \frac{\tau_d}{T} \tag{9b}$$

The combination of these three error sources will now be shown to be consistent with Mariner IV measurement data. For the Mariner IV data analyzed, the transit time is long as compared to the count time. The appropriate variance and autocorrelation function is then given by the following equations for the transit time an integral multiple of the count time.

$$\phi_n(o) = 2\left(\frac{K_q}{MT}\right)^2 + 2\left(\frac{K_1}{T}\right)^2 + \frac{K_2^2}{T} \tag{10}$$

$$\phi_n(T) = -\left(\frac{K_q}{MT}\right)^2 - \left(\frac{K_1}{T}\right)^2 \tag{11}$$

$$\phi_n(\tau_d) = -\frac{K_2^2}{2T} \tag{12}$$

$$\phi_n(rT) = o \qquad r \neq 1, \frac{\tau_d}{T} \tag{13}$$

Equations (12) and (13) must be modified for the more general situation with τ_d not an integer multiple of T. The replacement equations are as follows:

for $mT \leq \tau_d \leq (m+1)\,T$ and m a position integer 2 or greater

$$\phi_n(mT) = -\frac{K_2^2}{2T}\left(m+1-\frac{\tau_d}{T}\right) \tag{14}$$

$$\phi_n(mT+\tau) = \frac{K_2^2}{2\tau}\left(\frac{\tau_d}{T}-m\right) \tag{15}$$

$$\phi_n(rT) = o \qquad r \neq 1,\ m,\ m+1 \tag{16}$$

In addition, it should be noted that similar to Eq. (12)

$$\phi_n(mT) + \phi_n(mT+\tau) = \frac{-K_2^2}{2T} \tag{17}$$

The quantization error parameters K_q and m do not need to be determined since the values are well established. As a consequence, only the parameters K_1 and K_2 are required. τ_d may be estimated but far better estimates are available from the ODP. Although the quantization error does not need to be estimated from residual data, the variance in the quantization error can prevent accurate determination of K_1 and K_2. Quantization reduction techniques are necessary to accurately determine K_1 and K_2. This can be understood better by an examination of Figure 1. Figure 1 indicates separately the standard deviation for typical values of K_q, m, K_1, and K_2. Since σ_q and σ_1 have the same characteristics, the variance in the quantity error component must be made small as compared to random phase noise. Quantization reduction with m = 8 is adequate for this purpose. This value also allows K_2 to be determined from data sets greater than about 15-20 minutes for sample periods of one and six seconds.

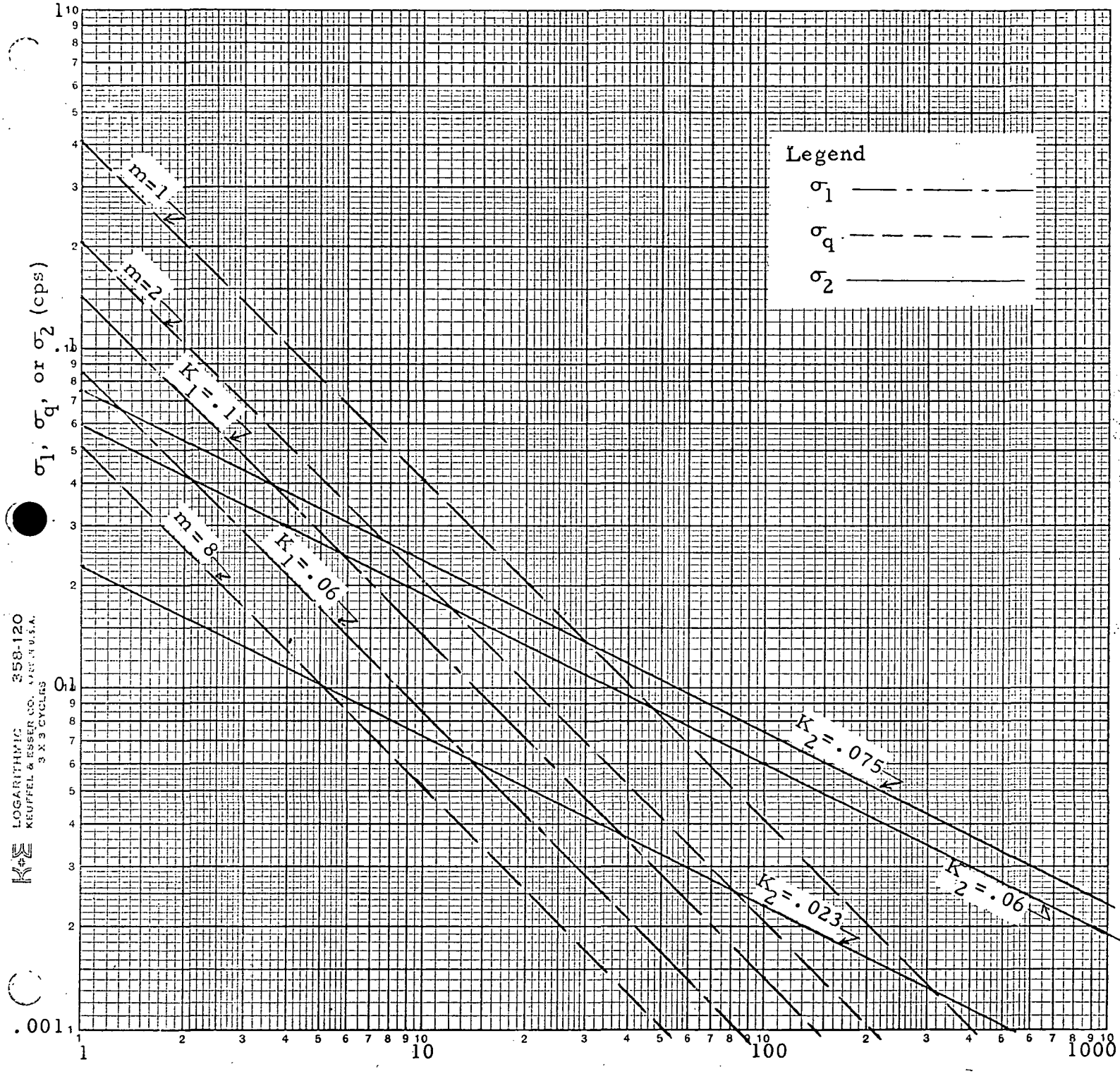
Legend
σ_1
σ_q
σ_2
m=1
m=2
m=8
K_1 = .1
K_1 = .06
K_2 = .075
K_2 = .06
K_2 = .023
σ_1, σ_q, or σ_2 (cps)
Count Time (seconds)
1
10
100
1000
.001
.01
.1
LOGARITHMIC
KEUFFEL & ESSER CO.
3 X 3 CYCLES
358-120

Figure 1.

The data employed for the determination of K_1 and K_2, and the estimates and variances in the quantities

$$\hat{\phi}_1 = \hat{K}_1^2 + .0013 \text{ and } \hat{\phi}_2 = \hat{K}_2^2$$

are tabulated in Figure 2. It should be noted that the estimates have an error with standard deviation of about 10 percent of the nominal value.

The equations to indicate the three-way doppler performance are simplier in nature. The correlation function is indicated below (K_2 is used in place of K_3 to simplify terminology in the comparison)

$$\phi_n(o) = 2\left(\frac{K_q}{mT}\right)^2 + 2\left(\frac{K_1}{T}\right)^2 + \frac{K_2^2}{T} \tag{18}$$

$$\phi_n(T) = -\left[\left(\frac{K_q}{mT}\right)^2 + \left(\frac{K_1}{T}\right)^2\right] \tag{19}$$

$$\phi_n(rT) = o \qquad r \neq o, 1 \tag{20}$$

The data employed to determine the parameters K_1 and K_2 for the five segments of three-way doppler measurement data and one segment of two-way doppler measurement data with a count time of six seconds are indicated in Figure 3. A summary of the primary results of the analysis is also indicated. For convenience,

$$\hat{\phi}_1 = 64\,(\hat{K}_1^2 + .0013)$$

and

$$\hat{\phi}_2 = 384\,\hat{K}_2^2 .$$

Experimental Basis for High Frequency Noise Model

Case	Date	Beginning GMT	Final GMT	No. of Points Used	No. of Missing Points	Total No.	Bias ($\dot{R}$) cps	Bias ($\dot{R}$) cm/sec
1-1-A	4-1-65	22:39:45	22:59:59	1199	16	1215	-.0267	-.174
B	4-2-65	09:40:03	10:00:01	1193	6	1199	-.0409	-.266
1-2-A	4-5-65	04:09:33	04:29:06	1162	12	1174	-.0103	-.067
B	4-5-65	09:32:02	09:51:59	1184	14	1198	-.0371	-.242
1-3-A	4-7-65	04:04:24	04:24:18	1173	22	1195	-.4384	-2.86
B	4-7-65	09:29:24	09:24:06	1164	19	1183	-.1249	-.815

$$\hat{\phi}_1 = \hat{K}_1^2 + .0013$$

$$\hat{\phi}_2 = \hat{K}_2^2$$

Case	$\phi_n(o)$ $(\text{counts})^2$	$\rho_N(T)$	$\hat{\phi}_1 \times 10^4$ $(\text{counts})^2$	$\Delta\phi_1 \times 10^4$ $(\text{counts})^2$	$\sqrt{\phi_1}$ counts	$\sqrt{\phi_1}$ $\dot{R}$ (cm)	$\hat{\phi}_2 \times 10^4$ $(\text{cps})^2$	$\Delta\phi_2 \times 10^4$ $(\text{cps})^2$	$\sqrt{\phi_2}$ cps	$\sqrt{\phi_2}$ $\frac{\dot{R}_1 + \dot{R}_2}{2}$ cm/sec
1-1-A	.0136	-.359	48.9	4.4	.070	.46	38.6	6.4	.062	.41
B	.0136	-.308	41.9	4.4	.065	.42	52.2	6.4	.072	.47
1-2-A	.0140	-.319	44.8	4.6	.067	.44	50.6	6.6	.071	.46
B	.0135	-.295	39.8	4.4	.063	.41	55.2	6.2	.074	.49
1-3-A	.0131	-.311	40.9	4.3	.064	.42	49.7	6.2	.071	.46
B	.0129	-.289	37.4	4.0	.061	.40	54.4	5.7	.074	.48

Figure 2. Mariner IV One-Second Count Time Two-Way Doppler Residuals (from ODP)

Case	Doppler	Date	Beginning GMT	Final GMT	No. of Points Used	No. of missing Pts	Total No.	$\phi_n(o)$ (counts)^2	$\rho_N(T)$
6-1-A	3-Way	4-2-65	22:51:25	23:08:55	175	0	175	1.332	-.021
B	3-Way		23:09:25	23:25:01	156	0	156	2.064	-.328
6-2-A	3-Way	4-4-65	06:47:06	07:02:06	150	0	150	2.264	-.289
B	3-Way		07:10:42	08:14:48	633	8	641	2.152	-.199
C	3-Way		08:43:24	09:16:06	323	4	327	2.437	-.280
6-3	2-Way	4-5-65	06:35:43	08:24:43	1090	0	1090	2.502	-.123

$$\phi_1 = 64\,(K_1^2 + .0013)$$

$$\phi_2 = 384\,K_2^2$$

Case	m	$\hat{\phi}_1$ (counts)^2	$\Delta\phi_1$ (counts)^2	$\frac{1}{m}\sqrt{\phi_1}$ counts	$\frac{1}{m}\sqrt{\phi_1}$ $\dot{R}$ cm	$\hat{\phi}_2$ (counts)^2	$\Delta\phi_2$ (counts)^2	$\frac{1}{mT}\sqrt{\phi_2}$ cps	$\frac{\dot{R}_1+\dot{R}_2}{2}$ cm/sec	$K_2^2 \times 10^4$ (counts)^2/sec
6-1-A	8	.028	.101	.0208	.14	1.276	.237	.0235	.154	33.1
B	8	.677	.190	.103	.67	.710	.263	.0175	.115	18.5
6-2-A	8	.654	.206	.102	.66	.956	.304	.0203	.133	24.8
B	8	.428	.091	.0818	.53	1.296	.158	.0237	.155	33.7
C	8	.682	.108	.104	.67	1.073	.208	.0215	.141	27.9
6-3	8	.307	.077	.0693	.45	1.888	.156	.0286	.187	49.0

Figure 3. Mariner IV Six-Second Count Time Doppler Residuals (from Raw Measurement Data)

For Case 6-1-A the standard deviation in the error of ϕ_1 is greater than the quantity estimated. As a consequence, the estimated value is only significant to the extent of being small. Due to the small sample size, the three-way coefficients have greater variance than the two-way 6 second data (Case 6-3) or the two-way one second data.

A summary of the experimental value of K_1^2 and K_2^2 is indicated in Figure 4. K_1^2 varies from about .0024 to .0036 (K_1 variation from about .05-.06) for all the two-way data and K_2^2 varies from about .0039 - .0055 (K_2 variation from about .063-.075). K_1^2 is somewhat larger for the three-way data while K_2^2 is somewhat smaller. This presumably reflects differences in the equipment at the various sites involved.

Figure 5 lists the highest values found for two-way and three-way performance. These numbers should be used for conservative error analyses.

The two-way expressions indicate that a correlated component should exist at a lag near the transit time. Table 6 indicates that such a component exists and that crude estimates of transit can be obtained by this technique as predicted by the theory.

Case	ϕ_1 (counts)^2	K_1^2 (counts)^2	K_2^2 counts^2/sec
1-1-A	.0049	.0036	.0039
B	.0042	.0029	.0052
1-2-A	.0045	.0032	.0051
B	.0040	.0027	.0055
1-3-A	.0041	.0028	.0050
B	.0037	.0024	.0054

Count Time = 1 Second

Case	$\hat{\phi}_1$ (counts)^2	$\frac{1}{64}\hat{\phi}_1$ (counts)^2	K_1^2 (counts)^2	K_2^2 (counts)^2/sec
6-1-A	.028	.0004	———	.0033
B	.677	.0106	.0093	.0019
6-2-A	.654	.0102	.0089	.0025
B	.428	.0067	.0054	.0034
C	.682	.0107	.0094	.0028
6-3	.307	.0048	.0035	.0049

Count Time = 6 Seconds

Figure 4. Experimental Values of K_1^2 and K_2^2 from Mariner IV Data

Experimental Nature of Predominant Mariner IV High Frequency Measurement Errors

$$\phi_n(o) = \sigma^2 = \frac{\left(K_1^2 + K_q^2\right)}{T^2} + \frac{K_2^2}{T}$$

Present Mariner IV Highest Values

	Two-Way	Three-Way
K_1 (cycles)	.06	.1
K_q (cycles)	$\frac{1}{m\sqrt{12}}$	$\frac{1}{m\sqrt{12}}$
K_2 (cycles/$\sqrt{\text{sec}}$)	.075	.075

Values for Parameters

	Two-Way		Three-Way	
	(cps)	(cm/sec) $\dot{R}$	(cps)	(cm/sec) $\frac{\dot{R}_1 + \dot{R}_2}{2}$
K_2	.075	.49	.075	.49
$K_1\sqrt{2}$	.085	.55	.14	.93
$K_q\sqrt{2}$	.408	2.66	.408	2.66
$\frac{K_q\sqrt{2}}{2}$	.204	1.33	.204	1.33
$\frac{K_q}{8}\sqrt{2}$	.051	.33	.051	.33

Noise Components for One-Second Count Time

Figure 5.

Case	$\hat{\tau}_d$ (sec)	$\Delta\hat{\tau}_d$ 1-2-A as Ref (sec)	Date	Mean GMT	Δt 1-2-A Ref (hrs)	$\Delta\tau_d$ * (sec)	$\Delta\tau_d - \Delta\hat{\tau}_d$ (sec)
1-1-A	477	-26	4-1-65	22:49:52	-77.5	-25.8	+.2
B	481	-22	4-2-65	09:50:03	-66.5	-22.2	-.2
1-2-A	503	0	4-5-65	04:19:20	0	0	0
B	505	2	4-5-65	09:42:01	5.4	1.8	-.2
1-3-A	519	16	4-7-65	04:14:21	47.9	16.0	0
B	520	17	4-7-65	09:39:15	53.3	17.7	.7
6-3	504	1	4-5-65	07:30:43	2.3	.8	-.2

Case	$\phi(\hat{\tau}_d - T) \times 10^4$ $(c)^2$	$\phi(\tau_d) \times 10^4$ $(c)^2$	$\phi(\hat{\tau}_d + T) \times 10^4$ $(c)^2$	$\hat{\phi}_2 \times 10^4$ $(c)^2$	$\frac{\phi(\hat{\tau}_d)}{\hat{\phi}_2}$	$\frac{\phi(\hat{\tau}_d)}{\hat{\phi}_2} + \frac{1}{2}$
1-1-A	11.1	-20.3	-8.2	38.6	-.53	-.03
B	4.5	-34.1	-.5	52.2	-.65	-.15
1-2-A	-11.6	-21.9	5.3	50.6	-.43	.07
B	-4.1	-14.1	-.8	55.2	-.26	.24
1-3-A	-3.8	-24.1	.5	49.7	-.48	.02
B	3.2	-27.5	-1.1	54.4	-.50	0
6-3	1230	-10,370	1180	18,880	-.55	-.05

Figure 6. Experimental Verification of Critical High Frequency Mariner IV Noise

*For $\frac{\Delta\tau_d}{\Delta t} = \frac{1}{3}$ sec/hr for $\dot{R}$ = 15 km/sec

The Bissett-Berman Corporation 2941 Nebraska Avenue, Santa Monica, California EXbrook 4-3270

APOLLO NOTE NO. 407
(Task II, Item II)

L. S. Lustick
4 February 1966

VISIBILITY AND MASTER MEASURABLE CHANGES

PURPOSE

The purpose of this note is to describe the following two changes that are being made in the Orbit Error Analysis Program.

1. The Orbit Error Analysis Program will automatically exclude data where the elevation angle from any station involved in the particular measurable is less than 5° or the vehicle is occluded by the Moon. This visibility provision can be overridden by an input control constant on the data sheet.

2. The range-rate measurable for a master station has been changed as follows:

Previously	Changed Version
$M = \dot{R}(t) + b + n(t)$	$M = 2\dot{R}(t) + b + n(t)$
where b = one way bias	b = two way bias
n(t) = one way noise	n(t) = two way noise

VISIBILITY CONSIDERATIONS

The elevation angle is calculated at each time for every station involved in the measurable. For example, for a slave station range-rate measurable, the elevation angle for the slave and the master is calculated if either of these are less than 5°, the point is excluded from the information matrix and a printout indicated the stations and the time excluded is provided. For measurables only involving one station, (range and angle information) the elevation angle for this station is checked and if below 5°, the point is excluded.

In addition to exclusion because of elevation angle, a point may be excluded because of occlusion by the Moon.

If the input defining Earth-Moon distance (R HOM) is within 7-1/2% of the mean Earth-Moon distance, the orbit is considered about the Moon and possible exclusion by the Moon is checked. Each station involved in the measurable is checked and if the vehicle is occluded by the Moon from any station, the point is excluded and a printout to this effect is provided.

The Moon occlusion calculation is indicated below:

X'_S = vector from station-to-vehicle in prime system

X' = vector from center of Moon to vehicle in prime system

S = magnitude of $\overrightarrow{X'_S}$

r = magnitude of $\overrightarrow{X'}$

r_m = radius of Moon

$$X'_S = \begin{bmatrix} x'_S \\ y'_S \\ z'_S \end{bmatrix}$$

$$X' = \begin{bmatrix} x' \\ y' \\ z' \end{bmatrix}$$

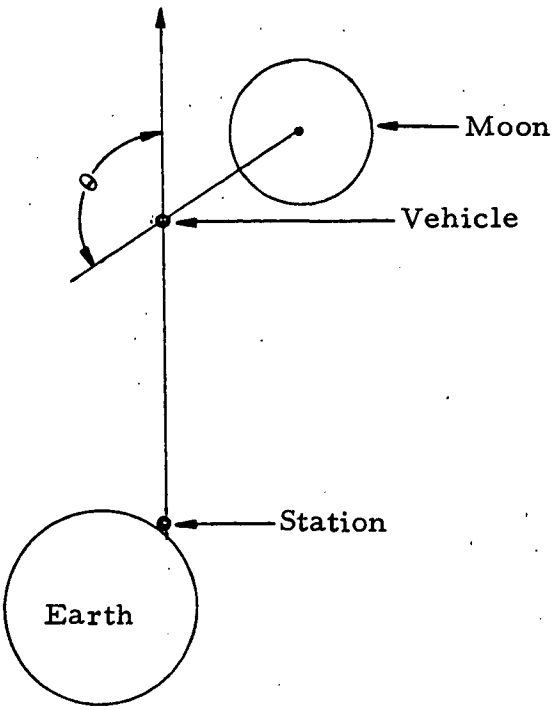

$$X'_S \cdot X' = |X'_S| \cdot |X'| \cos\theta = x'_S x' + y'_S y' + z'_S z'$$

$$\cos\theta = \frac{x'_S x' + y'_S y' + z'_S z'}{s \cdot r}$$

if,

$\cos\theta > 0$		$\cos\theta = 0$	$\cos\theta < 0$
$\sin\theta = +\sqrt{1 - \cos^2\theta}$		include point	include point
$\ell = r \sin\theta$			
if			
$\ell \geq r_m$	$\ell < r_m$		
include point	don't include point and printout occluded by Moon		

CHANGE IN $\dot{R}$ INFORMATION MATRIX FOR MASTER

The measurable in range-rate mode for a master was previously considered as $\dot{R}$ (one-way doppler) and the bias and the noise in the measurable were (one way).

That is,

$$M = R(\tau) + b + n(t)$$

where

b = two way bias

$n(t)$ = two way noise

This is now being changed to be handled similarly to a slave.

$$M = (2\dot{R}) + b + n(t)$$

where

b = two way bias

$n(t)$ = two way noise

The information matrix for a master (measurable range-rate) is as follows:

$$(C_{ij})_{\text{master}} = \frac{1}{\sigma_m^2} \begin{bmatrix} \sum \frac{\partial M}{\partial a_1}\frac{\partial M}{\partial a_1} & \cdots & \frac{\partial M}{\partial a_1}\frac{\partial M}{\partial a_6} & \frac{\partial M}{\partial a_1}\frac{\partial M}{\partial b} & \cdots & \frac{\partial M}{\partial a_1}\frac{\partial M}{\partial a_m} \\ & & & \vdots & & \\ & & & \sum \frac{\partial M}{\partial b}\frac{\partial M}{\partial b} & & \end{bmatrix}$$

where

$$\frac{\partial M}{\partial a_j} = 2\,\frac{\partial \dot{R}}{\partial a_j} \qquad \text{where } a_j \neq b$$

$$\frac{\partial M}{\partial b} = 1$$

σ_m^2 = two way noise (4 times previously used value)

σ_b^2 = a priori covariance of two way bias

EFFECT OF CHANGE IN RANGE-RATE MASTER

Let

σ_m^2 = one way noise

σ_b^2 = a priori on one way bias

$$\left[\begin{array}{c|c} A_{11} & A_{12} \\ \hline A_{21} & A_{22} \end{array}\right] = \frac{1}{\sigma_m^2} \left[\begin{array}{c|c} \sum\left(\frac{\partial M}{\partial a_1}\right)^2 \cdots \sum \frac{\partial M}{\partial a_1}\frac{\partial M}{\partial a_6} & \sum \frac{\partial M}{\partial a_1}\frac{\partial M}{\partial b} \\ \hline & \sum \frac{\partial M}{\partial a}\frac{\partial M}{\partial b} \end{array}\right] + \left[\begin{array}{c|c} \text{A priori information matrix} & \\ \hline & \end{array}\right]$$

Since

$$\frac{\partial M}{\partial a_j} \text{ (New Way)} = 2 \frac{\partial M}{\partial a_j} \text{ (Old Way)}$$

$$\sigma_m^2 \text{ (New Way)} = 4\, \sigma_m^2 \text{ (Old Way)}$$

$$\sigma_b^2 \text{ (New Way)} = 4\, \sigma_b^2 \text{ (Old Way)}$$

then

$$A_{11} \text{ (New)} = A_{11} \text{ (Old)}$$

$$A_{22} \text{ (New)} = \frac{1}{4} A_{22} \text{ (Old)}$$

$$A_{12} \text{ (New)} = \frac{1}{2} A_{22} \text{ (Old)}$$

Now, if we let

$$\left[\begin{array}{c|c} C_{11} & C_{12} \\ \hline C_{21} & C_{22} \end{array}\right] = \left[\begin{array}{c|c} A_{11} & A_{12} \\ \hline A_{21} & A_{22} \end{array}\right]^{-1}$$

then

$$C_{11} = \left(A_{11} - A_{12} A_{22}^{-1} A_{21}\right)^{-1} = \text{same either old or new way}$$

$$C_{22} = \left(A_{22} - A_{21} A_{11}^{-1} A_{12}\right)^{-1} \qquad \text{hence } C_{22}(\text{New}) = 4 \times C_{22}(\text{Old})$$

Hence, we see that excluding the bias all the other uncertainties are the same old or new way. Of course, the variance in the estimated bias is with the new way four times what it was with the old way. This is as it should be since with the new way we are estimating the two-way bias whereas with the old way we were estimating the one-way bias.

Thus far, we have looked at the filter where we update everything. Suppose we look at a filter where we partially update. Then,

$$C_{11} = A_{11}^{-1} + \left(A_{11}^{-1} A_{12}\right) \overline{A_{22}^{-1}} \left(A_{11}^{-1} A_{12}\right)^{T}$$

since

$$A_{12}\ (\text{New}) = \frac{1}{2}\ A_{12}(\text{Old})$$

$$\overline{A_{22}^{-1}}\ (\text{New}) = 4\ \overline{A_{22}^{-1}}\ (\text{Old})$$

$$A_{11}^{-1}\ (\text{New}) = A_{11}^{-1}\ (\text{Old})$$

then

$$C_{11}\ (\text{New}) = C_{11}\ (\text{Old})$$

The Bissett-Berman Corporation 2941 Nebraska Avenue, Santa Monica, California EXbrook 4-3270

APOLLO NOTE NO. 408
(Task 2, Item III)

L. Lustick
31 January 1966

EFFECT OF UNCERTAINTY IN REFRACTION PARAMETERS ON AN EARTH ORBIT

PURPOSE

The purpose of this report is to indicate the effect of the uncertainty in the troposphere refraction parameters (zenith range error, and surface refractivity) on the accuracy determination of an earth parking orbit.

INTRODUCTION

Previous reports (Apollo Note No. 372) have indicated how the partial derivatives of the measurables with respect to the refraction parameters are obtained. Briefly stated, the refraction model is summarized below:

$$\Delta R = \frac{(N_o H)}{\sin \mathcal{E} \ell} \tag{1}$$

$$\Delta \mathcal{E} \ell = N_o \operatorname{ctn} \mathcal{E} \ell \tag{2}$$

The purpose of this report will be to indicate how uncertainties in the parameters ($N_o H$ and N_o) affect the accuracy with which the state vector can be determined at a particular time.

ASSUMPTIONS

1. Orbit

The earth parking orbit selected is approximately consistent with the "Patched Conic, Reference Trajectory, September 17, 1969 Lunar Landing Mission." [1] The input data sheet for Part A of the OEA is shown in Figure 1.

[1] Apollo Navigation Working Group, Technical Report No. 65-AN-1.0, February 5, 1965.

2. Measurables

The measurable was vector range (range, azimuth, and elevation angle) from each of the observing stations. The observation intervals of the tracking station were selected so they did not overlap.

3. Accuracy of Measurables

Range σ= 20 meters
Azimuth σ= 0.5 mil
Elevation σ= 0.5 mil

A priori on insertion state vector was:

Position components - σ= 3 kilometers
Velocity components - σ= 10 meters/sec.

The data rate was one measurement every 6 seconds.

4. Tracking Stations

The tracking stations were chosen so that the tracking time did not overlap. Tracking for a station was at all times for which the elevation angles was above 5 degrees. The following stations and the tracking interval for each of these stations from time of insertion is indicated in the following table. The vehicle was tracked over approximately one orbit period and the uncertainties of the state vector 90 minutes after insertion was determined.

Station	Tracking Interval	
	Rise	Set
Grand Canary	6.4 min.	11.2 min.
Carnarvon	42.7 min.	45.1 min.
Canberra	49.5 min.	53.3 min.
Corpus Christi	81.2 min.	85.8 min.

5. Statistics of Refraction Parameters

The uncertainty in the parameter N_o for a station was assumed independent of the uncertainty in the parameter ($N_o H$) for the same station.

The cross correlation of refraction parameters uncertainties for different stations was taken as zero.

The standard deviation in the parameter ($N_o H$), the zenith range error, was approximately 5% of its mean value which is probably realistic.

The standard deviation in N_o, the surface refractivity, was taken as 5% of its average value of (300×10^{-6}). This is probably much greater than the uncertainty in the knowledge of N_o; if station calibrations are made.

METHOD

The results were obtained using the Multiple station version of the OEA program so that the effect of each "nuisance parameter" could be asscessed separately. Two filters were employed. The first filter (Filter 1) just updated the 6 orbit parameters and then the effect of each of the uncertainties in the non-updated refraction parameters was determined. The second filter (Filter 2) updated the 6 orbit parameters and a bias in each of the measurables. No apriori information was assumed on the bias and as before the effect of the non-updated refraction parameters was then determined. No other "nuisance" parameters but the refraction parameters were considered. If other parameters were considered they would not change the effect of the refraction parameters but would, of course, add an additional uncertainty to the final state vector.

RESULTS

The effect of the white noise and each of refraction parameters is presented separately. This serves as another illustration of the Multiple Station version of the program and allows the results to be extrapolated to other apriori uncertainties in the refraction parameters.

Figure 2. is the Part B data sheet used to obtain the results for Filter 1. Figure 3 shows the uncertainty in the predicted state vector due to the white noise. Figure 4 - Effect of N_o (Grand Canary), Figure 5 - Effect of (N_oH) (Grand Canary), Figure 6 - Effect of N_o (Carnarvon), Figure 7 - Effect of (N_oH) (Carnarvon), Figure 8 - Effect of (N_o) (Canberra), Figure 9 - Effect of (N_oH) (Canberra), Figure 10 - Effect of N_o (Corpus Christi), Figure 11 - Effect of (N_oH) (Corpus Christi), Figure 12 - Total due to white noise and all the refraction parameters. Figure 13 is the result obtained with the regular Orbit Error Analysis Program and its agreement with Figure 12 constitutes another check on the Multiple Station version of the OEA Program.

The following Table summarizes the preceding results:

	Due solely to White Noise	Total of White noise and Refraction Effects
Root mean Square Position Miss (at 90 min.)	8.769 meters	8.899 meters
Root mean Square Velocity Miss (at 90 min.)	.0130 m/sec.	.0132 m/sec.

As can be seen from this Table, the effect of the refraction parameters on the uncertainty is a negligible portion of that due to the white noise itself.

Figure 14 is the Part B data sheet for Filter 2 where in addition to the 6 orbit parameters a bias (with no apriori) in each of the measurables was updated. It is presented as another illustration of the use of the Multiple Station program. The following Table compares the two filters used:

	Root mean square position miss, m		Root mean square velocity miss, m/sec.	
Component	Filter 1	Filter 2	Filter 1	Filter 2
White noise	8.769	17.31	.0130	.0292
N_o Grand Canary	.613	.573	7.39×10^{-4}	5.07×10^{-4}
N_oH Grand Canary	.311	1.23	3.81×10^{-4}	1.73×10^{-3}
(N_o) Carnarvon	.272	4.33×10^{-3}	3.20×10^{-4}	5.10×10^{-6}
(N_oH) Carnarvon	.954	6.79×10^{-2}	1.19×10^{-3}	9.21×10^{-5}
(N_o) Canberra	.376	7.73×10^{-2}	4.61×10^{-4}	5.82×10^{-5}
(N_oH) Canberra	.407	.198	1.41×10^{-3}	3.53×10^{-4}
N_o Corpus Christi	.684	.867	8.06×10^{-4}	1.42×10^{-3}
N_oH Corpus Christi	.228	.782	8.56×10^{-4}	1.63×10^{-3}
Total	8.899	17.40	.0132	.0293

As can be seen from the preceding Table (comparing Filter 1 and Filter 2) for some stations the effect of refraction parameters stood about the same for other it was drastically reduced. The station for which it was reduced

significantly are the ones with small observation intervals which imply much less variation in the Elevation Angle. In this case the refraction effects would look like a bias and filter two discriminates against bias type errors in the measurables. The white noise effect for Filter 2 was approximately double that for Filter 1. The comparison of the two filters in the presences of all type non-updated nuisance parameter has not been made and cannot be inferred from the results of this report.

CONCLUSION

The conclusion of this study is that for the Earth parking orbit tracked over a significant portion of an orbit the refraction effects are negligible.

FUTURE STUDIES

1. The same type of studies should be performed on orbits consistent with other portions of Apollo mission.

2. It was assumed that there was no cross-correlation between refractions parameters of different stations. The effect of this could be studied.

3. The effect of refraction parameters on short arc tracking situations should also be investigated.

INPUT DATA

01	6.5633294E 06	A1
02	0	A4
03	7.7930648E 03	A5
04	-1.0000000E 00	GAM ID
05	3.3284000E 01	BETA
06	0	XI
07	0	ETA
08	0	ZETA
09	2.7736000E 01	LAMBDA
10	-1.5600000E 01	ALPHA
11	7.2921561E-05	OMEGAE
12	0	OMEGAM
13	6.3781650E 06	RHOE
14	0	RHOM
15	3.9860320E 14	MU
16	1.1200000E 01	D TIME
16	3.0000000E 01	D TIME
17	-0	REENTRY RAD
18	3.3166667E 01	BIG L
19	-5.4950000E 01	SMA L
20	0	RRATE IND
21	1.0000000E 00	RANGE IND
22	1.0000000E 00	Q IND
23	3.0000000E 01	QF IND
24	-1.0000000E 00	ANG 1 IND
25	-1.0000000E 00	ANG 2 IND
26	0	PVW IND
27	6.4000000E 00	T INIT
28	1.0000000E-01	T INCR
29	1.4000000E 01	DIMENS
30	-5.9565589-261	LAMBDA2
31	-5.9565589-261	ALPHA2
32	1.0000000E 00	M-S IND
33	-0	F-M IND

FIGURE 1.

```
DS  3  R   T=   11.20  SG=2.00000E 01  *
DS  3  A1  T=   11.20  SG=5.00000E-04  *
DS  3  A2  T=   11.20  SG=5.00000E-04        0 0 0 0 0 0 7 0 0 0 0 0 0 0 0 0 0 0 0 0 0 0 0 0 0
DS  4  Q   T=   90.00  SG=1.00000E 00  *
DS  1  A   T=      0   SG=1.00000E 00        7 0 0 0 0 0 0 0 0 0 0 0 0 0 0 0 0 0 0 0 0 0 0 0 0

DS  3  R   T=   11.20  SG=2.00000E 01        0 0 0 0 7 0 0 0 0 0 0 0 0 0 0 0 0 0 0 0 0 0 0 0 0
DS  3  A1  T=   11.20  SG=5.00000E-04  *
DS  3  A2  T=   11.20  SG=5.00000E-04  *
DS  4  Q   T=   90.00  SG=1.00000E 00  *
DS  1  A   T=     -0   SG=1.00000E 00        0 7 0 0 0 0 0 0 0 0 0 0 0 0 0 0 0 0 0 0 0 0 0 0 0

DS  4  R   T=   45.10  SG=2.00000E 01  *
DS  4  A1  T=   45.10  SG=5.00000E-04  *
DS  4  A2  T=   45.10  SG=5.00000E-04        0 0 0 0 0 0 7 0 0 0 0 0 0 0 0 0 0 0 0 0 0 0 0 0 0
DS  4  Q   T=   90.00  SG=1.00000E 00  *
DS  1  A   T=      0   SG=1.00000E 00        0 0 7 0 0 0 0 0 0 0 0 0 0 0 0 0 0 0 0 0 0 0 0 0 0

DS  4  R   T=   45.10  SG=2.00000E 01        0 0 0 0 7 0 0 0 0 0 0 0 0 0 0 0 0 0 0 0 0 0 0 0 0
DS  4  A1  T=   45.10  SG=5.00000E-04  *
DS  4  A2  T=   45.10  SG=5.00000E-04  *
DS  4  Q   T=   90.00  SG=1.00000E 00  *
DS  1  A   T=      0   SG=1.00000E 00        0 0 0 7 0 0 0 0 0 0 0 0 0 0 0 0 0 0 0 0 0 0 0 0 0

DS  5  R   T=   53.30  SG=2.00000E 01  *
DS  5  A1  T=   53.30  SG=5.00000E-04  *
DS  5  A2  T=   53.30  SG=5.00000E-04        0 0 0 0 0 0 7 0 0 0 0 0 0 0 0 0 0 0 0 0 0 0 0 0 0
DS  4  Q   T=   90.00  SG=1.00000E 00  *
DS  1  A   T=      0   SG=1.00000E 00        0 0 0 0 7 0 0 0 0 0 0 0 0 0 0 0 0 0 0 0 0 0 0 0 0

DS  5  R   T=   53.30  SG=2.00000E 01        0 0 0 0 7 0 0 0 0 0 0 0 0 0 0 0 0 0 0 0 0 0 0 0 0
DS  5  A1  T=   53.30  SG=5.00000E-04  *
DS  5  A2  T=   53.30  SG=5.00000E-04  *
DS  4  Q   T=   90.00  SG=1.00000E 00  *
DS  1  A   T=      0   SG=1.00000E 00        0 0 0 0 0 0 7 0 0 0 0 0 0 0 0 0 0 0 0 0 0 0 0 0 0

DS  6  R   T=   85.80  SG=2.00000E 01  *
DS  6  A1  T=   85.80  SG=5.00000E-04  *
DS  6  A2  T=   85.80  SG=5.00000E-04        0 0 0 0 0 0 7 0 0 0 0 0 0 0 0 0 0 0 0 0 0 0 0 0 0
DS  4  Q   T=   90.00  SG=1.00000E 00  *
DS  1  A   T=      0   SG=1.00000E 00        0 0 0 0 0 0 7 0 0 0 0 0 0 0 0 0 0 0 0 0 0 0 0 0 0

DS  6  R   T=   85.80  SG=2.00000E 01        0 0 0 0 7 0 0 0 0 0 0 0 0 0 0 0 0 0 0 0 0 0 0 0 0
DS  6  A1  T=   85.80  SG=5.00000E-04  *
DS  6  A2  T=   85.80  SG=5.00000E-04  *
DS  4  Q   T=   90.00  SG=1.00000E 00  *
DS  1  A   T=      0   SG=1.00000E 00        0 0 0 0 0 0 0 7 0 0 0 0 0 0 0 0 0 0 0 0 0 0 0 0 0
```

FIGURE 2.

(Q)(COV)(QT) - LOCAL COORDINATE SYSTEM

```
2.989951E 01 -2.654644E 01 -3.967330E 00  3.459923E-02 -3.204246E-02  4.890390E-03
2.654644E 01  3.920116E 01  3.410668E 00 -4.566034E-02  2.755697E-02 -9.606589E-03
3.967330E 00  3.410668E 00  7.802044E 00 -4.334282E-03  4.258177E-03 -2.403671E-03
3.459923E-02 -4.566034E-02 -4.334282E-03  5.742525E-05 -3.611889E-05  9.028825E-06
3.204246E-02  2.755697E-02  4.258177E-03 -3.611889E-05  3.443050E-05 -4.929500E-06
4.890390E-03 -9.606589E-03 -2.403671E-03  9.028825E-06 -4.929500E-06  7.732005E-05
```

```
SQRT((1,1)+(2,2)+(3,3)) =  8.7694201E 00
SQRT((4,4)+(5,5)+(6,6)) =  1.3006760E-02
SQRT( 1, 1) =  5.4680442E 00
SQRT( 2, 2) =  6.2610827E 00
SQRT( 3, 3) =  2.7932175E 00
SQRT( 4, 4) =  7.5779452E-03
SQRT( 5, 5) =  5.8677508E-03
SQRT( 6, 6) =  8.7931821E-03
```

PRINCIPAL POSITION UNCERTAINTIES

```
1ST AXIS =  7.873575E 00    PHI = -5.631044E 01
2ND AXIS =  2.882241E 00    CHI =  4.041272E 01
3RD AXIS =  2.569481E 00    PSI =  8.415115E 00
```

PRINCIPAL VELOCITY UNCERTAINTIES

```
1ST AXIS =  9.554535E-03    PHI = -3.632434E
2ND AXIS =  8.360040E-03    CHI = -9.113768E
3RD AXIS =  2.827793E-03    PSI = -3.618000E
```

FIGURE 3.

GROUP 1

```
                                                 6X6  07 08 09 10 11 12 13 14 15 16 17 18 19 20 21 22 23 24 25 26 27 28 29 30
                                                      BI US ES NS NH MU N* VA UM EM NM ED ND RM AM BS RS AS L1 L2 L3 L4 L5 L6
DS  3   R   T=   11.20  SG=2.00000E 01  *
DS  3   A1  T=   11.20  SG=5.00000E-04  *
DS  3   A2  T=   11.20  SG=5.00000E-04      0  0  0  0  0  0  7  0  0  0  0  0  0  0  0  0  0  0  0  0  0  0  0  0
DS  4   Q   T=   90.00  SG=1.00000E 00  *
DS  1   A   T=       0  SG=1.00000E 00      7  0  0  0  0  0  0  0  0  0  0  0  0  0  0  0  0  0  0  0  0  0  0  0
```

(Q)(COV)(QT) - LOCAL COORDINATE SYSTEM

```
 2.185797E-01 -1.836007E-01 -2.990267E-02  2.528974E-04 -2.344344E-04  2.097585E-05
-1.836007E-01  1.542194E-01  2.511739E-02 -2.124266E-04  1.969182E-04 -1.761912E-05
-2.990267E-02  2.511739E-02  4.090817E-03 -3.459748E-05  3.207165E-05 -2.869589E-06
 2.528974E-04 -2.124266E-04 -3.459748E-05  2.926031E-07 -2.712413E-07  2.426913E-08
-2.344344E-04  1.969182E-04  3.207165E-05 -2.712413E-07  2.514390E-07 -2.249733E-08
 2.097585E-05 -1.761912E-05 -2.869589E-06  2.426913E-08 -2.249733E-08  2.012933E-09
```

```
SQRT((1,1)+(2,2)+(3,3)) =  6.1391359E-01
SQRT((4,4)+(5,5)+(6,6)) =  7.3895538E-04
SQRT( 1, 1) =  4.6752511E-01
SQRT( 2, 2) =  3.9270772E-01
SQRT( 3, 3) =  6.3959492E-02
SQRT( 4, 4) =  5.4092799E-04
SQRT( 5, 5) =  5.0143696E-04
SQRT( 6, 6) =  4.4865723E-05
```

FIGURE 4.

```
                                                                07 08 09 10 11 12 13 14 15 16 17 18 19 20 21 22 23 24 25 26 27 28 29 30
                                                          6X6   BI US ES NS NH MU N* VA UM EM NM ED ND RM AM BS RS AS L1 L2 L3 L4 L5 L6

DS   3     R    T=     11.20   SG=2.00000E 01          0  0  0  0  7  0  0  0  0  0  0  0  0  0  0  0  0  0  0  0  0  0  0  0
DS   3     A1   T=     11.20   SG=5.00000E-04  *
DS   3     A2   T=     11.20   SG=5.00000E-04  *
DS   4     Q    T=     90.00   SG=1.00000E 00  *
DS   1     A    T=        0    SG=1.00000E 00          0  7  0  0  0  0  0  0  0  0  0  0  0  0  0  0  0  0  0  0  0  0  0  0


                                (Q)(COV)(QT) - LOCAL COORDINATE SYSTEM


  5.370047E-02 -4.783752E-02 -4.131746E-03  6.410770E-05 -5.759457E-05  1.941289E-05
 -4.783752E-02  4.261468E-02  3.680647E-03 -5.710850E-05  5.130647E-05 -1.729341E-05
 -4.131746E-03  3.680647E-03  3.178990E-04 -4.932484E-06  4.431361E-06 -1.493639E-06
  6.410770E-05 -5.710850E-05 -4.932484E-06  7.653186E-08 -6.875648E-08  2.317513E-08
 -5.759457E-05  5.130647E-05  4.431361E-06 -6.875648E-08  6.177106E-08 -2.082062E-08
  1.941289E-05 -1.729341E-05 -1.493639E-06  2.317513E-08 -2.082062E-08  7.017820E-09


                                SQRT((1,1)+(2,2)+(3,3)) =  3.1085856E-01
                                SQRT((4,4)+(5,5)+(6,6)) =  3.8120958E-04
                                          SQRT( 1, 1) =  2.3173361E-01
                                          SQRT( 2, 2) =  2.0643323E-01
                                          SQRT( 3, 3) =  1.7829722E-02
                                          SQRT( 4, 4) =  2.7664393E-04
                                          SQRT( 5, 5) =  2.4853784E-04
                                          SQRT( 6, 6) =  8.3772431E-05
```

FIGURE 5.

```
                                                                07 08 09 10 11 12 13 14 15 16 17 18 19 20 21 22 23 24 25 26 27 28 29 30
                                                          6X6   BI US ES NS NH MU N* VA UM EM NM ED ND RM AM BS RS AS L1 L2 L3 L4 L5 L6

DS   4     R    T=     45.10   SG=2.00000E 01  *
DS   4     A1   T=     45.10   SG=5.00000E-04  *
DS   4     A2   T=     45.10   SG=5.00000E-04          0  0  0  0  0  0  7  0  0  0  0  0  0  0  0  0  0  0  0  0  0  0  0  0
DS   4     Q    T=     90.00   SG=1.00000E 00  *
DS   1     A    T=        0    SG=1.00000E 00          0  0  7  0  0  0  0  0  0  0  0  0  0  0  0  0  0  0  0  0  0  0  0  0


                                (Q)(COV)(QT) - LOCAL COORDINATE SYSTEM


  4.833154E-02 -3.504205E-02 -1.045519E-03  4.651653E-05 -5.268143E-05 -2.186492E-06
 -3.504205E-02  2.540670E-02  7.588380E-04 -3.372610E-05  3.819587E-05  1.585282E-06
 -1.045519E-03  7.588380E-04  2.261693E-05 -1.006257E-06  1.139617E-06  4.729871E-08
  4.651653E-05 -3.372610E-05 -1.006257E-06  4.476968E-08 -5.070307E-08 -2.104382E-09
 -5.268143E-05  3.819587E-05  1.139617E-06 -5.070307E-08  5.742282E-08  2.383278E-09
 -2.186492E-06  1.585282E-06  4.729871E-08 -2.104382E-09  2.383278E-09  9.891564E-11


                                SQRT((1,1)+(2,2)+(3,3)) =  2.7158951E-01
                                SQRT((4,4)+(5,5)+(6,6)) =  3.1983030E-04
                                          SQRT( 1, 1) =  2.1984436E-01
                                          SQRT( 2, 2) =  1.5939480E-01
                                          SQRT( 3, 3) =  4.7557257E-03
                                          SQRT( 4, 4) =  2.1158847E-04
                                          SQRT( 5, 5) =  2.3963059E-04
                                          SQRT( 6, 6) =  9.9456343E-06
```

FIGURE 6.

```
                                                
```

```
                                                
```

						6X6	07 BI	08 US	09 ES	10 NS	11 NH	12 MU	13 N*	14 VA	15 UM	16 EM	17 NM	18 ED	19 ND	20 RM	21 AM	22 BS	23 RS	24 AS	25 L1	26 L2	27 L3	28 L4	29 L5	30 L6
DS	6	R	T=	85.80	SG=2.00000E 01		0	0	0	0	7	0	0	0	0	0	0	0	0	0	0	0	0	0	0	0	0	0	0	0
DS	6	A1	T=	85.80	SG=5.00000E-04	*																								
DS	6	A2	T=	85.80	SG=5.00000E-04	*																								
DS	4	Q	T=	90.00	SG=1.00000E 00	*																								
DS	1	A	T=	0	SG=1.00000E 00		0	0	0	0	0	0	0	7	0	0	0	0	0	0	0	0	0	0	0	0	0	0	0	0

(Q)(COV)(QT) - LOCAL COORDINATE SYSTEM

1.070882E-02	-6.451285E-03	2.002230E-02	1.073411E-05	-1.166886E-05	-8.711108E-05
-6.451285E-03	3.886429E-03	-1.206198E-02	-6.466520E-06	7.029641E-06	5.247809E-05
2.002230E-02	-1.206198E-02	3.743572E-02	2.006958E-05	-2.181729E-05	-1.628717E-04
1.073411E-05	-6.466520E-06	2.006958E-05	1.075946E-08	-1.169642E-08	-8.731680E-08
-1.166886E-05	7.029641E-06	-2.181729E-05	-1.169642E-08	1.271498E-08	9.492057E-08
-8.711108E-05	5.247809E-05	-1.628717E-04	-8.731680E-08	9.492057E-08	7.086066E-07

SQRT((1,1)+(2,2)+(3,3)) = 2.2810299E-01
SQRT((4,4)+(5,5)+(6,6)) = 8.5561734E-04
SQRT(1, 1) = 1.0348343E-01
SQRT(2, 2) = 6.2341233E-02
SQRT(3, 3) = 1.9348314E-01
SQRT(4, 4) = 1.0372781E-04
SQRT(5, 5) = 1.1276070E-04
SQRT(6, 6) = 8.4178774E-04

FIGURE 11.

(Q)(COV)(QT) - LOCAL COORDINATE SYSTEM

3.091787E 01	-2.742226E 01	-4.333581E 00	3.573103E-02	-3.313790E-02	5.548323E-03
-2.742226E 01	3.996608E 01	3.715030E 00	-4.664067E-02	2.849836E-02	-1.029186E-02
-4.333581E 00	3.715030E 00	8.303386E 00	-4.728020E-03	4.652760E-03	-2.536920E-03
3.573103E-02	-4.664067E-02	-4.728020E-03	5.868900E-05	-3.733581E-05	9.800839E-06
-3.313790E-02	2.849836E-02	4.652760E-03	-3.733581E-05	3.560890E-05	-5.632619E-06
5.548323E-03	-1.029186E-02	-2.536920E-03	9.800839E-06	-5.632619E-06	8.067819E-05

SQRT((1,1)+(2,2)+(3,3)) = 8.8987264E 00
SQRT((4,4)+(5,5)+(6,6)) = 1.3227853E-02
SQRT(1, 1) = 5.5603837E 00
SQRT(2, 2) = 6.3218730E 00
SQRT(3, 3) = 2.8815597E 00
SQRT(4, 4) = 7.6608747E-03
SQRT(5, 5) = 5.9673194E-03
SQRT(6, 6) = 8.9821039E-03

PRINCIPAL POSITION UNCERTAINTIES

1ST AXIS = 7.987957E 00 PHI =-5.510645E 01
2ND AXIS = 2.930349E 00 CHI =-4.658181E 01
3RD AXIS = 2.606325E 00 PSI = 7.997462E 00

PRINCIPAL VELOCITY UNCERTAINTIES

1ST AXIS = 9.748262E-03 PHI =-3.656102E 01
2ND AXIS = 8.479407E-03 CHI =-9.103637E 01
3RD AXIS = 2.836746E-03 PSI =-3.808957E 01

FIGURE 12.

(Q)(COV)(Q^T) - LOCAL COORDINATE SYSTEM

3.091787E 01	-2.742226E 01	-4.333581E 00	3.573103E-02	-3.313790E-02	5.548323E-03
-2.742226E 01	3.996608E 01	3.715030E 00	-4.664067E-02	2.849836E-02	-1.029186E-02
-4.333581E 00	3.715030E 00	8.303386E 00	-4.728020E-03	4.652760E-03	-2.536920E-03
3.573103E-02	-4.664067E-02	-4.728020E-03	5.868900E-05	-3.733581E-05	9.800839E-06
-3.313790E-02	2.849836E-02	4.652760E-03	-3.733581E-05	3.560890E-05	-5.632619E-06
5.548323E-03	-1.029186E-02	-2.536920E-03	9.800839E-06	-5.632619E-06	8.067819E-05

MISS TIME = 2.1285768E-01 MINIMUM MISS = 6.2626874E 00 REND MISS = 8.8987264E 00

SQRT((2,2)+(3,3)) =	6.9476229E 00
SQRT((4,4)+(5,5)+(6,6)) =	1.3227853E-02
SQRT(1, 1) =	5.5603837E 00
SQRT(2, 2) =	6.3218730E 00
SQRT(3, 3) =	2.8815597E 00
SQRT(4, 4) =	7.6608747E-03
SQRT(5, 5) =	5.9673194E-03
SQRT(6, 6) =	8.9821039E-03

FIGURE 13.

```
DS  3   R   T=   11.20  SG=2.00000E 01      7  0  0  0  0  0  0  0  0  0  0  0  0  0  0  0  0  0  0  0  0  0  0  0  0
DS  3   A1  T=   11.20  SG=5.00000E-04      8  0  0  0  0  0  0  0  0  0  0  0  0  0  0  0  0  0  0  0  0  0  0  0  0
DS  3   A2  T=   11.20  SG=5.00000E-04      9  0  0  0  0  0  0 19  0  0  0  0  0  0  0  0  0  0  0  0  0  0  0  0  0
DS  4   Q   T=   90.00  SG=1.00000E 00  *
DS  1   A   T=      -0  SG=1.00000E 00     19  0  0  0  0  0  0  0  0  0  0  0  0  0  0  0  0  0  0  0  0  0  0  0  0

DS  3   R   T=   11.20  SG=2.00000E 01      7  0  0  0 19  0  0  0  0  0  0  0  0  0  0  0  0  0  0  0  0  0  0  0  0
DS  3   A1  T=   11.20  SG=5.00000E-04      8  0  0  0  0  0  0  0  0  0  0  0  0  0  0  0  0  0  0  0  0  0  0  0  0
DS  3   A2  T=   11.20  SG=5.00000E-04      9  0  0  0  0  0  0  0  0  0  0  0  0  0  0  0  0  0  0  0  0  0  0  0  0
DS  4   Q   T=   90.00  SG=1.00000E 00  *
DS  1   A   T=      -0  SG=1.00000E 00      0 19  0  0  0  0  0  0  0  0  0  0  0  0  0  0  0  0  0  0  0  0  0  0  0

DS  4   R   T=   45.10  SG=2.00000E 01     10  0  0  0  0  0  0  0  0  0  0  0  0  0  0  0  0  0  0  0  0  0  0  0  0
DS  4   A1  T=   45.10  SG=5.00000E-04     11  0  0  0  0  0  0  0  0  0  0  0  0  0  0  0  0  0  0  0  0  0  0  0  0
DS  4   A2  T=   45.10  SG=5.00000E-04     12  0  0  0  0  0  0 19  0  0  0  0  0  0  0  0  0  0  0  0  0  0  0  0  0
DS  4   Q   T=   90.00  SG=1.00000E 00  *
DS  1   A   T=      -0  SG=1.00000E 00      0  0 19  0  0  0  0  0  0  0  0  0  0  0  0  0  0  0  0  0  0  0  0  0  0

DS  4   R   T=   45.10  SG=2.00000E 01     10  0  0  0 19  0  0  0  0  0  0  0  0  0  0  0  0  0  0  0  0  0  0  0  0
DS  4   A1  T=   45.10  SG=5.00000E-04     11  0  0  0  0  0  0  0  0  0  0  0  0  0  0  0  0  0  0  0  0  0  0  0  0
DS  4   A2  T=   45.10  SG=5.00000E-04     12  0  0  0  0  0  0  0  0  0  0  0  0  0  0  0  0  0  0  0  0  0  0  0  0
DS  4   Q   T=   90.00  SG=1.00000E 00  *
DS  1   A   T=      -0  SG=1.00000E 00      0  0  0 19  0  0  0  0  0  0  0  0  0  0  0  0  0  0  0  0  0  0  0  0  0

DS  5   R   T=   53.30  SG=2.00000E 01     13  0  0  0  0  0  0  0  0  0  0  0  0  0  0  0  0  0  0  0  0  0  0  0  0
DS  5   A1  T=   53.30  SG=5.00000E-04     14  0  0  0  0  0  0  0  0  0  0  0  0  0  0  0  0  0  0  0  0  0  0  0  0
DS  5   A2  T=   53.30  SG=5.00000E-04     15  0  0  0  0  0  0 19  0  0  0  0  0  0  0  0  0  0  0  0  0  0  0  0  0
DS  4   Q   T=   90.00  SG=1.00000E 00  *
DS  1   A   T=      -0  SG=1.00000E 00      0  0  0  0 19  0  0  0  0  0  0  0  0  0  0  0  0  0  0  0  0  0  0  0  0

DS  5   R   T=   53.30  SG=2.00000E 01     13  0  0  0 19  0  0  0  0  0  0  0  0  0  0  0  0  0  0  0  0  0  0  0  0
DS  5   A1  T=   53.30  SG=5.00000E-04     14  0  0  0  0  0  0  0  0  0  0  0  0  0  0  0  0  0  0  0  0  0  0  0  0
DS  5   A2  T=   53.30  SG=5.00000E-04     15  0  0  0  0  0  0  0  0  0  0  0  0  0  0  0  0  0  0  0  0  0  0  0  0
DS  4   Q   T=   90.00  SG=1.00000E 00  *
DS  1   A   T=      -0  SG=1.00000E 00      0  0  0  0  0 19  0  0  0  0  0  0  0  0  0  0  0  0  0  0  0  0  0  0  0

DS  6   R   T=   85.80  SG=2.00000E 01     16  0  0  0  0  0  0  0  0  0  0  0  0  0  0  0  0  0  0  0  0  0  0  0  0
DS  6   A1  T=   85.80  SG=5.00000E-04     17  0  0  0  0  0  0  0  0  0  0  0  0  0  0  0  0  0  0  0  0  0  0  0  0
DS  6   A2  T=   85.80  SG=5.00000E-04     18  0  0  0  0  0  0 19  0  0  0  0  0  0  0  0  0  0  0  0  0  0  0  0  0
DS  4   Q   T=   90.00  SG=1.00000E 00  *
DS  1   A   T=      -0  SG=1.00000E 00      0  0  0  0  0  0  0 19  0  0  0  0  0  0  0  0  0  0  0  0  0  0  0  0  0

DS  6   R   T=   85.80  SG=2.00000E 01     16  0  0  0 19  0  0  0  0  0  0  0  0  0  0  0  0  0  0  0  0  0  0  0  0
DS  6   A1  T=   85.80  SG=5.00000E-04     17  0  0  0  0  0  0  0  0  0  0  0  0  0  0  0  0  0  0  0  0  0  0  0  0
DS  6   A2  T=   85.80  SG=5.00000E-04     18  0  0  0  0  0  0  0  0  0  0  0  0  0  0  0  0  0  0  0  0  0  0  0  0
DS  4   Q   T=   90.00  SG=1.00000E 00  *
DS  1   A   T=      -0  SG=1.00000E 00      0  0  0  0  0  0  0 19  0  0  0  0  0  0  0  0  0  0  0  0  0  0  0  0  0
```

FIGURE 14.

The Bissett-Berman Corporation 2941 Nebraska Avenue, Santa Monica, California EXbrook 4-3270

APOLLO NOTE NO. 409
(Task 2, Item II)

B. Murphy
17 February 1966

THE Az-El PROGRAM

In generating the ionosphere range error by the ionosphere model as described in Apollo Note No. 388, it is necessary to know the azimuth and elevation from the tracking stations to the vehicle as functions of time for a particular orbit. For this purpose, the Az-$\mathcal{El}$ Program was generated by altering the Station Visibility Program. These alterations consist of finding the station-vehicle vector in a rotating (at ω_E) station-centered (UP-EAST-NORTH) coordinate system and then finding trig functions of the components.

Within the Station Visibility Program, the moon-vehicle vector in the primed system (x' axis along initial position vector, z' axis along angular momentum vector of vehicle about the moon) $\underline{R}'$, is available. This vector is rotated through Euler angles XI, ETA, and ZETA into the Tilde coordinate System by means of the $\mathbb{L}$ matrix (internally available in Station Visibility Program) to yield

$$\underline{\tilde{R}} = \mathbb{L}^T R'$$

where the Tilde System is moon-centered which has the $\tilde{x}$ axis along the initial earth-moon vector and the $\tilde{z}$ axis along the angular momentum vector of the moon about the earth.

Then the earth-vehicle vector is

$$\underline{\tilde{R}}_E = \underline{\tilde{R}} + \underline{\tilde{R}}_M$$

where $\underline{\tilde{R}}_M$ is the earth-moon vector

$$\underline{\tilde{R}}_M = \begin{bmatrix} r_M \cos \omega_M{}^T \\ r_M \sin \omega_M{}^T \\ 0 \end{bmatrix}$$

The earth-vehicle vector in the Tilde System is then rotated via the $\mathbb{K}$ matrix into a non-rotating earth based system ("unprimed") with the x and y axis in the equatorial plane, the x axis passing through the prime meridian at time zero.

$$\underline{R_E} = \mathbb{K}^T \underline{\tilde{R}_E}$$

A further rotation, G, carries the earth-vehicle vector into a rotating (at ω_E) earth-centered coordinate system with the $\hat{x}$ axis through the tracking station and the $\hat{y}$ still axis in the equatorial plane.

$$\underline{\hat{R}_E} = G\,\underline{R_E}$$

where

$$G = \mathbb{B}\mathbb{A} = \begin{bmatrix} \cos\lambda\cos\rho & \cos\lambda\sin\rho & \sin\lambda \\ -\sin\rho & \cos\rho & 0 \\ -\sin\lambda\cos\rho & -\sin\lambda\sin\rho & \cos\lambda \end{bmatrix}$$

$$\rho = \alpha + \omega_E T$$

and λ and α are the station's latitude and longitude respectively.

Now the station-vehicle vector, $\underline{\hat{R}_S}$, is

$$\underline{\hat{R}_S} = \underline{\hat{R}_E} - \begin{bmatrix} R_o \\ 0 \\ 0 \end{bmatrix}$$

in an UP-EAST-NORTH system where R_o is the earth radius. Finding the azimuth and elevation is now a simple matter of computing inverse trig functions of the components of the $\underline{\hat{R}_S}$ vector.

$$\text{Azimuth} = \tan^{-1}\left(\frac{\hat{R}_{Sy}}{\hat{R}_{Sz}}\right)$$

$$\text{Elevation} = \tan^{-1}\left(\frac{\hat{R}_{Sx}}{\sqrt{\hat{R}_{Sy}^2+\hat{R}_{Sz}^2}}\right)$$

In addition to azimuth-elevation information, the subsolar latitude and longitude (in lieu of local solar time and day of year) are needed as inputs to the ionosphere model. As it is unlikely that there will be tracking periods of more than a few days, the subsolar latitude is assumed to remain constant throughout this period and consequently will simply be an input. The longitude was computed from

$$\text{Subsolar longitude} = \text{Initial Subsolar long.} - \omega_E t$$

Then for a particular orbit as described in the same input form as for the Station Visibility Program (with the exception of initial subsolar latitude and longitude), the azimuth, elevation, subsolar latitude (SLAT) and subsolar longitude (SLONG) are stored on tape and printed out for each visible station as a function of time in the following manner:

Station No. , Station Name , Station Lat. , Station Long.

Time	Azimuth	Elevation	SLAT	SLONG
.25				
.50				

For further descriptions of the coordinate systems and rotation matrices utilized, see the Bissett-Berman Final Report on Contract NASw-688.

The Bissett-Berman Corporation 2941 Nebraska Avenue, Santa Monica, California EXbrook 4-3270

L. Lustick/
G. Hempstead
17 February 1966

APOLLO NOTE NO. 410
(Task II, Item II)

CHECKOUT OF VISIBILITY ADDITION TO OEA

PURPOSE

The purpose of this note is to indicate how the visibility position of the OEA program was checked out. The analysis for the visibility portion of the program is defined in Apollo Note No. 407.

METHOD

There is currently an existing visibility program at Bissett-Berman that has been checked out. The visibility additions to the OEA were checked against this program in the following manner. The orbit selection was a lunar orbit defined in Figure 1.

1. The first run made with the OEA (with the visibility additions) was with the following station locations.

	Slave	Master
LAT	40.4667°	0
LONG	-3.6667	-100

The vehicle was tracked with this station for 14 minutes.

The visibility program (current rise and set time program) indicated that the elevation angle for both of these stations was above 5 degrees during the tracking interval, but that the master was occulted by the Moon at 13.19 minutes and that the slave was occulted at 13.42 minutes.

In the OEA visibility addition the visibility of the receiving station is checked first and then the transmitting station. The OEA program should therefore have indicated that it excluded data because of master occulation for data at 13.2, 13.3 and 13.4 and then switch to excluding data because

```
01      1.7528160E 06     A1
02                -0      A4
03      1.6905030E 03     A5
04      1.0000000E 00     GAM ID
05      2.8500000E 01     BETA
06      9.0000000E 01     XI
07      1.7596000E 02     ETA
08      3.2500000E 02     ZETA
09      4.0466670E 01     LAMBDA
10     -3.6666670E 00     ALPHA
11      7.2911600E-05     OMEGAE
12      2.6690000E-06     OMEGAM
13      6.3786165E 06     RHOE
14      3.8440200E 08     RHOM
15      4.9027780E 12     MU
16      1.0000000E-01     D TIME
16      2.0000000E-01     D TIME
16      3.0000000E-01     D TIME
16      1.4000000E 01     D TIME
16      5.6710000E 01     D TIME
17                -0      REENTRY RAD
18     -2.0000000E 00     BIG L
19     -2.1526000E 01     SMA L
20      1.0000000E 00     RRATE IND
21      1.0000000E 00     RANGE IND
22      1.0000000E 00     Q IND
23      5.6710000E 01     QF IND
24      1.0000000E 00     ANG 1 IND
25      1.0000000E 00     ANG 2 IND
26                -0      PVW IND
27      1.0000000E-01     T INIT
28      1.0000000E-01     T INCR
29      3.0000000E 01     DIMENS
30                -0      LAMBDA2
31     -1.0000000E 02     ALPHA2
32                -0      M-S IND
33                -0      F-M IND
```

Figure 1. Input Data Defining Orbit

of slave occultation at 13.5 through 14. The OEA program did, in fact, indicate exactly this. To make sure that in fact no range-rate data beyond 13.1 minutes was included, the run was recalculated only to 13.1 minutes of tracking and the information matrix was for this case exactly the same as when the vehicle was tracked for 14 minutes. It was also confirmed that the range and angle information matrices were including data up to and including 13.4 minutes as should be.

2. As described in Apollo Note 407 if the input defining the Earth-Moon distance (RHOM) is not within 7-1/2% of its mean value, the occultation portion of the visibility program is not done. A rerun of the case used in (1) with a change in RHOM indicated that the occultation feature was indeed bypassed as it should be.

3. A third run was made with the following station locations:

	Slave	Master
LAT	0	40.4667
LONG	-111	-3.667

The tracking interval was 0 - 35 minutes. The rise and set time program indicated that the slave station was initially set (below 5° elevation angle). The OEA program indicated that data was initially excluded because the elevation angle of slave was below 5° and thereafter the station was above 5° (approximately 24 minutes) indicated that data was excluded because the slave was occulted as should be.

4. There is a control constant on the input data sheet that overrides all visibility considerations. This control constant was added to the input of run 3 and the run with the OEA indicated that no data was excluded as should be.

CONCLUSION

The visibility additions to the program have been checked out and will guard against including data in information matrices which is not applicable.

The Bissett-Berman Corporation 2941 Nebraska Avenue, Santa Monica, California EXbrook 4-3270

APOLLO NOTE NO. 411
(Task II, Item II)

CHECKOUT OF CHANGE TO RANGE-RATE INFORMATION MATRIX CALCULATIONS

L. Lustick/
G. Hempstead
18 February 1966

PURPOSE

The purpose of this note is to indicate how the change in the calculation of range-rate information matrices was checked.

INTRODUCTION

At the request of NASA (Houston) the calculation of range-rate information matrices has been changed. The analytical background for this change is described in Apollo Note 407.

METHOD

A lunar Hohman transfer orbit was selected and tracked from a master and two slaves for 24 minutes. The uncertainties in the position and velocity vector at the time corresponding to apolune were calculated. In addition to the orbit parameters, station location, lunar ephemeris, clock, gravitational constant, (pseudo bias in each measurable) parameters were considered.

Results for the following filters were obtained:

I. Update the orbit parameters with no errors in any of the other parameters.

II. Update orbit parameters and three pseudo-biases and include effect of uncertainty in the other nuisance parameters.

III. Update all the parameters.

The above was done with the old program and with the new program and the equivalence of the answers constitutes the check. The following table indicates the input differences required in the old and new program for the same problem.

	OLD	NEW
Standard Deviation in Measurables	$\frac{1}{2}\ \sigma$	σ where σ = (two-way noise)
Apriori Variance in Bias of Master	$\frac{1}{4}\ \sigma^2$ (bias) master	σ^2 (bias) master

Figures 1, 2, and 3 are the results with the old program for Filters I, II, and III, respectively. Figures 4, 5 and 6 are the results with the new program for Filters I, II, and III, respectively. Comparison of the results obtained with the old and the new program for corresponding filters indicate that the standard deviation in all the predicted parameters are the same except, $\sigma(7, 7)$, which is the standard deviation in the master bias. The standard deviation in the bias with the new program is twice that of the standard deviation in the bias with the old program. As explained in Apollo Note 407, this is exactly as should be since we are predicting a two-way master bias with the new program and we are only predicting a one-way bias with the old program.

```
SQRT((1,1)+(2,2)+(3,3)) =   6.8094252E 02
SQRT((4,4)+(5,5)+(6,6)) =   5.7288918E-01
          SQRT( 1, 1) =   2.2699477E 02
          SQRT( 2, 2) =   4.3670832E 02
          SQRT( 3, 3) =   4.7057617E 02
          SQRT( 4, 4) =   4.2407941E-01
          SQRT( 5, 5) =   1.4324396E-01
          SQRT( 6, 6) =   3.5754696E-01
```

Figure 1. Result of Filter I with Old Program

```
SQRT((1,1)+(2,2)+(3,3)) =   2.3202532E 03
SQRT((4,4)+(5,5)+(6,6)) =   2.5547623E 00
          SQRT( 1, 1) =   2.6270224E 02
          SQRT( 2, 2) =   5.0173747E 02
          SQRT( 3, 3) =   2.2500716E 03
          SQRT( 4, 4) =   4.8676514E-01
          SQRT( 5, 5) =   1.6454308E-01
          SQRT( 6, 6) =   2.5025578E 00
          SQRT( 7, 7) =   3.2331116E-02
          SQRT( 8, 8) =   1.1476991E-01
          SQRT( 9, 9) =   1.1151420E-01
```

Figure 2. Result of Filter II with Old Program

```
SQRT((1,1)+(2,2)+(3,3)) =  2.1620836E 03
SQRT((4,4)+(5,5)+(6,6)) =  2.2736933E 00
          SQRT( 1, 1) =  2.5749314E 02
          SQRT( 2, 2) =  4.9192406E 02
          SQRT( 3, 3) =  2.0895726E 03
          SQRT( 4, 4) =  4.7734174E-01
          SQRT( 5, 5) =  1.6118107E-01
          SQRT( 6, 6) =  2.2171709E 00
          SQRT( 7, 7) =  3.0897035E-02
          SQRT( 8, 8) =  1.1392395E-01
          SQRT( 9, 9) =  1.1147770E-01
          SQRT(10,10) =  1.7028188E 09
          SQRT(11,11) =  2.9998251E 03
          SQRT(12,12) =  5.9965654E 03
          SQRT(13,13) =  2.9999876E 03
          SQRT(14,14) =  2.9999996E-03
          SQRT(15,15) =  3.0000000E-03
          SQRT(16,16) =  3.0000000E-03
          SQRT(17,17) =  9.9978007E 01
          SQRT(18,18) =  9.9999027E 01
          SQRT(19,19) =  9.9984110E 01
          SQRT(20,20) =  1.0000000E-10
          SQRT(21,21) =  2.7748874E-14
          SQRT(22,22) =  9.1963261E-04
          SQRT(23,23) =  9.9995034E 01
          SQRT(24,24) =  9.9943852E 01
          SQRT(25,25) =  9.9998550E 01
          SQRT(26,26) =  8.7014125E-04
          SQRT(27,27) =  9.9998781E-11
          SQRT(28,28) =  7.6884373E-15
          SQRT(29,29) =  9.9994993E 01
          SQRT(30,30) =  9.9999774E 01
          SQRT(31,31) =  9.9999888E 01
          SQRT(32,32) =  9.9060514E-04
          SQRT(33,33) =  9.9998785E-11
          SQRT(34,34) =  9.7981033E-15
```

Figure 3. Result of Filter III with Old Program

```
SQRT((1,1)+(2,2)+(3,3)) =  6.8094250E 02
SQRT((4,4)+(5,5)+(6,6)) =  5.7288916E-01
          SQRT( 1, 1) =  2.2699476E 02
          SQRT( 2, 2) =  4.3670830E 02
          SQRT( 3, 3) =  4.7057617E 02
          SQRT( 4, 4) =  4.2407939E-01
          SQRT( 5, 5) =  1.4324395E-01
          SQRT( 6, 6) =  3.5754696E-01
```

Figure 4. Result of Filter I with New Program

```
SQRT((1,1)+(2,2)+(3,3)) =  2.3202532E 03
SQRT((4,4)+(5,5)+(6,6)) =  2.5547623E 00
          SQRT( 1, 1) =  2.6270222E 02
          SQRT( 2, 2) =  5.0173741E 02
          SQRT( 3, 3) =  2.2500716E 03
          SQRT( 4, 4) =  4.8676509E-01
          SQRT( 5, 5) =  1.6454306E-01
          SQRT( 6, 6) =  2.5025578E 00
          SQRT( 7, 7) =  6.4662232E-02
          SQRT( 8, 8) =  1.1476991E-01
          SQRT( 9, 9) =  1.1151420E-01
```

Figure 5. Result of Filter II with New Program

```
SQRT((1,1)+(2,2)+(3,3)) =  2.1620836E 03
SQRT((4,4)+(5,5)+(6,6)) =  2.2736933E 00
          SQRT( 1, 1) =  2.5749312E 02
          SQRT( 2, 2) =  4.9192403E 02
          SQRT( 3, 3) =  2.0895726E 03
          SQRT( 4, 4) =  4.7734171E-01
          SQRT( 5, 5) =  1.6118106E-01
          SQRT( 6, 6) =  2.2171709E 00
          SQRT( 7, 7) =  6.1794071E-02
          SQRT( 8, 8) =  1.1392396E-01
          SQRT( 9, 9) =  1.1147771E-01
          SQRT(10,10) =  1.7028188E 09
          SQRT(11,11) =  2.9998251E 03
          SQRT(12,12) =  5.9965659E 03
          SQRT(13,13) =  2.9999876E 03
          SQRT(14,14) =  2.9999996E-03
          SQRT(15,15) =  3.0000000E-03
          SQRT(16,16) =  3.0000000E-03
          SQRT(17,17) =  9.9978007E 01
          SQRT(18,18) =  9.9999027E 01
          SQRT(19,19) =  9.9984110E 01
          SQRT(20,20) =  1.0000000E-10
          SQRT(21,21) =  2.7748874E-14
          SQRT(22,22) =  9.1963261E-04
          SQRT(23,23) =  9.9995034E 01
          SQRT(24,24) =  9.9943852E 01
          SQRT(25,25) =  9.9998550E 01
          SQRT(26,26) =  8.7014125E-04
          SQRT(27,27) =  9.9998787E-11
          SQRT(28,28) =  7.6884373E-15
          SQRT(29,29) =  9.9994993E 01
          SQRT(30,30) =  9.9999774E 01
          SQRT(31,31) =  9.9999888E 01
          SQRT(32,32) =  9.9060514E-04
          SQRT(33,33) =  9.9998793E-11
          SQRT(34,34) =  9.7981033E-15
```

Figure 6. Result of Filter III with New Program

The Bissett-Berman Corporation 2941 Nebraska Avenue, Santa Monica, California EXbrook 4-3270

APOLLO NOTE NO. 412
(Task 2, Item II)

J. Childress
8 March 1966

THE EFFECTS OF BIAS UPDATING IN THE PRESENCE OF STATION AND CLOCK ERRORS DURING A TRANSLUNAR TRAJECTORY

INTRODUCTION

The presently planned MSC real-time ODP will batch data, and in each batch will estimate only the six element state vector and fixed biases in the measurables. A few computer runs performed previously for short arcs indicated that the estimates obtained from a single batch in this fashion are almost as good as though all of the nuisance parameters were estimated. For long arcs, on the other hand, analysis indicates that estimating only the six element state vector and fixed biases in the measurables, with just a single batch should lead to very poor estimates. This is so since in the latter case we are trying to fit the data with a very poor model.

In this Apollo note we investigate further the relative accuracies of position estimates obtained using different filters, in each case treating all the data as a single batch. The three kinds of filters considered are those in which:

1. Only the six orbit parameters are estimated.
2. The six orbit parameters and the fixed biases on the measurables are estimated.
3. All the parameters are estimated.

In addition, in order to see the loss of accuracy in the estimates attributable to errors in the a priori knowledge of the nuisance parameters, we also compute the uncertainty in the position estimates that would result if the nuisance parameter values were known perfectly.

DISCUSSION

The only nuisance parameters considered are fixed biases in the measurables, station location errors and clock parameters. The fixed biases in the measurables are included because they are part of the RTODP. The station location errors are included because we feel that for observations of several hours duration their effects cannot be compensated for by attaching a fixed bias to the measurable. The clock parameter errors are included because they are expected to be a major error source.

The orbit is that portion of a translunar trajectory outside the lunar sphere of influence. The measurable is range rate and the observing stations are a master at Canberra, and slaves at Madrid, Ascension and Hawaii. It will be noted that this is not a realistic situation, for Canberra cannot see the vehicle at the same time as Madrid or Ascension, but we do not need a realistic situation in order to establish the results we desire. Actually, the rule employed here is that data is used from a station if it can see the vehicle.

The orbit is specified by

$a_1 = 7.0861 \times 10^6$ m

$a_4 = 0$ m/sec.

$a_5 = 1.0510 \times 10^4$ m/sec.

$\beta = \xi = \eta = \zeta = 0$

There is no a priori estimate of position or velocity. The uncertainties in the a priori estimates of the other parameters, when these are not zero, are

Measurement Bias (old)		10 m/sec.
Measurement Bias (new)		.05 m/sec.
Station Location	(Up)	10 m.
	(East)	65.08 m.
	(North)	65.08 m.

Clock Offset	10^{-3} sec.
Rate	10^{-10}
Drift	10^{-14} sec.$^{-1}$

The range rate measurements are taken at 1 minute intervals with a standard deviation of 3.8×10^{-3} m/sec.

The curves in Figures 1 through 5 show the RMS uncertainty in the estimate of current position as a function of the time since the vehicle was injected into a translunar orbit. They illustrate the effects of using different kinds of filters (i. e., data processing techniques applied to the measurables to estimate the orbit, and also show the effects of different accuracies in the a priori estimates of the nuisance parameters. In all five figures, results are shown when

1. Only orbit parameters are estimated.
2. Orbit parameters and the biases are estimated.
3. All the parameters are estimated.

For comparison Figure 1 also shows how well position could be estimated if the a priori estimates of the nuisance parameters were known to be correct, and how well injection position can be estimated if all parameters are estimated.

Figures 1 through 5 differ in the assumptions that have been made concerning the quantities that are treated as nuisance parameters. The nuisance parameters for each figure are:

Figure 1: Old bias, station location, and clock errors.
Figure 2: Old bias, and station location errors.
Figure 3: New bias, station location, and clock errors.
Figure 4: New bias, and station location errors.
Figure 5: New bias, and clock errors.

Comparison of Figures 1 and 3, and of Figures 2 and 4 indicates that except in the case in which only the six orbit parameters are estimated, it does not matter greatly whether the a priori accuracy of the biases is 10 m/sec. or 0.05 m/sec.

In any figure, the fewer the parameters estimated the larger the RMS uncertainty in the estimate of position.

Comparison of Figures 1 and 2, and of Figures 3, 4 and 5 shows that if the orbit parameters and measurement biases are estimated, the clock errors contribute far more to the uncertainty in the estimate of position than do the station location errors.

For the time from injection small, the uncertainty in position depends strongly on both the noise in the measurements and the uncertainty in the parameters that are not being estimated. As the time from injection increases the effect of noise on the measurements decreases, but that of the uncertainty in the parameters that are not estimated increases. This accounts for the sharp breaks in some of the curves in the figures. For time since injection greater than 10 or 15 hours the uncertainty in the estimate of position is almost entirely due to uncertainties in the values of the parameters that are not estimated. Consequently, the accuracy of position estimation can be greatly improved by obtaining better a priori estimates for the parameters that are not estimated, or by using a more sophisticated data processing scheme (filter) that estimates more parameters.

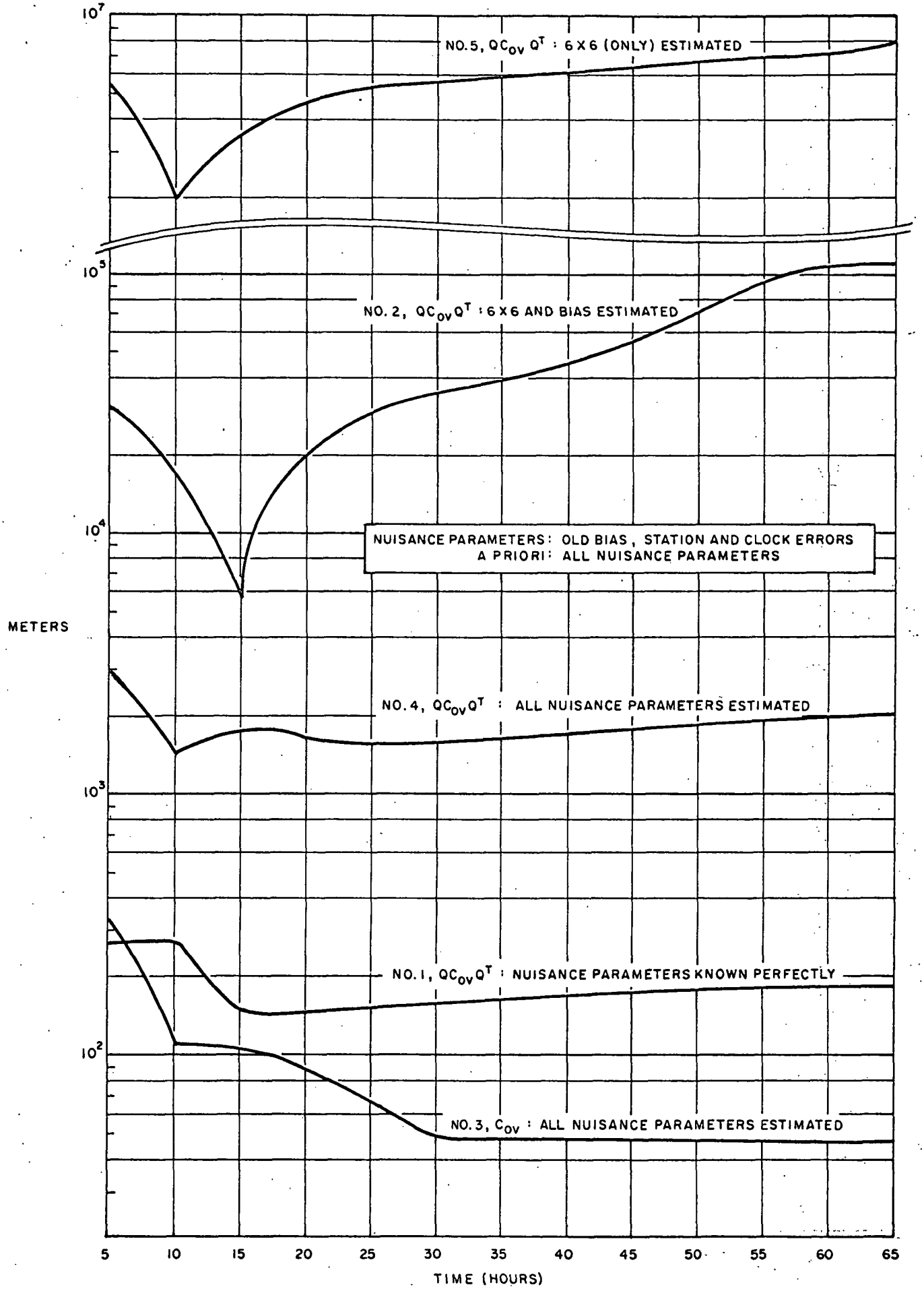
NO. 5, $QC_{OV}Q^T$: 6 X 6 (ONLY) ESTIMATED
NO. 2, $QC_{OV}Q^T$: 6 X 6 AND BIAS ESTIMATED
NUISANCE PARAMETERS: OLD BIAS, STATION AND CLOCK ERRORS
A PRIORI: ALL NUISANCE PARAMETERS
NO. 4, $QC_{OV}Q^T$: ALL NUISANCE PARAMETERS ESTIMATED
NO. 1, $QC_{OV}Q^T$: NUISANCE PARAMETERS KNOWN PERFECTLY
NO. 3, C_{OV} : ALL NUISANCE PARAMETERS ESTIMATED
METERS
10^7
10^5
10^4
10^3
10^2
5
10
15
20
25
30
35
40
45
50
55
60
65
TIME (HOURS)

Figure 1.

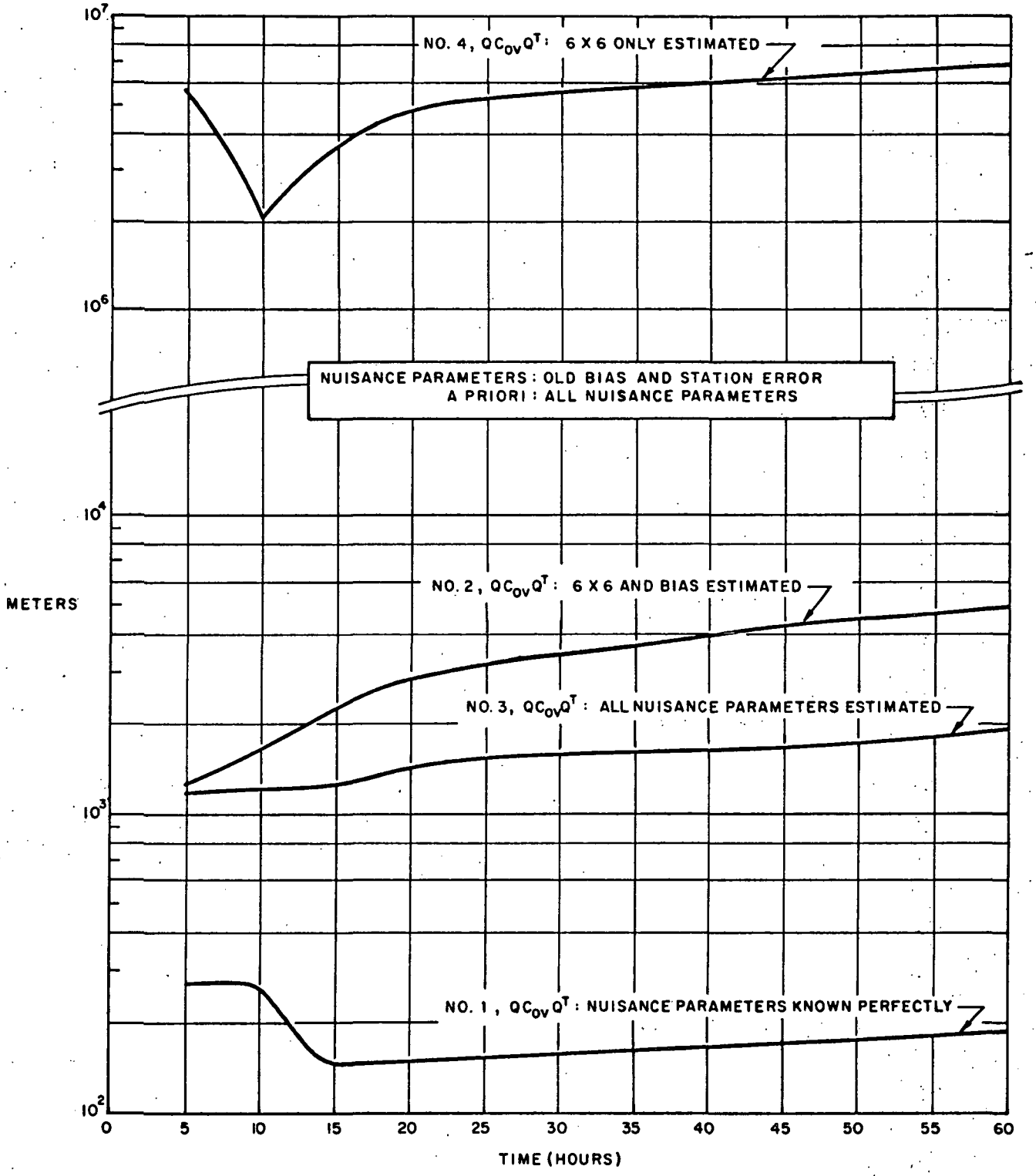
NO. 4, $QC_{OV}Q^T$: 6 X 6 ONLY ESTIMATED
NUISANCE PARAMETERS: OLD BIAS AND STATION ERROR
A PRIORI: ALL NUISANCE PARAMETERS
NO. 2, $QC_{OV}Q^T$: 6 X 6 AND BIAS ESTIMATED
NO. 3, $QC_{OV}Q^T$: ALL NUISANCE PARAMETERS ESTIMATED
NO. 1, $QC_{OV}Q^T$: NUISANCE PARAMETERS KNOWN PERFECTLY
METERS
10^7
10^6
10^4
10^3
10^2
0
5
10
15
20
25
30
35
40
45
50
55
60
TIME (HOURS)

Figure 2.

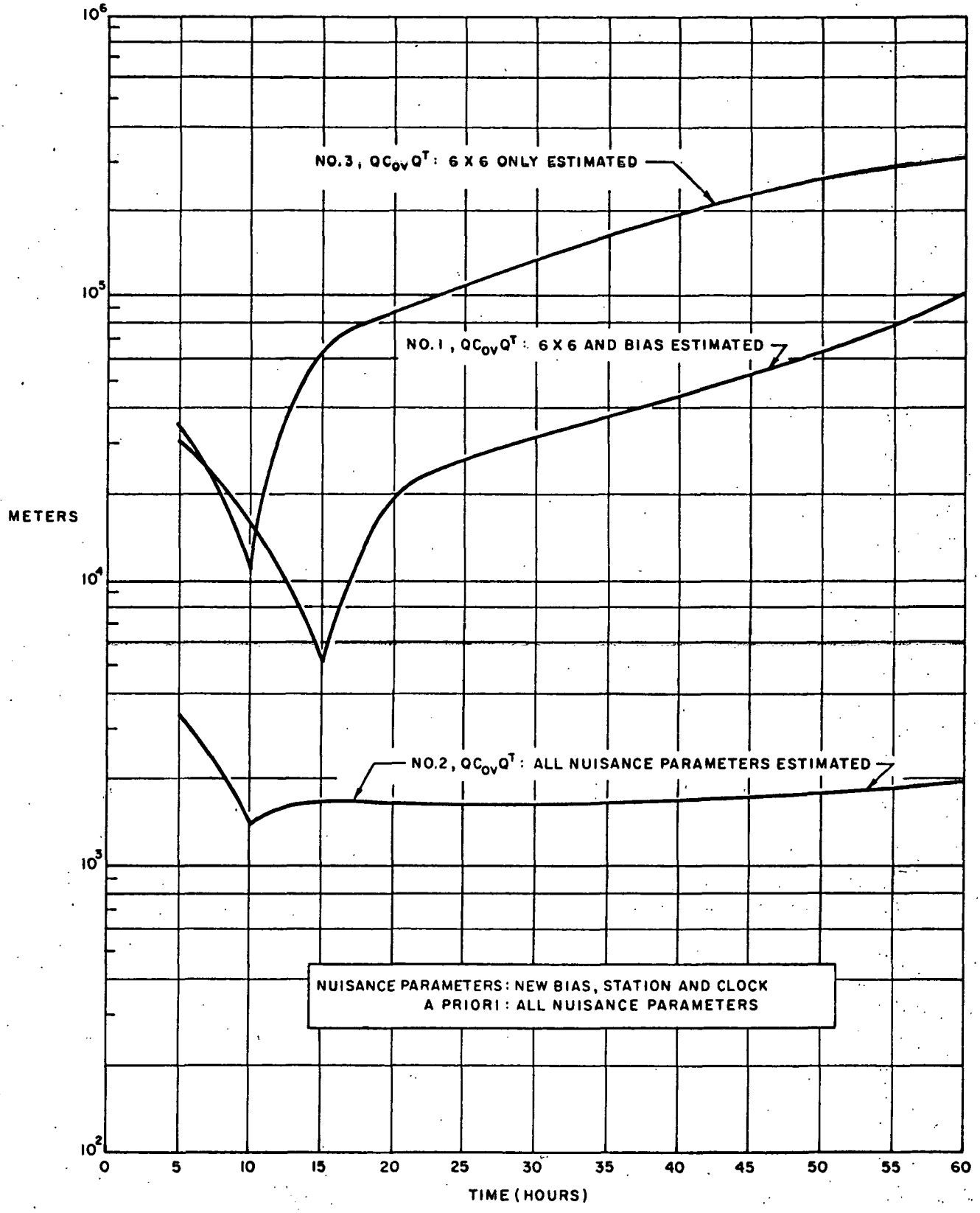
NO.3, $QC_{OV}Q^T$: 6 X 6 ONLY ESTIMATED
NO.1, $QC_{OV}Q^T$: 6 X 6 AND BIAS ESTIMATED
NO.2, $QC_{OV}Q^T$: ALL NUISANCE PARAMETERS ESTIMATED
NUISANCE PARAMETERS: NEW BIAS, STATION AND CLOCK
A PRIORI: ALL NUISANCE PARAMETERS
METERS
TIME (HOURS)
10^6
10^5
10^4
10^3
10^2
0
5
10
15
20
25
30
35
40
45
50
55
60

Figure 3.

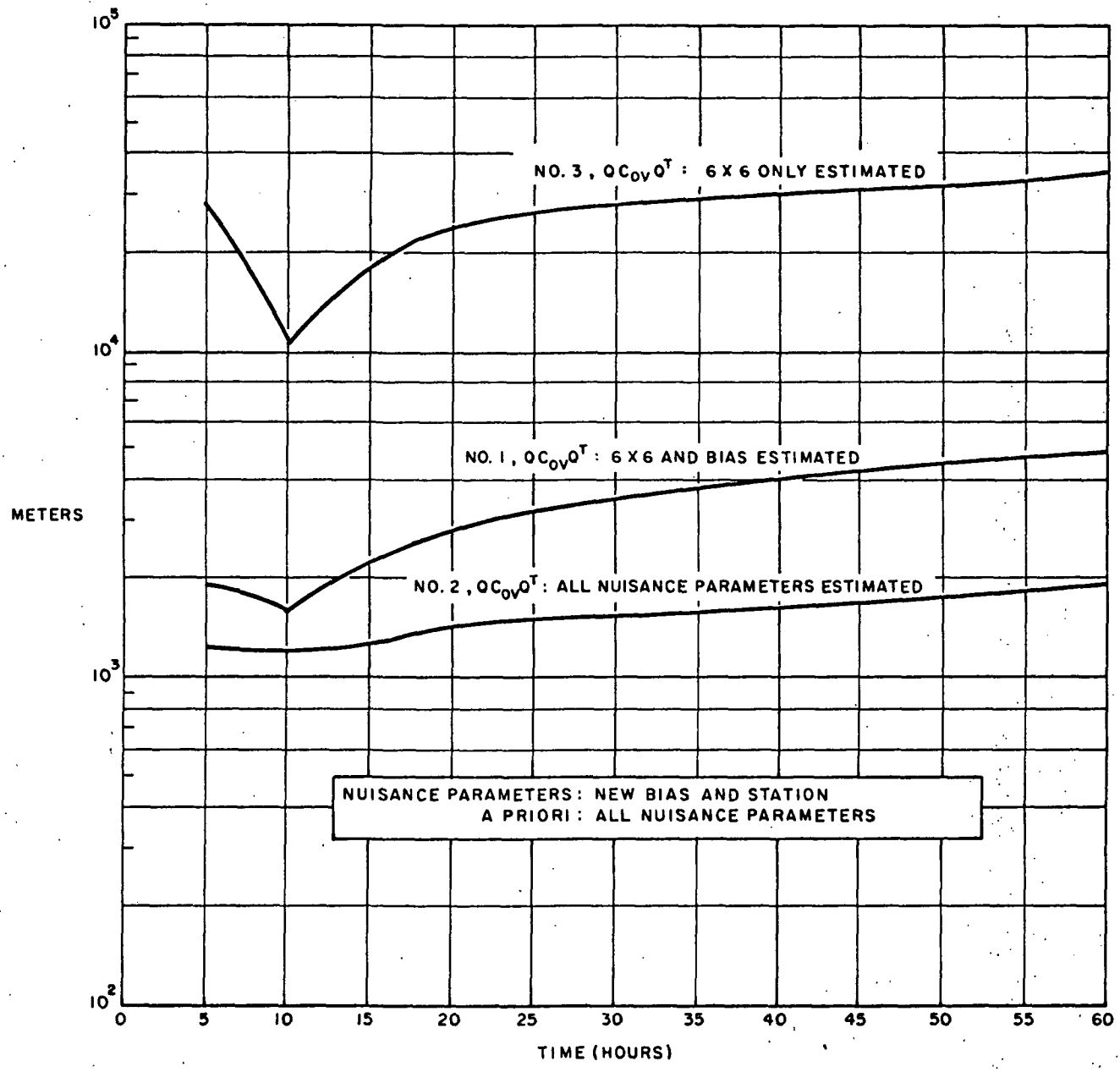
10^5
10^4
10^3
10^2
METERS
NO. 3 , $QC_{OV}Q^T$: 6 X 6 ONLY ESTIMATED
NO. 1 , $QC_{OV}Q^T$: 6 X 6 AND BIAS ESTIMATED
NO. 2 , $QC_{OV}Q^T$: ALL NUISANCE PARAMETERS ESTIMATED
NUISANCE PARAMETERS: NEW BIAS AND STATION
A PRIORI : ALL NUISANCE PARAMETERS
0
5
10
15
20
25
30
35
40
45
50
55
60
TIME (HOURS)

Figure 4.

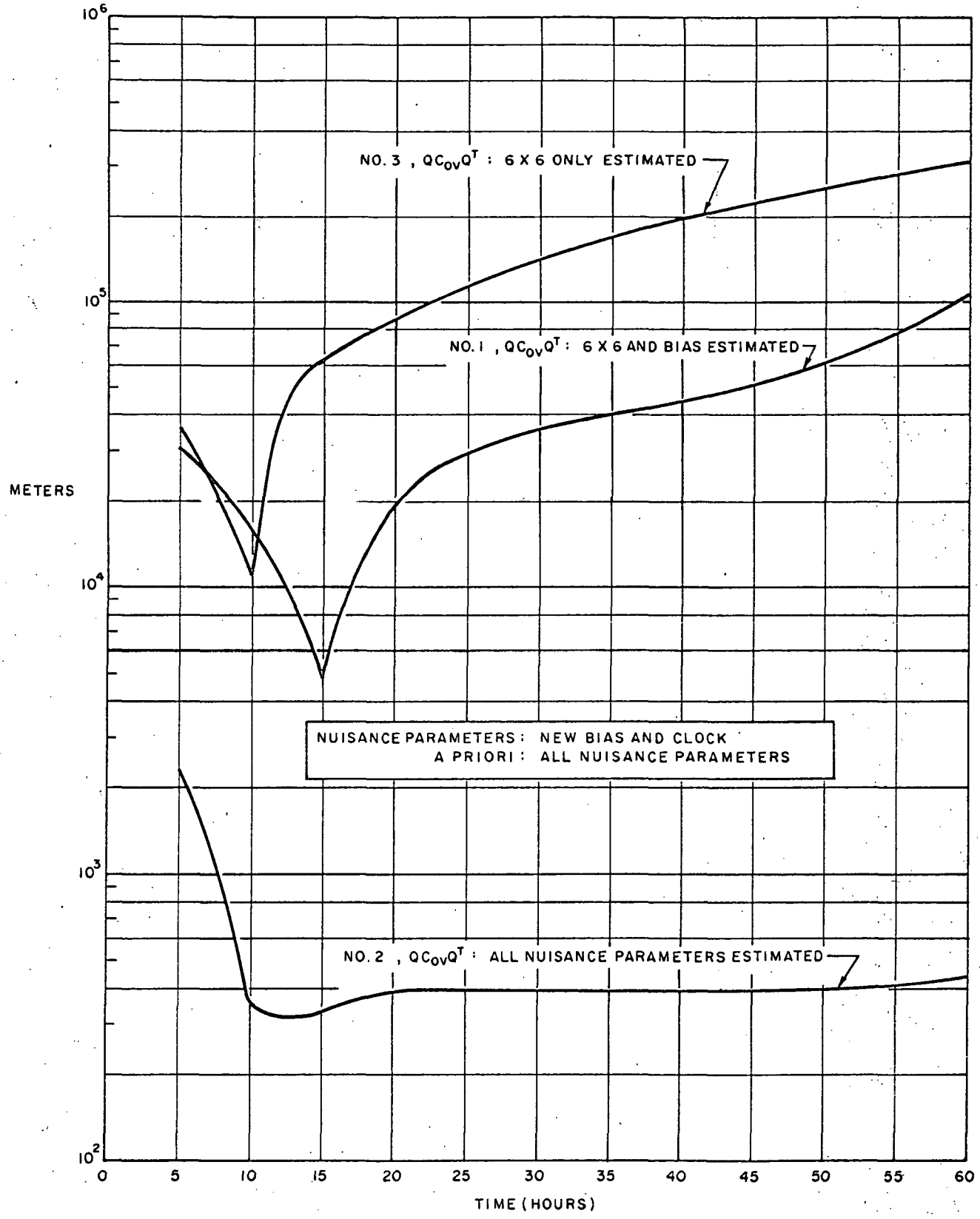
NO. 3 , $QC_{OV}Q^T$: 6 X 6 ONLY ESTIMATED
NO. 1 , $QC_{OV}Q^T$: 6 X 6 AND BIAS ESTIMATED
NUISANCE PARAMETERS : NEW BIAS AND CLOCK
A PRIORI : ALL NUISANCE PARAMETERS
NO. 2 , $QC_{OV}Q^T$: ALL NUISANCE PARAMETERS ESTIMATED
METERS
TIME (HOURS)
10^6
10^5
10^4
10^3
10^2
0
5
10
15
20
25
30
35
40
45
50
55
60

Figure 5.

The Bissett-Berman Corporation 2941 Nebraska Avenue, Santa Monica, California EXbrook 4-3270

APOLLO NOTE NO. 413
(Task II, Item 1)

C. P. Siska
2 March 1966

EFFECTS OF GRAVITATIONAL HARMONICS ON EARTH PARKING ORBIT PREDICTION

INTRODUCTION

This Note represents a preliminary investigation of the effects of harmonic terms in the Earth's gravitational potential upon the accuracy with which the Earth Parking Orbit is predicted. It also represents the first use of the integrated trajectory error analysis program (ITEAP), which is discussed in Apollo Notes 319 and 360.

The objectives in this investigation were twofold; first, to ascertain whether range and angle tracking by the Apollo ground station network could update the approximate current estimate of the harmonic terms over a relatively short period of time (9 orbits), and second, to determine how much the harmonic terms contribute to the uncertainty of parking orbit prediction in the Apollo mission phase. In the first instance, the a priori uncertainties in the zonal and tesseral harmonic coefficients were defined as twice the values obtained by KOZAI and IZSAK (Ref. 1 and 2). Inasmuch as these uncertainties were the result of processing several different orbits with many observations over long periods of time, no particular improvement in these uncertainties was expected. In pursuing the second objective, the program ITEAP is, at present, limited in the area of examining the effects of non-estimated parameters to a 40 x 40 matrix size. Consequently, the case of non-estimated harmonic terms in the Apollo mission phase was limited to examining effects over one parking orbit. The case of estimating (updating) the harmonic terms and other parameters had no limitation following the procedure outlined in Apollo Note No. 208.

INPUT PARAMETERS

Parking orbit insertion takes place over Cape Kennedy at

100 n. mi. altitude with a 90° azimuth. Since ITEAP can handle up to 20 stations only, the parking orbit is divided into two phases; the first phase is from t=0 to t=265 minutes flight time and the second phase is from t=265 to 809.25 minutes (actually this time range corresponds to 0 - 544.25 for the second phase).

Figure 1 shows the printout of input parameters for Phase I while Figure 2 does likewise for Phase II. Apollo Note No. 360 has a discussion of these parameters.

TRACKING DATA

A 6 second sample rate was used with range, azimuth, and elevation measurables, the sigmas being 15 meters for range (one-way path) and 0.8 milli-radians for each angle. Each station was considered to have an a priori uncertainty in the measurable bias of 100 meters in range and 1 milli-radian in angle.

The tracking schedule is shown in Table 1. Since the maximum matrix size for inversion is 40 x 40, this permitted a block of 3 stations to be processed at one time, yielding a 37 x 37 matrix for inversion. An outline of the parameters estimated is indicated in Figure 3. Within each block of data, the stations are numbered according to the values of Table 1.

RESULTS

All Parameters Estimated

Each data block was processed according to the "sequential" method of Apollo Note No. 208, the 19 "orbit" parameters in this case being position, velocity, gravitational constants of the Earth, mu of the Moon, and Earth-Moon distance.

Figure 3 shows the uncertainty in the values of the estimated parameters for accumulated observational data in the first phase of the parking orbit. That is to say, Block 3 values, for instance, are

the result of processing Blocks 1, 2, and 3 data and so forth. Some stations may appear in more than one data block (Table 1), however, the information concerning station location and measurable bias is always discarded and only a priori values are used for these parameters in each data block.

Figure 4 translates the results of Block 7 (corresponding to the t=0 position) to various times. The values of "orbit" parameters translated to the t=265 min. position are used as a priori values (19 x 19 marginal distribution matrix) for the second phase of the parking orbit.

Figure 5 shows the continuation of the parking orbit, except that the values in each column are associated with the t=265 min. position instead of the t=0 position. Harmonic terms are updated insignificantly as was expected for the short duration of approx. 9 orbits and the values of a priori uncertainties chosen.

Various Parameters Estimated During the First Orbit

Figure 6 shows results using Block 1 data (3 stations almost over one orbit) and estimating various groups of parameters out of the total of 37 parameters. The a priori values used are those shown in Figure 3 and the Block 1 results of Figure 3 can be directly compared with those of Figure 6.

Case 1 is the special case of no nuisance parameters, i. e. there is no uncertainty in any parameters excepting those of position and velocity.

Comparison of Case 3 and Case 2 indicates that adding as estimators, the "orbit" parameters other than position and velocity does not create much improvement in the knowledge of position and velocity. This is also evident in comparing Case 4 and the Block 1 results of Figure 3, in which instance not estimating these parameters has very little effect on position and velocity.

Comparison of Case 4 and 5 shows that there is a significant improvement when adding station location parameters to the list of estimators.

19 "Orbit" Parameters Only

In this case the list of estimators contains only the 19 "orbit" parameters, i. e. there is no uncertainty in the knowledge of station location and measurable bias.

During the Phase I parking orbit, all station data accumulated up to the indicated time in Figure 7 was processed. Table 1 indicates the number of stations involved.

This case again shows the insensitivity of the "orbit" parameters other than position and velocity, since the results are approximately equivalent to the no nuisance parameter case in both the case of estimating all 19 parameters and the case of estimating only the position and velocity parameters out of the set of 19 estimators.

CONCLUSIONS

During the Apollo mission phase involving the Earth parking orbit, neglecting Earth gravitational terms, as estimators in orbit prediction, has very little effect upon the accuracy with which position and velocity of the vehicle can be predicted. This is based on a conservative estimate of the uncertainties in current values of the harmonic terms. The effect of neglecting harmonic terms in the dynamical equations is left as a subject for future investigation.

Reference 1. Kozai, Y. Paper presented at the Symposium on the Use of Artificial Satellites for Geodesy. Wash., D. C. 1962.

Reference 2. Izsak, Jour. Geophysical Research, Vol. 69, No. 12, June 15, 1964.

PRIMARY BODY PARAMETERS			
14	MU		3.99689$_{00}$E 14
29	BODY RAD		6.378$_{1000}$E 0$_{6}$
26	PRI SPIN		7.2911600E-05
37	APM		1.2938000E 01
44	EAIND		1.0000000E 00
23	J2	2	1.0824800E-03
23	J3	3	-2.5660000E-06
23	J4	4	-1.8400000E-06
23	J5	5	-6.3000000E-08
24	C22	22	7.5500000E-07
24	C31	13	8.7500000E-07
24	C32	23	8.2000000E-08
25	S22	22	-6.1300000E-07
25	S31	13	-2.7000000E-07
25	S32	23	-8.5400000E-08
BODY TWO PARAMETERS			
19	MU2		4.896$_{0000}$E 12
20	MOON DIST		3.7836$_{000}$E 0^{8}
21	PHI		1.4622000E 01
22	V		1.5527000E 02
33	GAMID		1.0000000E 00
34	INCL		2.3000000E 01
60	OME2		2.6617000E-06
BODY THREE PARAMETERS			
15	MU SUN		1.327$_{1000}$E 20
16	DIST TO SUN		1.4737$_{000}$E 11
17	PHI		-1.7794000E 01
18	V		3.1226000E 02
31	GAMID		-1.0000000E 00
32	INCL		2.3500000E 01
ERROR ANALYSIS PARAMETERS			
27	DELTA T		2.5$_{0000000}$E-01
39	PRINT INTV		2.65$_{00000}$E 02
38	KEP ITER		2.0000000E-02
49	DEL TAU		2.5000000E-01
30	T Max		2.6600000E 02
41	T U MATRIX	1	1.2000000E 02
41	T U MATRIX	2	1.8000000E 02
41	T U MATRIX	3	2.4000000E 02
41	T U MATRIX	4	2.6500000E 02
43	QIND		1.0000000E 00
13	INP IND		-0

OMEGA	2.0236$_{100}$E 02
I	2.8482000E 01
U	9.0000000E 01
RZERO	6.5635$_{000}$E 0$_{6}$
VT	7.8$_{0}$367$_{00}$E 03
VR	-0
OMEGA(SM)	9.0000000E 01
ECC	2.5524583E-0$_{5}$

Figure 1.

Parameter Inputs For Phase I of Earth Parking Orbit

PRIMARY BODY PARAMETERS			
14	MU		3.99689$_{00}$E 14
29	BODY RAD		6.378$_{1000}$E 0^{6}
26	PRI SPIN		7.2911600E-05
37	APM		7.9360680E 01
44	EAIND		1.0000000E 00
23	J2	2	1.0824800E-03
23	J3	3	-2.5660000E-06
23	J4	4	-1.8400000E-06
23	J5	5	-6.3000000E-08
24	C22	22	7.5500000E-07
24	C31	13	8.7500000E-07
24	C32	23	8.2000000E-08
25	S22	22	-6.1300000E-07
25	S31	13	-2.7000000E-07
25	S32	23	-8.5400000E-08

BODY TWO PARAMETERS			
19	MU2		4.896$_{0000}$E 12
20	MOON DIST		3.7836000E 08
21	PHI		-1.8300000E 01
22	V		3.1400000E 02
33	GAMID		1.0000000E 00
34	INCL		2.3000000E 01
60	OME2		2.6617000E-06

BODY THREE PARAMETERS			
15	MU SUN		1.327$_{1000}$E 20
16	DIST TO SUN		1.473$_{7000}$E 11
17	PHI		-1.7794000E 01
18	V		3.1226000E 02
31	GAMID		-1.0000000E 00
32	INCL		2.3500000E 01

ERROR ANALYSIS PARAMETERS			
27	DELTA T		2.5$_{0000000}$E-01
49	DELTA TAU		2.5$_{0000000}$E-01
30	TMAX		9.6100000E 02
39	PRINT INTV		3.0000000E 01
38	KEP ITER		2.0000000E-02
41	T U MATRIX	1	2.5000000E 02
41	T U MATRIX	2	5.0000000E 02
41	T U MATRIX	3	7.5000000E 02
41	T UMATRIX	4	9.6000000E 02
43	QIND		1.0000000E 00
13	INP IND		1.0000000E 00

X	2.6855$_{0}$8E 0^{6}
Y	-5.1162438E 0^{6}
Z	3.1129111E 0^{6}
X DOT	6.9959214E 0^{3}
Y DOT	3.4359552E 0^{3}
Z DOT	-3.8822302E 02

ORBIT PARAMETERS TRANSFORMED	
OMEGA	-1.5911016E 02
I	2.8482135E 01
U	9.5988$_{1}$46E 01
RZERO	6.5634$_{0}$99E 0^{6}
VT	7.8$_{0}$38$_{0}$81E 0^{3}
VR	3.2616397E-02
OMEGA(SM)	9.0927373E 01
ECC	4.7382773E-05

Figure 2.

Parameter Inputs

Phase II of Earth Parking Orbit

TABLE 1.

TRACKING SCHEDULE FOR EARTH PARKING ORBIT - EAST LAUNCH

Station	Data Block	Station No.	Tracking Interval (min. after insertion)
Bermuda	2	1	2.00 - 5.75
Carnarvon		2	47.50 - 52.50
Hawaii		3	73.25 - 76.50
Pt. Arguello	2	1	83.00 - 85.00
Guaymas		2	86.00 - 88.00
G. Bahamas		3	91.50 - 96.00
Antigua	3	2	96.00 - 100.25
Ascension		3	110.00 - 114.00
Carnarvon		1	140.75 - 145.00
Hawaii	4	2	165.25 - 170.25
Pt. Arguello		3	175.25 - 178.00
Guaymas		1	178.00 - 181.00
Corpus Christie	5	2	181.00 - 184.75
G. Bahamas		3	184.75 - 187.50
G. Turk I.		1	187.50 - 190.00
Antigua	6	2	190.00 - 193.50
Ascension		3	202.75 - 207.25
Guam		1	245.5 - 249.75
Hawaii	7	1	259.00 - 263.25
Pt. Arguello	8	1	268.50 - 269.75
Guaymas		2	269.75 - 274.00
Corpus Christie		3	274.00 - 275.50
Guam	9	1	338.25 - 342.00
Hawaii		2	352.00 - 356.00
Hawaii		3	712.50 - 716.50
Hawaii	10	1	538.25 - 542.00
Ascension		2	671.75 - 675.00
Guam		3	712.50 - 716.50
Ascension	11	1	764.00 - 768.50
Guam		2	805.25 - 809.75

Parameter	A Priori	Block 1	Block 2	Block 3	Block 4
Position	8.6602540E 02	1.1515047E 02	6.2810949E 01	4.8035178E 01	3.9384497E 01
Velocity	5.1961524E 00	1.3444141E-01	8.8622050E-02	5.9396032E-02	4.9403435E-02
x	5.0000000E 02	7.0104459E 01	4.8215313E 01	3.5714122E 01	2.9480683E 01
y	5.0000000E 02	3.7373468E 01	2.2185976E 01	1.8843515E 01	1.5147113E 01
z	5.0000000E 02	8.3292009E 01	3.3589899E 01	2.6015414E 01	1.9948549E 01
x dot	3.0000000E 00	9.0771929E-02	3.2452494E-02	2.0936608E-02	1.8402114E-02
y dot	3.0000000E 00	5.6579013E-02	5.4413009E-02	3.7585864E-02	2.9649098E-02
z dot	3.0000000E 00	8.1777635E-02	6.1967151E-02	4.0950519E-02	3.5098339E-02
MU Earth	3.0000000E 08	2.9989083E 08	2.9975888E 08	2.9973368E 08	2.9967425E 08
J2	8.0000000E-08	7.9999789E-08	7.9995980E-08	7.9981974E-08	7.9965779E-08
J3	2.3874673E-08	2.3874432E-08	2.3873989E-08	2.3868716E-08	2.3843158E-08
J4	1.7888544E-07	1.7887480E-07	1.7882838E-07	1.7863671E-07	1.7823997E-07
J5	3.7416574E-08	3.7416202E-08	3.7414776E-08	3.7388689E-08	3.7332995E-08
C22	2.6076810E-08	2.6076701E-08	2.6076506E-08	2.6075568E-08	2.6046929E-08
C31	4.3538989E-08	4.3585430E-08	4.3578765E-08	4.3538169E-08	4.3470078E-08
C32	2.0000000E-08	1.9997604E-08	1.9994838E-08	1.9865521E-08	1.9747434E-08
S22	3.7416574E-08	3.7411325E-08	3.7398547E-08	3.7372428E-08	3.7326020E-08
S31	4.3538989E-08	4.3585536E-08	4.3582792E-08	4.3543215E-08	4.3510959E-08
S32	2.0000000E-08	1.9999464E-08	1.9991928E-08	1.9974887E-08	1.9939976E-08
MU-Moon	3.4641016E 07	3.4641016E 07	3.4641016E 07	3.4641016E 07	3.4641016E 07
E-M Dis.	2.0000000E 06	2.0000000E 06	2.0000000E 06	1.9999999E 06	1.9999996E 06
Sta 1 East	5.0000000E 01	4.6535634E 01	2.5513628E 01	3.7104841E 01	1.7132681E 01
Sta 1 North	5.0000000E 01	3.8639863E 01	4.2567358E 01	2.9549595E 01	3.1198548E 01
Sta 1 Up	5.0000000E 01	4.7967131E 01	4.9518813E 01	4.7502488E 01	2.3036657E 01
Sta 2 East	5.0000000E 01	2.5860620E 01	4.4430235E 01	1.9293216E 01	2.0021276E 01
Sta 2 North	5.0000000E 01	4.0373102E 01	4.8962595E 01	2.9787818E 01	3.2637398E 01
Sta 2 Up	5.0000000E 01	3.5000962E 01	4.5625767E 01	4.5739248E 01	3.4050760E 01
Sta 3 East	5.0000000E 01	4.7682486E 01	2.1065636E 01	3.0761559E 01	1.6849040E 01
Sta 3 North	5.0000000E 01	4.7611827E 01	3.6335972E 01	3.3557545E 01	3.4016135E 01
Sta 3 Up	5.0000000E 01	4.9701845E 01	2.4698418E 01	4.7534037E 01	4.8438958E 01
Sta 1 R	1.0000000E 02	2.8338224E 01	4.5663620E 01	1.4575490E 01	1.3202159E 01
Sta 1 Elev	1.0000000E-03	2.0728873E-04	2.2597334E-04	1.6347293E-04	2.4601596E-04
Sta 1 AZIM	1.0000000E-03	1.9418823E-04	2.2421624E-04	1.6940780E-04	2.5398659E-04
Sta 2 R	1.0000000E 02	1.0770581E 01	4.6661077E 01	1.0758080E 01	5.2651466E 00
Sta 2 Elev	1.0000000E-03	1.8183008E-04	1.7971484E-04	1.6827137E-04	1.5717289E-04
Sta 2 AZIM	1.0000000E-03	1.5532793E-04	1.7990427E-04	1.5751562E-04	1.4778674E-04
Sta 3 R	1.0000000E 02	3.3414382E 01	5.7888322E 00	1.3521942E 01	2.8055287E 01
Sta 3 Elev.	1.0000000E-03	2.0032305E-04	1.6745430E-04	1.6999035E-04	1.9742634E-04
Sta 3 AZIM	1.0000000E-03	2.0067818E-04	1.5878137E-04	1.6936773E-04	1.9067185E-04

Figure 3.
Sq. Rt. of Diagonal Cov Matrix Elements (t = o_position)

BLOCK 5	BLOCK 6	BLOCK 7
3.6710951E 01	3.2840716E 01	3.1828439E 01
4.6981222E-02	4.0751783E-02	4.0115093E-02
2.7499942E 01	2.4160951E 01	2.3768462E 01
1.4869685E 01	1.3212622E 01	1.2860248E 01
1.9244208E 01	1.7893789E 01	1.6814391E 01
1.6863867E-02	1.5174256E-02	1.5084659E-02
2.8601648E-02	2.5643338E-02	2.5183062E-02
3.3238396E-02	2.7800522E-02	2.7340211E-02
2.9966080E 08	2.9965010E 08	2.9964989E 08
7.9928953E-08	7.9844400E-08	7.9843080E-08
2.3861580E-08	2.3849234E-08	2.3846683E-08
1.7742390E-07	1.7543144E-07	1.7540450E-07
3.7357253E-08	3.7297539E-08	3.7285504E-08
2.6064921E-08	2.6049037E-08	2.6031732E-08
4.3414004E-08	4.3217430E-08	4.3205465E-08
1.9725965E-08	1.9387563E-08	1.9359705E-08
3.7277932E-08	3.7247214E-08	3.7238049E-08
4.3500037E-08	4.3390575E-08	4.3382312E-08
1.9881508E-08	1.9769534E-08	1.9718685E-08
3.4641016E 07	3.4641016E 07	3.4641016E 07
1.9999996E 06	1.9999993E 06	1.9999991E 06
2.2009897E 01	2.0882433E 01	2.0555276E 01
3.3022226E 01	2.8806609E 01	2.7308493E 01
4.7627348E 01	4.3598952E 01	4.7245196E 01
1.6600513E 01	2.0115927E 01	
3.1166010E 01	2.8805004E 01	
3.9188200E 01	4.6591356E 01	
2.1969627E 01	2.6658270E 01	
3.2683622E 01	2.6626996E 01	
4.8746960E 01	4.7507334E 01	
2.7071700E 01	9.7492494E 00	1.4893541E 01
2.0969044E-04	1.6893583E-04	1.6249725E-04
2.0294907E-04	1.6555317E-04	1.5693429E-04
1.0656828E 01	2.0045046E 01	
1.8114859E-04	1.7844127E-04	
1.6760901E-04	1.7159311E-04	
3.0569656E 01	1.4378854E 01	
1.9592016E-04	1.5756429E-04	
1.9072653E-04	1.5550493E-04	

Figure 3. (continued)

Parameter	t = 0 min.	t = 76.5 min.	t = 120.0 min.
Position	3.1828439E 01	2.9311560E 01	3.1449889E 01
Velocity	4.0115093E-02	2.7985649E-02	2.9344823E-02
x	2.3768463E 01	1.5693803E 01	2.0479040E 01
y	1.2860248E 01	1.3746335E 01	1.3209545E 01
z	1.6814391E 01	2.0589085E 01	1.9879948E 01
x dot	1.5084659E-02	8.6605091E-03	1.3511603E-02
y dot	2.5183062E-02	1.8398406E-02	1.6742022E-02
z dot	2.7340211E-02	1.9227344E-02	1.9956450E-02

t = 180.0 min.	t = 240.0 min.	t = 265.0 min.
2.2818676E 01	3.5725578E 01	2.9710821E 01
2.9736877E-02	3.6925043E-02	3.7544899E-02
1.0472022E 01	8.9179622E 00	1.8548209E 01
1.2121813E 01	2.5845065E 01	1.5924283E 01
1.6250857E 01	2.2996075E 01	1.6885320E 01
9.8707203E-03	2.5997406E-02	1.3626042E-02
1.5793439E-02	1.7261126E-02	2.2895056E-02
2.3182279E-02	1.9739483E-02	2.6453107E-02

Figure 4.

Block 7 Results Translated Forward in Time

Parameter	A Priori	BLOCK 8	BLOCK 9	BLOCK 10	BLOCK 11
	BLOCK 7				
Position	2.9710821E 01	2.6854710E 01	2.3293328E 01	2.2261177E 01	2.1974384E 01
Velocity	3.7544899E-02	3.4622603E-02	3.1961420E-02	2.9688429E-02	2.8759927E-02
x	1.8548209E 01	1.6573251E 01	1.5854450E 01	1.4757956E 01	1.4349456E 01
y	1.5924283E 01	1.3525542E 01	1.0106315E 01	9.7888702E 00	9.7641790E 00
z	1.6885320E 01	1.6234610E 01	1.3750562E 01	1.3488541E 01	1.3476924E 01
x dot	1.3626042E-02	1.2771526E-02	1.1706545E-02	1.1039527E-02	1.0768423E-02
y dot	2.2895056E-02	2.0579173E-02	1.9795651E-02	1.8554315E-02	1.8099617E-02
z dot	2.6453107E-02	2.4740865E-02	2.2195075E-02	2.0378152E-02	1.9585155E-02
MU Earth	2.9964989E 08	2.9960582E 08	2.8392796E 08	2.8186350E 08	2.8154789E 08
J2	7.9843080E-08	7.9788761E-08	7.9526560E-08	7.8473424E-08	7.7936547E-08
J3	2.3846683E-08	2.3844552E-08	2.3834114E-08	2.3678452E-08	2.3636988E-08
J4	1.7540450E-07	1.7415348E-07	1.6697745E-07	1.3996630E-07	1.2384344E-07
J5	3.7285504E-08	3.7275771E-08	3.7223222E-08	3.6456590E-08	3.6263950E-08
C22	2.6031732E-08	2.5999793E-08	2.5932394E-08	2.5812522E-08	2.5715834E-08
C31	4.3205465E-08	4.3160606E-08	4.1112943E-08	4.0801511E-08	4.0431908E-08
C32	1.9359705E-08	1.9301774E-08	1.8645396E-08	1.8490369E-08	1.8455953E-08
S22	3.7238049E-08	3.7204700E-08	3.7117149E-08	3.6740177E-08	3.6731006E-08
S31	4.3382312E-08	4.3307994E-08	4.2752744E-08	3.9296389E-08	3.8233869E-08
S32	1.9718685E-08	1.9681499E-08	1.8441280E-08	1.8034318E-08	1.7935543E-08
MU Moon	3.4641016E 07	3.4641016E 07	3.4641016E 07	3.4641016E 07	3.4641016E 07
E-M Distance	1.9999991E 06	1.9999990E 06	1.9999980E 06	1.9999975E 06	1.9999967E 06
Sta 1 East	5.0000000E 01	2.9482130E 01	2.1594877E 01	2.2461842E 01	4.5335927E 01
Sta 1 North	5.0000000E 01	4.3677225E 01	2.8747379E 01	2.7392684E 01	4.5189471E 01
Sta 1 Up	5.0000000E 01	4.9879975E 01	4.7874328E 01	4.7684653E 01	4.8668748E 01
Sta 1 R	1.0000000E 02	4.5873351E 01	1.8141086E 01	1.8011280E 01	5.1799749E 01
Sta 1 Elev	1.0000000E 03	2.7607132E-04	1.7112150E-04	1.7162932E-04	3.4783236E-04
Sta 1 AZIM	1.0000000E 03	2.7435447E-04	1.6687857E-04	1.6689528E-04	3.4878523E-04
Sta 2 East	5.0000000E 01	1.9437657E 01	1.7108087E 01	3.5679249E 01	3.0370785E 01
Sta 2 North	5.0000000E 01	2.5084801E 01	2.5959467E 01	3.3478812E 01	3.0282424E 01
Sta 2 Up	5.0000000E 01	4.6459700E 01	4.7383828E 01	4.8665204E 01	4.5237042E 01
Sta 2 R	1.0000000E 02	1.2808522E 01	1.5559329E 01	2.6668849E 01	1.0136430E 01
Sta 2 Elev	1.0000000E 03	1.6504596E-04	1.6690491E-04	1.8090598E-04	1.6520509E-04
Sta 2 AZIM	1.0000000E 03	1.5645171E-04	1.5987444E-04	1.8645548E-04	1.6273082E-04
Sta 3 East	5.0000000E 01	2.9227304E 01	2.9838141E 01	3.2610421E 01	
Sta 3 North	5.0000000E 01	4.2402042E 01	3.2878833E 01	2.9877994E 01	
Sta 3 Up	5.0000000E 01	4.9860763E 01	3.3289778E 01	4.7602571E 01	
Sta 3 R	1.0000000E 02	4.5601825E 01	5.3720490E 00	1.5990090E 01	
Sta 3 Elev	1.0000000E 03	2.5434871E-04	1.5776829E-04	1.6767339E-04	
Sta 3 AZIM	1.0000000E 03	2.5267613E-04	1.5909777E-04	1.7034275E-04	

Figure 5.

Sq. Rt. of Diagonal Cov Matrix Elements (t = 265 min. Position)

	CASE 1	CASE 2	CASE 3	CASE 4	CASE 5
Position	2.2276217E 01	3.4632851E 02	2.9522414E 02	1.1515049E 02	2.1459861E 02
Velocity	2.3498971E-02	3.7307446E-01	3.4383189E-01	1.3464145E-01	2.1947000E-01
x	1.4852898E 01	1.8153132E 02	1.4946534E 02	7.0180461E 01	1.1745282E 02
y	8.0257832E 00	1.2194216E 02	8.6330901E 01	3.7373501E 01	5.5413340E 01
z	1.4533000E 01	2.6855153E 02	2.3950863E 02	8.3292016E 01	1.7084133E 02
x dot	2.1681197E-02	3.1884018E-01	2.8731628E-01	9.0771963E-02	1.8040489E-01
y dot	5.7805780E-03	1.0411944E-01	1.0503214E-01	5.6579030E-02	6.0738922E-02
z dot	6.9794162E-03	1.6335430E-01	1.5696487E-01	8.1777657E-02	1.0923343E-01

	CASE 3	CASE 4		CASE 5	
MU-E	3.3006695E 09	R	2.8338228E 01	R	3.5077779E 01
J2	9.0315432E-08	EL	2.0728874E-04	EL	2.8181649E-04
J3	3.7404886E-08	AZ	1.9418824E-04	AZ	2.0080072E-04
J4	4.7111445E-07	R	1.0770583E 01	R	2.2918374E 01
J5	5.6291787E-08	EL	1.8183012E-04	EL	2.7266362E-04
C22	2.6118008E-08	AZ	1.5532793E-04	AZ	1.9375946E-04
C31	9.5875874E-08	R	3.3414383E 01	R	5.3860619E 01
C32	5.1205898E-08	EL	2.0032305E-04	EL	2.4533613E-04
S22	1.8927565E-07	AZ	2.0067819E-04	AZ	2.0214414E-04
S31	1.3246499E-07	E	4.6535636E 01		
S32	2.0221800E-08	N	3.8639877E 01		
MU-M	3.4641016E 07	UP	4.7967133E 01		
E-M D.	2.0007042E 06	E	2.5860620E 01		
		N	4.0373104E 01		
		UP	3.5000982E 01		
		E	4.7682487E 01		
		N	4.7611829E 01		
		UP	4.9701845E 01		

Case 1 - No nuisance parameters

Case 2 - Position, Velocity Estimated- Grav. constants, E-M Distance, Station Locations, R, EL, AZZ Biases not estimated.

Case 3 - Pos., Vel., Grav. Const., E-M Dist. estimated - Sta. Loc., R, EL, AZ biases not estimated.

Case 4 - Pos., Vel., Sta. Loc, R, EL, AZ biases estimated - Grav Const., E-M Dist. not estimated.

Case 5 - Pos., Vel., R, EL, AZ Biases estimated - Grav. Const., E-M Dist., Sta. Loc. not estimated.

Figure 6.

Block 1 Data with Various Parameters Estimates (t = o position)

All 19 Parameters Estimated

Parameter	A Priori	t = 88 min.	t = 178 min.	t = 265 min.
Position	8.66025400E 02	6.14427040E 00	4.03133540E 00	4.05259970E 00
Velocity	5.19615240E 00	8.01500980E-03	6.82789700E-03	5.19729300E-03
x	5.00000000E 02	3.68968400E 00	2.23497900E 00	2.23824710E 00
y	5.00000000E 02	2.62752890E 00	2.69488600E 00	2.83958490E 00
z	5.00000000E 02	4.15143150E 00	1.99853030E 00	1.83045680E 00
x dot	3.00000000E 00	3.61476800E-03	2.25598450E-03	2.48787420E-03
y dot	3.00000000E 00	4.64521870E-03	4.46560960E-03	3.12717970E-03
z dot	3.00000000E 00	5.44020020E-03	4.64640100E-03	3.32311360E-03
μ Earth	3.00000000E 08	2.81505760E 08	2.52190870E 08	2.48256940E 08
J2	8.00000000E-08	7.99021170E-08	7.77020430E-08	7.65150400E-08
J3	2.38746730E-08	2.38522340E-08	2.33709340E-08	2.29995910E-08
J4	1.78885440E-07	1.76893440E-07	1.31171450E-07	8.54029480E-08
J5	3.74165740E-08	3.73650670E-08	3.54596590E-08	3.36934110E-08
C22	2.60768100E-08	2.60714190E-08	2.48773830E-08	2.12540510E-08
C31	4.35889890E-08	4.34214530E-08	3.98571430E-08	3.39481750E-08
C32	2.00000000E-08	1.99282270E-08	1.30646950E-08	1.07784680E-08
S22	3.74165740E-08	3.55836470E-08	2.96238370E-08	2.70955130E-08
S31	4.35889890E-08	4.33858610E-08	3.87591540E-08	3.53876880E-08
S32	2.00000000E-08	1.99248480E-08	1.55852280E-08	1.23576330E-08
μ Moon	3.46410160E 07	3.46410160E 07	3.46410160E 07	3.46410160E 07
E-M Distance	2.00000000E 06	1.99999660E 06	1.99996300E 06	1.99990020E 06

Note: Cumulative Observations Up to Time t.

Figure 7.

Data Blocks 1 through 7 Using 19 Parameters Only
(coordinates at time t)

Position and Velocity Components Only (No Nuisance Parameters)

Parameter	t = 88 min.	t = 178 min.	t = 265 min.
Position	5.7160600E 00	3.0603007E 00	2.5503261E 00
Velocity	6.8143908E-03	3.6599841E-03	2.8189111E-03
x	3.4011140E 00	1.8418443E 00	1.7049557E 00
y	2.5837193E 00	1.8249542E 00	1.4445092E 00
z	3.7987050E 00	1.6256050E 00	1.2290982E 00
x dot	3.1994215E-03	1.3040943E-03	1.0442408E-03
y dot	4.0343440E-03	2.4946458E-03	1.9844857E-03
z dot	4.4635964E-03	2.3391374E-03	1.7081092E-03

Position and Velocity Components Estimated - Remaining 13 Parameters Not Estimated

Parameter	t = 88 min.	t = 178 min.	t = 265 min.
Position	6.2048879E 00	5.3122492E 00	6.7973675E 00
Velocity	8.0887259E-03	9.2849299E-03	1.2602858E-02
x	3.7170182E 00	2.9242178E 00	3.5357698E 00
y	2.6313669E 00	3.6487140E 00	5.0335936E 00
z	4.2142992E 00	2.5210766E 00	2.8923125E 00
x dot	3.6473072E-03	2.9596764E-03	6.3844662E-03
y dot	4.6733494E-03	5.9372116E-03	6.7868448E-03
z dot	5.5031302E-03	6.4961341E-03	8.4858321E-03

Figure 7 (continued)

The Bissett-Berman Corporation 2941 Nebraska Avenue, Santa Monica, California EXbrook 4-3270

APOLLO NOTE NO. 414
(Task 2, Item II)

C. H. Dale
L. Lustick

USING THE OEAP TO CALCULATE THE COVARIANCE OF THE FIRST CORRECTIVE BOOST AFTER THE ASCENT BURN

This note should be of interest only in showing how one can use the old Orbit Error Analysis Program to check the new LEM Guidance and Navigation Evaluation Program in the specific area of boost covariance calculations. Presented below is an example calculation.

The trajectory studied is shown in the following Figure:

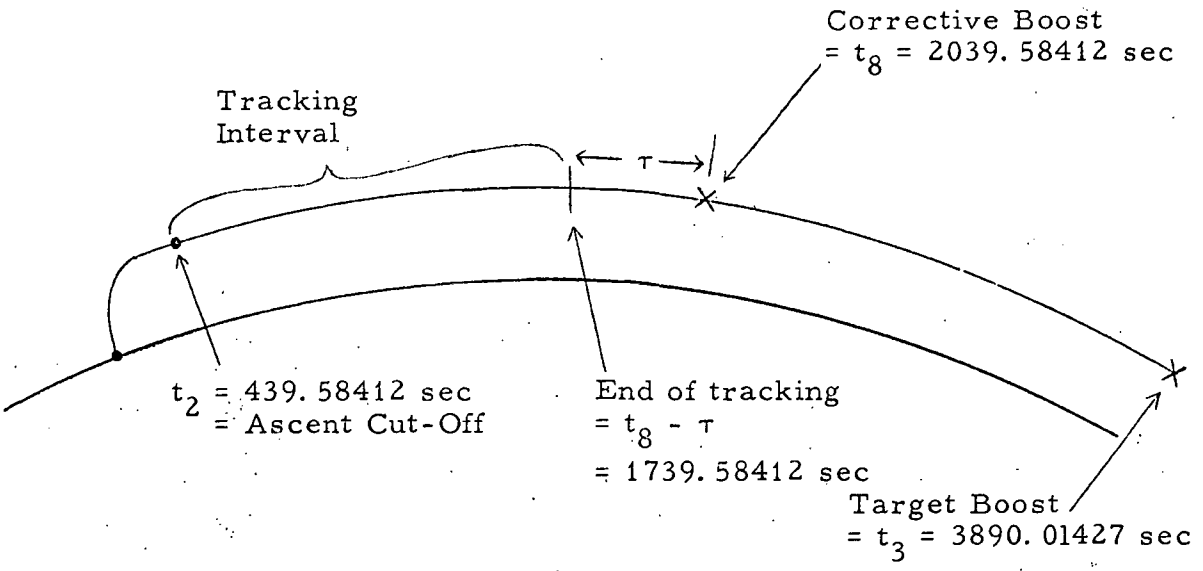

The operations that must be performed are the following:

1.) The a priori covariance of the Lift-Off point are used in conjunction with the Ascent Burn trajectory and uncertainties to produce an a priori covariance of the state vector at t_2.

2.) A priori values of all nuisance parameters are specified.

3.) Tracking is performed between t_2 and $t_8 - \tau$ using the OEAP for a group of stations. Two Q matrices are produced during these runs of Part A of the OEAP: $Q\left(\frac{t_3}{t_2}\right)$, $Q\left(\frac{t_8}{t_2}\right)$. Asking for the Q matrix from t_2 to t_8 causes the program to produce the state vector at t_8 and the angle between t_2 and t_8.

4.) Using the a priori inputs, the tracking information and $Q\left(\frac{t_3}{t_2}\right)$, the following outputs are produced using Part B of the OEAP.

$\overline{(\hat{a}-a_t)(\hat{a}-a_t)^T}$ = The covariance of the total state vector at t_3 updating 6 x 6 and biases but not other nuisance parameters and expressed in t_8 local coordinates. A 6 x 6 $Q\left(\frac{t_3}{t_2}\right)$ is used.

C_T^{-1} = The covariance of the 6 x 6 and updated biases (one for each tracking station) at t_3 in t_8 coordinates assuming all other parameters are known perfectly. A 6 x 6 $Q\left(\frac{t_3}{t_2}\right)$ is used.

C_{ap}^{-1} = The A priori covariance of the 6 x 6 expressed at t_3 in t_8 coordinates.

5.) Using the above outputs, the 3 x 3 position components are added by hand to produce

$$F_{ij} = C_{ap}^{-1} - 2\,C_T^{-1} + \overline{(\hat{a}-a_t)(\hat{a}-a_t)^T}$$

i = 1 to 3
j = 1 to 3

This is the position error covariance, with respect to the reference, at t_3 (expressed in t_8 coordinates) which must be corrected by a boost at t_8. An explanation of F_{ij} is found at the end of this Note.

6.) Using the output of Part A of the OEAP (wherein $Q\left(\frac{t_8}{t_2}\right)$ was called for, the radius (a_1), radius rate (a_4) and tangential velocity (a_5) are hand calculated at t_8, the time of the corrective boost. These are entered in a separate Part A to produce a Q matrix from t_8 to t_3. This is called $Q\left(\frac{t_3}{t_8}\right)$. From the first 6 x 6 set of components of $Q\left(\frac{t_3}{t_8}\right)$ we extract the upper right 3 x 3. We may define:

$$Q'\left(\frac{t_3}{t_8}\right) = \begin{bmatrix} \frac{\partial x(t_3)}{\partial \dot{x}(t_8)} & \frac{\partial x(t_3)}{\partial \dot{y}(t_8)} & \frac{\partial x(t_3)}{\partial \dot{z}(t_3)} \\ \frac{\partial y(t_3)}{\partial \dot{x}(t_8)} & \frac{\partial y(t_3)}{\partial \dot{y}(t_8)} & \frac{\partial y(t_3)}{\partial \dot{z}(t_8)} \\ \frac{\partial z(t_3)}{\partial \dot{x}(t_8)} & \frac{\partial z(t_3)}{\partial \dot{y}(t_8)} & \frac{\partial z(t_3)}{\partial \dot{z}(t_8)} \end{bmatrix}$$

Now

$$Q'\left(\frac{t_3}{t_8}\right)\begin{bmatrix} \Delta v_x(t_8) \\ \Delta v_y(t_8) \\ \Delta v_z(t_8) \end{bmatrix} = -\begin{bmatrix} \Delta x(t_3) \\ \Delta y(t_3) \\ \Delta z(t_3) \end{bmatrix}$$

expresses the fact that the boost at t_8 operated upon by the Q' matrix should remove (thus the minus sign) the position errors at t_3. Multiplying through by Q'^{-1} gives:

$$\begin{bmatrix} \Delta v_x(t_8) \\ \Delta v_y(t_8) \\ \Delta v_z(t_8) \end{bmatrix} = - Q'\left(\frac{t_3}{t_8}\right)^{-1} \begin{bmatrix} \Delta x(t_3) \\ \Delta y(t_3) \\ \Delta z(t_3) \end{bmatrix}$$

Now by multiplying the boost by its transpose and taking expected values,

$$\overline{\begin{bmatrix} \Delta v_x(t_8) \\ \Delta v_y(t_8) \\ \Delta v_z(t_8) \end{bmatrix} \begin{bmatrix} \Delta v_x(t_8), & \Delta v_y(t_8), & \Delta v_z(t_8) \end{bmatrix}} = Q'\left(\frac{t_3}{t_8}\right)^{-1} F_{ij}\ Q\left(\frac{t_3}{t_8}\right)^{-T}$$

we have the covariance of the boost. Thus we proceed.

7.) Using $Q'\left(\frac{t_3}{t_8}\right)$ which we enter as a Special Q Matrix, and F_{ij} which we enter as an a priori, we first get F_{ij} on tape with a single Part B run. Then we recall F_{ij} in a subsequent Part B run along with the special Q, called in under a QT command. The result of this second Part B run is $Q'\left[\frac{t_3}{t_8}\right]^T \left[F_{ij}\right]^{-1} Q'\left[\frac{t_3}{t_8}\right]$. and is stored on tape. Finally, a third run is made to invert this result giving:

$$Q'\left(\frac{t_3}{t_8}\right)^{-1} F_{ij}\ Q^{-T}\left(\frac{t_3}{t_8}\right)$$

which is the covariance of the boost at t_8 expressed in t_8 coordinates. The trace of this should equal the trace of the LEM G and N program results; or a

final rotation will put the above results in t_2 coordinate allowing an exact check with the new program.

The following is an example run using the OEAP which was done to enable checking the LEM G and N program. The a priori covariance at burnout was chosen to reasonably handle the nuisance parameters while making the 6 x 6 orbit parameter covariance small enough so as not to be swamped by radar tracking. The non-zero elements at burnout are:

A PRIORI 1

A(1, 1)	=	1.0000000E 03
A(2, 2)	=	9.0000000E 02
A(3, 3)	=	1.0000000E 03
A(4, 4)	=	4.0000000E-03
A(5, 5)	=	1.7000000E-04
A(6, 6)	=	3.2000000E-03
A(7, 7)	=	1.0000000E 30
A(8, 8)	=	1.0000000E 30
A(9, 9)	=	1.0000000E 30

A PRIORI 2

A(10,10)	=	2.9000000E 18
A(11,11)	=	9.0000000E 06
A(12,12)	=	3.6000000E 07
A(13,13)	=	9.0000000E 06
A(14,14)	=	9.0000000E-06
A(15,15)	=	9.0000000E-06
A(16,16)	=	9.0000000E-06
A(17,17)	=	1.0000000E 04
A(18,18)	=	1.0000000E 04
A(19,19)	=	1.0000000E 04
A(20,20)	=	1.0000000E-20
A(21,21)	=	7.7000000E-28
A(22,22)	=	1.0000000E-06
A(23,23)	=	1.0000000E 04
A(24,24)	=	1.0000000E 04
A(25,25)	=	1.0000000E 04
A(26,26)	=	1.0000000E-06

A PRIORI 3

A(7, 7)	=	1.0000000E-20
A(8, 8)	=	1.0000000E-28
A(9, 9)	=	1.0000000E 04
A(10,10)	=	1.0000000E 04
A(11,11)	=	1.0000000E 04
A(12,12)	=	1.0000000E-06
A(13,13)	=	1.0000000E-20
A(14,14)	=	1.0000000E-28

These were entered using three a priori data sets. The next inputs consist of the three radar stations: Madrid(Data Set 4), Kennedy(5), and Ascension(6).

(Madrid, Data Set 4)

01	5.7482400E	06	A1
02		-0	A4
03	5.5730580E	03	A5
04	1.0000000E	00	GAM ID
05	1.8000000E	01	BETA
06	1.8000000E	02	XI
07	1.8000000E	02	ETA
08	1.0394345E	01	ZETA
09	4.0417000E	01	LAMBDA
10	-3.6670000E	00	ALPHA
11	7.2911600E-05		OMEGAE
12	2.6638000E-06		OMEGAM
13	2.0922713E	07	RHOE
14	1.2600000E	09	RHOM
15	1.7313997E	14	MU
16	2.1000000E	01	D TIME
16	2.4000000E	01	D TIME
16	5.7507169E	01	D TIME
17		-0	REENTRY RAD
18	1.7999988E	01	BIG L
19	-4.1765746E	01	SMA L
20	1.0000000E	00	RRATE IND
21	1.0000000E	00	RANGE IND
22	1.0000000E	00	Q IND
23	5.7507169E	01	QF IND
24		-0	ANG 1 IND
25		-0	ANG 2 IND
26		-0	PVW IND
27	1.0000000E	00	T INIT
28	1.0000000E	00	T INCR
29	3.0000000E	01	DIMENS
30		-0	LAMBDA2
31		-0	ALPHA2
32	1.0000000E	00	M-S IND
33	1.0000000E	00	F-M IND

(Kennedy, Data Set 5)

01	5.7482400E	06	A1
02		-0	A4
03	5.5730580E	03	A5
04	1.0000000E	00	GAM ID
05	1.8000000E	01	BETA
06	1.8000000E	02	XI
07	1.8000000E	02	ETA
08	1.0394345E	01	ZETA
09	2.8482000E	01	LAMBDA
10	-8.0577000E	01	ALPHA
11	7.2911600E-05		OMEGAE
12	2.6638000E-06		OMEGAM
13	2.0922713E	07	RHOE
14	1.2600000E	09	RHOM
15	1.7313997E	14	MU
16	2.1000000E	01	D TIME
16	2.4000000E	01	D TIME
16	2.6666600E	01	D TIME
17		-0	REENTRY RAD
18	1.7999988E	01	BIG L
19	-4.1765746E	01	SMA L
20	1.0000000E	00	RRATE IND
21	1.0000000E	00	RANGE IND
22		-0	Q IND
23	2.6666600E	01	QF IND
24		-0	ANG 1 IND
25		-0	ANG 2 IND
26		-0	PVW IND
27	1.0000000E	00	T INIT
28	1.0000000E	00	T INCR
29	3.0000000E	01	DIMENS
30	4.0417000E	01	LAMBDA2
31	-3.6670000E	00	ALPHA2
32		-0	M-S IND
33	1.0000000E	00	F-M IND

(Ascension, Data Set 6)

01	5.7482400E	06	A1
02		-0	A4
03	5.5730580E	03	A5
04	1.0000000E	00	GAM ID
05	1.8000000E	01	BETA
06	1.8000000E	02	XI
07	1.8000000E	02	ETA
08	1.0394345E	01	ZETA
09	-7.9520000E	00	LAMBDA
10	-1.4413000E	01	ALPHA
11	7.2911600E	-05	OMEGAE
12	2.6638000E	-06	OMEGAM
13	2.0922713E	07	RHOE
14	1.2600000E	09	RHOM
15	1.7313997E	14	MU
16	2.1000000E	01	D TIME
16	2.4000000E	01	D TIME
16	2.6666600E	01	D TIME
17		-0	REENTRY RAD
18	1.7999988E	01	BIG L
19	-4.1765746E	01	SMA L
20	1.0000000E	00	RRATE IND
21	1.0000000E	00	RANGE IND
22		-0	Q IND
23	2.6666600E	01	QF IND
24		-0	ANG 1 IND
25		-0	ANG 2 IND
26		-0	PVW IND
27	1.0000000E	00	T INIT
28	1.0000000E	00	T INCR
29	3.0000000E	01	DIMENS
30	4.0417000E	01	LAMBDA2
31	-3.6670000E	00	ALPHA2
32		-0	M-S IND
33	1.0000000E	00	F-M IND

Now, from Data Set 6, the QF indication $\left(1600/60\right)$ min. produced the radius and x and y components of velocity (in t_2 coordinates) at t_8, along with the sine and cosine of the central angle between t_2 and t_8.

$$\text{radius} = 5.9177775 \times 10^{6} \text{ ft}$$

$$\dot{x} = -5.3973982 \times 10^{3} \text{ ft/sec}$$

$$\dot{y} = 4.4858884 \times 10^{2} \text{ ft/sec}$$

$$\sin(\theta - \theta_o) = 9.9865522 \times 10^{-1}$$

$$\cos(\theta - \theta_o) = 5.1843555 \times 10^{-2}$$

Using these numbers it is possible to calculate the angel between t_2 and t_8

$$< t_2, t_8 = \sin^{-1}(\sin(\theta - \theta_o)) = 87.017^{o}$$

and the state vector at t_8 in t_8 coordinates

$$a_1 = \text{radius}$$

$$\begin{bmatrix} a_4 \\ a_5 \end{bmatrix} = \begin{bmatrix} \cos(\theta - \theta_o) & \sin(\theta - \theta_o) \\ -\sin(\theta - \theta_o) & \cos(\theta - \theta_o) \end{bmatrix} \begin{bmatrix} \dot{x} \\ \dot{y} \end{bmatrix}$$

These are used as an input to a Program A along with the time between t_8 and t_3 (QF entry).

INPUT DATA

01	5.9177775E 06	A1
02	1.6816525E 02	A4
03	5.4133963E 03	A5
04	1.0000000E 00	GAM ID
05	1.8000000E 01	BETA
06	1.8000000E 02	XI
07	1.8000000E 02	ETA
08	1.0394345E 01	ZETA
09	4.0417000E 01	LAMBDA
10	-3.6670000E 00	ALPHA
11	7.2911600E-05	OMEGAE
12	2.6638000E-06	OMEGAM
13	2.0922713E 07	RHOE
14	1.2600000E 09	RHOM
15	1.7313997E 14	MU
16	3.0840503E 01	D TIME
17	-0	REENTRY RAD
18	1.7999988E 01	BIG L
19	-4.1765746E 01	SMA L
20	-0	RRATE IND
21	-0	RANGE IND
22	-0	Q IND
23	3.0840503E 01	QF IND
24	-0	ANG 1 IND
25	-0	ANG 2 IND
26	-0	PVW IND
27	1.0000000E 00	T INIT
28	1.0000000E 00	T INCR
29	3.0000000E 01	DIMENS
30	-0	LAMBDA2
31	-0	ALPHA2
32	1.0000000E 00	M-S IND
33	1.0000000E 00	F-M IND

The output of this program is a Q matrix between t_8 and t_3.

Q MATRIX 11 Q T = 30.8405

2.836653E 00	1.084206E 00	0	2.341314E 03	8.839092E 02	0
2.306369E 00	1.056281E 00	0	1.289916E 03	2.466824E 03	0
0	0	-8.566589E-02	0	0	1.128631E 03
7.768567E-04	8.328669E-04	0	8.898587E-01	9.507633E-01	0
3.565316E-03	9.736923E-04	0	2.121778E 00	2.941720E 00	0
0	0	-8.822233E-04	0	0	-5.014383E-02
0	0	0	0	0	0
0	0	0	0	0	0
0	0	0	0	0	0
0	0	0	0	0	0
0	0	0	0	0	0
0	0	0	0	0	0
0	0	0	0	0	0
0	0	0	0	0	0

The $Q'\left(\frac{t_3}{t_8}\right)$ matrix is the 3 x 3 blocked in above.

In Data Set 8, all of the a priori and radar information is used to obtain the covariance of the total state vector at t_2 using tracking between t_2 and $t_8 - \tau$, assuming the nuisance parameters (past the 9 x 9) are not updated. Following are the inputs

DATA SET 8 CASE 0 6X6

```
DS   4    RD   T=     21.00   SG=1.00000E-02
DS   5    RD   T=     21.00   SG=1.00000E-02
DS   6    RD   T=     21.00   SG=1.00000E-02
DS   1    A    T=       -0    SG=1.00000E 00
DS   2    A    T=       -0    SG=1.00000E 00
DS   3    A    T=       -0    SG=1.00000E 00
DS   4    Q    T=     57.51   SG=1.00000E 00   *
```

07	08	09	10	11	12	13	14	15	16	17	18	19	20	21	22	23	24	25	26	27	28	29	30
BI	US	ES	NS	NH	MU	N*	VA	UM	EM	NM	ED	ND	RM	AM	BS	RS	AS	L1	L2	L3	L4	L5	L6

EULER ANGLES A= -0 B= -0 G= 87.017

7	17	18	19	0	10	0	0	0	0	0	0	0	20	21	22	0	0	11	12	13	14	15	16
8	23	24	25	0	10	0	0	17	18	19	0	0	20	21	26	27	28	11	12	13	14	15	16
9	29	30	31	0	10	0	0	17	18	19	0	0	20	21	32	33	34	11	12	13	14	15	16

27	28	29	30	31	32	33	34	0	0	0	0	0	0	0	0	0	0	0	0	0	0	0	0

Notice that a Q matrix is used to obtain results at t_3. This Q matrix is restricted to a 6 x 6 since the LEM assumes μ to be perfectly known. The angle G = 87.017° is used to rotate Q Cov Q^T from t_2 coordinates to t_8 coordinates since this is the coordinate system of the $Q'\left(\frac{t_3}{t_8}\right)$ matrix.

The particular result we are interested in, consists of Q Cov Q^T with parameters 1 through 9 updated, (other parameters not updated)shown below.

(Q) (COV)(QT) - COORDINATE ROTATION

1.051464E 05	3.751642E 04	1.715332E 01	1.481415E 01	8.913839E 01
3.751642E 04	1.684538E 04	1.151610E 01	7.240058E 00	3.431105E 01
1.715332E 01	1.151610E 01	1.133329E 03	5.520406E-03	1.750958E-02
1.481415E 01	7.240058E 00	5.520406E-03	3.200160E-03	1.395995E-02
8.913839E 01	3.431105E 01	1.750958E-02	1.395995E-02	7.744148E-02
-2.108384E-02	3.713946E-03	1.136465E-03	4.136177E-06	-1.336206E-05
1.927668E 00	-7.732109E-01	-6.717201E-03	-4.862801E-04	4.405210E-04
3.026030E 00	-1.949121E 00	-2.451331E-02	-1.154092E-03	1.351218E-04
3.003597E 00	-1.963496E 00	-1.911435E-02	-1.161184E-03	1.169884E-04

-2.108384E-02	1.927668E 00	3.026030E 00	3.003597E 00
3.713946E-03	-7.732109E-01	-1.949121E 00	-1.963496E 00
1.136465E-03	-6.717201E-03	-2.451331E-02	-1.911435E-02
4.136177E-06	-4.862801E-04	-1.154092E-03	-1.161184E-03
-1.336206E-05	4.405210E-04	1.351218E-04	1.169884E-04
2.827035E-03	2.952471E-06	-2.659564E-05	-5.219839E-05
2.952471E-06	1.826001E-03	3.572678E-03	3.559808E-03
-2.659564E-05	3.572678E-03	2.691767E-02	1.706891E-02
-5.219839E-05	3.559808E-03	1.706891E-02	2.686939E-02

Of the above results we are interested in the first 3 x 3 which we call $(\hat{a}-a_t)(\hat{a}-a_t)^T$.

The next data set (9) is identical to data set 8 except parameters 1 through 9 are updated with no further nuisance parameters. This produces C_T^{-1} at t_3 in t_8 coordinates.

(Q) (COV) - COORDINATE ROTATION

2.166016E 04	9.003525E 03	2.047519E 01	3.995317E 00	1.947046E 01
9.003525E 03	6.995964E 03	8.311577E 00	3.469021E 00	1.049628E 01
2.047519E 01	8.311577E 00	1.132349E 03	3.387560E-03	1.795270E-02
3.995317E 00	3.469021E 00	3.387560E-03	1.745864E-03	4.918565E-03
1.947046E 01	1.049628E 01	1.795270E-02	4.918565E-03	1.929616E-02
8.602674E-03	6.694027E-03	-9.114370E-04	3.903546E-06	6.977727E-06
2.112081E 00	-9.054498E-01	-3.266484E-03	-6.045187E-04	5.891885E-04
4.165190E 00	-1.831303E 00	-4.879801E-03	-1.217642E-03	1.128391E-03
4.224251E 00	-1.810990E 00	1.374846E-03	-1.209100E-03	1.178393E-03

8.602674E-03	2.112081E 00	4.165190E 00	4.224251E 00
6.694027E-03	-9.054498E-01	-1.831303E 00	-1.810990E 00
-9.114370E-04	-3.266484E-03	-4.879801E-03	1.374846E-03
3.903546E-06	-6.045187E-04	-1.217642E-03	-1.209100E-03
6.977727E-06	5.891885E-04	1.128391E-03	1.178393E-03
2.822677E-03	1.289326E-05	1.735069E-05	-6.472923E-06
1.289326E-05	1.193108E-03	2.368580E-03	2.376575E-03
1.735069E-05	2.368580E-03	4.740176E-03	4.737031E-03
-6.472923E-06	2.376575E-03	4.737031E-03	4.772385E-03

Again we are interested in the first 3 x 3.

Data Set 10 updates the a priori state vector with a 6 x 6 Q.

```
DATA SET   10          CASE   0              6 x 6

DS    1      A   T=        -0   SG=1.00000E 00
DS    4      Q   T=     57.51   SG=1.00000E 00   *


07 08 09 10 11 12 13 14 15 16 17 18 19 20 21 22 23 24 25 26 27 28 29 30
BI US ES NS NH MU N* VA UM EM NM ED ND RM AM BS RS AS L1 L2 L3 L4 L5 L6

      EULER ANGLES        A=       -0    B=       -0    G=  87.017
```

The result, C_{ap}^{-1}, is presented at t_3 in t_8 coordinates where again the first 3 x 3 position components are of interest

(Q) (COV) (QT) - COORDINATE ROTATION

1.893110E 05	4.884629E 04	0	1.518641E 01	1.506527E 02	0
4.884629E 04	1.874395E 04	0	7.360838E 00	4.337505E 01	0
0	0	1.132771E 03	0	0	-2.017928E-07
1.518641E 01	7.360838E 00	0	3.165051E-03	1.457324E-02	0
1.506527E 02	4.337505E 01	0	1.457324E-02	1.233016E-01	0
0	0	-2.017928E-07	0	0	2.824930E-03

Now, using the results of the last three Data Sets, we may form by hand:

$$F_{ij} = C_{ap}^{-1} - 2C_T^{-1} + \overline{(\hat{a}-a_t)(\hat{a}-a_t)^T}$$

Starting a new run F_{ij} is entered as an a priori as Data Set 1.

A PRIORI 1

A(1, 1)	=	2.5113710E 05
A(1, 2)	=	6.8355660E 04
A(1, 3)	=	-2.3797060E 01
A(2, 1)	=	6.8355660E 04
A(2, 2)	=	2.1597400E 04
A(2, 3)	=	-5.1070500E 00
A(3, 1)	=	-2.3797060E 01
A(3, 2)	=	-5.1070500E 00
A(3, 3)	=	1.4020000E 00
A(4, 4)	=	1.0000000E 00
A(5, 5)	=	1.0000000E 00
A(6, 6)	=	1.0000000E 00

The $Q'\left(\frac{t_3}{t_8}\right)$ Matrix is entered by a "Special Q" as Data Set 2. The non-zero elements of this 3 x 3 are:

Q MATRIX 2

Q(1, 1)	=	2.3413140E 03
Q(1, 2)	=	8.8390920E 02
Q(2, 1)	=	1.2899160E 03
Q(2, 2)	=	2.4668240E 03
Q(3, 3)	=	1.1286310E 03
Q(4, 4)	=	1.0000000E 00
Q(5, 5)	=	1.0000000E 00
Q(6, 6)	=	1.0000000E 00

Data Set 3 simply enters the a priori 1 (F_{ij}) and places it on tape so that it may be recalled by a subsequent data set without inverting it. On tape as a result of Data Set 3 is:

(COV) - LOCAL COORDINATE SYSTEM

2.511371E 05	6.835566E 04	-2.379706E 01	0	0	0
6.835566E 04	2.159740E 04	-5.107050E 00	0	0	0
-2.379706E 01	-5.107050E 00	1.402000E 00	0	0	0
0	0	0	1.000000E 00	0	0
0	0	0	0	1.000000E 00	0
0	0	0	0	0	1.000000E 00

Data Set 4 calls in the previous results of Data Set 3, shown above, by a P command. The special Q from Data Set 2 is called in by a QT command.

DATA SET 4 CASE 1 6 x 6

DS	3-1	P	T=	-0	SG=1,00000E 00
DS	2	QT	T=	-0	SG=1,00000E 00

The result of Data Set 4 is stored on tape. This result is actually $Q'\left(\frac{t_3}{t_8}\right)^T F_{ij} Q'\left(\frac{t_3}{t_8}\right)$ and is shown below.

(Q) (C)V) (QT) - LOCAL COORDINATE SYSTEM

1.641921E 02	4.938958E 02	-6.212170E 01	-6.629953-261	-6.629953-261	-6.629953-261
4.938958E 02	1.660177E 03	-7.548073E 02	-5.220515-261	-5.220515-261	-5.220515-261
-6.212170E 01	-7.548073E 02	9.104366E 05	-4.809808-258	-4.809808-258	-4.809808-258
-6.629953-261	-5.220515-261	-4.809808-258	1.000000E 00	-1.191312-260	-1.191312-260
-6.629953-261	-5.220515-261	-4.809808-258	-1.191312-260	1.000000E 00	-1.191312-260
-6.629953-261	-5.220515-261	-4.809808-258	-1.191312-260	-1.191312-260	1.000000E 00

Data Set 5 simply recalls the above results and inverts it. The Euler angles (G = -87.017°) are used to present the results in t_2 coordinates. The inputs for Data Set 5 are:

```
DATA SET     5          CASE 1          6 x 6
DS   4 - 1 P   T=          -0   SG=1.00000E 00

EULER ANGLES  A=       -0     B=        -0     G= - 87.017
```

and the final results are:

(COV) - COORDINATE ROTATION

7.678260E-03	1.989383E-02	-4.115981E-06	-7.567450-263	8.399491-263	7.994303-263
1.989383E-02	5.609795E-02	-1.015738E-05	-2.280908-262	2.531694-262	2.409566-262
-4.115981E-06	-1.015738E-05	1.100637E-06	-4.963884-264	5.509664-264	5.243879-264
-7.567450-263	-2.280908-262	-4.963884-264	1.000000E 00	0	-1.127702-260
8.399491-263	2.531694-262	5.509664-264	0	1.000000E 00	1.251693-260
7.994303-263	2.409566-262	5.243879-264	-1.127702-260	1.251693-260	1.000000E 00

```
SQRT((1,1)+(2,2)+(3,3)) =  2.5254170E-01
SQRT((4,4)+(5,5)+(6,6)) =  1.7320508E 00
          SQRT( 1, 1) =  8.7625684E-02
          SQRT( 2, 2) =  2.3685006E-01
          SQRT( 3, 3) =  1.0491124E-03
          SQRT( 4, 4) =  1.0000000E 00
          SQRT( 5, 5) =  1.0000000E 00
          SQRT( 6, 6) =  1.0000000E 00
```

The upper left 3 x 3 is the covariance of the boost at t_8 in t_2 coordinates. Note that the variance in the magnitude of the boost is .2525 ft/sec. which is ridiculously small because of the excellent a priori state vector at t_2.

Defining:

$\hat{a}$	=	the estimate of the state vector
a_{ref}	=	the reference state vector used
a_{ap}	=	the a priori estimate of the state vector at t_2
a_t	=	the actual or true state vector
$n_i(j)$	=	noise on the ith measurement of the jth measurable
$m_i(j)$	=	the actual ith measurement of the jth measurable
$mc_i(j)$	=	the computed value of the above along the reference trajectory
C_T	=	the information matrix of the k parameters where k includes the orbit parameters and the updated biases (k = 9 in our example)
σ_j^2	=	variance in the jth one-shot measurable

We proceed to estimate $\overline{(\hat{a}-a_{ref})(\hat{a}-a_{ref})^T}$:

$$\hat{a}-a_{ref} = C_T^{-1} \sum_j \frac{1}{\sigma_j^2} \begin{bmatrix} \sum_i \frac{\partial m_i(j)}{\partial a_1} \left(m_i(j) - mc_i(j)\right) \\ \vdots \\ \sum_i \frac{\partial m_i(j)}{\partial a_k} \left(m_i(j) - mc_i(j)\right) \end{bmatrix}$$

where:

$$m_i(j) - mc_i(j) = \sum_{\ell=1}^{L} \frac{\partial m(j)}{\partial a(\ell)} \left(a_t(\ell) - a_{ref}(\ell) \right) + n_i(j)$$

and $n_i(j)$ is the i<u>th</u> noise on the j<u>th</u> measurable. But, $a_{ref} = a_{ap}$, thus:

$$\hat{a} - a_{ref} = C_T^{-1} \sum_j \frac{1}{\sigma_j^2} \left\{ \begin{bmatrix} \sum_i \frac{\partial m_i(j)}{\partial a_1} \left\{ - \sum_\ell \frac{\partial m_i(j)}{\partial a_\ell} \left(a_{ap} - a_t \right)_\ell \right\} \\ \vdots \\ \sum_i \frac{\partial m_i(j)}{\partial a_k} \left\{ \quad \right\} \end{bmatrix} + n_i(j) \right\}$$

$$= C_T^{-1} \sum_j \frac{1}{\sigma_j^2} \left[- A_{x\ell}(j) \begin{bmatrix} a_{ap}(1) - a_t(1) \\ \vdots \\ a_{ap}(L) - a_t(L) \end{bmatrix} \right] + \text{noise}$$

where x, goes from 1 to k and ℓ goes from 1 to L. Therefore:

$$(\hat{a} - a_{ref}) = C_T^{-1} \left[- B_{x\ell} \right] \begin{bmatrix} a_{ap}(1) - a_t(1) \\ \vdots \\ a_{ap}(L) - a_t(L) \end{bmatrix} + \text{noise}$$

where we have summed over the j measurables. Then we may partition the above

$$(\hat{a} - a_{ref}) = C_T^{-1} \left[C_T - C_{ap} \;\vdots\; B_{12} \right] \begin{bmatrix} a_{ap}(1) - a_t(1) \\ \vdots \\ a_{ap}(k) - a_t(k) \\ \vdots \\ a_{ap}(L) - a_t(L) \end{bmatrix} + \text{noise}$$

where $C_T - C_{ap}$ is the k x k information due to radar measurements alone and B_{12} is the $(L-k) \times (L-k)$ upper right hand of the total information matrix. Now we multiply the above by its transpose and take expected values:

$$\overline{(\hat{a} - a_{ref})(\hat{a} - a_{ref})^T} = C_T^{-1} (C_T + C_{ap}) C_{ap}^{-1} (k \times k) (C_T + C_{ap})^T C_T^{-T}$$

$$+ C_T^{-1} B_{12} \left[C_{ap}^{-1} (L-k) \times (L-k) \right] B_{12}^T C_T^{-T}$$

$$+ C_T^{-1} C_m (k \times k) C_T^{-T}$$

where $C_{ap}^{-1}(k \times k)$, in the first term, is the a priori covariance of the updated parameters; $C_{ap}^{-1}(L-k) \times (L-k)$ is the covariance of the non-updated parameters, elsewhere referred to as $\hat{C}_{ap}^{-1}$; and $C_m(k \times k)$ is the noise covariance on the k x k set caused by radar measurements. Now:

$$C_T^{-1} (C_T + C_{ap}) C_{ap}^{-1} (C_T + C_{ap})^T C_T^{-T}$$

$$= C_T^{-1} (C_T + C_{ap}) C_{ap}^{-1} (C_T + C_{ap}) C_T^{-1}$$

(since covariance matrices are symmetric)

$$= C_T^{-1}(C_T C_{ap}^{-1} - I)\,(C_T - C_{ap})\,C_T^{-1}$$

$$= C_T^{-1}\,(C_T C_{ap}^{-1} C_T - C_T - C_T + C_{ap})\,C_T^{-1}$$

$$= (C_{ap}^{-1} C_T - 2I + C_T^{-1} C_{ap})\,C_T^{-1}$$

$$= C_{ap}^{-1} - 2C_T^{-1} + C_T^{-1} C_{ap} C_T^{-1}$$

Substituting this into the equation for the covariance for the boost gives:

$$\overline{(\hat{a}-a_{ref})(\hat{a}-a_{ref})^T} = C_{ap}^{-1} - 2C_T^{-1} + C_T^{-1} C_{ap} C_T^{-1} + C_T^{-1} C_m(k\times k)\, C_T^{-1}$$

$$= C_T^{-1} B_{12} \hat{C}_{ap}^{-1} B_{12}^T C_T^{-1}$$

Now $C_{ap} + C_m$ = the total information, C_T. Thus

$$\overline{(\hat{a}-a_{ref})(\hat{a}-a_{ref})^T} = C_{ap}^{-1} - 2C_T^{-1} + C_T^{-1} \left[C_{ap}+C_m = C_T\right] C_T^{-1}$$

$$+ C_T^{-1} B_{12} \hat{C}_{ap}^{-1} B_{12}^T C_T^{-1}$$

$$= \left\{ C_T^{-1} + C_T^{-1} B_{12} \hat{C}_{ap}^{-1} B_{12}^T C_T^{-1} \right\} - 2C_T^{-1} + C_{ap}^{-1}$$

Now, note that the bracketed term above is just the normal result

$\overline{(\hat{a}-a_t)(\hat{a}-a_t)^T}$ of the OEAP when certain parameters (1⟶k) are updated and other parameters (k+1⟶L) are effective but not updated. C_T^{-1} is the same covariance assuming perfect knowledge of the k + 1 through L parameters, and C_{ap}^{-1} is the covariance with no tracking at all, i. e. the inverse of the a priori information at t_2.

The Bissett-Berman Corporation 2941 Nebraska Avenue, Santa Monica, California EXbrook 4-3270

APOLLO NOTE NO. 415
(Task III)

J. W. Childress, III
29 March 1966

LONG PERIOD STATION-KEEPING FOR A LUNAR ORBIT

INTRODUCTION

This study evaluated tracking station location errors when long periods occur between trackings. Specifically two weeks elapsed between trackings. Both one and two slave stations were used with a master station. Four cases were run in each of these two configurations. In the first case the vehicle was tracked for two orbits. In the second case the vehicle was tracked for four orbits. For the third case the vehicle was tracked for two orbits; there was a two week wait, then the vehicle was tracked for two orbits. The fourth case was comprised of a four orbit track, a two week wait, and finally; a four orbit track.

DISCUSSION

In this study the only nuisance parameters considered were the uncertainties in the stations. All other parameters were assumed to be known perfectly a priori. Range rate was used as a measurable with a sigma of 0.03 m/s for 1 second observations. The a priori matrix contains sigmas of the vehicle position and velocity and the station. The three components of the vehicle position uncertainty each had sigmas of 3 km, while the vehicle velocity uncertainty components each had sigmas of 1 m/sec. The sigmas of the components of the station location uncertainty were 100 m.

Because of the period involved and the trajectory selected (see Figure 1.), it was not possible to continuously track from any particular station. As a result it was necessary to use more than one master and more than two slave stations. The stations used as masters were Cape Kennedy and Grand Canary; while the slaves were Ascension, Hawaii,

Madrid, and Grand Turk. When it became necessary to switch stations, the station location error was transferred from the old to the new station. That is, all of the tracking data which had been collected prior to the station switch was used to estimate the station location uncertainties after the switch, although the new (second) station actually had not been in use prior to the switch. This was reasonable since the new station could have tracked at some time prior and thus have the assumed error. Further, since it is assumed that the stations are fixed relative to the coordinate system imbedded in the Earth, the waiting period between tracking periods does not change the station location uncertainties. If all of the tracking stations at some time or other tracked a particular object or several objects, it should be possible to reduce the a priori station position uncertainties.

Figures 2 through 4 shows the station position uncertainties as a function of time (orbits) for two stations. (Actually, data from a third station was included for the 4 orbit-second and fourth cases.) Figures 5 through 7 illustrate the station position uncertainties as a function of time for the three stations.

CONCLUSIONS

It is easily seen that a relatively small amount of tracking data will practically minimize the station location errors. Unfortunately, this "minimum" is not always considerably smaller than the a priori assumption. Some components have sigmas which are not 10% smaller than the a priori values in some cases. This is particularly true of the North (or z)-component (in this study) which is practically orthogonal to the orbit selected. The East (or y)-component uncertainty shows the greatest reduction, while the uncertainty in the Up (or x)-component lies between uncertainties in the East and North-components. The rms station location uncertainty was reduced less than 45%, i. e., from 173 meters to some value greater than 100 meters. Likewise the reduction in the uncertainty associated with a particular station location is virtually independent of the locations of the

other stations and is solely a function of the tracking data. To verify this conclusion Grand Turk was substituted for Madrid and the results examined. Although the rms vehicle position uncertainty was practically doubled, e. g., 161 meters when the former was used versus 72 meters (in one case) when the latter was used, the uncertainty in the components of the station position was essentially unchanged. For example, the three sigmas for the master station (Cape Kennedy) were $\{50.0,\ 131.6,\ 86.7\}$ and $\{49.9,\ 13.3,\ 86.5\}$ for the inclusion of data from Grand Turk and Madrid, respectively. Likewise the Ascension (slave) location uncertainty was unaffected. The distribution of location uncertainties in Grand Turk differed significantly from that of Madrid, e. g., 43. 8, 21. 5, 91. 9 and 67. 8, 19. 0, 78. 8 , respectively. The rms uncertainties differ very little, however. In comparing the Up and North components of location error for the two stations remember that Madrid is at a latitude of 40.417° while Grand Turk is at a latitude of 21.434°. In addition, the orbital plane is at an angle of 28.5° with the Earth's equator. Since changing the initial position of the vehicle in its orbit will not change the amount of tracking data, during an orbit, from each station, a different vehicle orbit would have to be used in order to significantly reduce North components of error further. (The rms uncertainties in the station's position could be slightly smaller depending on the initial vehicle position in the orbit but this reduction does not appear to warrant the effort required to find the minimum uncertainty as a function of initial position).

It can also be seen from these results that while tracking for four orbits rather than two significantly reduces the rms positional uncertainty of the vehicle, this additional tracking often has a considerably smaller effect on the station location uncertainty, with the exception of either the East or Up component. One of these two components is usually reduced proportionally greater than the other components.

In the two-station runs, the East-component of the master station position error was significantly reduced while the Up-component of the

slave station error was significantly reduced.

If the tracking station locations are optimally selected, then the component errors can be reduced (although, the replacement of Madrid with Grand Turk produced little change in the station location uncertainty after four orbits). As previously indicated if equal (identical) amounts of data are used for each station, then the rms vehicle position uncertainty could be changed while the master station location uncertainties are essentially unchanged. The relative magnitude of the station uncertainties is variable, however. In fact, the rms vehicle position uncertainty is seriously affected by the initial position of the vehicle (at the start of tracking) although the orbit, station locations, and total tracking period are unchanged.

This leads to interesting conclusions already discussed in Apollo Notes describing the effects of station and clock uncertainties in bias estimating, i. e., equal amounts of data could produce.

$$\sigma_{cp1} > \sigma_{cp2}$$

while:

$$\sigma_{QcQ^T1} < \sigma_{QcQ^T2}$$

where σ_{cpi} (i = 1, 2), the rms vehicle position uncertainty found from the covariance matrix, Cov, while $\sigma_{QcQ^T_i}$ is the rms vehicle position uncertainty found from Q Cov Q^T and the index i is used to distinguish one case from the other. Finally, it is concluded that a relatively short tracking period will significantly reduce the station location errors although large reduction, e. g., an order-of-magnitude, seems impractical. Obviously, these errors are independent of the working period for lunar orbits. It also seems likely that the initial conditions, for given tracking periods and stations, which will minimize the rms position error will be close to minimizing the station location errors.

INPUT DATA

01	1.9373000E 06	A1
02	0	A4
03	1.5897300E 03	A5
04	1.0000000E 00	GAM ID
05	0	BETA
06	0	XI
07	1.8000000E 02	ETA
08	1.8000000E 02	ZETA
09	2.8482000E 01	LAMBDA
10	-8.0577000E 01	ALPHA
11	7.2911600E -05	OMEGAE
12	2.6638000E -06	OMEGAM
13	6.3781000E 06	RHOE
14	3.8500000E 08	RHOM
15	4.8960000E 12	MU

FIGURE 1.

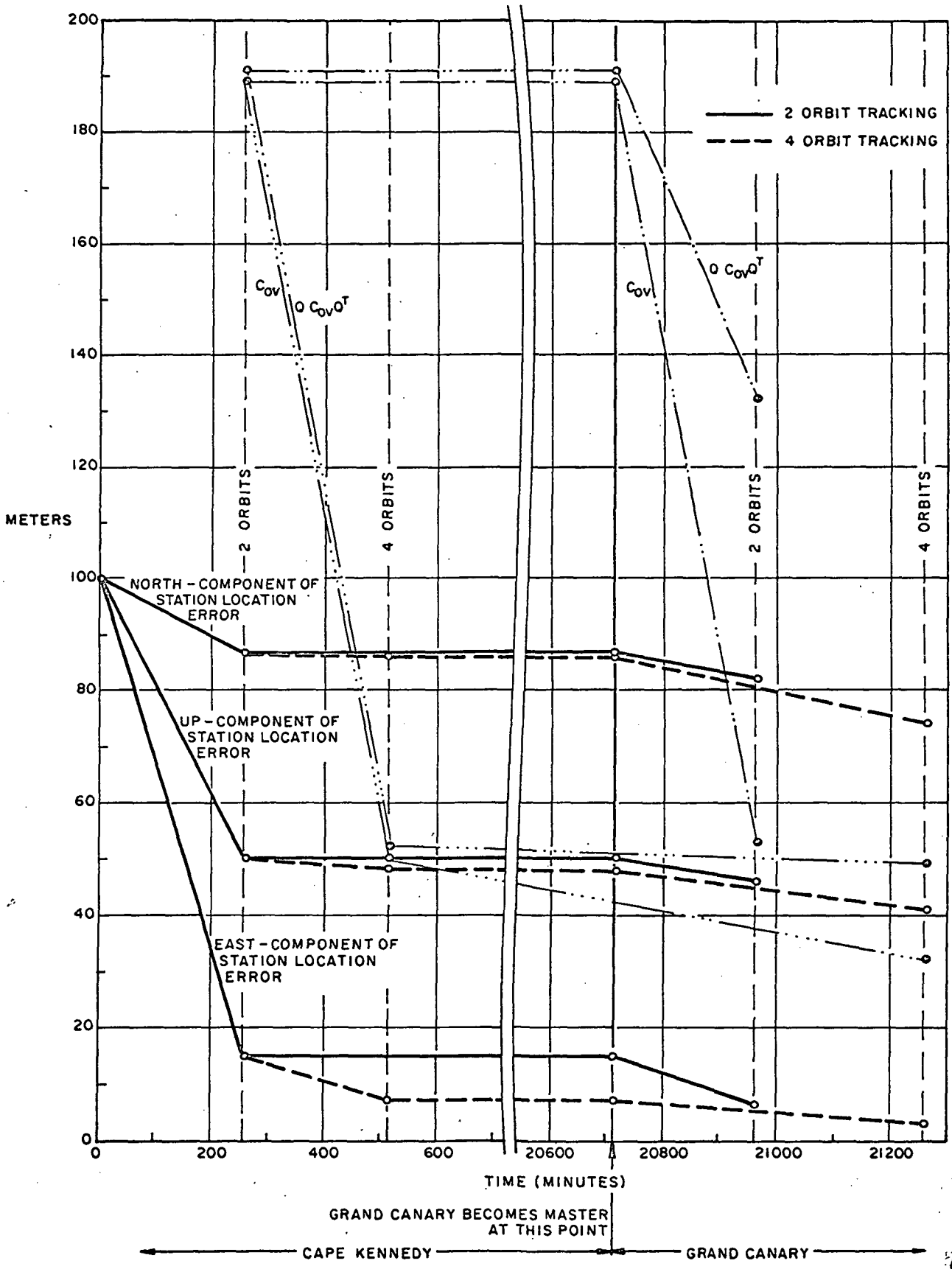
2 ORBIT TRACKING
4 ORBIT TRACKING
C_{ov}
$Q\ C_{ov}Q^T$
2 ORBITS
4 ORBITS
NORTH - COMPONENT OF STATION LOCATION ERROR
UP - COMPONENT OF STATION LOCATION ERROR
EAST - COMPONENT OF STATION LOCATION ERROR
METERS
TIME (MINUTES)
GRAND CANARY BECOMES MASTER AT THIS POINT
CAPE KENNEDY
GRAND CANARY

FIGURE 2.

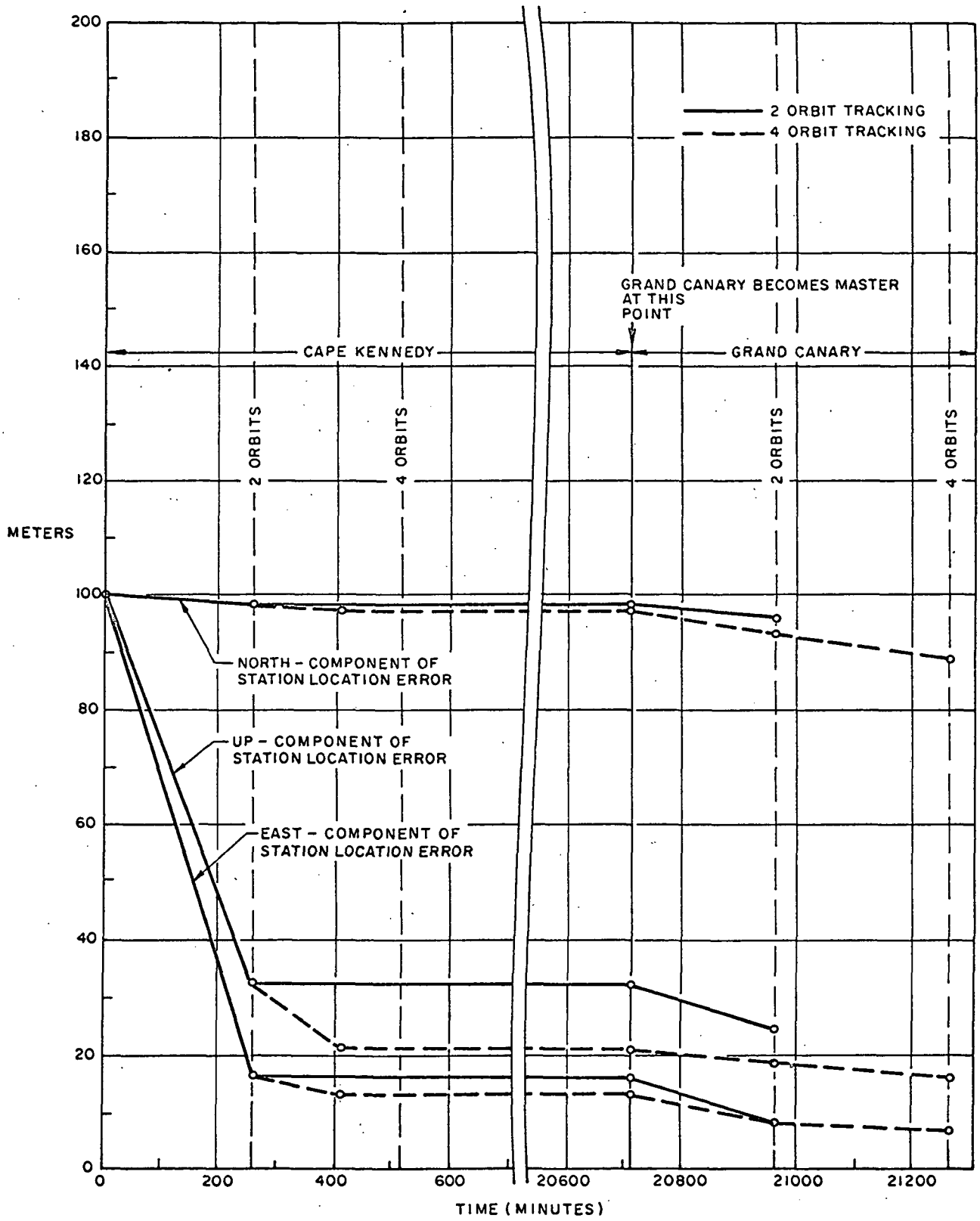
2 ORBIT TRACKING
4 ORBIT TRACKING
GRAND CANARY BECOMES MASTER AT THIS POINT
CAPE KENNEDY
GRAND CANARY
2 ORBITS
4 ORBITS
2 ORBITS
4 ORBITS
METERS
NORTH - COMPONENT OF STATION LOCATION ERROR
UP - COMPONENT OF STATION LOCATION ERROR
EAST - COMPONENT OF STATION LOCATION ERROR
200
180
160
140
120
100
80
60
40
20
0
0
200
400
600
20600
20800
21000
21200
TIME (MINUTES)

FIGURE 3.

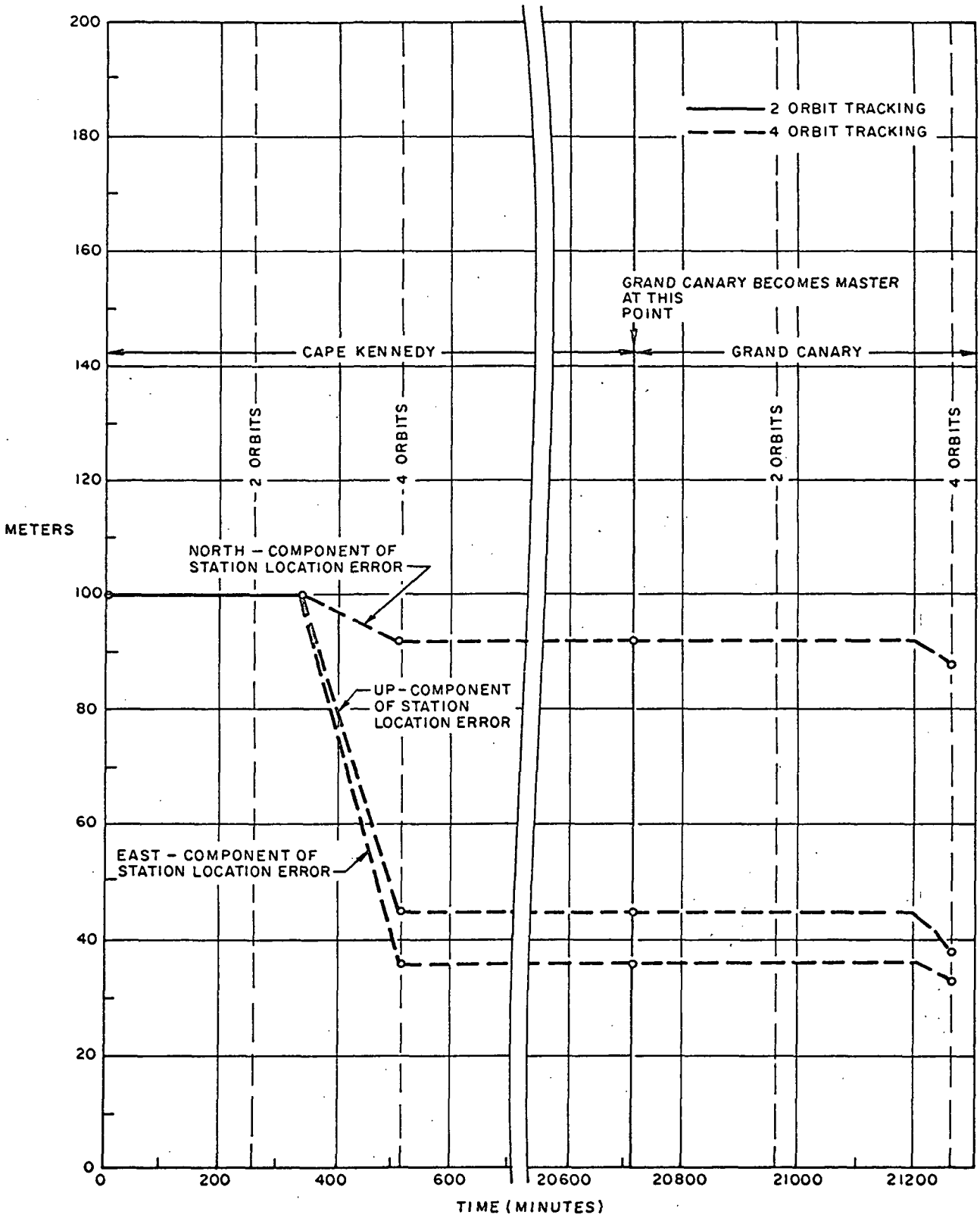
200
180
160
140
120
100
80
60
40
20
0
METERS
2 ORBIT TRACKING
4 ORBIT TRACKING
GRAND CANARY BECOMES MASTER AT THIS POINT
CAPE KENNEDY
GRAND CANARY
2 ORBITS
4 ORBITS
2 ORBITS
4 ORBITS
NORTH – COMPONENT OF STATION LOCATION ERROR
UP – COMPONENT OF STATION LOCATION ERROR
EAST – COMPONENT OF STATION LOCATION ERROR
0
200
400
600
20600
20800
21000
21200
TIME (MINUTES)

FIGURE 4.

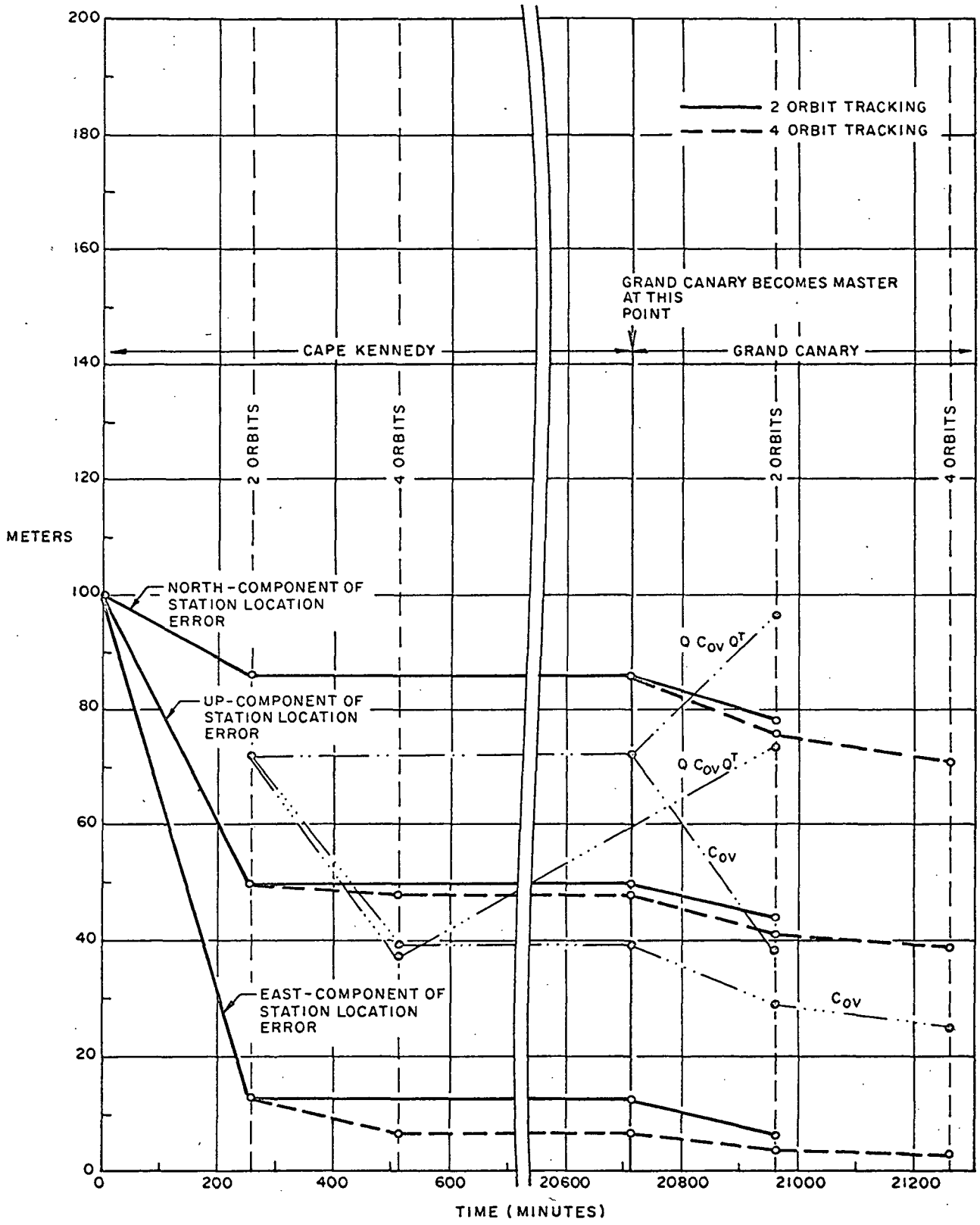
2 ORBIT TRACKING
4 ORBIT TRACKING
GRAND CANARY BECOMES MASTER AT THIS POINT
CAPE KENNEDY
GRAND CANARY
2 ORBITS
4 ORBITS
2 ORBITS
4 ORBITS
METERS
NORTH-COMPONENT OF STATION LOCATION ERROR
UP-COMPONENT OF STATION LOCATION ERROR
EAST-COMPONENT OF STATION LOCATION ERROR
Q Cov Q^T
Q Cov Q^T
Cov
Cov
200
180
160
140
120
100
80
60
40
20
0
0
200
400
600
20600
20800
21000
21200
TIME (MINUTES)

FIGURE 5.

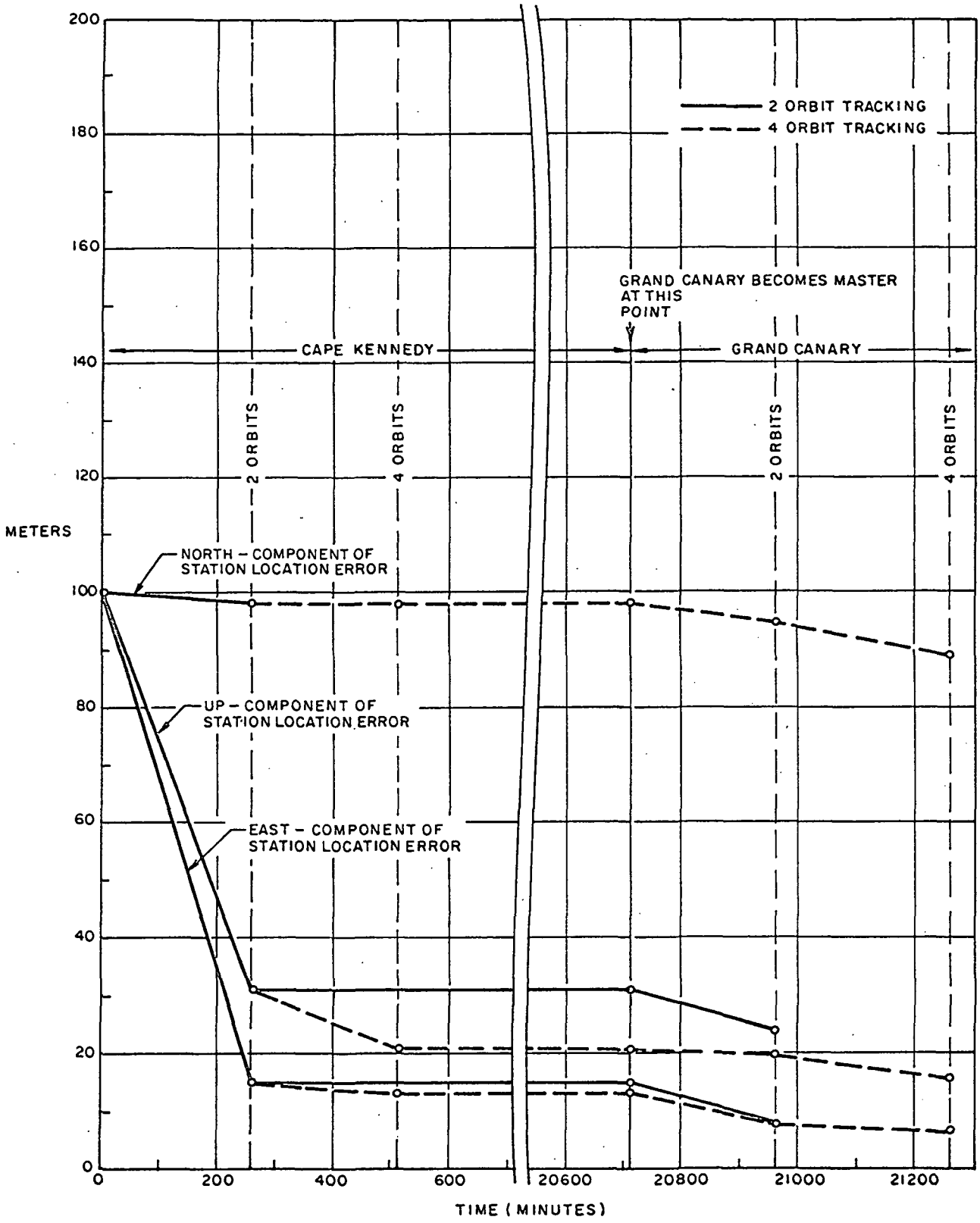
2 ORBIT TRACKING
4 ORBIT TRACKING
GRAND CANARY BECOMES MASTER AT THIS POINT
CAPE KENNEDY
GRAND CANARY
2 ORBITS
4 ORBITS
2 ORBITS
4 ORBITS
METERS
NORTH – COMPONENT OF STATION LOCATION ERROR
UP – COMPONENT OF STATION LOCATION ERROR
EAST – COMPONENT OF STATION LOCATION ERROR
200
180
160
140
120
100
80
60
40
20
0
0
200
400
600
20600
20800
21000
21200
TIME (MINUTES)

FIGURE 6.

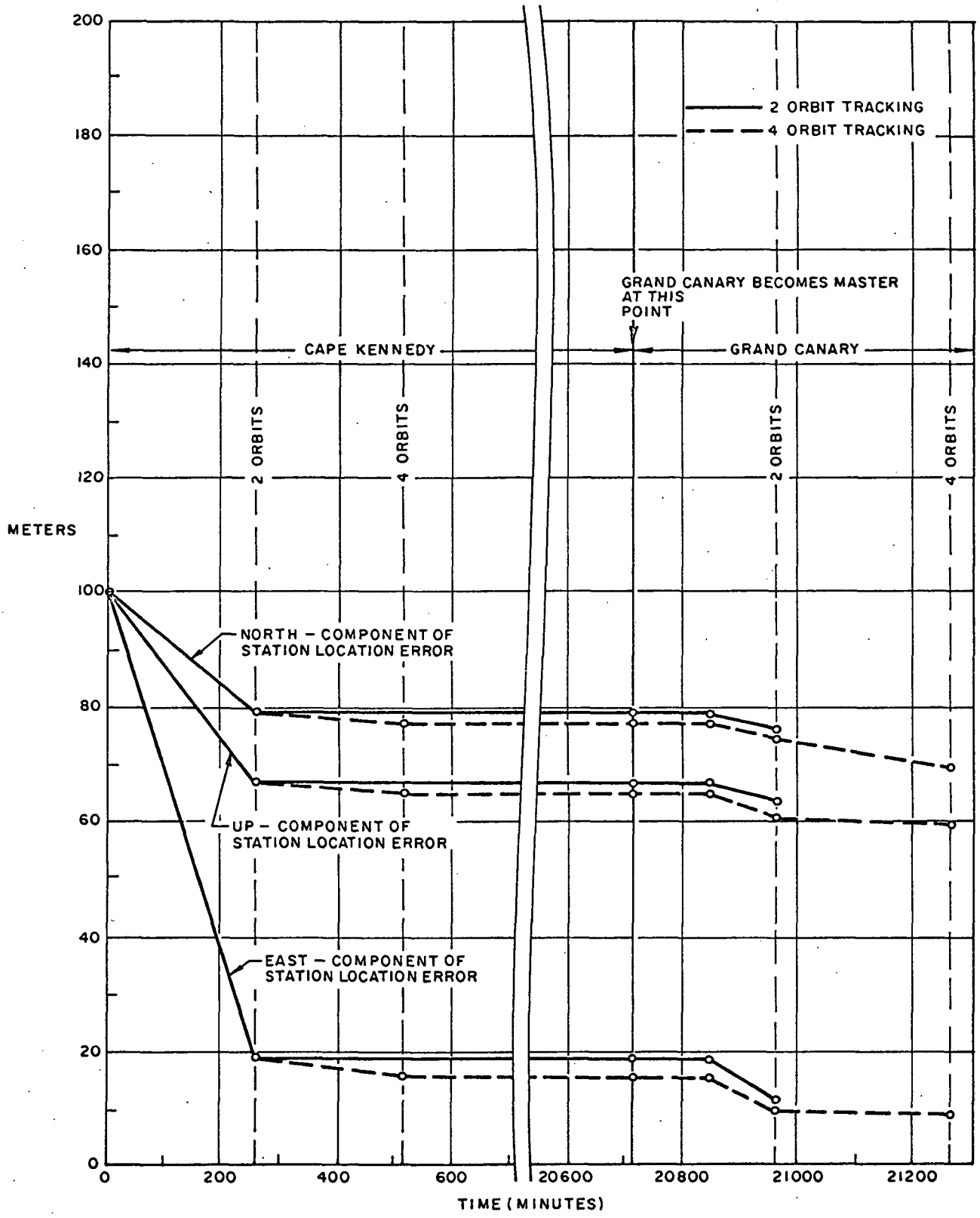
2 ORBIT TRACKING
4 ORBIT TRACKING
GRAND CANARY BECOMES MASTER AT THIS POINT
CAPE KENNEDY
GRAND CANARY
2 ORBITS
4 ORBITS
2 ORBITS
4 ORBITS
METERS
NORTH – COMPONENT OF STATION LOCATION ERROR
UP – COMPONENT OF STATION LOCATION ERROR
EAST – COMPONENT OF STATION LOCATION ERROR
200
180
160
140
120
100
80
60
40
20
0
0
200
400
600
20600
20800
21000
21200
TIME (MINUTES)

FIGURE 7.

The Bissett-Berman Corporation 2941 Nebraska Avenue, Santa Monica, California EXbrook 4-3270

APOLLO NOTE NO. 417
(Task II, Item 1)

J. B. Murphy
31 March 1966

EFFECT OF IONOSPHERE ON DETERMINATION OF ORBIT PARAMETERS

In Apollo Note No. 388, an ionosphere model was described and programmed that determines ionosphere range error as a function of solar cycle and emanations, time of day and year and specifically, azimuth and elevation from tracking station to vehicle. The next step is to see how this tracking error couples into an orbit. That is, how much does the ionosphere hamper the determination of the orbit parameter.

A method previously used for similar problems was to consider the characterizing parameters as nuisance parameters in the OEA (Orbit Error Analysis) program. However, in order to do so requires the partials of the measurables by the characterizing parameters (e. g. sunspot number, geomagnetic index, etc). This, as one can see after examining the ionosphere model description, is somewhat difficult. An alternative approach is to employ the concept of weighting functions as described in Apollo Note No. 353 to determine the effect on the orbit parameters of the measurable differing from the true value. It should be pointed out that this method will yield larger errors in the orbit parameters than the first method since the weighting functions method assumes that no correction of the measurement to account for the ionosphere is made. Thus, a "worst case" type of result will be achieved.

More specifically, the process used to find the orbit parameter errors using the above method involves a number of steps:

1) For a specific orbit, generation of azimuth and elevation from ground stations to vehicle by means of the Az-El Program (Apollo Note No. 409).

2) Introducing this Az-El information (in addition to subsolar location) into the ionosphere slab model

much as depicted in Apollo Note No. 388 to find the range errors as a function of time from start of orbit.

3) Generating the weighting functions (range or range-rate) for the orbit and for tracking times corresponding to Az-El information chosen from 2).

4) Multiply the range weighting functions in 3) by the associated range error in 2) (or the range-rate weighting function by the first-difference derivative of the range error) and sum these products over the total tracking time.

The alterations required for the ionosphere model as described in Apollo Note No. 377 and 388 are such that local solar time and day of the year are no longer used as inputs. Instead, sub-solar latitude, longitude and an additional indicator are used. In particular, these alterations consist of replacing Equations (1) - (6) in Apollo Note No. 388 by the following:

$$\delta = \text{subsolar latitude.} \tag{1}$$

$$\sin\theta_3 = \frac{360\delta}{2\pi\,(23.56)} \tag{2}$$

$$\cos\theta_3 = \text{SUND}\sqrt{1 - \sin^2\theta_3} \tag{3}$$

$$\cos\theta_1 = (1 - 2\sin^2\theta_3)\cos\frac{68\pi}{365} + 2\sin\theta_3\cos\theta_3\sin\frac{68\pi}{365} \tag{4}$$

$$\theta'_4 = \text{SLOG} - \frac{\pi}{6} - \text{subsolar longitude} \tag{5}$$

$$\theta'_5 = \text{SLOG} - \frac{2\pi}{3} \text{ - subsolar longitude}$$

where:

$$\text{SUND} = \begin{cases} +1 \text{ Dec. 21} - \text{June 21} \\ -1 \text{ June 22} - \text{Dec. 20} \end{cases}$$

Other terms in these equations are defined in either of the previously mentioned notes.

The ionosphere parameters shown are to represent a day in the middle of May with solar conditions somewhat more excited than probably will exist in 1969. Specifically, these parameters are:

$R = 300$
$\overline{R} = 200$
$F = 160$
$\overline{F} = 160$
$a_p = 0$
$f = 2.3\,10^9$ cps
$K = L = 10^{-4}$

The four steps mentioned previously with the above ionosphere parameters are applied to a number of tracking situations, typical of the Apollo mission. These situations were:

1. Earth Orbit - Range and 2 angle information
   (a) One orbit ($\backsim$ 95 min.) of tracking - no nuisance parameters.
   (b) One orbit - bias in range.
   (c) One station (4.25 min.) - bias in range.

2. Translunar Orbit - Track from Injection to LSOI.

(a) Range and 2 angles - no nuisance parameters.

(b) Range and 2 angles - bias in range.

(c) Range rate (2 way) - no nuisance parameters.

(d) Range rate - bias in range rate.

In both cases the location of the sun (subsolar longitude) was chosen so as to maximize the portion of tracking done in sunlight, further increasing the ionosphere range error.

The orbital data for the Earth orbit (1) are as follows:

A1 = $6.56342 \cdot 10^6$ m.

A4 = 0

A5 = $7.82074 \cdot 10^3$ m/sec.

GAMID = 1.0

BETA = 28.482 deg.

OMEGA E = $7.45135\ 10^{-5}$ rad/sec.

OMEGA M = 0

RHO E = $6.3781 \cdot 10^6$

MU = $4.014424 \cdot 10^{14}$ m^3/sec^2

BIG L = 28.48 deg.

SMA L = 80.6 deg.

The associated tracking data are:

(1) One second samples with σ_R = 15 meters/sample and $\sigma_{\phi_1} = \sigma_{\phi_2} = .8 \cdot 10^{-3}$ radians/sample.

(2) Track for 95.25 min. using tracking stations:

Grand Bahamas	0 - 1.25 min.
* Bermuda	1.25 - 5.50
Carnarvon	47.25 - 52.25
Hawaii	73.00 - 76.50
Pt. Arguello	82.50 - 85.50
Guaymas	85.50 - 88.25
White Sands	88.25 - 89.00
Corpus Christi	89.00 - 91.00
Eglin	91.00 - 92.75
Cape Kennedy	92.75 - 95.25

* Single station track

It should be noted that the altitude for this orbit is about 200 kilometers whereas in fact the ionosphere extends up to about 1500 km (although it is extremely rarified at this altitude). Thus, the range error generated by this ionosphere model (which assumes that the orbit is entirely above the ionosphere) for this orbit is somewhat larger and of a different form than the actual situation.

The orbital data used for the translunar (2) orbit are:

A1	=	$6.56006 \cdot 10^6$ m.
A4	=	0.0
A5	=	$1.095085 \cdot 10^4$ m/sec.
GAMID	=	+ 1.0
BETA	=	24.782278 deg.

OMEGA E	=	$7.29216\ 10^{-4}$ rad/sec.
OMEGA M	=	0.0
RHO E	=	$6.3781\ 10^{6}$ m.
RHO M	=	0.0
MU	=	$3.986032\ 10^{14}\ m^3/sec^2$
BIG L	=	-7.93 deg.
SMA L	=	16.129 deg.

While the associated tracking data are:

(1) Both Range and 2 angle data, and range-rate (2-way) with 10 sec. samples ($\sigma_{\dot{R}}$ = 3 cm/sec/sample).

(2) Tracks for 3340 minutes (to LSOI).

Using stations and tracking times of:

Carnarvon	0 - 400 min.
Madrid	400 - 1040
Hawaii	1040 - 1700
Woomera	1700 - 1940
Ascension	1940 - 2320
Pt. Arguello	2320 - 2720
Canberra	2720 - 3340

For the Earth orbit, the initial subsolar longitude was 45° W (3:00 pm GMT); for the translunar orbit, the subsolar longitude was 135° W (9:00 pm GMT).

Since the Az-El program prints out all of the stations that are visible to the vehicle and the radar system does not have the capability of simultaneous tracking, it is necessary to manually select those

stations that are to track for the ionosphere range error program and the weighting functions program. When more than one station can see the vehicle, that station that appears to have the better tracking geometry is chosen.

The weighted errors in the orbit parameters that result from this process for the seven situations mentioned are compiled in Table I. Keeping in mind that this is a "worst case" type answer, these numbers are relatively small, especially the relevant situations, (1b) and (2d), the tracking modes that will be used for those phases of the mission. It is interesting to note that in the course of computing the weighting functions, the covariance of the orbit parameters for the depicted tracking situations are found (exclusive of the ionospheric errors). For the range rate tracking mode, these standard deviations of the orbit parameters are 3 to 10 times the corresponding weighted ionosphere errors (Table I) while the standard deviation of the orbit parameters for the vector range tracking mode are $\frac{1}{3}$ to $\frac{1}{10}$ of these weighted ionosphere error.

If these errors prove to be significant at some future time because of the reduction of other contributing errors, (e. g., station location error, clock errors, etc.), the radar data received can be corrected by use of this ionosphere model (Apollo Note No. 388). The remaining error will be the result of not knowing the ionosphere parameters exactly; however a reduction to one fifth of the errors in Table I by this correction is not at all unrealistic.

Tracking Station	Meters				cm/sec.			
	δa_1	δa_2	δa_3	S_1	δa_4	δa_5	δa_6	S_2
(1) Earth Orbit								
(a) No bias in range	-1.6	-9.6	-16.2	18.9	0.6	0.2	-.02	.63
(b) Bias in range	2.6	-0.8	1.2	3.0	-.02	-0.2	0.1	.23
(c) One station tracking- bias in range	-20.0	12.6	8.8	25.2	8.6	-7.2	2.4	11.5
(2) Translunar Orbit								
(a) Range Track - no bias	10.0	10.0	4.2	14.8	-1.84	-0.84	2.4	3.14
(b) Range - bias	29.2	70.6	63.2	100.8	-9.0	-2.4	-.46	9.3
(c) Range rate - no bias	9.0	14.2	-27.2	32.6	-2.14	-.76	-.38	2.35
(d) Range rate- bias in range rate	-4.4	-1.1	-22.8	23.2	1.54	0.26	-19.6	19.7

$$S_1 = \sqrt{\delta a_1^2 + \delta a_2^2 + \delta a_3^2} \qquad S_2 = \sqrt{\delta a_4^2 + \delta a_5^2 + \delta a_6^2}$$

TABLE 1.

The Bissett-Berman Corporation 2941 Nebraska Avenue, Santa Monica, California EXbrook 4-3270

APOLLO NOTE NO. 416
(Task I, Item I)

H. Epstein
30 March 1966

TECHNIQUES FOR ESTIMATION OF PARAMETERS ASSOCIATED WITH STATISTICAL TYPE NOISE

PART I

The general objective of this note is to establish a criteria for the validity of estimates of parameters associated with statistical type measurement error sources. This general objective may be considered in terms of a number of features. One such factor deals with how well can the parameters of interest be estimated. In addition, specific simple analysis techniques will be investigated to indicate their performance relative to the optimum performance. The third feature will be to establish requirements on data to be taken to allow satisfactory estimates to be made. It is necessary for the satisfaction of this objective that theoretical models for statistical type noise be established which yield the precise nature of the functional dependence and only require scale factors or parameters to be estimated.

The term statistical type error source or statistical type noise is defined as those error sources whose most appropriate description is made either in terms of its correlation function or spectral distribution. These error sources most frequently are assumed to possess a multidimensional gaussian probability distribution with a zero mean. Unless otherwise specified, this characteristic should be assumed. In addition, where a number of error sources are present, it is assumed that no correlation exists between different error sources. The error sources themselves are treated with their appropriate correlation. The functional dependent of the auto-correlation function is determined completely by the normalized auto-correlation function. Theoretical model will be employed wherein the normalized value of the auto-correlation function is completely determined. In addition, the noise sources will be pre-whitened to the extent that they become stationary. For these

individual error sources, it is only necessary to estimate their variation (this corresponds to the zero lag value of the auto-correlation function).

Our experience at Bissett-Berman in the analysis of doppler residual data and frequency standard data for Apollo has indicated that these data sets can be almost invariably separated into sets of statistical error sources with either one or two dominant noise sources. The analysis which follows in this note assumes that no more than two noise sources needs to be considered. The basic technique which will be indicated can be simply extended to more error sources if the added complexity is warranted at a future time. No a priori knowledge of the variance of the individual error sources is assumed in this part of the analysis. This is a possible area for a simple extension of the technique. To establish good estimates for the variance of the individual noise sources, it is necessary that large numbers of samples of noise sources be taken. As a consequence, we are interested in large sample estimates of the variance of the errors of the estimated variances. The asymptotic performance of the maximum likelihood estimators then provides the optimum estimators. This estimate is an unbiased estimate. The analysis proceeds as follows. The basic equation is given by:

I. Initial General Analysis

$$n(r) = x(r) + y(r) \qquad (1)$$

where

$n(r)$ = measured value of the combined noise

$x(r)$ = one noise source

$y(r)$ = the other noise source

r = the number of the measurement

The following assumptions are made:

$$E\left\{x(r)\right\} = E\left\{y(r)\right\} = E\left\{x(r)\, y(s)\right\} = 0 \tag{2}$$

$$E\left\{x(r)\; x(r+k)\right\} = \phi_x(k) = \phi_x\, \rho_x(k) \tag{3}$$

$$E\left\{y(r)\;\; y(r+k)\right\} = \phi_y(k) = \phi_y\, \rho_y(k) \tag{4}$$

where

$E\{\;\}$ = expected value of the quantity

$\phi_{\substack{x \\ y}}$ = variance or zero lag value of the $\substack{x \\ y}$ error

$\phi_{\substack{x \\ y}}(k)$ = auto-correlation function for the $\substack{x \\ y}$ error source

$\rho_{\substack{x \\ y}}(k)$ = normalized value of the auto-correlation function which is assumed as being known exactly

From Eqs. (1), (2), (3), and (4), it can readily be shown that

$$E\left\{n(r)\right\} = 0 \tag{5}$$

$$E\left\{n(r)\; n(r+k)\right\} = \phi_n(k) = \phi_x(k) + \phi_y(k) \tag{6a}$$

$$= \phi_x\, \rho_x(k) + \phi_y\, \rho_y(k) \tag{6b}$$

The covariance matrix for the combined noise (C) may be written as

$$C = \left[\, c_y \,\right] \tag{7}$$

where

c_y = i, j element of the square matrix C

From Eqs. (6a) and (6b)

$$c_{ij} = \phi_n(j-i) = \phi_x(j-i) + \phi_y(j-i) = \phi_x\rho_x(j-i) + \phi_y\rho_y(j-i) \tag{8}$$

Let

$$C^{-1} = \left[c^{-1}(i,j)\right] = \text{inverse of the matrix C} \tag{9}$$

where

$c^{-1}(i,j)$ = i, j element of the inverse of the square matrix C

With the assumption that the noise sources are gaussian, the likelihood function (L) is given by the following equation:

$$-\ell n L = \frac{1}{2}\sum_{i=1}^{N}\sum_{j=1}^{N} n_i n_j\, c^{-1}(i,j) + \frac{1}{2}\ell n\, D + \frac{N}{2}\ell n\, 2\pi \tag{10}$$

where

D = determinant of the matrix C

N = number of samples of the noise

The maximum likelihood estimates for ϕ_x and ϕ_y are then found by taking partials derivates with respect to ϕ_x and then ϕ_y. These partials are then set equal to zero and then the resulting two equations are solved for ϕ_x and ϕ_y. The two equations to be solved are indicated below as:

$$\frac{-\partial \ell n L}{\partial \phi_x} = 0 = \frac{1}{2}\sum_{i=1}^{N}\sum_{j=1}^{N} n_i n_j \frac{\partial c^{-1}(i,j)}{\partial \phi_x} + \frac{1}{2D}\frac{\partial D}{\partial \phi_x} \tag{11}$$

$$= \frac{1}{2}\sum_{i=1}^{N}\sum_{j=1}^{N} n_i n_j \frac{\partial c^{-1}(i,j)}{\partial \phi_y} + \frac{1}{2D}\frac{\partial D}{\partial \phi_y} \tag{12}$$

Since unbiased estimators are being used, Eqs. (6a), (6b) and (7) may be used with the expected values of Eqs. (11) and (12) to obtain the following results:

$$-\frac{1}{2D}\frac{\partial D}{\partial \phi_x} = \frac{1}{2}\sum_{i=1}^{N}\sum_{j=1}^{N} c_{ij}\frac{\partial c^{-1}(i,j)}{\partial \phi_y} \tag{13}$$

and

$$-\frac{1}{2D}\frac{\partial D}{\partial \phi_y} = \frac{1}{2}\sum_{i=1}^{N}\sum_{j=1}^{N} c_{ij}\frac{\partial c^{-1}(i,j)}{\partial \phi_y} \tag{14}$$

Now Eq. (13) may be substituted into Eq. (11) and Eq. (14) into Eq. (12) to yield the desired forms:

$$-\frac{\partial \ell nL}{\partial \phi_x} = \frac{1}{2}\sum_{i=1}^{N}\sum_{j=1}^{N}(n_i n_j - c_{ij})\frac{\partial c^{-1}(i,j)}{\partial \phi_x} = 0 \tag{15}$$

$$-\frac{\partial \ell nL}{\partial \phi_y} = \frac{1}{2}\sum_{i=1}^{N}\sum_{j=1}^{N}(n_i n_j - c_{ij})\frac{\partial c^{-1}(i,j)}{\partial \phi_y} = 0 \tag{16}$$

Fortunately, in order to find the variance in the maximum likelihood estimators, it is not necessary to find the explicit forms of the equations which indicate how the data is to be processed to obtain the maximum likelihood estimators. This allows us to find how well we can do in estimators. This result can be compared to simple processing techniques to arrive at simple quasi optimum estimates which retain the same quality of performance. Where simple techniques are not readily available, it then becomes necessary to solve for the likelihood estimators and from this one may assume that a simple technique will be suggested. At any rate, the variances in $\hat{\phi}_x$ and $\hat{\phi}_y$ may be found from the found equations:

$$\begin{bmatrix} A, & B \\ B, & D \end{bmatrix}^{-1} = \frac{1}{AD - B^2}\begin{bmatrix} D, & B \\ -B, & A \end{bmatrix} \tag{17}$$

$$A = E\left\{-\frac{\partial^2 \ell nL}{\partial \phi_x^2}\right\} \tag{18}$$

$$B = E\left\{-\frac{\partial^2 \ell nL}{\partial \phi_x \partial \phi_y}\right\} \tag{19}$$

$$D = E\left\{-\frac{\partial^2 \ell n L}{\partial \phi_y^2}\right\} \tag{20}$$

Letting

$$\Delta\phi_x^2 = E\left\{\phi_x^2\right\} - \phi_x^2 \tag{21}$$

$$\Delta\phi_y^2 = E\left\{\phi_y^2\right\} - \phi_y^2 \tag{22}$$

then

$$\Delta\phi_x^2 = \frac{D}{AD - B^2} \tag{23}$$

$$\Delta\phi_y^2 = \frac{A}{AD - B^2} \tag{24}$$

The correlation between errors in the estimate of ϕ_x and ϕ_y (ρ_{x-y}) is given by:

$$\rho_{x-y} = \frac{-B}{\sqrt{AD}} \tag{25}$$

Clearly, at this point, the remaining effort needs to be devoted to arriving at suitable expressions for A, B, and D, (at times, care must be taken with the quantity $AD - B^2$ also).

A, B, and D, can be found from Eqs. (6a), (6b), (7), (15), (16), (18), (19), and (20).

$$A = -\frac{1}{2}\sum_{i=1}^{N}\sum_{j=1}^{N}\left(\frac{\partial c_{ij}}{\partial \phi_x}\right)\left(\frac{\partial c^{-1}(i,j)}{\partial \phi_x}\right) \tag{26}$$

$$B = -\frac{1}{2} \sum_{i=1}^{N} \sum_{j=1}^{N} \left(\frac{\partial c_{ij}}{\partial \phi_x} \right) \left(\frac{\partial c^{-1}(i,j)}{\partial \phi_y} \right) \tag{27a}$$

$$= -\frac{1}{2} \sum_{i=1}^{N} \sum_{j=1}^{N} \left(\frac{\partial c_{ij}}{\partial \phi_y} \right) \left(\frac{\partial c^{-1}(i,j)}{\partial \phi_x} \right) \tag{27b}$$

$$D = -\frac{1}{2} \sum_{i=1}^{N} \sum_{j=1}^{N} \left(\frac{\partial c_{ij}}{\partial \phi_y} \right) \left(\frac{\partial c^{-1}(i,j)}{\partial \phi_y} \right) \tag{28}$$

Differentiating Eq. (8)

$$\frac{\partial c_{ij}}{\partial \phi_x} = \rho_x(j-i) \tag{29}$$

$$\frac{\partial c_{ij}}{\partial \phi_y} = \rho_y(j-i) \tag{30}$$

The substitution of Eqs. (29) and (30) into Eqs. (26), (27a), (27b), and (28), yields the following results:

$$A = -\frac{1}{2} \sum_{i=1}^{N} \sum_{j=1}^{N} \rho_x(j-i) \frac{\partial c^{-1}(i,j)}{\partial \phi_x} \tag{31}$$

$$B = -\frac{1}{2} \sum_{i=1}^{N} \sum_{j=1}^{N} \rho_y(j-i) \frac{\partial c^{-1}(i,j)}{\partial \phi_y} \tag{32a}$$

$$= -\frac{1}{2} \sum_{i=1}^{N} \sum_{j=1}^{N} \rho_y(j-i) \frac{\partial c^{-1}(i,j)}{\partial \phi_x} \tag{32b}$$

$$D = -\frac{1}{2}\sum_{i=1}^{N}\sum_{j=1}^{N}\rho_y(j-i)\,\frac{\partial c^{-1}(i,j)}{\partial \phi_y} \tag{33}$$

Since ρ_x and ρ_y are only function of (j-i) and C^{-1} is a symmetric matrix, the form for A, B, and D, may be written as follows:

$$A = -\frac{1}{2}\sum_{i=1}^{N}\frac{\partial c^{-1}(i,i)}{\partial \phi_x} - \sum_{r=1}^{N-1}\rho_x(r)\sum_{i=1}^{N-r}\frac{\partial c^{-1}(i,i+r)}{\partial \phi_x} \tag{34}$$

$$B = -\frac{1}{2}\sum_{i=1}^{N}\frac{\partial c^{-1}(i,i)}{\partial \phi_y} - \sum_{r=1}^{N-1}\rho_x(r)\sum_{i=1}^{N-r}\frac{\partial c^{-1}(i,i+r)}{\partial \phi_y} \tag{35a}$$

$$= -\frac{1}{2}\sum_{i=1}^{N}\frac{\partial c^{-1}(i,i)}{\partial \phi_x} - \sum_{r=1}^{N-1}\rho_y(r)\sum_{i=1}^{N-r}\frac{\partial c^{-1}(i,i+r)}{\partial \phi_x} \tag{35b}$$

$$D = -\frac{1}{2}\sum_{i=1}^{N}\frac{\partial c^{-1}(i,i)}{\partial \phi_y} - \sum_{r=1}^{N-1}\rho_y(r)\sum_{i=1}^{N-r}\frac{\partial c^{-1}(i,i+r)}{\partial \phi_y} \tag{36}$$

By inspection of Eqs. (34), (35a), (35b), and (36), A, B, and D are determined from the trace of the diagonal and sums of super diagonal elements.

$$\text{defining } T_r^{-1} = \sum_{i=1}^{N-r} c^{-1}(i,i+r) \tag{37}$$

The final desired forms for A, B, and D can now be obtained.

$$A = -\frac{1}{2}\frac{\partial T_o^{-1}}{\partial \phi_x} - \sum_{r=1}^{N-1} \rho_x(r)\frac{\partial T_r^{-1}}{\partial \phi_x} \tag{38}$$

$$B = -\frac{1}{2}\frac{\partial T_o^{-1}}{\partial \phi_y} - \sum_{r=1}^{N-1} \rho_x(r)\frac{\partial T_r^{-1}}{\partial \phi_y} \tag{39a}$$

$$B = -\frac{1}{2}\frac{\partial T_o^{-1}}{\partial \phi_x} - \sum_{r=1}^{N-1} \rho_y(r)\frac{\partial T_r^{-1}}{\partial \phi_x} \tag{39b}$$

$$D = -\frac{1}{2}\frac{\partial T_o^{-1}}{\partial \phi_y} - \sum_{r=1}^{N-1} \rho_y(r)\frac{\partial T_r^{-1}}{\partial \phi_y} \tag{40}$$

The two equivalent forms for B are given even though somewhat redundant. As one should expect $AD - B^2 = 0$ if $\rho_x(r) = \rho_y(r)$ for all values of r. Such noise sources are to be combined and considered as one noise source. Equations (37) through (40) are particularly good forms for the situation wherein theoretical models indicate that few significant values for the correlation function exist.

The result for the situation wherein only one significant noise source exists can readily be obtained from Eq. (26). With only one noise source,

$$c_{ij} = \phi\, d_{ij} \tag{41}$$

$$c^{-1}(i,j) = \phi\, d^{-1}(i,j) \tag{42}$$

where d_{ij} and $d^{-1}(i,j)$ are independent of the variance ϕ

$$\therefore A = \frac{1}{2\phi^2} \sum_{i=1}^{N} \sum_{j=1}^{N} d_{ij}\, d^{-1}(i,j) = \frac{N}{2\phi^2} \tag{43}$$

and

$$\Delta\phi^2 = \frac{2\phi^2}{N} \tag{44}$$

or

$$\frac{\Delta\phi^2}{\phi^2} = \frac{2}{N} \tag{45}$$

This is the same results as is obtained for uncorrelated samples. Therefore, the maximum likelihood data processor may simply be considered as a device which makes the noise sample uncorrelated and of equal variance. With only one noise source, processing techniques may be readily compared to maximum likelihood values. One simple numerical example will be indicated here without the proof. If one takes unbiased, uncorrelated noise samples and estimates the variance by the sum of squares of the values divided by the number of samples, one will obtain the result indicated in Eq. (45). On the other hand, if one takes the difference between samples, and estimates the variance by the sum of the squares divided by the number of samples, one will obtain a value of $\frac{3}{N}$ rather than $\frac{2}{N}$. A factor of 1.5 exists for this case. Much more dramatic illustrations can be given. The important factor is that a standard of performance is readily obtainable for this case.

Numerical values for the case of two noise sources is much more difficult to obtain. At this point, I will arrive at numerical values for an example which is indicative of doppler measurement error sources. The example corresponds to a random frequency

noise combined with a random phase noise. Mathematically this corresponds to the case of the first difference of a random noise in the presence of a random walk type noise. These error sources are dominant high frequency measurement error sources for the three-way doppler mode.

II. Numerical Example

The properties of the noise sources are given below as:

$$\phi_x(r) = \phi_x \qquad r = 0$$
$$= 0 \qquad r \neq 0$$

and

$$\phi_y(r) = \phi_y \qquad r = 0$$
$$= -\frac{\phi_y}{2} \qquad (r) = 1$$
$$= 0 \qquad |r| \neq 0, 1$$

A, B, and D are then given from Eqs. (38), (39a), and (40) as:

$$A = -\frac{1}{2} \frac{\partial T_o^{-1}}{\partial \phi_x} \tag{46}$$

$$B = -\frac{1}{2} \frac{\partial T_o^{-1}}{\partial \phi_y} \tag{47}$$

$$D = -\frac{1}{2} \frac{\partial}{\partial \phi_y} (T_o^{-1} - T_1^{-1}) \tag{48}$$

$$T_o^{-1} = \sum_{i=1}^{N} c^{-1}(i, i) \tag{49}$$

$$T_1^{-1} = \sum_{i=1}^{N-1} c^{-1}(i, i+1) \tag{50}$$

Equation (22) of Apollo Note 305 with a slight modification in nomenclature yields:

$$c^{-1}(i, i) = \frac{2}{N+1} \sum_{\ell=1}^{N} \frac{\sin^2 \frac{\ell \pi i}{N+1}}{\phi_x + \phi_y \left(1 - \cos \frac{\ell \pi}{N+1}\right)} \tag{51}$$

$$c^{-1}(i, i+1) = \frac{2}{N+1} \sum_{\ell=1}^{N} \frac{\sin \frac{\ell \pi i}{N+1} \sin \frac{\ell \pi (i+1)}{N+1}}{\phi_x + \phi_y \left(1 - \cos \frac{\pi \ell}{N+1}\right)} \tag{52}$$

Making use of the easily obtainable relationships

$$\sum_{i=1}^{N} \sin^2 \frac{\ell \pi i}{N+1} = \frac{N+1}{2} \tag{53}$$

$$\sum_{i=1}^{N-1} \sin \frac{\ell \pi i}{N+1} \sin \frac{\ell \pi (i+1)}{N+1} = \frac{N+1}{2} \cos \frac{\pi \ell}{N+1} \tag{54}$$

Then

$$T_o^{-1} = \sum_{\ell=1}^{N} \frac{1}{\phi_x + \phi_y \left(1 - \cos \frac{\pi \ell}{N+1}\right)} \tag{55}$$

and

$$T_o^{-1} - T_1^{-1} = \sum_{\ell=1}^{N} \frac{1 - \cos \frac{\pi \ell}{N+1}}{\phi_x + \phi_y \left(1 - \cos \frac{\pi \ell}{N+1}\right)} \tag{56}$$

These equations [(55) and (56)] may be simplified by replacing the sum by an integral for large N provided that

$$\phi_x >> \phi_y \left(1 - \cos \frac{\pi}{N+1}\right) \sim \frac{\phi_y}{2} \left(\frac{\pi}{N+1}\right)^2 \sim \frac{5\phi_y}{N^2} \tag{57}$$

for N = 500, this corresponds to $\frac{\phi_x}{\phi_y} >> 2 \times 10^{-5}$ which is certainly a trivial restriction.

It can readily be shown that

$$T_o^{-1} \sim \int_o^N \frac{d\ell}{\phi_x + \phi_y \left(1 - \cos \frac{\pi\ell}{N}\right)} = \frac{N}{\sqrt{\phi_x^2 + 2\phi_x\phi_y}} \tag{58}$$

$$T_o^{-1} - T_1^{-1} \sim \int_o^N \frac{d\ell \left(1 - \cos \frac{\pi\ell}{N}\right)}{\phi_x + \phi_y \left(1 - \cos \frac{\pi\ell}{N}\right)} = \frac{N}{\phi_y} - \frac{N\phi_x}{\phi_y \sqrt{\phi_x^2 + 2\phi_x\phi_y}} \tag{59}$$

From Eqs. (46), (47), (48), (58), and (59),

$$A \sim \frac{N\left(\phi_x + \phi_y\right)}{2\left(\phi_x^2 + 2\phi_x\phi_y\right)^{3/2}} \tag{60}$$

$$B \sim \frac{N\phi_x}{2\left(\phi_x^2 + 2\phi_x\phi_y\right)^{3/2}} \tag{61}$$

$$D \sim \frac{N}{2\phi_y^2} \left[1 - \frac{\phi_x^2\left(\phi_x + 3\phi_y\right)}{\left(\phi_x^2 + 2\phi_x\phi_y\right)^{3/2}}\right] \tag{62}$$

After some manipulation,

$$AD - B^2 = \frac{N^2}{4\left(\phi_x^2 + 2\phi_x\phi_y\right)^{3/2}\left[\phi_x + \phi_y + \sqrt{\phi_x^2 + 2\phi_x\phi_y}\right]} \tag{63}$$

$$\frac{N\Delta\phi_x^2}{\phi_x^2} \sim \frac{2\left(3 + \frac{8\phi_y}{\phi_x}\right)\left[1 + \frac{\phi_y}{\phi_x} + \sqrt{1 + \frac{2\phi_y}{\phi_x}}\right]}{1 + \frac{3\phi_y}{\phi_x} + \left(1 + 2\frac{\phi_y}{\phi_x}\right)^{3/2}} \tag{64}$$

$$\frac{N\Delta\phi_y^2}{\phi_y^2} \sim 2\left(1 + \frac{\phi_x}{\phi_y}\right)\left[1 + \frac{\phi_x}{\phi_y} + \sqrt{\frac{\phi_x^2}{\phi_y} + \frac{2\phi_x}{\phi_y}}\right] \tag{65}$$

and

$$\rho_{x-y} \sim -\left[\frac{\left(1 + \frac{2\phi_y}{\phi_x}\right)^{3/2} + 1 + \frac{3\phi_y}{\phi_x}}{\left(1 + \frac{\phi_y}{\phi_x}\right)\left(3 + \frac{8\phi_y}{\phi_x}\right)}\right]^{1/2} \tag{66}$$

It is of interest how these expressions behave for large values of $\frac{\phi_y}{\phi_x}$ and $\frac{\phi_x}{\phi_y}$.

$$\text{for } \frac{\phi_x}{\phi_y} >> 1 \ , \quad \frac{\Delta\phi_x^2}{\phi_x^2} \sim \frac{6}{N} \tag{67}$$

$$\frac{\Delta\phi_y^2}{\phi_y^2} \sim \frac{4}{N}\left(\frac{\phi_x}{\phi_y}\right)^2 \tag{68}$$

$$\rho_{x-y} \sim -\sqrt{\frac{2}{3}} = -.817 \tag{69}$$

for $\frac{\phi_y}{\phi_x} >> 1$, $\frac{\Delta\phi_x^2}{\phi_x^2} \sim \frac{4}{N}\sqrt{\frac{2\phi_y}{\phi_x}}$ (70)

$$\frac{\Delta\phi_y^2}{\phi_y^2} \sim \frac{2}{N} \tag{71}$$

$$\rho_{x-y} \sim -\sqrt{\frac{\phi_x}{8\phi_y}} \tag{72}$$

Examination of Eq. (71) indicates that for $\frac{\phi_y}{\phi_x} >> 1$ that $\frac{\Delta\phi_y^2}{\phi_y^2} \sim \frac{2}{N}$ which is the same result as though only one noise source was estimated. This can be explained by the fact that the correlation between the errors in this case approaches zero as $\frac{\phi_x}{\phi_y}\sqrt{\frac{\phi_y}{\phi_x}}$ goes to zero. In addition, for this situation $\frac{\Delta\phi_x^2}{\phi_x^2}$ is proportional to $\sqrt{\frac{\phi_y}{\phi_x}}$. This error component as a consequence deteriorates in performance very slowly as $\frac{\phi_y}{\phi_x}$ increases.

Equation (67) indicates that for $\frac{\phi_x}{\phi_y} >> 1$ that $\frac{\Delta\phi_x^2}{\phi_x^2} \sim \frac{6}{N}$. This indicates a deterioration in the estimate of ϕ_x due to the uncertainty in ϕ_y even though $\frac{\phi_y}{\phi_x} << 1$. Another indication of the rational for this behavior is indicated by the strong correlation between errors in the estimates. Equation (68) indicates that accurate estimates of ϕ_y are difficult and perhaps even impractical for this case.

A graphical representation of Eqs. (64) and (65) are left to a later section of this report to enable a comparison to be made with a simple processing technique to be indicated in the next portion.

III. Estimation of Parameters From The Correlation Function

The previous portions of this report has treated the problem of how well can the noise parameters be estimated. The problem of how to obtain the indicated level of performance was not treated. For many cases of interest, it might be expected that simple processing techniques will provide a satisfactory level of performance. This section will indicate the accuracy which may be obtained for variance estimation by use of the zero lag value of the auto-correlation function and one other lag value.

The properties of the gaussian noise source are indicated below as:

$$E\left\{n(r)\right\} = 0 \tag{73}$$

$$E\left\{n(r)\ n(r+k)\right\} = \phi_n(k) \tag{74}$$

$$\hat{\phi}_n(k) = \frac{1}{N} \sum_{i=1}^{N} n(r)\ n(r+k) \tag{75}$$

$$E\left\{\phi_n(k)\right\} = \phi_n(k) \tag{76}$$

$$\hat{\phi}_n(k)^2 = \frac{1}{N^2} \sum_{r=1}^{N} \sum_{s=1}^{N} n(r)\ n(r+k)\ n(s)\ n(s+k) \tag{77}$$

Letting

$$\Delta\phi_n^2(k) = E\left\{\phi_n^2(k)\right\} - \phi_n^2(k) \tag{78}$$

then it can be shown that

$$\Delta\phi_n^2(k) = \frac{1}{N^2}\sum_{r=1}^{N}\sum_{s=1}^{N}\left[\phi_n^2(s-r) + \phi_n(s-r+k)\,\phi_n(s-r-k)\right] \tag{79}$$

$$= \frac{1}{N}\left[\phi_n^2(o) + \phi_n^2(k)\right] + \frac{2}{N}\sum_{r=1}^{N-1}\left(1 - \frac{r}{N}\right)\left[\phi_n^2(r) + \phi_n(r+k)\,\phi_n(r-k)\right] \tag{80}$$

and

$$\Delta\phi_n^2(o) = \frac{2}{N}\,\phi_n^2(o) + \frac{4}{N}\sum_{r=1}^{N-1}\left(1 - \frac{r}{N}\right)\phi_n^2(r) \tag{81}$$

With only one noise source present, Eq. (81) is ample for an estimation of the variance. Rewritten this equation in a slightly different form

$$\frac{\Delta\phi_n^2(o)}{\phi_n^2(o)} = \frac{2}{N} + \frac{4}{N}\sum_{r=1}^{N-1}\left(1 - \frac{r}{N}\right)\rho_n^2(r) = 0 \tag{82}$$

For uncorrelated noise sample $\rho_n(r) = 0$ which leads to:

$$\frac{\Delta\phi_n^2(o)}{\phi_n^2(o)} = \frac{2}{N}$$

which corresponds to the value for the maximum likelihood estimator.

For

$$\rho_n(r) = -\frac{1}{2} \qquad |r| = 1$$

$$= 0 \qquad |r| \geq 2$$

Then

$$\frac{\Delta\phi_n^2(o)}{\phi_n^2(o)} = \frac{3}{N}$$

which corresponds to a degradation in performance level associated with this simple estimation technique.

By inspection of Eq. (82), it can be seen that if few significant values for the normalized auto-correlation function exist, only a moderate degradation in the quality of estimator will be encountered through the use of this simple technique.

The extension to the use with two noise sources can be made as follows. Using the same nomenclature and properties as indicated earlier.

$$n(r) = x(r) + y(r) \tag{83}$$

$$\phi_n(o) = \phi_x + \phi_y \tag{84}$$

$$\phi_n(k) = \phi_x\rho_x(k) + \phi_y\rho_y(k) \tag{85}$$

Solving for ϕ_x and ϕ_y, one obtains

$$\phi_x = \frac{\rho_y(k)\,\phi_n(o) - \phi_n(k)}{\rho_y(k) - \rho_x(k)} \tag{86}$$

$$\phi_y = \frac{\phi_n(k) - \rho_x(k)\,\phi_n(o)}{\rho_y(k) - \rho_x(k)} \tag{87}$$

Our estimators ($\hat{\phi}_x$ and $\hat{\phi}_y$) are then determined from $\hat{\phi}_n(k)$ and $\hat{\phi}_n(o)$. Formally, dependent on the nature of $\rho_y(k)$ and $\rho_x(k)$, one could find the optimum value of k to use. However, one might expect to find that the optimum or near-optimum performance to be obtained with $\left|\rho_y(k) - \rho_x(k)\right|$ equal to maximum.

After some mathematical manipulations the following results may be obtained:

$$\left[\rho_y(k) - \rho_x(k)\right]^2 \Delta\phi_x^2(o,k) = \frac{c(o,k)}{N} + \frac{2}{N}\sum_{i=1}^{N-1}\left(1 - \frac{r}{N}\right)c(r,k) \tag{88}$$

$$\left[\rho_y(k) - \rho_x(k)\right]^2 \Delta\phi_y^2(o,k) = \frac{d(o,k)}{N} + \frac{2}{N}\sum_{i=1}^{N-1}\left(1 - \frac{r}{N}\right)d(r,k) \tag{89}$$

$$\left[\rho_y(k) - \rho_x(k)\right]^2 \Delta\phi_x \Delta\phi_y = \frac{e(o,k)}{N} + \frac{2}{N}\sum_{i=1}^{N-1}\left(1 - \frac{r}{N}\right)e(r,k) \tag{90}$$

where

$$c(o,k) = 2\phi_x^2\left[\rho_y(k) - \rho_x(k)\right]^2 + \phi_n^2(o) - \phi_n^2(k) \tag{91}$$

$$c(r,k) = \left[1 + 2\rho_y^2(k)\right]\phi_n^2(r) - 2\rho_y(k)\,\phi_n(r)\left[\phi_n(r-k) + \phi_n(r+k)\right] + \phi_n(r-k)\,\phi_n(r+k) \tag{92}$$

$$d(o,k) = 2\phi_y^2\left[\rho_y(k) - \rho_x(k)\right]^2 + \phi_n^2(o) - \phi_n^2(k) \tag{93}$$

$$d(r,k) = \left[1+2\rho_x^2(k)\right]\phi_n^2(r) - 2\rho_x(k)\,\phi_n^2(r)\left[\phi_n(r-k)+\phi_n(r+k)\right] + \phi_n(r+k)\,\phi_n(r-k) \tag{94}$$

$$e(o,k) = 2\phi_x\phi_y\left[\rho_y(k)-\rho_x(k)\right]^2 - \phi_n^2(o) + \phi_n^2(k) \tag{95}$$

$$e(r,k) = -\left[1+2\rho_x(k)\,\rho_y(k)\right]\phi_n^2(r) - \phi_n(r\mp k)\,\phi_n(r-k) + \left[\rho_y(k)+\rho_x(k)\right]\phi_n(r)\left[\phi_n(r-k)+\phi_n(r+k)\right] \tag{96}$$

To cite an example of the results that can be obtained with this technique, we will consider the same model as was used for the numerical results obtained in the previous section.

Model $\quad \rho_x(r) = 0$

$$\rho_y(r) = -1/2 \qquad |r| = 1$$

$$= 0 \qquad |r| \geq 2$$

$k = 1$ is the obvious optimum value of k.

It can be show that

$$\frac{N\Delta\phi_x^2}{\phi_x^2} = 2\left(3+\frac{2\phi_y}{\phi_x}+\frac{\phi_y^2}{\phi_x^2}\right) + \frac{1}{N}\left(\frac{4\phi_y}{\phi_x}+\frac{\phi_y^2}{\phi_x^2}\right) \tag{97a}$$

$$\sim 2\left(3+\frac{2\phi_y}{\phi_x}+\frac{\phi_y^2}{\phi_x^2}\right) = 6+\frac{4\phi_y}{\phi_x}+\frac{2\phi_y^2}{\phi_x^2} \tag{97b}$$

$$\frac{N\Delta\phi_y^2}{\phi_y^2} = \left(7 + \frac{8\phi_x}{\phi_y} + \frac{4\phi_x^2}{\phi_y^2}\right) - \frac{2}{N} \tag{98a}$$

$$\sim 7 + \frac{8\phi_x}{\phi_y} + \frac{4\phi_x^2}{\phi_y^2} \tag{98b}$$

$$\frac{N\Delta\phi_x\,\Delta\phi_y}{\phi_x\phi_y} = -\left[\frac{4\phi_x}{\phi_y} + 4 + \frac{3\phi_y}{\phi_x}\right] + \frac{2}{N} \tag{99a}$$

$$\sim -\left[\frac{4\phi_x}{\phi_y} + 4 + \frac{3\phi_y}{\phi_x}\right] \tag{99b}$$

$$\rho_{x-y} \sim -\frac{\left(4\frac{\phi_x}{\phi_y} + 3 + \frac{3\phi_y}{\phi_x}\right)}{\left[\left(6 + \frac{4\phi_y}{\phi_x} + \frac{2\phi_y^2}{\phi_x^2}\right)\left(7 + \frac{8\phi_x}{\phi_y} + \frac{4\phi_x^2}{\phi_y^2}\right)\right]^{1/2}} \tag{100}$$

Corresponding expressions for the variance obtained in this section and the previous section on maximum likelihood estimators will now be indicated graphically.

Figure 1 is a graphical representation of Eqs. (64) and (97b). The correlation technique leads to results within a factor of 2 of the results for the maximum likelihood estimation for $\frac{\phi_y}{\phi_x} < 2$ and is within a factor of 10 for $\frac{\phi_y}{\phi_x} < 9$. We would like to keep $\frac{\Delta\phi_x^2}{\phi_x^2} < .01$ since this would lead to a standard deviation of the error in the estimate less than 10%. Corresponding upper limits for $\frac{\phi_y}{\phi_x}$ for the two techniques are 1.5 and .7 for 1000 noise samples and 300 and 6 for 10,000 noise samples. This should give a good quantitative insight into when more complex processing techniques (than the simple correlation) are required.

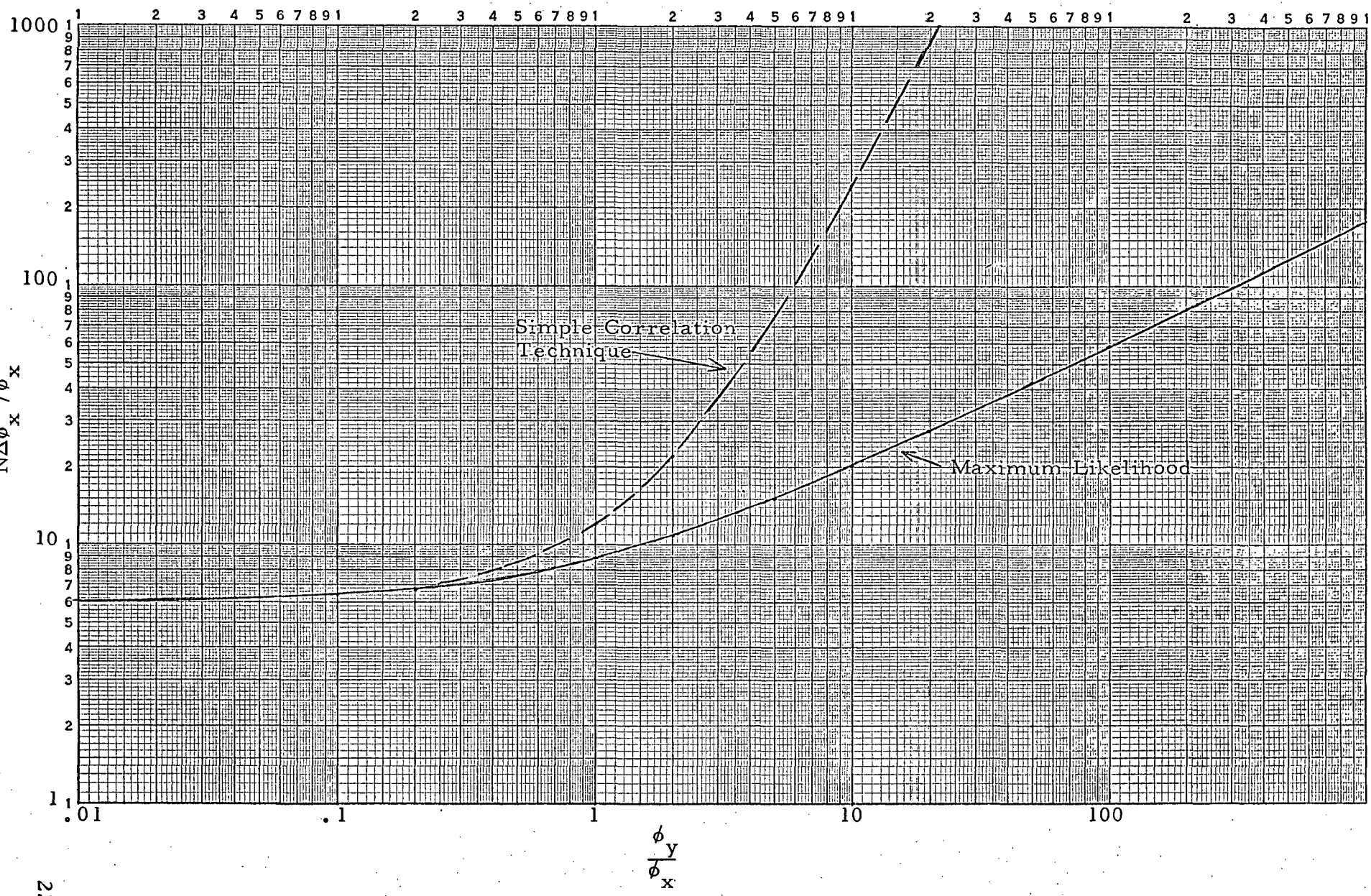
K+E LOGARITHMIC 358-125
KEUFFEL & ESSER CO. MADE IN U.S.A.
3 X 5 CYCLES
1000
100
10
1
.01
.1
1
10
100
$N\Delta\phi_x^2/\phi_x^2$
$\frac{\phi_y}{\phi_x}$
Simple Correlation Technique
Maximum Likelihood

Figure 1

Figure 2 is a graphical representation of Eqs. (65) and (98b). In this case, the simple correlation technique and the maximum likelihood technique are within a factor of 3.5 for all values of $\frac{\phi_x}{\phi_y}$. Again retaining a standard deviation of 10%, the corresponding upper limits for $\frac{\phi_x}{\phi_y}$ for the two techniques are 2/3 and 1/3 for 1000 samples and about 4 for both with 10,000 samples. As a consequence, for large samples sizes the simple correlation technique should be an adequate approximation to the maximum likelihood estimate for this component.

It is of practical importance to indicate that simple techniques can be employed in an intelligent fashion to obtain nearly maximum likelihood results. Specifically, consider the situation where two sets of noise samples are available. Choosing these two sets to correspond to one set of data with $\frac{\phi_y}{\phi_x} \ll 1$ and the other with $\frac{\phi_x}{\phi_y} \gg 1$, almost trivial extensions of the simple correlation techniques would lead to near optimum maximum likelihood solutions for the case indicated above.

One further comment should be made. Linear combinations of maximum likelihood estimates are also maximum likelihood estimates. Since the simple correlation technique involves a linear combination of the zero lag and another lag value of the correlation function with a non-zero expected value, maximum likelihood estimates of these quantities would yield the maximum likelihood estimates. Furthermore, by virtue of the discrepancy indicated, the simple technique obviously only approximates the maximum likelihood estimates of the zero lag and k lag values of the auto-correlation function.

IV. Extension of Initial General Analysis

An improved form for Eqs. (38) through (40) indicated in Section I can be found where one noise source has few non-zero expected values for the normalized auto-correlation function. Arbitrarily selecting x(r) to be the noise source with few non-zero values for its auto-correlation function, (Eqs. (38) and (39a) are already satisfactory forms). It then

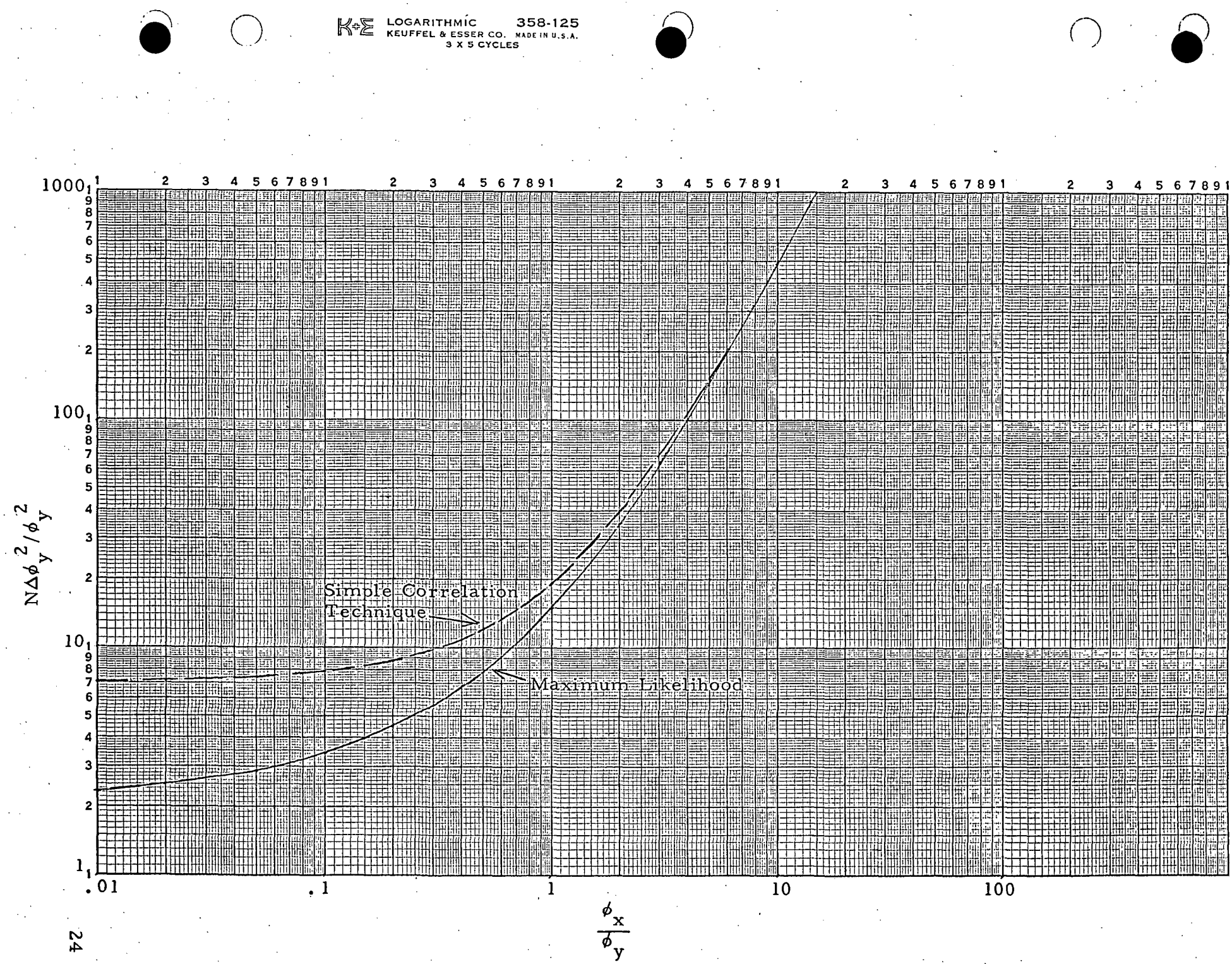
LOGARITHMIC 358-125
KEUFFEL & ESSER CO. MADE IN U.S.A.
3 X 5 CYCLES
1000
100
10
1
$N\Delta\phi_y^2/\phi_y^2$
Simple Correlation Technique
Maximum Likelihood
.01
.1
1
10
100
$\frac{\phi_x}{\phi_y}$

Figure 2

becomes necessary only to find an alternate form for Eq. (40). Re-writing Eq. (28),

$$D = -\frac{1}{2} \sum_{i=1}^{N} \sum_{j=1}^{N} \left(\frac{\partial c_{ij}}{\partial \phi_y} \right) \left(\frac{\partial c^{-1}(i,j)}{\partial \phi_y} \right) \tag{101}$$

$$\frac{\partial c_{ij}}{\partial \phi_y} = \rho_y(j-i) = \frac{1}{\phi_y} \left[c_{ij} - \phi_x(j-i) \right] \tag{102}$$

Then

$$D = \frac{1}{2\phi_y} \sum_{i=1}^{N} \sum_{j=1}^{N} \phi_x(j-i) \frac{\partial c^{-1}(i,j)}{\partial \phi_y} - \frac{1}{2\phi_y} \sum_{i=1}^{N} \sum_{j=1}^{N} c_{ij} \frac{\partial c^{-1}(i,j)}{\partial \phi_y} \tag{103}$$

Making use of Eq. (102) and the following relationships,

$$\sum_{i=1}^{N} \sum_{j=1}^{N} c_{ij}\, c^{-1}(i,j) = N \tag{104}$$

and

$$c_{ij} \frac{\partial c^{-1}(i,j)}{\partial \phi_y} = c_{ij}\, c^{-1}(i,j) - c^{-1}(i,j) \frac{\partial c_{ij}}{\partial \phi_y} \tag{105}$$

One can readily obtain the following result

$$D = \frac{N}{2\phi_y^2} - \frac{\phi_x}{2\phi_y^2} \sum_{i=1}^{N} \sum_{j=1}^{N} \rho_x(j-i)\ c^{-1}(i,j) + \frac{\phi_x}{2\phi_y} \sum_{i=1}^{N} \sum_{j=1}^{N} \rho_x(j-i)\ \frac{\partial c^{-1}(i,j)}{\partial \phi_y} \tag{106}$$

This can also be written as

$$D = \frac{N}{2\phi_y^2} - \frac{\phi_x T_o^{-1}}{2\phi_y^2} + \frac{\phi_x}{2\phi_y} \frac{\partial T_o^{-1}}{\partial \phi_y} - \frac{\phi_x}{\phi_y^2} \sum_{r=1}^{N-1} \rho_x(r)\ T_r^{-1} + \frac{\phi_x}{\phi_y} \sum_{r=1}^{N-1} \rho_x(r)\ \frac{\partial T_r^{-1}}{\partial \phi_y} \tag{107}$$

Where T_r^{-1} is given by Eq. (37).

For completeness, Eqs. (37),(38), and (39a) are indicated below.

$$A = -\frac{1}{2} \frac{\partial T_o^{-1}}{\partial \phi_x} - \sum_{r=1}^{N-1} \rho_x(r)\ \frac{\partial T_r^{-1}}{\partial \phi_x} \tag{108}$$

$$B = -\frac{1}{2} \frac{\partial T_o^{-1}}{\partial \phi_y} - \sum_{r=1}^{N-1} \rho_x(r)\ \frac{\partial T_r^{-1}}{\partial \phi_y} \tag{109}$$

$$T_r^{-1} = \sum_{i=1}^{N-r} c^{-1}(i, i+r) \tag{110}$$

For the situation where x(r) is uncorrelated noise, a simplification occurs regarding Eqs. (107), (108), and (109). For this case, the following simple equations are obtained.

$$A = -\frac{1}{2} \frac{\partial T_o^{-1}}{\partial \phi_x} \tag{111}$$

$$B = -\frac{1}{2} \frac{\partial T_o^{-1}}{\partial \phi_y} \tag{112}$$

$$D = \frac{N}{2\phi_y^2} - \frac{\phi_x T_o^{-1}}{2\phi_y^2} + \frac{\phi_x}{2\phi_y} \left(\frac{\partial T_o^{-1}}{\partial \phi_y} \right) \tag{113}$$

All of the computational difficulty in the determination of the variance of the estimated values of ϕ_x and ϕ_y are contained within the problem of determination of the trace of the inverse of the covariance matrix.

The last portion of this section will treat a somewhat fundamental characteristic of the asymptotic behavior $\left(\frac{\phi_x}{\phi_y} \gg 1 \right)$ with one noise source, an uncorrelated noise source.

First an approximation to the inverse of a matrix is required. Letting M be a general matrix

$$M = M_o + M_1 \tag{114}$$

$$M^{-1} = M_o^{-1} + \Delta M_o^{-1} \tag{115}$$

$$MM^{-1} = I = \left(M_o + M_1\right)\left(M_o^{-1} + \Delta M_o^{-1}\right) \tag{116}$$

$$M_1 M_o^{-1} + M_o \Delta M_o^{-1} + M_1 \Delta M_o^{-1} = 0 \tag{117}$$

Taking M_o^{-1} to be the approximate inverse and $M_o M_o^{-1} = 1$ to a first order approximation.

$$\Delta M_o^{-1} = - M_o^{-1} M_1 M_o^{-1} \tag{118}$$

The second order approximation may be obtained by using the value indicated in Eq. (118) for the third term in Eq. (117).

The second order approximation is then obtained as:

$$\Delta M_o^{-1} = -M_o^{-1} M_1 M_o^{-1} + M_o^{-1} M_1 M_o^{-1} M_1 M_o^{-1} \tag{119}$$

and

$$M^{-1} = M_o^{-1} - M_o^{-1} M_1 M_o^{-1} + M_o^{-1} M_1 M_o^{-1} M_1 M_o^{-1} \tag{120}$$

Taking the situation where M_o is a diagonal matrix with each diagonal element equal to ϕ_x

$$M^{-1} = \frac{1}{\phi_x} I - \frac{1}{\phi_x^2} M_1 + \frac{1}{\phi_x^3} M_1 M_1 \tag{121}$$

Letting M_1 be the covariance matrix of the other noise source, it can be shown that:

$$T_o^{-1} = \frac{N}{\phi_x} - \frac{N\phi_y}{\phi_x^2} + \frac{N\phi_y^2}{\phi_x^3} t_o \tag{122}$$

where

$$t_o = 1 + 2 \sum_{r=1}^{N-1} \left(1 - \frac{r}{N}\right) \rho_y^2(r) \tag{123}$$

This representation may be considered to be satisfactory provided that $\frac{\phi_y}{\phi_x} t_o << 1$. For $\frac{\phi_x}{\phi_y} >> 1$, this condition will be met provided that the correlation length of the y(r) noise source is short as compared to N. The substitution of Eq. (122) into Eqs. (111), (112), and (113) leads to the following results.

$$A \sim \frac{N}{2}\left[\frac{1}{\phi_x^2} - \frac{2\phi_y}{\phi_x^3} + \frac{3\phi_y^2}{\phi_x^4} t_o\right] \sim \frac{N}{2\phi_x^2} \tag{124}$$

$$B \sim \frac{N}{2}\left[\frac{1}{\phi_x^2} - \frac{2\phi_y}{\phi_x^3} t_o\right] \sim \frac{N}{2\phi_x^2} \tag{125}$$

$$D \sim \frac{Nt_o}{2\phi_x^2} \tag{126}$$

$$\frac{N\Delta\phi_x^2}{\phi_x^2} \sim \frac{2t_o}{(t_o-1)} \tag{127}$$

$$\frac{N\Delta\phi_y^2}{\phi_y^2} \sim \frac{2}{(t_o-1)} \frac{\phi_x^2}{\phi_y} \tag{128}$$

$$\rho_{x-y} \sim -\frac{1}{\sqrt{t_o}} \tag{129}$$

As a check of this result, the model taken in Section 2 will be compared.

$$\rho_y(r) = -1/2 \qquad |r| = 1$$
$$= 0 \qquad |r| \geq 2$$

then from Eq. (123),

$$t_o = 1 + \frac{1}{2}\left(1 - \frac{1}{N}\right) \sim \frac{3}{2} \tag{130}$$

$$\frac{N\Delta\phi_x^2}{\phi_x^2} \sim 6 \tag{131}$$

$$\frac{N\Delta\phi_y^2}{\phi_y^2} \sim 4\left(\frac{\phi_x}{\phi_y}\right)^2 \tag{132}$$

$$\rho_{x-y} \sim -\sqrt{\frac{2}{3}} = -.817 \tag{133}$$

These equations [(131), (132), and (133)] compare exactly with the corresponding equations [(67), (68), and (69)] of Section 2.

The equations for $\frac{\phi_y}{\phi_x} >> 1$ cannot be checked by this technique since a limitation was placed on this quantity by the analysis technique to obtain simple solutions. From the nature of the results obtained, one would expect to find, at least for a large class of noise sources of interest, that for $\frac{\phi_y}{\phi_x} >> 1$

$$\frac{\Delta\phi_y^2}{\phi_y^2} \sim \frac{2}{N}$$

A later part will be written to indicate the characteristics of some measurement error sources which have been observed in doppler tracking data.

H. Epstein
15 April 1966

APOLLO NOTE NO. 416
(Task I, Item I)

APPENDIX A
IMPROVED FORMS FOR MAXIMUM LIKELIHOOD ESTIMATORS

During the analysis effort being performed for Part II, a highly desirable form for the variance of the estimators of the variance of the two noise noises and for the correlation between the errors in the estimated values of the variance was indicated.

This formulation will now be given. Rewriting Eq. (8),

$$c_{ij} = \phi_x \rho_x(j-i) + \phi_y \rho_y(j-i) \tag{A1}$$

Letting

$$\alpha = \frac{\phi_x}{\phi_y} \tag{A2}$$

Then

$$c_{ij} = \phi_y d_{ij} \tag{A3}$$

where

$$d_{ij} = \alpha \rho_x(j-i) + \rho_y(j-i) = d(i, j; \alpha) \tag{A4}$$

$$\therefore \quad c^{-1}(i, j) = \frac{1}{\phi_y} d^{-1}(i, j) \tag{A5}$$

From Eq. (37),

$$T_r^{-1} = \sum_{i=1}^{N-r} c^{-1}(i, i+r) \tag{A6}$$

Letting

$$S_r^{-1} = \sum_{i=1}^{N-r} d^{-1}(i, i+r) \tag{A7}$$

then

$$T_r^{-1} = \frac{1}{\phi_y} S_r^{-1} \tag{A8}$$

It can then be shown that

$$\frac{\partial T_r^{-1}}{\partial \phi_x} = \frac{1}{\phi_y^2} \frac{\partial S_r^{-1}}{\partial \alpha} \tag{A9}$$

and

$$-\frac{\partial T_r^{-1}}{\partial \phi_y} = \frac{S_r^{-1}}{\phi_y^2} + \frac{\phi_x}{\phi_y^3} \frac{\partial S_r^{-1}}{\partial \alpha} \tag{A10}$$

The substitution of Eqs. (A9) and (A10) into Eqs. (107), (108), and (109), leads to the following results.

$$A = \frac{NH}{2\phi_y^2} \tag{A11}$$

$$B = \frac{N(F - H\alpha)}{2\phi_y^2} \tag{A12}$$

$$D = \frac{N}{2\phi_y^2} \left[1 - 2F\alpha + \alpha^2 H\right] \tag{A13}$$

where

$$F = \frac{1}{N} \left[S_o^{-1} + 2 \sum_{r=1}^{N-1} \rho_x(r) S_r^{-1} \right] \tag{A14}$$

and

$$H = -\frac{\partial F}{\partial \alpha} = -\frac{1}{N} \left[\frac{\partial S_o^{-1}}{\partial \alpha} + 2 \sum_{r=1}^{N-1} \rho_x(r) \frac{\partial S_r^{-1}}{\partial \alpha} \right] \tag{A15}$$

then

$$AD - B^2 = \left(\frac{N}{2\phi_y^2}\right)^2 \left[H - F^2\right] \tag{A16}$$

After manipulations are performed on Eqs. (23), (24), and (25), using the expressions indicated in Eqs.(A11), (A12), (A13), and (A16), the following results can be obtained.

$$\frac{N\Delta\phi_x^2}{\phi_x^2} = \frac{2\left(1 - \frac{2F}{\alpha H} + \frac{1}{\alpha^2 H}\right)}{1 - \frac{F^2}{H}} \tag{A17}$$

$$\frac{N\Delta\phi_y^2}{\phi_y^2} = \frac{2}{1 - \frac{F^2}{H}} \tag{A18}$$

$$\rho_{x-y} = -\frac{\left|\frac{F}{H\alpha} - 1\right|}{\left[1 - \frac{2F}{\alpha H} + \frac{1}{\alpha^2 H}\right]^{1/2}} \tag{A19}$$

Eqs. (A17), (A18), and (A19), together with Eqs. (A14) and (A15), allow a great deal to be inferred regarding the nature of the errors. For example, in regions wherein F may be considered independent of N, the variance in the estimated values of the variance of the noise sources is inversely proportional to N and the errors in the estimated values are independent of N. In addition, for this situation, the right-hand quantities in Eqs. (A17), (A18), and (A19) only involve

the parameter α $\left(\alpha = \frac{\phi_x}{\phi_y}\right)$. This considerably simplifies the task associated with obtained numerical values when either analytical or numerical values are used for the covariance matrix elements and the information matrix elements.

For finite values of N and α and α non-zero,

$$2 < \frac{N\Delta\phi_y^2}{\phi_y^2} < \infty \tag{A20}$$

which, in turn, places the restriction that

$$0 < \frac{F^2}{H} < 1 \tag{A21}$$

Since F is a real quantity, Eq. (A21) indicates that H $\left(H = -\frac{\partial F}{\partial \alpha}\right)$ is a positive quantity.

To illustrate the reduction in effort accompanied by the set of equations contained within this appendix, the results of Section II will be duplicated.

From Eqs. (58), (A8), (A14), and (A15),

$$F = (\alpha^2 + 2\alpha)^{-1/2} \tag{A22}$$

$$H = -\frac{\partial F}{\partial \alpha} = \frac{\alpha + 1}{(\alpha^2 + 2\alpha)^{3/2}} \tag{A23}$$

Substituting Eqs. (A22) and (A23) into Eqs. (A17), (A18), and (A19), one can obtain

$$\frac{N\Delta\phi_x^2}{\phi_x^2} = \frac{2\,(3\alpha+8)\left[\alpha+1\sqrt{\alpha^2+2\alpha}\right]}{\alpha\,(\alpha+3)+(\alpha+2)\sqrt{\alpha^2+2\alpha}} \tag{A24}$$

$$\frac{N\Delta\phi_y^2}{\phi_y^2} = 2\,(\alpha+1)\left[\alpha+1+\sqrt{\alpha^2+2\alpha}\right] \tag{A25}$$

$$\rho_{x-y} = -\left[\frac{(\alpha+2)\sqrt{\alpha^2+2\alpha}+\alpha\,(\alpha+3)}{(\alpha+1)\,(3\alpha+8)}\right]^{1/2} \tag{A26}$$

Although the forms are different in appearance, corresponding values from Eqs. (64), (65), and (66) are identical.

The Bissett-Berman Corporation 2941 Nebraska Avenue, Santa Monica, California EXbrook 4-3270

APOLLO NOTE NO. 418
(Task 2, Item I)

C. P. Siska
28 March 1966

EFFECTS OF GRAVITATIONAL HARMONICS ON LUNAR PARKING ORBIT PREDICTION

INTRODUCTION

This note represents a preliminary investigation of the harmonic terms in the Moon's gravitational potential and their effect upon the accuracy with which the lunar parking orbit is predicted. Results were obtained using the Integrated Trajectory Error Analysis Program (ITEAP) discussed in Apollo Notes 319 and 360.

At the present time, very little is known about the absolute values of gravitational constants of the Moon, with the exception of the MU, J2, and C22 terms, and the location of the center of mass and the principal axes directions.

In this analysis it is assumed that the latter two items are known very well, so that in effect there is no uncertainty in the values of the terms J1, C11, S11, C21, S21, and S22.

Information on uncertainties, MU excepted, appears to be negligible, so that the first objective in this investigation is to obtain reasonable uncertainties in harmonic coefficient values. These values will eventually be determined by Lunar Orbiter, which has as a secondary mission, the definition of selenodetic parameters.

To obtain uncertainty estimates, therefore, the CSM lunar parking orbit was tracked in the Moon's orbit plane ($i = 180^{\circ}$) over a one day interval (12 orbits) using 3-way Doppler data. A secondary investigation examined the effects of inclining the parking orbit 45° ($i = 135^{\circ}$) to the Moon orbit plane and tracking 6 orbits.

Finally, the data for both the $i = 180^{\circ}$ and $i = 135^{\circ}$ cases were processed "simultaneously" in order to see if different orbit geometries

permitted an improvement in determining selenodetic parameter values.

After determining the selenodetic uncertainties in the $i = 180^{\circ}$ case, these values were used as a priori estimates in examining the accuracy with which one CSM orbit could be predicted, for various groups of estimators.

It is noted here, that originally it was intended to include drift and drift rate clock parameters for each station in addition to clock bias. However, difficulty was experienced in obtaining a good matrix inverse, so therefore the drift and drift rate parameters were left out of the analysis.

INPUT PARAMETERS

CSM parking orbit insertion takes place at the backside of the Moon (x axis at t = o points toward the Earth) at 80 n. mi. altitude, with retrograde motion in the Moon's orbit plane (x-y plane). Figure 1 shows the inputs for this case - the parameters are discussed in Apollo Note No. 360. The first six orbits are labeled Phase I (t = o to 744 minutes after insertion). Continuation of the trajectory for approximately another six orbits is labeled Phase II and starts with position and velocity components at t = 744 minutes. Trajectory time in this phase, however, is defined from t = o to t = 701 minutes. The inputs for Phase II are shown in Figure 2.

Inputs for the 135° inclination case are identical to the Phase I inputs of the 180° inclination case, except for the change of inclination. Phase II for the $i = 135^{\circ}$ case was not examined.

Input values for higher order harmonic terms are arbitrary estimates. Errors in these values will have a negligible effect on the uncertainties computed in this report.

TRACKING DATA

A one-minute sample rate was used with a 3-way Doppler mode, i. e., a Master-Slave operation. The measurement sigma was 0. 388 cm/sec for a "one-way path measurable".

Table 1. shows the tracking schedule and categorizes the stations by data block and station number so that one can identify a particular station's parameters in the results. Generally, the stations in each data block are treated as new stations even though some may appear in more than one data block. The exception to this arises in the case of Blocks 1 and 2 data, in which three stations are considered to be the same. That is to say, information concerning station parameters (location, etc.) is considered as a priori only at the start of tracking in each data block except as noted.

RESULTS

All Parameters Estimated - 180° Inclination

Figure 3 shows the results of tracking Phase I of the CSM orbit for the selected list of 30 estimators in each data block. The procedure used is outlined in Apollo Note No. 208, and in this instance, the station parameters are updated with tracking data accumulated up to the time associated with each data block (see Table 1.).

Figure 4. illustrates the translation of Phase I results forward in time. Since the trajectory is continued from t = 744 minutes, the translated results for this time (18 x 18 matrix) are used as a priori for Phase II.

Figure 5 shows results for the continuation of the CSM orbit, representing the completion of one day's tracking data. Note that the uncertainty in MU of the Moon has been reduced by approximately 50 percent, while the Earth-Moon distance uncertainty remains unaffected. The program treats these two parameters as independent, i. e., no constraining relation between these two parameters is used, such as appears in Kepler's third law.

Note that even after one day's tracking, the CSM position uncertainty is still approximately 200 meters.

All Parameters Estimated - 135° Inclination

This case used the same tracking schedule as shown in Table 1. The parking orbit was inclined 45° to the Moon's orbit plane so as to ascertain the effects of orbit geometry in determining harmonic terms.

Comparison of the Block 6 results in Figures 3 and 6 indicates a significant improvement for inclined orbits, not only in the uncertainties in gravitational coefficients, but also in position and velocity. This undoubtedly results from the more favorable orbit-station geometry resulting for inclined orbits. That is to say, the station can achieve larger normal displacements to the orbit plane than in the i= 180° case, and, consequently determines the orbit plane and position in the plane more precisely.

All Parameters - Both Orbits

The previous results have treated the i = 180° and i = 135° cases independently. To determine gravitational constants, it is desirable to simultaneously process various orbits with different geometries. As an indication of the type of accuracy which can be attained, the tracking data of the i = 180° case (Phase I and II data) and the i = 135° case were combined.

The procedure used was to take the marginal distribution of the gravitational constants (including MU of the Earth and Earth-Moon distance) pertaining to the Block 12 results of Figure 5, and then to use this matrix (12 x 12) as a priori for continuation with the i = 135° tracking data. As before, the stations in each data block were considered as new stations.

Figure 8 shows the results of this procedure. Note that the uncertainties in MU of the Moon has been improved by approximately an order of magnitude over the presently accepted value of 3.467 + 07 m^3/sec^2. (computed from data in JPL Technical Report No. 32-604).

One Orbit - Six Estimators

One problem of interest is to estimate the uncertainty in CSM position when using only position and velocity components as estimators. It has already been ascertained that the position uncertainty of the CSM after one day's tracking should be like 200 meters using a fairly complete set of estimators.

In this instance, tracking will be limited to that corresponding to one CSM orbit. Various combinations of a priori values for position and velocity, and gravitational constants will be examined with the following definitions:

Parameters	Good A Priori	Poor A Priori
Position; Velocity components	100 m;3m/sec.	500 m; 10 m/sec.
Gravitational Constants	Values of Block 12 results - Figure 5. (one day's tracking)	Arbitrary estimates shown in Figure 3.

Figures 10. through 13. show results not only for the case of 6 estimators (24 not estimated), but also, the cases of 6 estimators only (no nuisance parameters), and 30 estimators. The position-velocity results pertain to initial condition coordinates.

If gravitational constants are known as well as might be expected from one day's tracking of the CSM, it appears from Figures 12. and 13. that orbit prediction using 6 estimators yields accuracies comparable to that which uses all 30 estimators. This applies for tracking duration on the order of one CSM orbit period.

Concluding Remarks

This preliminary investigation indicates that selenodetic parameters can be determined fairly accurately with one day's tracking of the CSM. However, more accuracy can be attained by tracking lunar satellites with orbit geometries which differ mainly in inclination angle.

Since Lunar Orbiter is to be tracked for several months, one can expect selenodetic parameters to be determined with less uncertainty than the values used in this investigation. Consequently, orbit prediction of lunar satellites using position, velocity estimators should yield satisfactory results for tracking durations of short periods, such as required for the rendezvous mission.

PRIMARY BODY PARAMETERS

14	MU OF MOON		4,896 0000E 12
23	J2	2	2,048 0000E-04
23	J3	3	8,6300000E-05
23	J4	4	-2,6280000E-04
23	J5	5	1,0000000E-04
24	C22	22	-2,3000000E-05
24	C31	13	-1,0000000E-06
24	C32	23	-6,9000000E-06
25	S22	22	0
25	S31	13	-2,9600000E-05
25	S32	23	-1,0000000E-06
29	MOON RADIUS		1,7380900E 06
26	MOON SPIN		2,6616990E-06
37	RT ASC PR ME		0
44	EA IND		0

BODY TWO PARAMETERS

19	MU EARTH		3,986 0000E 14
20	E/M DISTANCE		3,9000000E 08
21	LAT TO E/M P		0
22	RT ASC EARTH		0
33	GAMID		1,0000000E 00
34	INC EARTH OR		0
60	ANG VEL EAOR		2,6616990E-06

BODY THREE PARAMETERS

15	MU OF SUN		1,327154 0E 20
16	MOON SUN DIS		1,47366 10E 11
17	LAT TO E/M P		3,0000000E 00
18	RT ASC SUN		1,6717000E 02
31	GAMID SUN		1,0000000E 00
32	INCL SUN ORB		-5,6000000E 00

TRANSFORMATION PARAMETERS

46	MOON LAT INI		-3,558 0000E 00
47	RT ASC MOON		1,84828 00E 02
47	RT ASC MOON		1,84828 00E 02
45	INCL MOON OR		2,8600000E 01
48	RT ASC GR ME		1,6500000E 02
59	GAMID MOON		1,0000000E 00

ERROR ANALYSIS PARAMETERS

27	DELTA T1		1,0000000E 00
49	DELTA TAU		1,0000000E 00
39	PRINT INTV1		3,1000000E 01
41	T UMATRIX	1	6,2000000E 01
41	T UMATRIX	2	1,2400000E 02
41	T UMATRIX	3	6,2000000E 02
41	T UMATRIX	4	7,4400000E 02
43	QIND		0
38	KEP INTV		2,0000000E-01
30	T MAX		7,4500000E 02
13	INPUT IND		0

OMEGA	1,8000000E 02
I	1,8000000E 02
U	0
RZERO	1,8855930E 06
VT	1,6223750E 03
VR	0
OMEGA(SM)	0
ECC	1,3699049E-02

Figure 1.

Inputs for Phase I of Lunar Parking Orbit ($i = 180^{\circ}$)

PRIMARY BODY PARAMETERS			
14	MU OF MOON		4.89600000E 12
23	J2	2	2.04800000E-04
23	J3	3	8.63000000E-05
23	J4	4	-2.62800000E-04
23	J5	5	1.00000000E-04
24	C22	22	-2.30000000E-05
24	C31	13	-1.00000000E-06
24	C32	23	-6.90000000E-06
25	S22	22	0
25	S31	13	-2.96000000E-05
25	S32	23	-1.00000000E-06
29	MOON RADIUS		1.73809000E 06
26	MOON SPIN		2.66169900E-06
37	RTASC PRI ME		6.80770000E 00
44	EA IND		0

BODY TWO PARAMETERS			
19	MU EARTH		3.98600000E 14
20	E/M DISTANCE		3.90000000E 08
21	LAT TO E/M P		0
22	RT ASC EARTH		6.80770000E 00
33	GAMID		1.00000000E 00
34	INC EARTH OR		0
60	ANG VEL EAOR		2.66169900E-06

BODY THREE PARAMETERS			
15	MU OF SUN		1.32715400E 20
16	MOON SUN DIS		1.47366100E 11
17	LAT TO E/M P		3.00000000E 00
18	RT ASC SUN		1.67170000E 02
31	GAMID SUN		1.00000000E 00
32	INCL SUN ORB		-5.60000000E 00

TRANSFORMATION PARAMETERS			
46	MOON LAT INI		-6.84000000E 00
45	INCL MOON OR		2.86000000E 01
47	RT ASC MOON		1.90800000E 02
47	RT ASC MOON		1.90800000E 02
48	RTASC GR MER		2.14600000E 02
59	GAMID MOON		1.00000000E 00

ERROR ANALYSIS PARAMETERS			
27	DELTA T1		1.00000000E 00
49	DEL TAU		1.00000000E 00
39	PRINT INTV 1		3.00000000E 01
41	T UMATRIX	1	5.30000000E 02
41	T UMATRIX	2	6.00000000E 02
41	T UMATRIX	3	6.30000000E 02
41	T UMATRIX	4	7.00000000E 02
43	OIND		0
38	KEP INTV		2.00000000E-01
30	T MAX		7.01000000E 02
13	INPUT IND		1.00000000E 00

X	-1.80313380E 06
Y	-5.60781110E 05
Z	3.18132190E 01
X DOT	-4.74455970E 02
Y DOT	1.54815320E 03
Z DOT	-9.98365750E-02

ORBIT PARAMETERS TRANSFORMED	
OMEGA	1.97719320E 00
I	1.79996350E 02
U	1.64701320E 02
RZERO	1.88832380E 06
VT	1.61921020E 03
VR	-6.70831810E 00
OMEGA(SM)	1.85192270E 02
ECC	1.19676850E-02

Figure 2.

Inputs for Phase II of Lunar Parking Orbit (i = 180°)

TABLE I

LUNAR PARKING ORBIT

TRACKING SCHEDULE

Station	Data Block	Station No.	Tracking Period (min. after insertion)
*Canberra	1	1	23 - 99
Guam	1	2	23 - 98
Hawaii	1	3	23 - 97
*Canberra	2	1	145 - 222
Guam	2	2	145 - 221
Hawaii	2	3	145 - 192
*Canberra	3	1	267 - 344
Guam	3	2	267 - 343
Carnarvon	3	3	267 - 342
*Madrid	4	1	389 - 465
Carnarvon	4	2	389 - 464
Grand Canary	4	3	412 - 463
*Madrid	5	1	511 - 588
Carnarvon	5	2	511 - 568
Grand Canary	5	3	511 - 587
*Madrid	6	1	534 - 710
Bermuda	6	2	634 - 709
Ascension	6	3	634 - 708
*Madrid	8	1	878 - 955
Goldstone	8	2	878 - 954
Ascension	8	3	878 - 953
*Goldstone	9	1	1000 - 1076
Ascension	9	2	1000 - 1075
Grand Canary	9	3	1000 - 1070
*Goldstone	10	1	1122 - 1199
Hawaii	10	2	1122 - 1198
Antigua	10	3	1122 - 1197
*Goldstone	11	1	1245 - 1321
Guam	11	2	1245 - 1320
Canberra	11	3	1245 - 1319
*Goldstone	12	1	1367 - 1442
Guam	12	2	1367 - 1441
Canberra	12	3	1367 - 1440

* Master Station in Each Data Block

Parameter	A Priori	Block 1	Block 1 and 2	Block 3	Block 4
Position	8.6602540E 02	5.6341585E 02	3.1982387E 02	2.9988389E 02	2.7900685E 02
Velocity	1.7320508E 01	7.7213635E 00	7.3737895E-01	5.5347749E-01	3.5640617E-01
x	5.0000000E 02	7.8105041E 01	8.4841044E 00	4.4308056E 00	2.7612030E 00
y	5.0000000E 02	3.1790804E 02	2.3887439E 01	9.7884610E 00	8.1970674E 00
z	5.0000000E 02	4.5855371E 02	3.1881769E 02	2.9969134E 02	2.7887274E 02
x dot	1.0000000E 01	3.3282536E-01	1.5683699E-02	6.6721771E-03	5.8054884E-03
y dot	1.0000000E 01	2.3782441E-01	4.5537135E-03	3.9699203E-03	3.1079216E-03
z dot	1.0000000E 01	7.7105202E 00	7.3719808E-01	5.5342303E-01	3.5634533E-01
MU Moon	3.4641016E 07	3.4635626E 07	3.4609843E 07	3.4600509E 07	3.4591432E 07
J2	2.0000000E-04	1.5869388E-04	4.4043183E-05	2.4104793E-05	2.0700162E-05
J3	1.0000000E-04	9.8507175E-05	9.4311227E-05	9.3807170E-05	9.2981950E-05
J4	1.0000000E-04	9.5417386E-05	4.5742787E-05	2.1197662E-05	1.8594601E-05
J5	1.0000000E-04	9.8379797E-05	9.3719243E-05	9.3019887E-05	9.1264246E-05
C22	1.0000000E-04	9.4688576E-06	4.6927704E-07	2.5082025E-07	1.7565190E-07
C31	1.0000000E-04	6.1716281E-05	5.7556605E-07	2.7839426E-07	2.5781335E-07
C32	1.0000000E-04	4.2245873E-05	1.5252258E-05	1.1725023E-05	4.3757817E-06
S31	1.0000000E-04	8.1025064E-05	1.5824954E-07	8.4407779E-08	4.9462949E-08
S32	1.0000000E-04	5.1975277E-05	2.2139568E-05	1.5429542E-05	4.6354188E-06
MU Earth	3.0000000E 08	3.0000000E 08	3.0000000E 08	3.0000000E 08	3.0000000E 08
E-M Distance	1.0000000E 03	1.0000000E 03	1.0000000E 03	1.0000000E 03	1.0000000E 03
Station East	5.0000000E 01	4.5766881E 01	3.5159078E 01	3.3842022E 01	4.8963873E 01
1 North	5.0000000E 01	4.9563465E 01	4.5239051E 01	4.7387850E 01	4.1014245E 01
Location Up	5.0000000E 01	4.9249677E 01	4.2085137E 01	4.3933211E 01	3.5717625E 01
Station East	5.0000000E 01	4.4860152E 01	3.5863830E 01	3.5203562E 01	3.2781061E 01
2 North	5.0000000E 01	4.9914882E 01	4.9516569E 01	4.9616244E 01	4.9160968E 01
Location Up	5.0000000E 01	4.8028916E 01	4.0684522E 01	4.4616736E 01	4.5155156E 01
Station East	5.0000000E 01	3.8554279E 01	3.5154537E 01	2.4258779E 01	4.9500733E 01
3 North	5.0000000E 01	4.9671702E 01	4.8218178E 01	4.9739075E 01	4.8189751E 01
Location Up	5.0000000E 01	4.8412486E 01	3.9153538E 01	4.8785667E 01	4.2398851E 01
Clock Sta. 1	4.4721360E-02	3.2019779E-02	5.4885754E-03	4.1927772E-03	7.6324201E-03
Time Sta. 2	4.4721360E-02	3.0455250E-02	6.1835861E-03	4.5190476E-03	5.0926061E-03
Bias Sta. 3	4.4721360E-02	2.5949024E-02	5.9455454E-03	4.2656546E-03	7.5552486E-03

Figure 3.

Sq. Rt. of Diagonal Elements of Covariance Matrix - Phase I Orbit -

Inclination = 180° - T = 0 coordinates

Block 5	Block 6
2.7612332E 02	2.7103351E 02
3.3716509E-01	3.2117599E-01
1.8542764E 00	1.3263086E 00
7.1599394E 00	6.2052002E 00
2.7602425E 02	2.7095922E 02
5.2110167E-03	4.6219325E-03
2.6144692E-03	2.1960549E-03
3.3711468E-01	3.2113522E-01
3.4538700E 07	3.4410997E 07
1.7997886E-05	1.5373578E-05
9.2889382E-05	9.2769124E-05
1.6534172E-05	1.4466353E-05
9.0015019E-05	8.7575648E-05
1.4279596E-07	1.2620854E-07
2.3940334E-07	2.2037176E-07
3.9932060E-06	3.8346201E-06
4.0510273E-08	3.4680981E-08
3.9275092E-06	3.6687238E-06
3.0000000E 08	3.0000000E 08
1.0000000E 03	1.0000000E 03
4.1538070E 01	2.6110175E 01
4.3117138E 01	4.7537414E 01
3.9293144E 01	4.6175851E 01
4.4709283E 01	4.9245593E 01
4.7854455E 01	4.4028104E 01
3.7511286E 01	3.1475658E 01
4.6915160E 01	3.5566151E 01
4.6193687E 01	4.9766205E 01
3.2501153E 01	4.0578590E 01
7.6373871E-03	7.5483498E-03
5.0525975E-03	7.7927202E-03
7.5232923E-03	6.6491937E-03

Figure 3.

(continued)

Minutes After Insertion

Parameter	T = 0	T = 62	T = 124	T = 744
Position	2.7103353E 02	2.4345495E 02	2.7123472E 02	2.4561962E 02
Velocity	3.2117594E-01	2.9197303E-01	3.1897578E-01	3.3190997E-01
x	1.3263081E 00	2.0808586E 00	1.0951899E 00	4.2878939E 00
y	6.2052095E 00	3.9694660E 00	4.9134966E 00	1.1525921E 01
z	2.7095924E 02	2.4341369E 02	2.7118800E 02	2.4531157E 02
x dot	4.6219389E-03	3.2217631E-03	3.8508990E-03	9.3190345E-03
y dot	2.1960602E-03	9.1810302E-04	1.9302922E-03	2.9387958E-03
z dot	3.2113518E-01	2.9195381E-01	3.1894669E-01	3.3176610E-01
MU Moon	3.4410807E 07	3.4410807E 07	3.4410807E 07	3.4410807E 07
J2	1.5373604E-05	1.5373604E-05	1.5373604E-05	1.5373604E-05
J3	9.2769123E-05	9.2769123E-05	9.2769123E-05	9.2769123E-05
J4	1.4466436E-05	1.4466436E-05	1.4466436E-05	1.4466436E-05
J5	8.7575675E-05	8.7575675E-05	8.7575675E-05	8.7575675E-05
C22	1.2620861E-07	1.2620861E-07	1.2620861E-07	1.2620861E-07
C31	2.2037289E-07	2.2037289E-07	2.2037289E-07	2.2037289E-07
C32	3.8346226E-06	3.8346226E-06	3.8346226E-06	3.8346226E-06
S31	3.4680989E-08	3.4680989E-08	3.4680989E-08	3.4680989E-08
S32	3.6687237E-06	3.6687237E-06	3.6687237E-06	3.6687237E-06
MU Earth	3.0000000E 08	3.0000000E 08	3.0000000E 08	3.0000000E 08
E-M Distance	1.0000000E 03	1.0000000E 03	1.0000000E 03	1.0000000E 03

Figure 4.

Block 6 Results ($i = 180^{o}$) Translated Forward In Time

Parameter	A Priori	Block 7	Block 8	Block 9
Position	2.4561962E 02	2.2608397E 02	2.2155588E 02	2.1502938E 02
Velocity	3.3190997E-01	3.0310480E-01	2.5474363E-01	2.5192955E-01
x	4.2878939E 00	2.5058778E 00	1.4549482E 00	1.0691019E 00
y	1.1525921E 01	9.2274613E 00	4.3961061E 00	2.8834578E 00
z	2.4531157E 02	2.2588169E 02	2.2150748E 02	2.1500739E 02
x dot	9.3190345E-03	7.3379323E-03	3.5448902E-03	2.4365039E-03
y dot	2.9387958E-03	2.1875333E-03	1.1436094E-03	8.5210363E-04
z dot	3.3176610E-01	3.0300807E-01	2.5471639E-01	2.5191633E-01
MU Moon	3.4410807E 07	3.1564311E 07	3.0494690E 07	2.9235780E 07
J2	1.5373604E-05	5.9451198E-06	5.3963519E-06	4.9969504E-06
J3	9.2769123E-05	9.2409116E-05	9.2028527E-05	9.1684988E-05
J4	1.4466436E-05	5.3147276E-06	4.6444143E-06	4.1230291E-06
J5	8.7575675E-05	7.9564520E-05	7.7579329E-05	7.6110697E-05
C22	1.2620861E-07	9.6673760E-08	8.5870409E-08	7.7767357E-08
C31	2.2037289E-07	1.2455446E-07	1.1630865E-07	1.0738609E-07
C32	3.8346226E-06	3.1397807E-06	3.0837321E-06	3.0210259E-06
S31	3.4680989E-08	3.0293244E-08	2.6581063E-08	2.5995527E-08
S32	3.6687237E-06	3.4094749E-06	3.1386313E-06	2.8748556E-06
MU Earth	3.0000000E 08	3.0000000E 08	3.0000000E 08	3.0000000E 08
E-M Distance	1.0000000E 03	9.9999999E 02	9.9999999E 02	9.9999999E 02
Station East	5.0000000E 01	1.4322374E 01	2.4668335E 01	4.1608784E 01
1 North	5.0000000E 01	4.9604189E 01	4.7234342E 01	4.3732908E 01
Location Up	5.0000000E 01	4.9531501E 01	4.6724773E 01	3.8008785E 01
Station East	5.0000000E 01	4.5639804E 01	4.9661387E 01	3.6910196E 01
2 North	5.0000000E 01	4.4121785E 01	4.1424184E 01	4.9712292E 01
Location Up	5.0000000E 01	3.5279934E 01	3.2693120E 01	3.8033712E 01
Station East	5.0000000E 01	2.2257229E 01	2.1505438E 01	3.6394261E 01
3 North	5.0000000E 01	4.9988283E 01	4.9934067E 01	4.7984261E 01
Location Up	5.0000000E 01	4.8198767E 01	4.8408073E 01	4.1123452E 01
Clock Sta. 1	4.4721360E-02	6.7578774E-03	5.3354051E-03	5.5694918E-03
Time Sta. 2	4.4721360E-02	6.3418891E-03	5.0255974E-03	5.5576070E-03
Bias Sta. 3	4.4721360E-02	5.9798044E-03	4.9457356E-03	5.7152894E-03

Figure 5.

Sq. Rt. of Diagonal Elements of Covariance Matrix Phase II
Orbit - Inclination = 180° - T = 744 Coordinates

Block 10	Block 11	Block 12
2.0410354E 02	1.9793295E 02	1.9714938E 02
2.4930009E-01	2.4779004E-01	2.4758998E-01
8.9839095E-01	8.4757358E-01	8.4534732E-01
2.5236903E 00	2.4465500E 00	2.4193210E 00
2.0408596E 02	1.9791602E 02	1.9713272E 02
2.1468927E-03	2.0843547E-03	2.0714235E-03
7.2949648E-04	6.8941303E-04	6.8170792E-04
2.4928977E-01	2.4778031E-01	2.4758038E-01
2.7527786E 07	2.7117831E 07	2.7111430E 07
4.6875135E-06	4.5765471E-06	4.5382256E-06
9.1275503E-05	9.1135233E-05	9.1125352E-05
3.7509467E-06	3.6278304E-06	3.5630380E-06
7.2702567E-05	7.0719856E-05	7.0361917E-05
7.1704866E-08	6.9727976E-08	6.9700833E-08
1.0004078E-07	9.8759187E-08	9.8456891E-08
2.9852626E-06	2.8614202E-06	2.8566722E-06
2.4939091E-08	2.4674510E-08	2.4581338E-08
2.7705788E-06	2.6598911E-06	2.6486651E-06
3.0000000E 08	3.0000000E 08	3.0000000E 08
9.9999999E 02	9.9999999E 02	9.9999999E 02
2.3818595E 01	3.3817047E 01	4.9892648E 01
4.7873867E 01	4.9977612E 01	4.9990952E 01
4.4986839E 01	4.9929383E 01	4.9983819E 01
4.7086593E 01	4.9955741E 01	4.9996933E 01
4.6818445E 01	4.9530944E 01	4.9998899E 01
2.9015313E 01	4.2584487E 01	4.9980059E 01
2.7459712E 01	4.9987812E 01	4.9996107E 01
4.9689498E 01	4.7747014E 01	4.9993133E 01
4.5445833E 01	4.4999258E 01	4.9986740E 01
6.4523858E-03	7.7362954E-03	8.7999486E-03
6.3923434E-03	7.5669308E-03	8.5123719E-03
6.4747720E-03	7.6328324E-03	8.5562299E-03

Figure 5.

(continued)

Parameter	A Priori	Block 1 and 2	Block 3	Block 4	Block 5
Position	8.6602540E 02	3.3540508E 02	2.0157096E 02	1.5016007E 02	1.2809875E 02
Velocity	1.7320508E 01	2.7450212E-01	1.8957307E-01	1.6706656E-01	1.5445631E-01
x	5.0000000E 02	6.8225318E 00	4.7904486E 00	4.1242678E 00	3.7253122E 00
y	5.0000000E 02	2.4136834E 02	1.4560496E 02	1.0872697E 02	9.3055805E 01
z	5.0000000E 02	2.3279035E 02	1.3930936E 02	1.0348663E 02	8.7954700E 01
x dot	1.0000000E 01	1.9274241E-02	7.1363589E-03	5.6105075E-03	4.9829545E-03
y dot	1.0000000E 01	1.9318137E-01	1.3395048E-01	1.1814551E-01	1.0933650E-01
z dot	1.0000000E 01	1.9406409E-01	1.3395630E-01	1.1798896E-01	1.0898373E-01
MU Moon	3.4641016E 07	3.0582669E 07	2.5163219E 07	2.0559141E 07	1.9432344E 07
J2	2.0000000E-04	2.1952670E-05	1.1757983E-05	7.8086036E-06	5.9961743E-06
J3	1.0000000E-04	4.5183442E-05	8.8094378E-06	3.2658867E-06	1.9852147E-06
J4	1.0000000E-04	8.6500808E-06	4.6365896E-06	3.4265165E-06	2.5816608E-06
J5	1.0000000E-04	7.2450542E-06	3.9618749E-06	3.2724822E-06	2.8796422E-06
C22	1.0000000E-04	3.5858070E-06	1.8267101E-06	1.3392455E-06	1.0774943E-06
C31	1.0000000E-04	1.5690911E-06	7.1981476E-07	5.1431676E-07	3.5522615E-07
C32	1.0000000E-04	7.6718076E-06	1.4694055E-06	5.4937222E-07	3.1738667E-07
S31	1.0000000E-04	3.0069516E-05	5.9281384E-06	2.2602223E-06	1.4536290E-06
S32	1.0000000E-04	2.5207997E-07	1.0550039E-07	7.3380649E-08	5.0963643E-08
MU Earth	3.0000000E 08	3.0000000E 08	3.0000000E 08	3.0000000E 08	3.0000000E 08
E-M Distance	1.0000000E 03	1.0000000E 03	1.0000000E 03	1.0000000E 03	1.0000000E 03
Station East	5.0000000E 01	2.7725062E 01	3.4579670E 01	4.8803993E 01	4.2189250E 01
1 North	5.0000000E 01	4.3936153E 01	4.7417513E 01	4.1071210E 01	4.3448437E 01
Location Up	5.0000000E 01	4.4333707E 01	4.4032820E 01	3.5831562E 01	3.9679398E 01
Station East	5.0000000E 01	2.9236441E 01	3.3482893E 01	3.4426017E 01	4.4663921E 01
2 North	5.0000000E 01	4.9462857E 01	4.9609219E 01	4.9175811E 01	4.7796710E 01
Location Up	5.0000000E 01	3.9277276E 01	4.4682087E 01	4.5283701E 01	3.6866518E 01
Station East	5.0000000E 01	3.8726281E 01	2.6345508E 01	4.9392959E 01	4.7186900E 01
3 North	5.0000000E 01	4.8129259E 01	4.9778880E 01	4.8199942E 01	4.6364234E 01
Location Up	5.0000000E 01	3.8803701E 01	4.9060437E 01	4.2495398E 01	3.3133109E 01
Clock Sta. 1	4.4721360E-02	9.5364565E-03	4.4517896E-03	3.9551852E-03	4.3299858E-03
Time Sta. 2	4.4721360E-02	9.4363750E-03	4.3798986E-03	3.9846662E-03	4.3504037E-03
Bias Sta. 3	4.4721360E-02	9.4931624E-03	4.4086505E-03	4.1004122E-03	4.3240755E-03

Figure 6.

Sq. Rt. of Diagonal Elements of Covariance Matrix - Phase I Orbit - Inclination = 135° - T = 0 Coordinates

Block 6

```
9.6518073E 01
1.5001048E-01
3.2116055E 00
7.0470070E 01
6.5874072E 01
4.5775653E-03
1.0621193E-01
1.0583580E-01
1.6492943E 07
3.3220398E-06
1.3682835E-06
2.1816231E-06
2.5928865E-06
6.6403922E-07
2.7731138E-07
2.0046527E-07
1.0717700E-06
3.9185405E-08
3.0000000E 08
1.0000000E 03
2.7789386E 01
4.7680475E 01
4.6171445E 01
4.9388910E 01
4.4229503E 01
3.1940699E 01
3.5799486E 01
4.9767567E 01
4.1464485E 01
4.8159561E-03
4.8205347E-03
4.8606356E-03
```

Figure 6.
(continued)

Parameter	T = 0	T = 62	T = 124	T = 744
Position	9.6509915E 01	8.9317182E 01	6.9629994E 01	1.5196014E 02
Velocity	1.4990944E-01	1.4614777E-01	1.5078316E-01	1.4096122E-01
x	3.2111101E 00	1.3416294E 00	2.9358049E 00	1.3057475E 01
y	7.0463600E 01	6.1995714E 01	5.0044888E 01	1.0776894E 02
z	6.5869064E 01	6.4282894E 01	4.8324179E 01	1.0633552E 02
x dot	4.5770415E-03	2.9046873E-03	3.3342725E-03	1.3288713E-02
y dot	1.0614032E-01	1.0375998E-01	1.0682735E-01	9.7325739E-02
z dot	1.0576447E-01	1.0288148E-01	1.0635959E-01	1.0109983E-01
MU Moon	1.6491892E 07	1.6491892E 07	1.6491892E 07	1.6491892E 07
J2	3.3220246E-06	3.3220246E-06	3.3220246E-06	3.3220246E-06
J3	1.3682184E-06	1.3682184E-06	1.3682184E-06	1.3682184E-06
J4	2.1815976E-06	2.1815976E-06	2.1815976E-06	2.1815976E-06
J5	2.5928855E-06	2.5928855E-06	2.5928855E-06	2.5928855E-06
C22	6.6403849E-07	6.6403849E-07	6.6403849E-07	6.6403849E-07
C31	2.7730182E-07	2.7730182E-07	2.7730182E-07	2.7730182E-07
C32	2.0045735E-07	2.0045735E-07	2.0045735E-07	2.0045735E-07
S31	1.0717481E-06	1.0717481E-06	1.0717481E-06	1.0717481E-06
S32	3.9185380E-08	3.9185380E-08	3.9185380E-08	3.9185380E-08
MU Earth	3.0000000E 08	3.0000000E 08	3.0000000E 08	3.0000000E 08
E-M Distance	1.0000000E 03	1.0000000E 03	1.0000000E 03	1.0000000E 03

Figure 7.

Block 6 Results (i = 135°) Translated Forward in Time

Parameter	A Priori	Blocks 1 and 2	Block 3	Block 4
Position	8.6602540E 02	1.3276895E 02	9.5185021E 01	5.2108009E 01
Velocity	1.7320508E 01	2.6089945E-01	1.3247559E-01	1.1894222E-01
x	5.0000000E 02	4.4857451E 00	2.6412229E 00	1.7230674E 00
y	5.0000000E 02	9.9140713E 01	7.1008344E 01	3.9399255E 01
z	5.0000000E 02	8.8196317E 01	6.3332670E 01	3.4058395E 01
x dot	1.0000000E 01	7.8984043E-03	5.8732832E-03	4.2428038E-03
y dot	1.0000000E 01	1.8370369E-01	9.3437043E-02	8.4330354E-02
z dot	1.0000000E 01	1.8509211E-01	9.3727288E-02	8.3771366E-02
MU Moon	2.7111430E 07	1.7404287E 07	1.0637350E 07	7.9174534E 06
J2	4.5382256E-06	3.9205091E-06	2.5489265E-06	2.1351413E-06
J3	9.1125352E-05	1.4267925E-06	8.1430548E-07	5.7307970E-07
J4	3.5630380E-06	2.5121218E-06	1.7848476E-06	1.4246306E-06
J5	7.0361917E-05	5.3835964E-06	3.5401753E-06	2.7338252E-06
C22	6.9700833E-08	6.2863949E-08	5.6960297E-08	5.5807967E-08
C31	9.8456891E-08	5.3711895E-08	3.5051194E-08	2.5083615E-08
C32	2.8566722E-06	5.0593389E-07	3.4387204E-07	2.6879840E-07
S31	2.4581338E-08	1.6880196E-08	1.5512772E-08	1.5020131E-08
S32	2.6486651E-06	5.6066133E-08	3.2068738E-08	2.4379765E-08
MU Earth	3.0000000E 08	3.0000000E 08	3.0000000E 08	3.0000000E 08
E-M Distance	9.9999999E 02	9.9999999E 02	9.9999998E 02	9.9999998E 02
Station East	5.0000000E 01	2.3306030E 01	3.3577306E 01	4.8534433E 01
1 North	5.0000000E 01	4.2568700E 01	4.7246200E 01	4.0500246E 01
Location Up	5.0000000E 01	3.9197558E 01	4.3643232E 01	3.4762455E 01
Station East	5.0000000E 01	2.3930162E 01	3.3056139E 01	3.3099710E 01
2 North	5.0000000E 01	4.9425840E 01	4.9577263E 01	4.9098805E 01
Location Up	5.0000000E 01	3.8144354E 01	4.4105390E 01	4.4896528E 01
Station East	5.0000000E 01	2.9935959E 01	2.5004682E 01	4.9380491E 01
3 North	5.0000000E 01	4.7883189E 01	4.9761109E 01	4.8070700E 01
Location Up	5.0000000E 01	3.7132588E 01	4.8991782E 01	4.1914236E 01
Clock Sta 1	4.4721360E-02	5.3295109E-03	3.9038659E-03	3.4414335E-03
Time Sta 2	4.4721360E-02	5.3218077E-03	3.5588987E-03	3.6027622E-03
Bias Sta 3	4.4721360E-02	5.4809648E-03	3.8569111E-03	3.5981495E-03

Figure 8.

Covariance Matrix Elements of 135° Inclination Orbit With A Priori Containing Phase I and II Results of 180° Orbit

Block 5	Block 6
4.4578179E 01	3.9830106E 01
1.1657166E-01	1.1319704E-01
1.4111731E 00	1.2253793E 00
3.3485682E 01	2.9763093E 01
2.9392716E 01	2.6440388E 01
3.7648621E-03	3.5510738E-03
8.2660231E-02	8.0246382E-02
8.2110077E-02	7.9758879E-02
6.3682654E 06	5.1674466E 06
1.7901329E-06	1.4891441E-06
4.4835030E-07	3.5479912E-07
1.1945113E-06	1.0431950E-06
2.0527342E-06	1.5175767E-06
5.4913756E-08	5.4265144E-08
2.0397689E-08	1.7811393E-08
1.9931880E-07	1.4669840E-07
1.4827347E-08	1.4736909E-08
2.2481232E-08	1.9817224E-08
3.0000000E 08	3.0000000E 08
9.9999998E 02	9.9999998E 02
4.1208764E 01	2.5141679E 01
4.3044221E 01	4.7599605E 01
3.9014833E 01	4.6035379E 01
4.4328304E 01	4.9375837E 01
4.7688692E 01	4.3935910E 01
3.6101268E 01	3.0823690E 01
4.6881910E 01	3.5090798E 01
4.6194212E 01	4.9753182E 01
3.2181596E 01	4.0939841E 01
3.9645083E-03	4.4924177E-03
4.1212879E-03	4.5483007E-03
4.0130672E-03	4.6894096E-03

Figure 8.
(continued)

Minutes After Insertion

Parameter	T = 0	T = 62	T = 124	T = 744
Position	3.98285$_0$6E 01	4.0999292E 01	4.1137124E 01	9.5548233E 01
Velocity	1.13149$_0$4E-01	1.0969000E-01	1.1322165E-01	1.0154376E-01
x	1.22537$_1$6E 00	6.1100098E-01	1.3730969E 00	8.5092124E 00
y	2.97619$_2$9E 01	2.9118181E 01	3.0475846E 01	6.9180061E 01
z	2.64392$_8$7E 01	2.8856545E 01	2.7597108E 01	6.5354244E 01
x dot	3.55$_1$05$_1$3E-03	2.6925583E-03	3.2803004E-03	7.9116364E-03
y dot	8.02123$_1$6E-02	7.7597397E-02	8.0200729E-02	6.9408983E-02
z dot	7.97250$_2$0E-02	7.7480897E-02	7.9851260E-02	7.3694876E-02
MU Moon	5.1674423E 06	5.1674423E 06	5.1674423E 06	5.1674423E 06
J2	1.48911$_1$7E-06	1.4891117E-06	1.4891117E-06	1.4891117E-06
J3	3.54798$_8$1E-07	3.5479881E-07	3.5479881E-07	3.5479881E-07
J4	1.04314$_9$8E-06	1.0431498E-06	1.0431498E-06	1.0431498E-06
J5	1.51757$_6$2E-06	1.5175762E-06	1.5175762E-06	1.5175762E-06
C22	5.42641$_1$3E-08	5.4264113E-08	5.4264113E-08	5.4264113E-08
C31	1.78$_1$0988E-08	1.7810988E-08	1.7810988E-08	1.7810988E-08
C32	1.46698$_0$7E-07	1.4669807E-07	1.4669807E-07	1.4669807E-07
S31	1.47369$_0$9E-08	1.4736909E-08	1.4736909E-08	1.4736909E-08
S32	1.98165$_9$2E-08	1.9816592E-08	1.9816592E-08	1.9816592E-08
MU Earth	3.0000000E 08	3.0000000E 08	3.0000000E 08	3.0000000E 08
E-M Distance	9.9999998E 02	9.9999998E 02	9.9999998E 02	9.9999998E 02

Figure 9.

Block 6 Results of Figure 8 Translated Forward in Time

Parameter	A Priori			
Position	8.660 + 02	2.1596687E 02	5.6341585E 02	8.4047301E 03
Velocity	1.732 + 01	2.4646429E-01	7.7213635E 00	1.5271972E 01
x	5.000 + 02	2.3275291E 01	7.8105041E 01	3.8320061E 03
y	5.000 + 02	4.0759562E 01	3.1790804E 02	7.0999826E 03
z	5.000 + 02	2.1080467E 02	4.5855371E 02	2.3548810E 03
x dot	5.000 + 02	3.9606385E-02	3.3282536E-01	6.6095571E 00
y dot	1.000 + 01	1.4818131E-02	2.3782441E-01	2.9102332E 00
z dot	1.000 + 01	2.4280940E-01	7.7105202E 00	1.3456501E 01
MU Moon	3.467 + 07		3.4635626E 07	
J2	2.000 + 04		1.5869388E-04	
J3	1.000 - 04		9.8507175E-05	
J4	1.000 - 04		9.5417386E-05	
J5	1.000 - 04		9.8379797E-05	
C22	1.000 - 04		9.4688576E-06	
C31	1.000 - 04		6.1716281E-05	
C32	1.000 - 04	No Uncertainty	4.2245873E-05	These Parameters Not Estimated
S31	1.000 - 04		8.1025064E-05	
S32	1.000 - 04		5.1975277E-05	
MU Earth	3.000 + 08		3.0000000E 08	
E-M Distance	1.000 + 03		1.0000000E 03	
Station 1 East	5.000 + 01		4.5766881E 01	
North	5.000 + 01		4.9563465E 01	
Location Up	5.000 + 01		4.9249677E 01	
Station 2 East	5.000 + 01		4.4860152E 01	
North	5.000 + 01		4.9914882E 01	
Location Up	5.000 + 01		4.8028916E 01	
Station 3 East	5.000 + 01		3.8554279E 01	
North	5.000 + 01		4.9671702E 01	
Location Up	5.000 + 01		4.8412486E 01	
Clock Sta. 1	4.472 - 02		3.2019779E-02	
Time Sta. 2	4.472 - 02		3.0455250E-02	
Bias Sta. 3	4.472 - 02		2.5949024E-02	

Figure 10.

Block 1 Data With Poor A Priori Values - One Orbit

Parameter	A Priori			
Position	1.7320000E 02	1.0125715E 02	1.5063187E 02	6.6905177E 03
Velocity	5.1960000E 00	2.2711493E-01	2.9358924E 00	1.4784560E 01
x	1.0000000E 02	2.1123638E 01	5.8248789E 01	3.1439637E 03
y	1.0000000E 02	3.7018124E 01	9.6827658E 01	5.8853997E 03
z	1.0000000E 02	9.1850214E 01	9.9606437E 01	4.9049889E 02
x dot	3.0000000E 00	3.5963038E-02	3.2708968E-01	5.4353182E 00
y dot	3.0000000E 00	1.3446767E-02	2.0854130E-01	2.4761471E 00
z dot	3.0000000E 00	2.2384601E-01	2.9101524E 00	1.3524394E 01
MU Moon	3.4670000E 07		3.4634545E 07	
J2	2.0000000E-04		1.4952669E-04	
J3	1.0000000E-04		9.8149109E-05	
J4	1.0000000E-04		9.4481610E-05	
J5	1.0000000E-04		9.7989608E-05	
C22	1.0000000E-04		5.4013371E-06	
C31	1.0000000E-04		6.0825291E-05	
C32	1.0000000E-04	No uncertainty	4.1942608E-05	These Parameters Not Estimated
S31	1.0000000E-04		4.9658317E-05	
S32	1.0000000E-04		4.5059623E-05	
MU Earth	3.0000000E 08		3.0000000E 08	
E-M Distance	1.0000000E 03		1.0000000E 03	
Station 1 East	5.0000000E 01		4.5199187E 01	
1 North	5.0000000E 01		4.9507825E 01	
Location Up	5.0000000E 01		4.9153717E 01	
Station 2 East	5.0000000E 01		4.4259084E 01	
2 North	5.0000000E 01		4.9905101E 01	
Location Up	5.0000000E 01		4.7802484E 01	
Station 3 East	5.0000000E 01		3.8204186E 01	
3 North	5.0000000E 01		4.9663231E 01	
Location Up	5.0000000E 01		4.8371134E 01	
Clock Sta. 1	4.4720000E - 02		2.6887690E-02	
Time Sta. 2	4.4720000E - 02		2.6524778E-02	
Bias Sta. 3	4.4720000E - 02		2.5766324E-02	

Figure 11.

Block 1 Data With Good A Priori Values For Position

And Velocity and Poor A Priori Values For Gravitational Constants - one orbit

Parameter	A Priori			
Position	1.7320000E 02	1.0125715E 02	1.1145221E 02	1.3977630E 02
Velocity	5.1960000E 00	2.2711493E-01	1.9483016E 00	2.7054161E 00
x	1.0000000E 02	2.1123638E 01	2.7497370E 01	3.5417953E 01
y	1.0000000E 02	3.7018124E 01	4.4742863E 01	5.5612859E 01
z	1.0000000E 02	9.1850214E 01	9.8303434E 01	1.2324850E 02
x dot	3.0000000E 00	3.5963038E-02	4.6831595E-02	6.0024134E-02
y dot	3.0000000E 00	1.3446767E-02	2.1151532E-02	2.8327111E-02
z dot	3.0000000E 00	2.2384601E-01	1.9476239E 00	2.7046019E 00
MU Moon	2.7110883E 07		2.5020132E 07	
J2	4.5387223E-06		4.1881730E-06	
J3	9.1104336E-05		8.4832969E-05	
J4	3.5637059E-06		3.3990043E-06	
J5	7.0356236E-05		6.7201257E-05	
C22	6.9641941E-08		6.9535018E-08	
C31	9.8437798E-08		9.8425800E-08	
C32	2.8565714E-06	No uncertainty	2.8422988E-06	These parameters not estimated
S31	2.4576411E-08		2.4576407E-08	
S32	2.6495283E-06		2.6394447E-06	
MU Earth	3.0000000E 08		3.0000000E 08	
E-M Distance	1.0000000E 03		1.0000000E 03	
Station East	5.0000000E 01		3.9848898E 01	
1 North	5.0000000E 01		4.8990417E 01	
Location Up	5.0000000E 01		4.8259304E 01	
Station East	5.0000000E 01		4.0892377E 01	
2 North	5.0000000E 01		4.9854091E 01	
Location Up	5.0000000E 01		4.6577427E 01	
Station East	5.0000000E 01		3.7065486E 01	
3 North	5.0000000E 01		4.9633126E 01	
Location Up	5.0000000E 01		4.8232202E 01	
Clock Sta. 1	8.9440000E -03		7.2164061E-03	
Time Sta. 2	8.9440000E -03		6.7260876E-03	
Bias Sta. 3	8.9440000E -03		5.2662906E-03	

Figure 12.

Block 1 Data with Good A Priori Values - one orbit

Parameter	A Priori			
Position	8.6602540E 02	2.1596687E 02	3.7266140E 02	4.8489734E 02
Velocity	1.7320508E 01	2.4646429E-01	2.5140585E 00	2.6655757E 00
x	5.0000000E 02	2.3275291E 01	3.2084795E 01	4.0296476E 01
y	5.0000000E 02	4.0759562E 01	5.2413096E 01	6.4515865E 01
z	5.0000000E 02	2.1060467E 02	3.6755946E 02	4.7889386E 02
x dot	1.0000000E 01	3.9606385E-02	5.4861785E-02	6.8706484E-02
y dot	1.0000000E 01	1.4818131E-02	2.4503721E-02	3.1449542E-02
z dot	1.0000000E 01	2.4280940E-01	2.5133404E 00	2.6645045E 00
MU Moon	2.7110883E 07		2.5234061E 07	
J2	4.5387223E-06		4.2247861E-06	
J3	9.1104336E-05		8.7726041E-05	
J4	3.5637059E-06		3.4166831E-06	
J5	7.0356236E-05		6.8644770E-05	
C22	6.9641941E-08		6.9578244E-08	
C31	9.8437798E-08		9.8426220E-08	
C32	2.8565714E-06	No uncertainty	2.8453164E-06	These parameters not estimated
S31	2.4576411E-08		2.4576409E-08	
S32	2.6495283E-06		2.6435716E-06	
MU Earth	3.0000000E 08		3.0000000E 08	
E-M Distance	1.0000000E 03		1.0000000E 03	
Station 1 East	5.0000000E 01		4.2542196E 01	
North	5.0000000E 01		4.9250101E 01	
Location Up	5.0000000E 01		4.8713857E 01	
Station 2 East	5.0000000E 01		4.2763109E 01	
North	5.0000000E 01		4.9883777E 01	
Location Up	5.0000000E 01		4.7278974E 01	
Station 3 East	5.0000000E 01		3.7371974E 01	
North	5.0000000E 01		4.9640291E 01	
Location Up	5.0000000E 01		4.8267320E 01	
Clock Sta. 1	8.9442719E-03		8.2541568E-03	
Time Sta. 2	8.9442719E-03		7.5752689E-03	
Bias Sta. 3	8.9442719E-03		5.3121315E-03	

Figure 13.

Block 1 Data With Poor A Priori Values for Position-Velocity and Good A Priori Values For Gravitational Constants-one orbit

The Bissett-Berman Corporation 2941 Nebraska Avenue, Santa Monica, California EXbrook 4-3270

H. Epstein
27 April 1966

APOLLO NOTE NO. 419
(Task I, Item I)

TECHNIQUES FOR ESTIMATION OF PARAMETERS ASSOCIATED WITH STATISTICAL TYPE ERROR SOURCES

PART II - Maximum Likelihood Estimators

INTRODUCTION

The purpose of this note is to indicate how suitable processing networks can be found to determine the variance of each noise source when two noise sources are present. It is expected that standard processing techniques such as the simple correlation technique indicated in Part I, (Apollo Note 416) will be used to form initial estimates of the desired variances. The variability of the variance of this class of estimators is then to be compared with results obtained from Appendix A of Apollo Note 416. A favorable comparison or suitable accuracy at this point would conclude the required estimation procedure. An unfavorable comparison stimulates the requirements for better data processing techniques. Interest has been directed towards situations wherein accurate estimates can be made from the measurement data with a maximum likelihood estimators. This condition allows an iterative technique to be employed to arrive at the required accuracy of estimation. Unbiased estimators are employed and no a priori knowledge is assumed pertaining to the variance of either noise source. The properties of the noise sources and terminology will be consistent with Apollo Note 416.

I. Derivation of Estimator Equation

Equation (15) of Apollo Note 416 may be written in the following fashion:

$$\sum_{i=1}^{N} \sum_{j=1}^{N} n_i n_j \frac{\partial c^{-1}(i,j)}{\partial \phi_x} = \sum_{i=1}^{N} \sum_{j=1}^{N} c_{ij} \frac{\partial c^{-1}(i,j)}{\partial \phi_x} \qquad (1)$$

but

$$c_{ij} \frac{\partial c^{-1}(i,j)}{\partial \phi_x} = \frac{\partial}{\partial \phi_x}\left[c_{ij}\, c^{-1}(i,j)\right] - c^{-1}(i,j) \frac{\partial c_{ij}}{\partial \phi_x} \tag{2}$$

Since

$$c_{ij} = \phi_x \rho_x(j-i) + \phi_y \rho_y(j-i) \tag{3}$$

$$\frac{\partial c_{ij}}{\partial \phi_x} = \rho_x(j-i) \tag{4}$$

Recalling that

$$\sum_{i=1}^{N} \sum_{j=1}^{N} c_{ij}\, c^{-1}(i,j) = N \tag{5}$$

The substitution of Eqs. (2), (4), and (5) into Eq. (1) leads to the following result.

$$\sum_{i=1}^{N} \sum_{j=1}^{N} \rho_x(j-i)\, c^{-1}(i,j) = -\sum_{i=1}^{N} \sum_{j=1}^{N} n_i n_j \frac{\partial c^{-1}(i,j)}{\partial \phi_x} \tag{6}$$

By a similar technique, Eq. (16), (Apollo Note 416), may be transformed to:

$$\sum_{i=1}^{N} \sum_{j=1}^{N} \rho_y(j-i)\, c^{-1}(i,j) = \sum_{i=1}^{N} \sum_{j=1}^{N} n_i n_j \frac{\partial c^{-1}(i,j)}{\partial \phi_y} \tag{7}$$

Combining Eqs. (6) and (7) using Eqs. (3) and (5), it can readily be shown that

$$-\frac{1}{N}\sum_{i=1}^{N}\sum_{j=1}^{N} n_i n_j \left[\phi_x \frac{\partial c^{-1}(i,j)}{\partial \phi_x} + \phi_y \frac{\partial c^{-1}(i,j)}{\partial \phi_x}\right] = 1 \tag{8}$$

Eqs. (A2) and (A5) of Appendix A, (Apollo Note 416) are as follows:

$$\alpha = \frac{\phi_x}{\phi_y} \tag{9}$$

$$c^{-1}(i,j) = \frac{1}{\phi_y} d^{-1}(i,j) \tag{10}$$

Eqs. (9) and (10) can be used to find the following quantities:

$$\frac{\partial c^{-1}(i,j)}{\partial \phi_x} = \frac{1}{\phi_y^2} \frac{\partial d^{-1}(i,j)}{\partial \alpha} \tag{11}$$

$$\frac{\partial c^{-1}(i,j)}{\partial \phi_y} = -\frac{1}{\phi_y^2} d^{-1}(i,j) - \frac{1}{\phi_y^3} \frac{\partial d^{-1}(i,j)}{\partial \alpha} \tag{12}$$

$$\therefore \quad \phi_x \frac{\partial c^{-1}(i,j)}{\partial \phi_x} + \phi_y \frac{\partial c^{-1}(i,j)}{\partial \phi_y} = -\frac{d^{-1}(i,j)}{\phi_y} = -c_{ij} \tag{13}$$

It can now be shown from Eqs. (8), (10), and (13) that

$$\phi_y = -\frac{1}{N}\sum_{i=1}^{N}\sum_{j=1}^{N} n_i n_j \, d^{-1}(i,j) \tag{14}$$

From Eqs. (A5), (A6), (A7), and (A14), (Apollo Note 416), the following result can be obtained

$$\sum_{i=1}^{N} \sum_{j=1}^{N} \rho_x(j-i)\, c^{-1}(i,j) = T_o^{-1} + 2 \sum_{r=1}^{N-1} \rho_x(r)\, T_r^{-1} = \frac{NF}{\phi_y} \tag{15}$$

It can readily be shown from Eqs. (6), (11), and (15), that

$$\phi_y F = - \frac{1}{N} \sum_{i=1}^{N} \sum_{j=1}^{N} n_i n_j \frac{\partial d^{-1}(i,j)}{\partial \alpha} \tag{16}$$

Eqs. (14) and (16) are two equations which could be employed with an iterative technique to find the maximum likelihood estimates of ϕ_x and ϕ_y. Fortunately, it is also possible to find linear, unbiased estimates of ϕ_x and ϕ_y which will be the maximum likelihood value provided that the value of α chosen equals the true value of the ratio ϕ_x/ϕ_y. From this point onward, α is the assumed value of ϕ_x/ϕ_y and not the true value.

For present purposes, dummy parameters will be temporarily associated with Eqs. (14) and (16).

$$\hat{a} = \frac{1}{N} \sum_{i=1}^{N} \sum_{j=1}^{N} n_i n_j\, d^{-1}(i,j) \tag{17}$$

$$\hat{b} = -\frac{1}{N} \sum_{i=1}^{N} \sum_{j=1}^{N} n_i n_j \frac{\partial d^{-1}(i,j)}{\partial \alpha} \tag{18}$$

but

$$E\left\{n_i n_j\right\} = \phi_x\, \rho_x(j-i) + \phi_y\, \rho_y(j-i) \tag{19}$$

From Eq. (A4) of Apollo Note 416,

$$d_{ij} = \alpha \rho_x(j-i) + \rho_y(j-i) \tag{20}$$

$$\therefore \ \phi_n(j-i) = E\{n_i n_j\} = \phi_x \rho_x(j-i) + \phi_y \left[d_{ij} - \alpha \rho_x(j-i) \right] \tag{21}$$

Using the technique indicated by Equations (2) through (5), and Eqs. (15), (17), (18), and (19), it can be shown that

$$a = E\{a\} = F\phi_x + (1-\alpha F)\phi_y \tag{22}$$

$$b = E\{b\} = H\phi_x + (F-\alpha H)\phi_y \tag{23}$$

where

$$H = -\frac{\partial F}{\partial \alpha} \tag{24}$$

The solution of Eqs. (22) and (23) yields the result

$$\phi_x = \frac{(\alpha H - F)a + (1-\alpha F)b}{H - F^2} \tag{25}$$

$$\phi_y = \frac{Ha - Fb}{H - F^2} \tag{26}$$

The desired linear estimation equations for ϕ_x and ϕ_y can now be obtained by substitution of Eqs. (17) and (18) into Eqs. (25) and (26). The results are as indicated below:

$$\hat{\phi}_x = \frac{1}{N(H-F^2)} \sum_{i=1}^{N} \sum_{j=1}^{N} n_i n_j \, K_x(i,j) \tag{27}$$

and

$$\hat{\phi}_y = \frac{1}{N(H - F^2)} \sum_{i=1}^{N} \sum_{j=1}^{N} n_i n_j K_y(i, j) \tag{28}$$

where

$$K_x(i, j) = (\alpha H - F)\, d^{-1}(i, j) - (1 - \alpha F) \frac{\partial d^{-1}(i, j)}{\partial \alpha} \tag{29}$$

and

$$K_y(i, j) = H d^{-1}(i, j) + F \frac{\partial d^{-1}(i, j)}{\partial \alpha} \tag{30}$$

Equations (27) and (28) are the equations which ideally would be used for estimation purposes. Equations (29) and (30) are subsidiary equations employed for convenience. The estimates obtained are unbiased. In addition, the maximum likelihood estimate will be obtained with the proper value of α employed. To this point, two important problems still need to be resolved. One, how closely must the values of α be known? Basically, this deals with the convergence characteristic of the iterative technique to be employed. The present approach would be as indicated below:

Step 1. An initial estimate of the variance of each noise source is obtained by using an appropriate form of the simple correlation technique. At least ideally, this form will correspond to the limiting expression with one noise source dominant.

Step 2. An initial estimate of α is obtained from the ratio of the variance of the two noise sources. ϕ_x will be selected as the noise source with the fewest non-zero values for the normalized auto-correlation function.

Step 3. The variance of the maximum likelihood estimator for the value of α computed in Step 2 is calculated from the expressions given in Appendix A of Apollo Note 416.

Step 4. The variance of the simple correlation technique estimator is calculated from the expressions given in Section III of Apollo Note 416.

Step 5. The results of Steps 3 and 4 are compared. If these results are suitably close in agreement the process is terminated. An unfavorable comparison would necessitate an iteration process to be performed.

Step 6. Repeat Steps 1 through 5 for the maximum likelihood estimator with the value of α computed in Step 2 in place of the simple correlation technique.

Step 7. Repeat Step 6 for the improved estimator of α until suitable convergence is obtained.

Step 8. The final result will then be indicated by estimates for each ϕ_x and ϕ_y and estimates of the standard deviation of each quantity.

The second problem should treat how closely the typically complex forms required to obtain the maximum likelihood estimators need be represented to obtain nearly maximum likelihood estimates. Naturally, simple processing techniques are preferred where suitable results may be obtained.

Section II of Part II which follows derives the equations associated with the lack of performance associated with errors in the value of α used.

II. Effect of Incorrect Value of α

The variation with α of the variance of the estimates indicated in Eqs. (27) and (28) is the desired result of this section. Treating $\hat{\phi}_x$ first and employing the following definition

$$\Delta\phi_x^2 = E\left\{\phi_x^2\right\} - \phi_x^2 \tag{31}$$

$$E\left\{\phi_x^2\right\} = \frac{1}{N^2(H-F^2)^2} \sum_{i=1}^{N} \sum_{j=1}^{N} \sum_{k=1}^{N} \sum_{\ell=1}^{N} K_x(i,j)\, K_x(k,\ell)\, E\left\{n_i n_j\, n_k n_\ell\right\} \tag{32}$$

since

$$E\left\{n_i n_j\, n_k n_\ell\right\} = \phi_n(j-i)\,\phi_n(k-\ell) + \phi_n(k-i)\,\phi_n(\ell-j) + \phi_n(\ell-i)\,\phi_n(k-j) \tag{33}$$

Taking advantage of the symmetry involved and using Eqs. (31), (32), and (33),

$$\Delta\phi_x^2 = \frac{2}{N^2(H-F^2)^2} \sum_{i=1}^{N} \sum_{j=1}^{N} \sum_{k=1}^{N} \sum_{\ell=1}^{N} \phi_n(k-i)\,\phi_n(\ell-j)\, K_x(i,j)\, K_x(k,\ell) \tag{34}$$

Using Eq. (21),

$$\phi_n(k-i) = (\phi_x - \alpha\phi_y)\,\rho_x(k-i) + \phi_y\, d_{i,k} \tag{35}$$

and

$$\phi_n(\ell-j) = (\phi_x - \alpha\phi_y)\,\rho_x(\ell-j) + \phi_y\, d_{j,\ell} \tag{36}$$

By substitution of Eqs. (35) and (36) into Eq. (34) and taking advantage of the symmetry,

$$\Delta\phi_x^2 = \frac{2}{N^2(H-F^2)^2} \left[M_{x-1}\phi_y^2 + 2\, M_{x-2}\,\phi_y(\phi_x - \alpha\phi_y) + M_{x-3}(\phi_x - \alpha\phi_y)^2\right] \tag{37}$$

where

$$M_{x-1} = \sum_{i=1}^{N}\sum_{j=1}^{N}\sum_{k=1}^{N}\sum_{\ell=1}^{N} d_{ik}d_{j\ell}\, K_x(i,j)\, K_x(k,\ell) \tag{38}$$

$$M_{x-2} = \sum_{i=1}^{N}\sum_{j=1}^{N}\sum_{k=1}^{N}\sum_{\ell=1}^{N} \rho_x(k-i)\, d_{j\ell}\, K_x(i,j)\, K_x(k,\ell) \tag{39}$$

$$M_{x-3} = \sum_{i=1}^{N}\sum_{j=1}^{N}\sum_{k=1}^{N}\sum_{\ell=1}^{N} \rho_x(k-i)\, \rho_x(\ell-j)\, K_x(i,j)\, K_x(k,\ell) \tag{40}$$

The form for Eq. (37) was selected for several reasons. Note that for $\alpha = \phi_x/\phi_y$, $\Delta\phi_x^2$ is independent of M_{x-2} and M_{x-3}. The demonstration for this situation that $\Delta\phi_x^2$ calculated from Eq. (37) corresponds to the variance indicated in Apollo Note 416 would show that the processing network resulted in a maximum likelihood estimate. The terms of $\Delta\phi_x^2$ associated with M_{x-2} and M_{x-3} then correspond to the degradation in performance associated with incorrect value for α (if one may assure that the error in α is sufficiently small as to make the variation of M_{x-1} negligible).

More convenient forms for Eqs. (38), (39), and (40) can be obtained. An alternate set will be indicated below. These results are obtained by substitution of indices and by making use of the symmetry involved.

$$M_{x-1} = (\alpha+1)^2 \sum_{i=1}^{N}\sum_{j=1}^{N} K_x^2(i,j) + 4(\alpha+1)\sum_{r=1}^{N-1} d(r) \sum_{i=1}^{N-r}\sum_{j=1}^{N} K_x(i,j)\, K_x(i+r,j)$$

$$+ 2\sum_{r=1}^{N-1} d(r)\sum_{s=1}^{N-1} d(s)\sum_{i=1}^{N-r}\sum_{j=1}^{N-s}\left[K_x(i,j)\,K_x(i+r,j+s) + K_x(i,j+s)\,K_x(i+r,j)\right] \tag{41}$$

$$M_{x-2} = (\alpha+1) \sum_{i=1}^{N} \sum_{j=1}^{N} K_x^2(i,j) + 2(\alpha+1) \sum_{r=1}^{N-1} \rho_x(r) \sum_{i=1}^{N-r} \sum_{j=1}^{N} K_x(i,j)\, K_x(i+r,j)$$

$$+ 2 \sum_{s=1}^{N-1} d(s) \sum_{i=1}^{N} \sum_{j=1}^{N-s} K_x(i,j)\, K_x(i,j+s) \qquad (42)$$

$$+ 2 \sum_{r=1}^{N-1} \rho_x(r) \sum_{s=1}^{N-1} d(s) \sum_{i=1}^{N-r} \sum_{j=1}^{N-s} \left[K_x(i,j) K_x(i+r,j+s) + K_x(i+r,j) K_x(i,j+s) \right]$$

$$M_{x-3} = \sum_{i=1}^{N} \sum_{j=1}^{N} K_x^2(i,j) + 4 \sum_{r=1}^{N-1} \rho_x(r) \sum_{i=1}^{N-r} \sum_{j=1}^{N} K_x(i,j)\, K_x(i+r,j)$$

$$+ 2 \sum_{r=1}^{N-1} \rho_x(r) \sum_{s=1}^{N-1} \rho_x(s) \sum_{i=1}^{N-r} \sum_{j=1}^{N-s} \left[K_x(i,j) K_x(i+r,j+s) + K_x(i,j+s) K_x(i+r,j) \right] \qquad (43)$$

These equations become greatly simplified for the x noise source uncorrelated. A set of preferred forms are given below for use in a later portion of this note.

For

$$\rho_x(r) = 0 \qquad |r| \geq 1$$

$$M_{x-1} = (\alpha+1)^2 \sum_{i=1}^{N} \sum_{j=1}^{N} K_x^2(i,j) + 4(\alpha+1) \sum_{r=1}^{N-1} \rho_y(r) \sum_{i=1}^{N-r} \sum_{j=1}^{N} K_x(i,j)\, K_x(i+r,j)$$

$$+ 2 \sum_{r=1}^{N-1} \rho_y(r) \sum_{s=1}^{N-1} \rho_y(s) \sum_{i=1}^{N-r} \sum_{j=1}^{N-s} \left[K_x(i,j) K_x(i+r,j+s) + K_x(i,j+s) K_x(i+r,j) \right] \qquad (44)$$

$$M_{x-2} = (\alpha+1) \sum_{i=1}^{N} \sum_{j=1}^{N} K_x^2(i,j) + 2 \sum_{s=1}^{N-1} \rho_y(s) \sum_{i=1}^{N} \sum_{j=1}^{N-s} K_x(i,j)\, K_x(i,j+s) \tag{45}$$

$$M_{x-3} = \sum_{i=1}^{N} \sum_{j=1}^{N} K_x^2(i,j) \tag{46}$$

The implication to this point is that the results derived in this section to this point apply only to the situation where exact values are used for the elements of the inverse of the covariance matrix of the combined noise sources. The results are actually much more broad in scope. The formulation is consistent with simplified representations so long as K_x, K_y, F, and H are derived from the approximation to matrix elements employed. As a matter of fact, major simplifications can be made to the equations (particularly M_{x-1}) when exact values are employed. For example, for $\alpha = \phi_x / \phi_y$ one should expect the variance of the estimators to correspond to the variance for the maximum likelihood estimator.

Rewriting Eqs. (38) and (29),

$$M_{x-1} = \sum_{i=1}^{N} \sum_{j=1}^{N} \sum_{k=1}^{N} \sum_{\ell=1}^{N} d_{ik}\, d_{j\ell}\, K_x(i,j)\, K_x(k,\ell) \tag{47}$$

$$K_x(k,\ell) = (\alpha H - F)\, d^{-1}(k,\ell) - (1-\alpha F)\, \frac{\partial d^{-1}(k,\ell)}{\partial \alpha} \tag{48}$$

A number of relationships allow the final result to be obtained.

Some properties of a matrix and its inverse are:

$$\sum_{\ell=1}^{N} d_{j\ell}\, d^{-1}(\ell,k) = 1 \qquad k = j \tag{49a}$$

$$= 0 \qquad k \neq j \tag{49b}$$

$$\sum_{i=1}^{N} \sum_{j=1}^{N} d_{ij}\, d^{-1}(i,j) = N \tag{50}$$

By an earlier definition,

$$F = \frac{1}{N} \sum_{i=1}^{N} \sum_{j=1}^{N} \rho_x(j-i)\, d^{-1}(i,j) \tag{51}$$

$$H = -\frac{\partial F}{\partial \alpha} = -\frac{1}{N} \sum_{i=1}^{N} \sum_{j=1}^{N} \rho_x(j-i)\, \frac{\partial d^{-1}(i,j)}{\partial \alpha} \tag{52}$$

By differentiation of Eq. (20),

$$\frac{\partial d_{ij}}{\partial \alpha} = \rho_x(j-i) \tag{53}$$

Using Eq. (49a) and (49b) and integration by parts,

$$-\sum_{\ell=1}^{N} d_{j\ell}\, \frac{\partial d^{-1}(\ell,k)}{\partial \alpha} = -\frac{\partial}{\partial \alpha}\left[\sum_{\ell=1}^{N} d_{j\ell}\, d^{-1}(\ell,k)\right] + \sum_{\ell=1}^{N} \rho_x(\ell-j)\, d^{-1}(\ell,k)$$

$$= \sum_{\ell=1}^{N} \rho_x(\ell-j)\, d^{-1}(\ell,k) \tag{54}$$

Substitution of Eq. (48) into Eq. (47) summing over ℓ, and making use of relationships (48), (49a), (49b), (50), (53), and (54),

$$M_{x-1} = (\alpha H - F) \sum_{i=1}^{N} \sum_{j=1}^{N} d_{ij} K_x(i,j) + (1-\alpha F) \sum_{i=1}^{N} \sum_{j=1}^{N} \sum_{k=1}^{N} \sum_{\ell=1}^{N} \rho_x(\ell - j)\, d_{ik}\, d^{-1}(\ell, k)\, K_x(i,j) \tag{55}$$

Now summing over k,

$$M_{x-1} = (\alpha H - F) \sum_{i=1}^{N} \sum_{j=1}^{N} d_{ij} K_x(i,j) + (1-\alpha F) \sum_{i=1}^{N} \sum_{j=1}^{N} \rho_x(i-j) K_x(i,j) \tag{56}$$

Using the same relationships and Eqs. (51) and (52), it can be shown that

$$\sum_{i=1}^{N} \sum_{j=1}^{N} d_{ij} K_x(i,j) = N(\alpha H - F) + N(1-\alpha F) F = \alpha N (H - F^2) \tag{57}$$

$$\sum_{i=1}^{N} \sum_{j=1}^{N} \rho_x(i-j) K_x(i,j) = (\alpha H - F) NF + (1-\alpha F) HN = N(H - F^2) \tag{58}$$

The substitution of Eqs. (57) and (58) into Eq. (56), yields the desired result:

$$M_{x-1} = N(H - F^2) \left[\alpha^2 H - 2F\alpha + 1 \right] \tag{59}$$

By similar manipulations on Eq. (39) and use of Eq. (40),

$$M_{x-2} = N(\alpha H-F)\,(H-F^2) + N(\alpha H-F)\,(1-\alpha F)\,P - \frac{N(1-\alpha F)^2}{2}\,\frac{\partial P}{\partial \alpha} \tag{60}$$

and

$$M_{x-3} = N(\alpha H-F)^2\,P - N(\alpha H-F)\,(1-\alpha F)\,\frac{\partial P}{\partial \alpha} + N(1-\alpha F)^2\,Q \tag{61}$$

where

$$P = \frac{1}{N}\sum_{i=1}^{N}\sum_{j=1}^{N}\sum_{k=1}^{N}\sum_{\ell=1}^{N}\rho_x(k-i)\,\rho_x(\ell-j)\,d^{-1}(k,\ell)\,d^{-1}(i,j) \tag{62}$$

and

$$Q = \frac{1}{N}\sum_{i=1}^{N}\sum_{j=1}^{N}\sum_{k=1}^{N}\sum_{\ell=1}^{N}\rho_x(k-i)\,\rho_x(\ell-j)\left[\frac{\partial d^{-1}(k,\ell)}{\partial \alpha}\right]\left[\frac{\partial d^{-1}(i,j)}{\partial \alpha}\right] \tag{63}$$

Equations (59), (60), and (61) yield the desired forms for M_{x-1}, M_{x-2}, and M_{x-3}. Computational difficulty is limited to the determination of F, P, and Q.

The substitution of Eq. (59) into Eq. (37) yields the following result:

$$\Delta\phi_x^2 = \frac{2\phi_y^2(\alpha^2 H-2F\alpha+1)}{N(H-F^2)} + \frac{2}{N^2(H-F^2)^2}\left[2M_{x-2}\,\phi_y(\phi_x-\alpha\phi_y) + M_{x-3}(\phi_x-\alpha\phi_y)^2\right] \tag{64}$$

This result is in exact agreement (as one should expect) with Eq. (A17) of Apollo Note 416 for $\alpha = \phi_x/\phi_y$.

Corresponding expressions for M_{y-1}, M_{y-2}, and M_{y-3} may be found by a similar approach. The results are as follows:

$$M_{y-1} = NH(H-F^2) \tag{65}$$

$$M_{y-2} = -NHFP - \frac{NF^2}{2}\frac{\partial P}{\partial \alpha} \tag{66}$$

and

$$M_{y-3} = NH^2P + NHF\frac{\partial P}{\partial \alpha} + NF^2Q \tag{67}$$

with

$$\Delta\phi_y^2 = E\left\{\phi_y^2\right\} - \phi_y^2 \tag{68}$$

and

$$\Delta\phi_y^2 = \frac{2}{N^2(H-F^2)^2}\left[M_{y-1}\phi_y^2 + 2M_{y-2}\phi_y(\phi_x - \alpha\phi_y) + M_{y-3}(\phi_x - \alpha\phi_y)^2\right] \tag{69}$$

The substitution of Eq. (65) into Eq. (69) yields the following result:

$$\Delta\phi_y^2 = \frac{2\phi_y^2}{N\left(1-\frac{F^2}{H}\right)} + \frac{2}{N^2(H-F^2)^2}\left[2M_{y-2}\phi_y(\phi_x - \alpha\phi_y) + M_{y-3}(\phi_x - \alpha\phi_y)^2\right] \tag{70}$$

Again, this result is in exact agreement with Eq. (A18), (Apollo Note 416) for $\alpha = \phi_x/\phi_y$.

The major effort for this section is now concluded. A technique has been demonstrated to attain at least nearly the maximum likelihood estimator results where good accuracy can be obtained with a maximum

likelihood estimator. It now remains only to indicate suitable forms for the variance for simpler estimators which only approximate the results which are obtained by the more complex processing technique. Eqs. (44), (45), and (46) are suitable expressions for M_{x-1}, M_{x-2}, and M_{x-3} for this purpose. Corresponding results for M_{y-1}, M_{y-2}, and M_{y-3} may be obtained by the following substitutions in Eqs. (44), (45), and (46).

$$M_{x-1} \rightarrow M_{y-1}$$

$$M_{x-2} \rightarrow M_{y-2}$$

$$M_{x-3} \rightarrow M_{y-3}$$

$$K_x \rightarrow K_y$$

Where K_y is given by Eq. (30).

The section which follows will treat a numerical example where exact values are used for $d^{-1}(i, j)$.

III. Numerical Example – Exact Form of $d^{-1}(i, j)$

The numerical example will treat the standard example used in Apollo Note 416. Briefly,

$$\begin{aligned} \rho_x(r) &= 1 && r = 0 \\ &= 0 && r \neq 0 \end{aligned}$$

$$\begin{aligned} \rho_y(r) &= 1 && r = 0 \\ &= -1/2 && |r| = 1 \\ &= 0 && |r| \geq 2 \end{aligned}$$

For this case, from Eqs. (51), (62), and (63),

$$NF = \sum_{i=1}^{N} d^{-1}(i,i) \tag{71}$$

$$NP = \sum_{i=1}^{N}\sum_{j=1}^{N}\left[d^{-1}(i,j)\right]^2 \tag{72}$$

$$NQ = \sum_{i=1}^{N}\sum_{j=1}^{N}\left[\frac{\partial d^{-1}(i,j)}{\partial \alpha}\right]^2 \tag{73}$$

where

$$d^{-1}(i,j) = \frac{2}{N+1}\sum_{\ell=1}^{N}\frac{\sin\frac{\ell\pi i}{N+1}\sin\frac{\ell\pi 1}{N+1}}{\alpha+1-\cos\frac{\pi\ell}{N+1}} \tag{74}$$

by differentiation,

$$\frac{\partial d^{-1}(i,j)}{\partial \alpha} = -\frac{2}{N+1}\sum_{\ell=1}^{N}\frac{\sin\frac{\ell\pi i}{N+1}\sin\frac{\ell\pi 1}{N+1}}{\left(\alpha+1-\cos\frac{\pi\ell}{N+1}\right)^2} \tag{75}$$

Making use of the geometric relationship

$$\sum_{i=1}^{N}\sum_{j=1}^{N}\sin\frac{\ell_1\pi i}{N+1}\sin\frac{\ell_2\pi i}{N+1} = \frac{N+1}{2} \qquad \ell_1 = \ell_2 \tag{76a}$$

$$= 0 \qquad \ell_1 \neq \ell_2 \tag{76b}$$

Equation (71) may be written as:

$$F = \frac{1}{N} \sum_{\ell=1}^{N} \frac{1}{\left(\alpha+1 - \cos \frac{\pi\ell}{N+1}\right)} \tag{77}$$

then

$$H = - \frac{\partial F}{\partial \alpha} = \frac{1}{N} \sum_{\ell=1}^{N} \frac{1}{\left(\alpha+1 - \cos \frac{\pi\ell}{N+1}\right)^2} \tag{78}$$

Equations (72) and (73) may be written as:

$$P = \frac{1}{N} \sum_{\ell=1}^{N} \frac{1}{\left(\alpha+1 - \cos \frac{\pi\ell}{N+1}\right)^2} = H \tag{79}$$

$$Q = \frac{1}{N} \sum_{\ell=1}^{N} \frac{1}{\left(\alpha+1 - \cos \frac{\pi\ell}{N+1}\right)^4} = \frac{1}{6} \frac{\partial^2 P}{\partial \alpha^2} = \frac{1}{6} \frac{\partial^2 H}{\partial \alpha^2} \tag{80}$$

The quantity $\partial P/\partial \alpha$ is also required. By differentiation of Eq. (79),

$$\frac{\partial P}{\partial \alpha} = - \frac{2}{N} \sum_{\ell=1}^{N} \frac{1}{\left(\alpha+1 - \cos \frac{\pi\ell}{N+1}\right)^3} = \frac{\partial H}{\partial \alpha} \tag{81}$$

At least for this case, H, P, $\partial P/\partial \alpha$, and Q may all be determined from F.

M_{x-2} and M_{x-3} as given in Eqs. (60) and (61) may now be written as:

$$M_{x-2} = N(\alpha H - F)\,(2H - \alpha FH - F^2) - \frac{N(1-\alpha F)^2}{2} \frac{\partial H}{\partial \alpha} \tag{82}$$

$$M_{x-3} = N(\alpha H-F)^2 H - N(\alpha H-F)(1-\alpha F)\frac{\partial H}{\partial \alpha} + \frac{N(1-\alpha F)^2}{2}\frac{\partial^2 H}{\partial \alpha^2} \quad (83)$$

Similarly, M_{y-2} and M_{y-3} as given by Eqs. (66) and (67) may be written as follows:

$$M_{y-2} = - NH^2F - \frac{NF^2}{2}\frac{\partial H}{\partial \alpha} \quad (84)$$

$$M_{y-3} = - NH^3 + NHF\frac{\partial H}{\partial \alpha} + \frac{NF^2}{6}\frac{\partial^2 H}{\partial \alpha^2} \quad (85)$$

To obtain a greater insight into the characteristic of the sensitivity of the technique to differences in α from ϕ_x/ϕ_y, the approximate value of F from Apollo Note 416 will be used. All equations which follow are then approximate. However, an equal sign will be used in place of the approximate sign. From Eq. (A22), Apollo Note 416,

$$F = (\alpha^2 + 2\alpha)^{-1/2} \quad (86)$$

By differentiation,

$$H = -\frac{\partial F}{\partial \alpha} = \frac{\alpha + 1}{(\alpha^2+2\alpha)^{3/2}} \quad (87)$$

$$\frac{\partial H}{\partial \alpha} = -\frac{(2\alpha^2 + 4\alpha + 3)}{(\alpha^2 + 2\alpha)^{5/2}} \quad (88)$$

$$\frac{\partial^2 H}{\partial \alpha^2} = \frac{3(\alpha+1)}{(\alpha^2+2\alpha)^{7/2}}\left[2\alpha^2 + 4\alpha + 5\right] \quad (89)$$

Substituting the expressions indicated in Eqs. (86), (87), (88), and (89) into Eqs. (82), (83), (84), and (85), the following results can be obtained.

$$\frac{M_{x-2}}{N} = \frac{\alpha\left[2\alpha^3 + 8\alpha^2 + 10\alpha + 3 - (2\alpha^2 + 6\alpha + 5)\sqrt{\alpha^2 + 2\alpha}\right]}{(\alpha^2 + 2\alpha)^{7/2}} \tag{90}$$

$$\frac{M_{x-3}}{N} = \frac{\alpha}{(\alpha^2 + 2\alpha)^{9/2}}\left[2\alpha^4 + 10\alpha^3 + 20\alpha^2 + 18\alpha + 5 - (2\alpha^3 + 8\alpha^2 + 13\alpha + 8)\sqrt{\alpha^2 + 2\alpha}\right] \tag{91}$$

$$\frac{M_{y-2}}{N} = \frac{1}{2(\alpha^2 + 2\alpha)^{7/2}} \tag{92}$$

$$\frac{M_{y-3}}{N} = \frac{(\alpha + 1)}{2(\alpha^2 + 2\alpha)^{9/2}} \tag{93}$$

Other quantities required for computation are:

$$H - F^2 = \frac{\alpha + 1 - \sqrt{\alpha^2 + 2\alpha}}{(\alpha^2 + 2\alpha)^{3/2}} = \frac{1}{(\alpha^2 + 2\alpha)^{3/2}\left[\alpha + 1 + \sqrt{\alpha^2 + 2\alpha}\right]} \tag{94}$$

$$\alpha^2 H - 2F\alpha + 1 = 1 - \frac{\alpha^2(\alpha + 3)}{(\alpha^2 + 2\alpha)^{3/2}} \tag{95}$$

Letting

$$\beta = \frac{\phi_x}{\phi_y}$$

After extensive mathematical manipulations, it can be shown that:

$$\frac{N\Delta\phi_x^2}{\phi_x^2} = 2\left[1+\sqrt{1+\frac{2}{\alpha}} + \frac{\left(1+\frac{1}{\alpha}+\frac{1}{\beta}\right)^2}{\left(1+\frac{2}{\alpha}\right)^{3/2}}\right] \tag{96}$$

and

$$\frac{N\Delta\phi_y^2}{\phi_y^2} = 1+\frac{\left(1+\frac{1}{\alpha}+\sqrt{1+\frac{2}{\alpha}}\right)^2}{\left(1+\frac{2}{\alpha}\right)^{3/2}}\left[\alpha^2\left(1+\frac{2}{\alpha}\right)^{3/2} - \alpha^2\left(1+\frac{3}{\alpha}\right) + 2\beta + \left(1+\frac{1}{\alpha}\right)\beta^2\right] \tag{97}$$

Equations (96) and (97) are the desired final forms for the variance of the estimators. As a check of the Eqs. (96) and (97), a comparison will now be made with results previously obtained in Apollo Note 416.

For

$$\alpha = \beta\ , \quad \frac{N\Delta\phi_x^2}{\phi_x^2} = 2\left[1+2\sqrt{1+\frac{2}{\alpha}}\right] \tag{98}$$

and

$$\frac{N\Delta\phi_y^2}{\phi_y^2} = 1+\alpha^2\left(1+\frac{1}{\alpha}+\sqrt{1+\frac{2}{\alpha}}\right)^2 = 2(\alpha+1)\left[\alpha+1+\sqrt{\alpha^2+2\alpha}\right] \tag{99}$$

Equations (98) and (99) compare exactly with Eqs. (A24) and (A25) of Apollo Note 416. The form given in Eq. (98) is a simpler form for Eq. (A24).

The limiting forms for Eqs. (96) and (97) for $\alpha = \infty$ are as follows:

$$\frac{N\Delta\phi_x^2}{\phi_x^2} = 2\left[2 + \left(1+\frac{1}{\beta}\right)^2\right] = 2\left[3 + \frac{2}{\beta} + \frac{1}{\beta^2}\right] \tag{100}$$

$$\frac{N\Delta\phi_y^2}{\phi_y^2} = 1 + 4\left(\frac{3}{2} + 2\beta + \beta^2\right) = 7 + 8\beta + 4\beta^2 \tag{101}$$

These results compare exactly with Eqs. (97b) and (98b) of Apollo Note 416. The simple correlation technique is asymptotically the maximum likelihood estimator for $\beta \gg 1$ as was previously noted.

The task remaining in this section is to indicate numerical results on the sensitivity of use of values other than optimal for α much less than one. The simple correlation technique is satisfactory for $\alpha > 1$.

Equation (96) is plotted on Figure 1 for $\beta = .01$, $.1$, and $.5$. As the equation indicates for a given value of α, the normalized variance decreases as β ($\beta = \phi_x/\phi_y$) increases. It should also be noted that for a given value of β, the normalized variance is a minimum for $\alpha = \beta$. In addition, for a given value of β, the minimum value for the variance is nearly achieved over a rather broad range of α. This indicates considerable tolerance to deviations in the value of α that may be used.

Equation (97) is plotted on Figure 2 for $\beta = .01$, $.1$, and $.5$. As the form of the equation would indicate, the smaller the value of β the smaller the normalized variance for this component as one should expect. Again, for a fixed value of β, the normalized variance is a minimum for $\alpha = \beta$ and a nearly minimum is achieved over a broad range of α.

K+E LOGARITHMIC 46 7320
2 X 3 CYCLES MADE IN U.S.A.
KEUFFEL & ESSER CO.

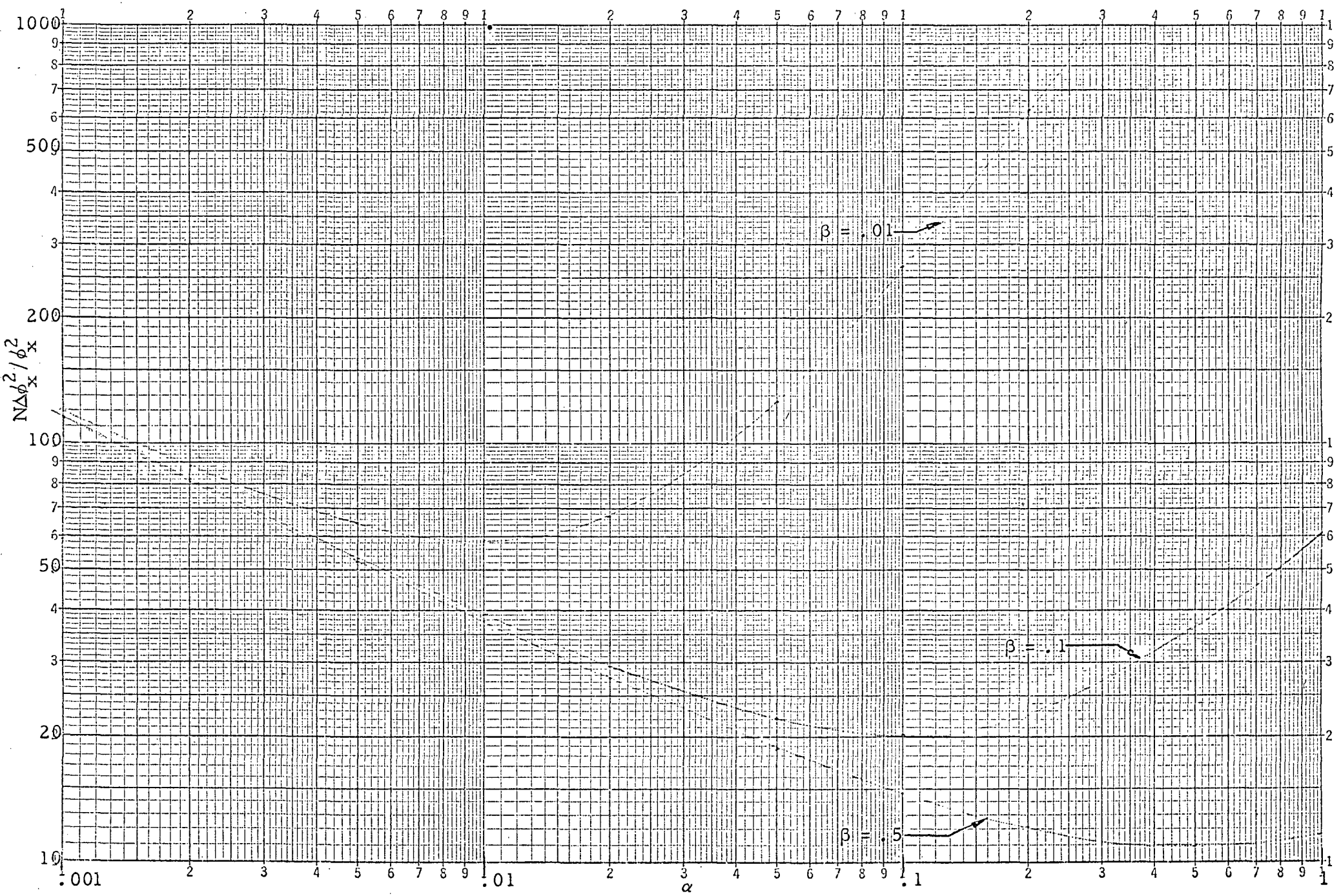

Figure 1. Normalized Variance - Ideal Form for Matrix Inverse Coefficients

K&E LOGARITHMIC 46 7320
2 X 3 CYCLES MADE IN U.S.A.
KEUFFEL & ESSER CO.

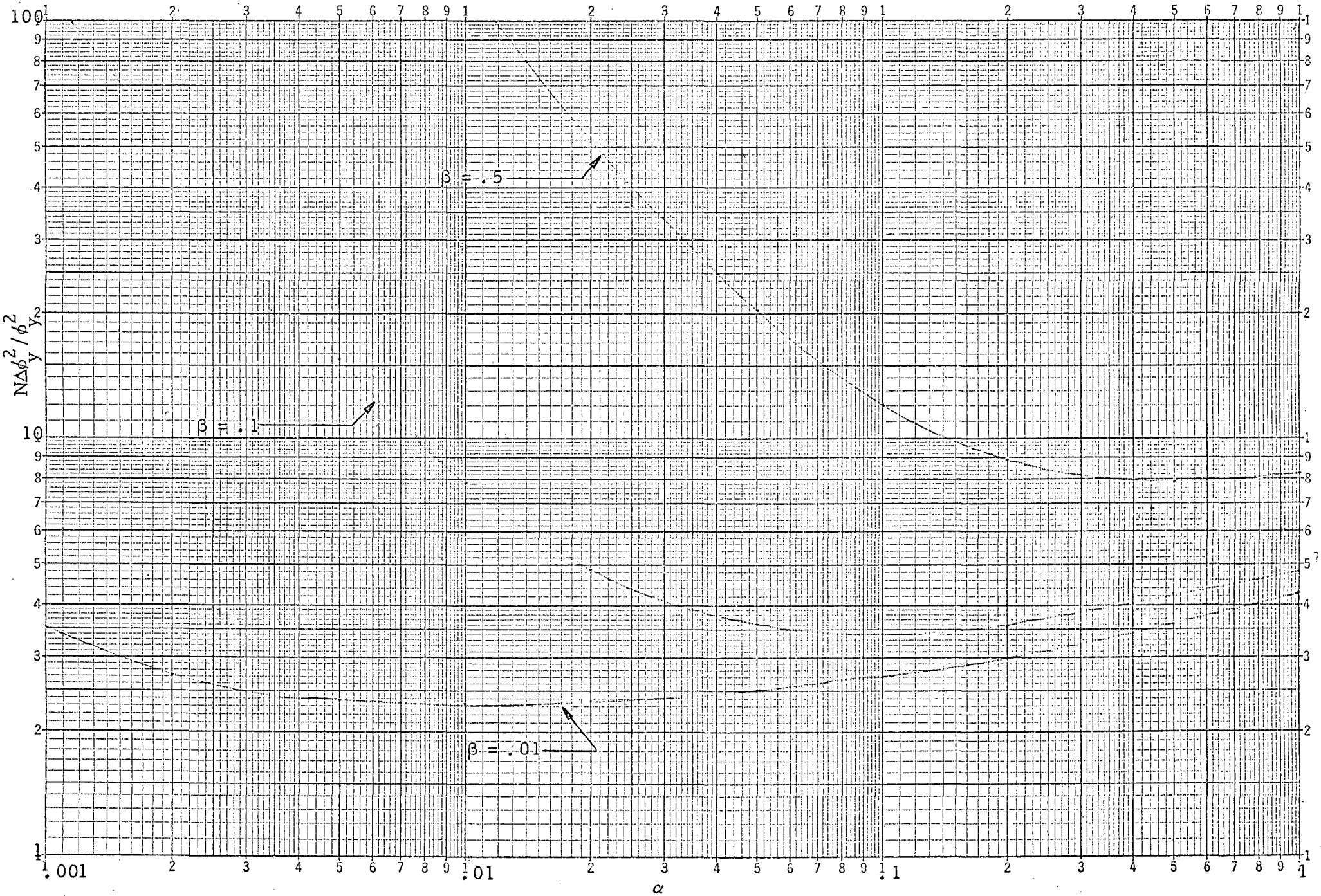

Figure 2. Normalized Variance - Ideal Form for Matrix Inverse Coefficients

In a somewhat arbitrary fashion, the range of α to be tolerated was selected as the range dictated by the normalized variance increasing 50% over the minimum value. Table 1, which follows, indicates the allowable range for α with $\beta = .01, .1, .5$, and ∞. (The infinity value was found from Figures 1 and 2 of Apollo Note 416.) It can be noted that the range of α is broad for either component with $N\Delta\phi_y^2/\phi_y^2$ component being less sensitive than the $N\Delta\phi_x^2/\phi_x^2$ component. One could further surmise from the table that the use of three values of α ($\alpha = .03, .5$, and ∞) would allow the estimate of both components to be made within 50% of the maximum likelihood estimator for $\beta > .01$.

Normalized Variance Component	Allowable Range for α			
	$\beta = .01$	$\beta = .1$	$\beta = .5$	$\beta = \infty$
$\frac{N\Delta\phi_x^2}{\phi_x^2}$	.002-.032	.019-.37	.074-4.8	.85-∞
$\frac{N\Delta\phi_y^2}{\phi_y^2}$	.001-.35	.0019-1.3	.1-50	.54-∞

Table 1. Allowable Range for α

The last section of this report will treat the variance form, approximate form of the matrix inverse.

IV. Numerical Example - Approximate Form of $d^{-1}(i, j)$

Work performed previously on first order linear regression techniques involved a matrix and its inverse which were similar to the matrices involved with our present techniques. After some manipulation, a suggested form for our purposes is indicated below for the example given in Section III.

Let

$$f^{-1}(i, j) = F e^{-\gamma r} \tag{102}$$

where

$$r = |j-i| \tag{103}$$

$$e^{\gamma} = \alpha + 1 + \sqrt{\alpha^2 + 2\alpha} \tag{104}$$

and

$$F = \frac{1}{\sqrt{\alpha^2 + 2\alpha}} \tag{105}$$

Recalling that

$$d_{ij} = \alpha + 1 \qquad j = i \tag{106a}$$

$$= -1/2 \qquad |j - i| = 1 \tag{106b}$$

$$= 0 \qquad |j - i| \geq 2 \tag{106c}$$

and letting

$$G = \left[g_{ij} \right] \tag{107}$$

where

$$g_{ij} = \sum_{k=1}^{N} d_{ij} f^{-1}(i, j) \tag{108}$$

It can be shown that

$$g_{ij} = 1 \qquad j = i \quad \text{and} \quad i \neq 1, N \tag{109a}$$

$$= 0 \qquad j \neq i \quad \text{and} \quad i \neq 1, N \tag{109b}$$

$$g_{ij} = \frac{F}{2} e^{\gamma} = \frac{1}{2}\left[1 + \frac{\alpha+1}{\sqrt{\alpha^2 + 2\alpha}}\right] \quad j = 1 \tag{110a}$$

$$= \frac{F}{2} e^{-\gamma j} \qquad j \geq 2 \tag{110b}$$

$$g_{Nj} = \frac{F}{2} e^{\gamma} = \frac{1}{2}\left[1 + \frac{\alpha+1}{\sqrt{\alpha^2\, 2\alpha}}\right] \quad j = N \tag{111a}$$

$$= \frac{F}{2} e^{-\gamma(N+1-j)} \qquad j \leq N-1 \tag{111b}$$

Equations (109a) through (111b) indicate that an approximate inverse would be obtained by using $f^{-1}(i, j)$ for $d^{-1}(i, j)$ at least for α sufficiently large. At any rate, this network may be used with the appropriate equations of Section II provided that F and H are made compatible, which already has been accomplished.

Some additional relationships to be employed are as follows. By differentiation of Eqs. (102) and (104), and using Eqs. (104) and (105),

$$\frac{\partial e^{\gamma}}{\partial \alpha} = 1 + \frac{\alpha+1}{\sqrt{\alpha^2\, 2\alpha}} = F e^{\gamma} \tag{112}$$

$$\frac{\partial f^{-1}(i, j)}{\partial \alpha} = \frac{\partial f^{-1}(r)}{\partial \alpha} = -He^{-\gamma r} - rF^2 e^{-\gamma r} \tag{113}$$

It can easily be shown that

$$H - F^2 = F^3 e^{-\gamma} \tag{114}$$

and

$$\frac{1}{F} - \alpha = 1 - e^{-\gamma} \tag{115}$$

Substitution of Eqs. (102) and (113) into Eq. (29) yields

$$K_x(i, j) = K_x(r) = \left[(H-F^2) + rF^2\,(1 - \alpha F)\right] e^{-\gamma r} \tag{116}$$

Substitution of Eqs. (114) and (115) into Eq. (116) yields

$$K_x(r) = F^3 \left[e^{-\gamma} + r\,(1 - e^{-\gamma})\right] e^{-\gamma r} \tag{117}$$

The substituion of Eqs. (102) and (113) into Eq. (30) yields

$$K_y(i, j) = K_y(r) = -rF^3\, e^{-\gamma r} \tag{118}$$

For the numerical case of interest, Eqs. (44), (45), and (46) may be written as follows:

$$M_{x-1} = (\alpha+1)^2 \sum_{i=1}^{N}\sum_{j=1}^{N} K_x^2(r) - 2(\alpha+1) \sum_{i=1}^{N-1}\sum_{j=1}^{N} K_x(r)\, K_x(i+1, j) + \frac{1}{2} \sum_{i=1}^{N-1}\sum_{j=1}^{N-1} \left[K_x^2(r) + K_x(i, j+1)\, K_x(i+1, j)\right] \tag{119}$$

$$M_{x-2} = (\alpha+1) \sum_{i=1}^{N}\sum_{j=1}^{N} K_x^2(r) - \sum_{i=1}^{N}\sum_{j=1}^{N-1} K_x(r)\, K_x(i, j+1) \tag{120}$$

and

$$M_{x-3} = \sum_{i=1}^{N} \sum_{j=1}^{N} K_x^2(r) \tag{121}$$

It can also be shown that

$$\sum_{i=1}^{N} \sum_{j=1}^{N} K_x^2(i, j) = N\, K_x^2(0) + 2 \sum_{r=1}^{N-1} (N-r)\, K_x^2(r) \tag{122}$$

$$\sum_{i=1}^{N-1} \sum_{j=1}^{N} K_x(i, j)\, K_x(i+1, j) = \sum_{i=1}^{N} \sum_{j=1}^{N-1} K_x(i, j)\, K_x(i, j+1) = 2 \sum_{r=1}^{N-1} (N-r)\, K_x(r-1) K_x(r) \tag{123}$$

$$\sum_{i=1}^{N-1} \sum_{j=1}^{N-1} K_x(i, j)\, K_x(i+1, j+1) = (N-1)\, K_x^2(0) + 2 \sum_{r=1}^{N-1} (N-1-r)\, K_x^2(r) \tag{124}$$

and

$$\sum_{i=1}^{N-1} \sum_{j=1}^{N-1} K_x(i, j+1)\, K_x(i+1, j) = (N-1)\, K_x^2(1) + 2 \sum_{r=2}^{N-1} (N-r)\, K_x(r-2)\, K_x(r) \tag{125}$$

To find the simplified asymptotic response, we will limit our processing network to values of α or γ wherein $K_x(r)$ is substantially zero for a value of $r << N$.

Equations (122), (123), (124), and (125), may be written as follows:

$$\frac{1}{N} \sum_{i=1}^{N} \sum_{j=1}^{N} K_x^2(i, j) \sim K_x^2(0) + 2 \sum_{r=1}^{\infty} K_x^2(r) \tag{126}$$

$$\frac{1}{N}\sum_{i=1}^{N-1}\sum_{j=1}^{N} K_x(i,j)\,K_x(i+1,j) \sim 2\sum_{r=1}^{\infty} K_x(r-1)\,K_x(r) \tag{127}$$

$$\frac{1}{N}\sum_{i=1}^{N-1}\sum_{j=1}^{N-1} K_x(i,j)\,K_x(i+1,j+1) \sim K_x^2(0) + 2\sum_{r=1}^{\infty} K_x^2(r) \tag{128}$$

and

$$\frac{1}{N}\sum_{i=1}^{N-1}\sum_{j=1}^{N-1} K_x(i,j+1)\,K_x(i+1,j) \sim K_x^2(1) + 2\sum_{r=2}^{\infty} K_x(r-2)\,K_x(r) \tag{129}$$

Corresponding equations for M_{y-1}, M_{y-2}, and M_{y-3}, may be found from Eqs. (119) through (129) by the substitution of y for x in all places.

The following relationships are employed to arrive at closed form expressions for the infinite series employed in Eqs. (126), (127), (128), and (129):

$$\sum_{k=o}^{\infty} e^{-2\gamma k} = \frac{1}{1-e^{-2\gamma}} \tag{130}$$

$$\sum_{k=o}^{\infty} k\, e^{-2\gamma k} = \frac{e^{-2\gamma}}{\left(1-e^{-2\gamma}\right)^2} \tag{131}$$

$$\sum_{k=o}^{\infty} k^2\, e^{-2\gamma k} = \frac{e^{-2\gamma}\left(1+e^{-2\gamma}\right)}{\left(1-e^{-2\gamma}\right)^3} \tag{132}$$

After considerable manipulation, it can be shown that

$$\frac{2}{K_x^2(0)} \sum_{r=1}^{\infty} K_x^2(r) = \frac{2\alpha^2 + 6\alpha + 5}{(\alpha+2)\sqrt{\alpha^2+2\alpha}} \tag{133}$$

$$\frac{2}{K_x^2(0)} \sum_{r=1}^{\infty} K_x(r-1)\, K_x(r) = 1 + \frac{\alpha^2 + 5\alpha + 5}{(\alpha+2)\sqrt{\alpha^2+2\alpha}} \tag{134}$$

$$\frac{2}{K_x^2(0)} \sum_{r=2}^{\infty} K_x(r-2)\, K_x(r) = \frac{2\alpha+5}{(\alpha+2)\sqrt{\alpha^2+2\alpha}} \tag{135}$$

Furthermore,

$$K_x(0) = K_x(1) = F^3\, e^{-\gamma} = H - F^2 \tag{136}$$

Substitution of Eqs. (126), (127), (128), (129), (133), (134), (135), and (136) into Eqs. (119), (120), and (121), yields the following results after simplification.

$$\frac{M_{x-1}}{N\left|H - F^2\right|^2} = \alpha^2 \left[1 + 2\sqrt{1+\frac{2}{\alpha}}\right] \tag{137}$$

$$\frac{M_{x-2}}{N\left|H - F^2\right|^2} = \alpha \left[1 + \frac{2\alpha + 3}{\sqrt{\alpha^2+2\alpha}}\right] \tag{138}$$

and

$$\frac{M_{x-3}}{N\left|H - F^2\right|^2} = 1 + \frac{2\alpha^2 + 6\alpha + 5}{(\alpha+2)\sqrt{\alpha^2+2\alpha}} = 1 + \frac{2(\alpha+1)}{\sqrt{\alpha^2+2\alpha}} + \frac{1}{(\alpha+2)\sqrt{\alpha^2+2\alpha}} \tag{139}$$

Letting $\beta = \phi_x/\phi_y$, the substitution of Eqs. (137), (138), and (139) into Eq. (37) yields, after simplification,

$$\frac{N\Delta\phi_x^2}{\phi_x^2} = \frac{2}{N|H-F^2|^2}\left[M_{x-3} + \frac{2}{\beta}\left(M_{x-2} - \alpha M_{x-3}\right) + \frac{1}{\beta^2}\left(M_{x-1} - 2\alpha M_{x-2} + \alpha^2 M_{x-3}\right)\right] \quad (140a)$$

$$= 2\left[1 + \frac{2\alpha^2+6\alpha+5}{(\alpha+2)\sqrt{\alpha^2+2\alpha}} + \frac{2\alpha(\alpha+1)}{\beta(\alpha+2)\sqrt{\alpha^2+2\alpha}} + \frac{\alpha^2}{\beta^2(\alpha+2)\sqrt{\alpha^2+2\alpha}}\right] \quad (140b)$$

$$= 2\left[1 + \sqrt{1+\frac{2}{\alpha}} + \frac{\left(1+\frac{1}{\alpha}+\frac{1}{\beta}\right)^2}{\left(1+\frac{2}{\alpha}\right)^{3/2}}\right] \quad (140c)$$

The result indicated in Eq. (140c) corresponds exactly to the expression indicated in Eq. (96). As a consequence, this is nearly the maximum likelihood technique for α not too small.

By a similar technique, the results can be derived for $\Delta\phi_y^2$. A few of the relationships will be indicated below.

$$K_y(r) = -rF^3 e^{-\gamma r} \quad (141)$$

$$K_y(0) = 0 \quad (142)$$

$$-K_y(1) = F^3 e^{-\gamma} = H - F^2 = K_x(0) = K_x(1) \quad (143)$$

$$\frac{1}{|H-F^2|^2}\sum_{r=1}^{\infty} K_y^2(r) = \frac{(\alpha+1)^2}{2(\alpha^2+2\alpha)} + \frac{(\alpha+1)^3 - \frac{\alpha+1}{2}}{2|\alpha^2+2\alpha|^{3/2}} \quad (144)$$

$$\frac{1}{\left|H - F^2\right|^2} \sum_{r=2}^{\infty} K_y(r)\, K_y(r-1) = \frac{\alpha+1}{2(\alpha^2+2\alpha)} + \frac{(\alpha+1)^2 - \frac{1}{2}}{2(\alpha^2+2\alpha)^{3/2}} \tag{145}$$

$$\frac{1}{\left|H - F^2\right|^2} \sum_{r=2}^{\infty} K_y(r)\, K_y(r-2) = \frac{1}{2(\alpha^2+2\alpha)} + \frac{\alpha+1}{4(\alpha^2+2\alpha)^{3/2}} \tag{146}$$

$$\frac{M_{y-1}}{N\left|H - F^2\right|^2} = (\alpha+1)^2 + (\alpha+1)\sqrt{\alpha^2+2\alpha} \tag{147}$$

$$\frac{M_{y-2}}{N\left|H - F^2\right|^2} = \alpha+1 + \frac{2\alpha^2+4\alpha+1}{2\sqrt{\alpha^2+2\alpha}} \tag{148}$$

$$\frac{M_{y-3}}{N\left|H - F^2\right|^2} = \left(\frac{\alpha+1}{\alpha^2+2\alpha}\right)\left[\alpha+1+\frac{2\alpha^2+4\alpha+1}{2\sqrt{\alpha^2+2\alpha}}\right] \tag{149}$$

and finally,

$$\frac{N\Delta\phi_y^2}{\phi_y^2} = \frac{4\left(1+\frac{1}{\alpha}\right)}{1+\frac{2}{\alpha}} + \frac{3+\frac{5}{\alpha}}{\left(1+\frac{2}{\alpha}\right)^{3/2}} + \left[\frac{2\left(1+\frac{1}{\alpha}\right)}{1+\frac{2}{\alpha}} + \frac{2+\frac{4}{\alpha}+\frac{1}{\alpha^2}}{\left(1+\frac{2}{\alpha}\right)^{3/2}}\right]\left[2\beta + \left(1+\frac{1}{\alpha}\right)\beta^2\right] \tag{150}$$

Equations (150) and (99) are different but equivalent forms.

It has been demonstrated to this point that the approximate inverse will yield excellent results subject to α being sufficiently large. The condition on α is stated by Eq. (57) of Apollo Note 416, ($\alpha >> 5/N^2$). This means that for large samples α can be very small. For example, the approximation will be good for N = 1000 with $\alpha >> .000005$. Values of α greater than .001 (with $N \geq 1000$) certainly should allow the approximations to be adequate. An examination of the expressions for the variance would indicate that the approximations are valid where high confidence estimates can be made for the two noise sources.

The conclusion of the part will be to indicate particular characteristics of the estimator indicated in this section.

Rewriting Eqs. (27) and (117),

$$\hat{\phi}_x = \frac{1}{N\left(H - F^2\right)} \sum_{i=1}^{N} \sum_{j=1}^{N} n_i n_j \, K_x(i, j) \tag{151}$$

$$K_x(i, j) = K_x(r) = (H - F^2) \left[1 + r(e^{\gamma} - 1)\right] e^{-\gamma r} \tag{152}$$

It can be shown that

$$\hat{\phi}_x = \frac{1}{N} \sum_{i=1}^{N} n_i^2 + \frac{2}{N} \sum_{r=1}^{N-1} \left[1 + r(e^{\gamma} - 1)\right] e^{-\gamma r} \sum_{i=1}^{N-r} n_i n_{i+r} \tag{153}$$

If we define $\hat{\phi}_m(r)$ by the following equation

$$\hat{\phi}_m(r) = \frac{1}{N} \sum_{i=1}^{N-r} n_i \, n_{i+r} \tag{154}$$

Then,

$$\hat{\phi}_x = \hat{\phi}_m(0) + 2 \sum_{r=1}^{N-1} \left[1 + r(e^{\gamma} - 1)\right] e^{-\gamma r} \, \hat{\phi}_m(r) \tag{155}$$

Now $\hat{\phi}_m(r)$ is a form which is frequently used to find the correlation function. The different values of α or γ then simply correspond to different weighting factors on the correlation function estimated as indicated in Eq. (154). Computationally, this is a highly desirable form.

Making use of Eqs. (28), (118), and (154), it can be shown that

$$\hat{\phi}_y = -2 \sum_{r=1}^{N-1} r\, e^{-\gamma(r-1)} \hat{\phi}_m(r) \tag{156}$$

The limiting form of Eqs. (155) and (156) as $\gamma \to \infty$ is given by the following formulae:

$$\lim_{\gamma \to \infty} \hat{\phi}_x = \hat{\phi}_m(0) + 2\hat{\phi}_m(1) \tag{157}$$

$$\lim_{\gamma \to \infty} \hat{\phi}_y = -2\hat{\phi}_m(r) \tag{158}$$

These equations, (157) and (158), are the same as that employed for the simple correlation technique. The results contained with this note and Apollo Note 416 indicate an approach to processing measurement noise data has been obtained for a large class of noise sources which will allow relatively simple techniques to be employed to arrive at highly efficient estimates provided that reliable estimates can be made by any technique.

The third part of this report will indicate the characteristics of some noise sources pertinent to the Apollo effort.

The Bissett-Berman Corporation 2941 Nebraska Avenue, Santa Monica, California EXbrook 4-3270

H. Epstein
27 April 1966

APOLLO NOTE NO. 420
(Task I, Item I)

A TECHNIQUE FOR THE RTCC TO CORRECT MEASUREMENT DATA FOR THE EFFECT OF THE TROPOSPHERE

This note is addressed to a technique for compensation of measurement data for the effect of regular tropospheric effect. Analysis performed to date have indicated that the effect of the troposphere on range, doppler, and angle measurement data can readily be reduced by an order of magnitude with simple compensation techniques. Apollo Note No. 293 provides the basis for the correction. Later Apollo notes indicated that the simple slab model will yield suitable accuracy for present purposes. Equations (14) and (18) of Appendix D, (Apollo Note 293), yield the desired results. A slightly different terminology will be employed to emphasize the predominant parameter on measurement data above five degrees elevation angle. The two parameters employed are zenith range error (R_z) and surface reflectivity (N_o). N_o as used here is defined differently from the common form in the literature N_s for mathematical convenience ($N_s = N_o \times 10^{+6}$). For elevation angles above five degrees, the range and doppler errors are primarily influenced by R_z while the elevation angle error is primarily influenced by N_o.

The results of Apollo Note 293 are most simply applied to situations wherein negligible spacecraft motion occurs during the transit time of the signal. The more general results can be had by a simple extension of the previous results. One other factor should be mentioned prior to the analytical results. It is expected that a troposhere correction will be made to measurement data by the RTCC. It is highly desirable that the RTODP be tested against more accurate post flight quality ODP's. A post flight ODP employed to test the RTODP should at least equal, or preferably excel in all aspects, the performance of the RTODP.

The geometry of the situation is indicated in Figure 1. The times, position vectors, and elevation angles of interest are indicated below.

Let

t_r = time the signal is being received

Δt_v = time difference between the time the signal is received at the receiving station and the time the signal was received at the spacecraft

$\Delta t_s = \tau$ = time difference between the time that the signal was received at the receiving station and the time the signal was transmitted by the transmitting station

$\vec{R}_R(t)$ = position of the receiving station at time t

$\vec{R}_T(t)$ = position of the transmitting station at time t

$\vec{R}_V(t)$ = position of the spacecraft at time t

$\phi_2(t_R)$ = true elevation angle measured at the receiving station determined by the position of the receiving station at time t_r and the spacecraft at time $t_r - \Delta t_v$

$\phi_1(t_R)$ = true elevation angle measured at the transmitting station determined by the transmitting station location at time $t_r - \tau$ and the spacecraft at time $t_r - \Delta t_v$

ϕ_{o-1} = apparent elevation angle corresponding to ϕ_1

ϕ_{o-2} = apparent elevation angle corresponding to ϕ_2

$\Delta\phi_1$ = troposphere elevation error corresponding to ϕ_{o-1}

$\Delta\phi_2$ = " " " " " ϕ_{o-2}

The equations are written in terms of apparent elevation angle in the referenced Apollo notes. As a consequence, the appropriate apparent elevation angles need to be computed first. An iterative

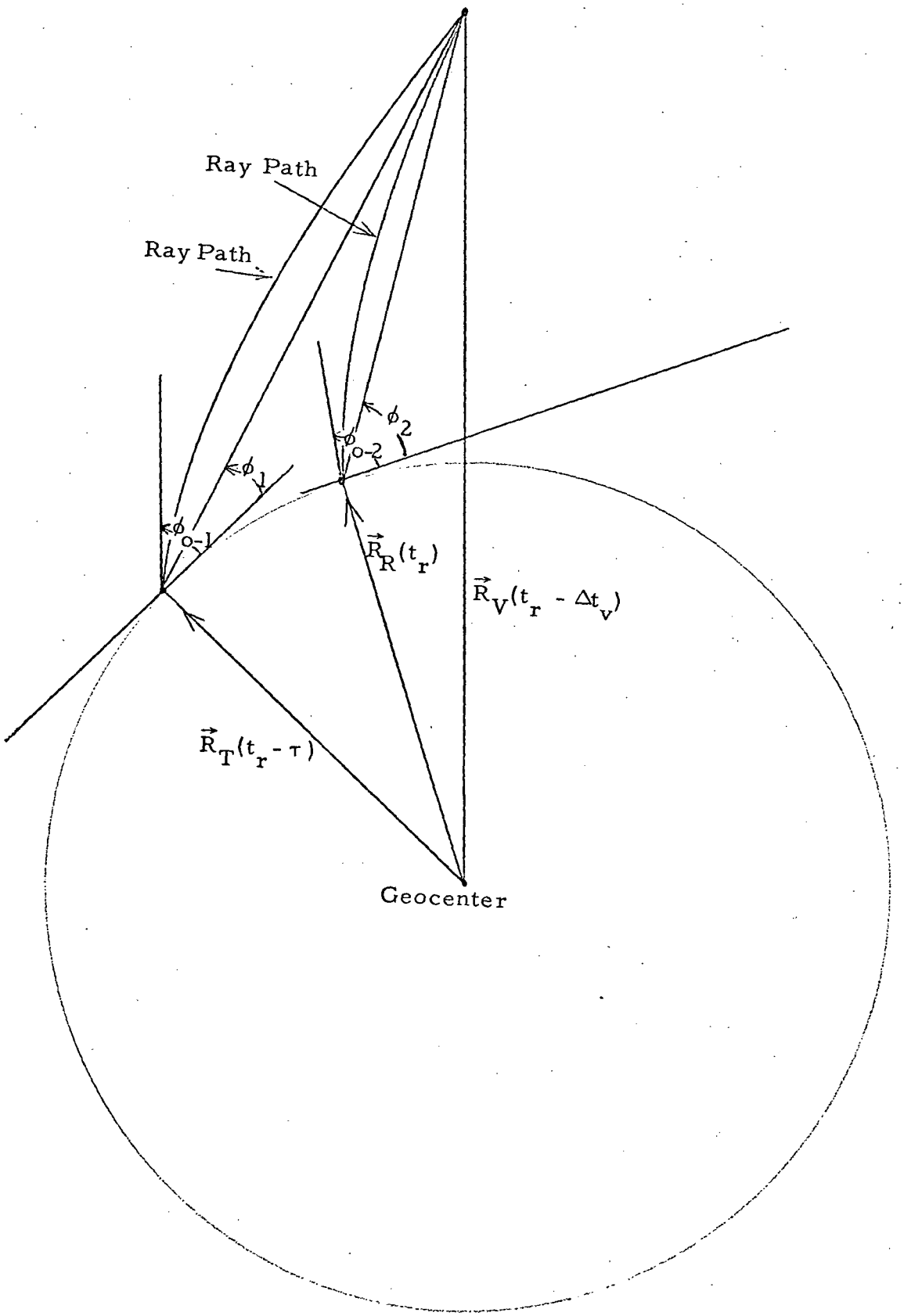

Figure 1. Geometry for Troposphere Correction

technique is required to find the proper apparent elevation angle. The ODP can provide the proper true elevation angles from the location of stations and spacecraft at appropriate times involved (see Figure 1).

It will be assumed in the analysis that the altitude of any station above sea level is negligibly small with respect to the radius of the earth. (This does not restrict the zenith range errors at the various stations to the same value.) With this minor limitation in mind, Eq. (14) and (18), (Appendix D, Apollo Note 293), may be written in terms of R_z and N_o as follows at each station as follows:

$$\Delta\phi = \frac{2N_o \cos\phi_o}{\sqrt{\sin^2\phi_o + \frac{2R_z}{N_o R_o}} + \sqrt{\sin^2\phi_o + 2\left(\frac{R_z}{N_o R_o} - N_o\right)}} \qquad (1)$$

$$\Delta R = \frac{4R_z}{\left[\sin\phi_o + \sqrt{\sin^2\phi_o + \frac{2R_z}{N_o R_o}}\right]\left[1 + \sqrt{\frac{\sin^2\phi_o + 2\left(\frac{R_z}{N_o R_o} - N_o\right)}{\sin^2\phi_o + \frac{2R_z}{N_o R_o}}}\right]} \qquad (2)$$

where for the 1959 ARDC atmosphere

N_o = index of refraction minus one = 2.73×10^{-4}

R_z = zenith range error = 2.31 meters

ϕ_o = apparent elevation elevation

ϕ = true elevation angle

$\Delta\phi$ = error in elevation angle = $\phi_o - \phi$

R_o = radius of the earth = 6.378×10^6 meters

The equations as written allow both two-way and three-way doppler (and range) tropospheric effects to be accommodated. The nature of the angle measurement equipment is to make tropospheric angle measurement errors a characteristic of the receiving station only, (independent of tropospheric errors at the transmitting station). The range measurable will be considered to be the total round trip distance. As a result, caution must be employed in factor of two which can occur for other quantities being considered the measurable.

The time t_r is the time at which the measurement is made at the receiving station.

The angle measurement error is then obtained from an iteration of:

$$\Delta\phi_2(t_r) = \frac{2N_{o-2}\cos\phi_{o-2}(t_r)}{\sqrt{\sin^2\phi_{o-2}(t_r) + \frac{2R_{z-2}}{N_{o-2}R_o}} + \sqrt{\sin^2\phi_{o-2}(t_r) + 2\left|\frac{R_{z-2}}{N_{o-2}R_o} - N_{o-2}\right|}} \quad (3)$$

and

$$\Delta\phi_2(t_r) = \phi_{o-2}(t_r) - \phi_2(t_r) \quad (4)$$

In the iteration process, particularly for elevation angles above 5 degrees, a good initial estimate for $\phi_{o-2}(t_r)$ to use in Eq. (3) is $\phi_2(t_r)$. It should be expected that no more than two iterations will be required to attain the desired accuracy if the initial estimate is used as suggested.

It is also necessary to obtain ϕ_{o-1} to compute the range and doppler errors. The iteration equations for this case are as follows:

$$\Delta\phi_1(t_r-\tau) = \frac{2N_{o-1}\cos\phi_{o-1}(t_r-\tau)}{\sqrt{\sin^2\phi_{o-1}(t_r-\tau) + \frac{2R_{z-1}}{N_{o-1}R_o}} + \sqrt{\sin^2\phi_{o-1}(t_r-\tau) + 2\left|\frac{R_{z-1}}{N_{o-1}R_o} - N_{o-1}\right|}} \quad (5)$$

and

$$\Delta\phi_1(t_r-\tau) = \phi_{o-1}(t_r-\tau) - \phi_1(t_r-\tau) \tag{6}$$

The round trip troposhere range error is then computed from the following equations:

$$\Delta R(t_r) = \Delta R_1(t_r-\tau) + \Delta R_2(t_r) \tag{7}$$

where

$$\Delta R_1(t_r-\tau) = \frac{4R_{z-1}}{\left[\sin\phi_{o-1}(t_r-\tau) + \sqrt{\sin^2\phi_{o-1}(t_r-\tau) + \frac{2R_{z-2}}{N_{o-2}R_o}}\right]\left[1+\sqrt{\frac{\sin^2\phi_{o-1}(t_r-\tau) + 2\left(\frac{R_{z-1}}{N_{o-2}R_o} - N_{o-1}\right)}{\sin^2\phi_{o-1}(t_r-\tau) + \frac{2R_{z-1}}{N_{o-2}R_o}}}\right]} \tag{8}$$

$$\Delta R_2(t_r) = \frac{4R_{z-2}}{\left[\sin\phi_{o-2}(t_r) + \sqrt{\sin^2\phi_{o-2}(t_r) + \frac{2R_{z-2}}{N_{o-2}R_o}}\right]\left[1+\sqrt{\frac{\sin^2\phi_{o-2}(t_r) + 2\left(\frac{R_{z-2}}{N_{o-2}R_o} - N_{o-2}\right)}{\sin^2\phi_{o-2}(t_r) + \frac{2R_{z-2}}{N_{o-2}R_o}}}\right]} \tag{9}$$

The round trip troposphere doppler error (ΔR_D) is then computed from the first difference of the range error at time t_r minus the range error at time $t_r - T$. T is the count time of the doppler counter and $t_r - T$ is the previous measurement time.

$$\therefore \quad \Delta R_D(t_r) = \Delta R(t_r) - \Delta R(t_r - T) \tag{10}$$

The Bissett-Berman Corporation 2941 Nebraska Avenue, Santa Monica, California EXbrook 4-3270

APOLLO NOTE NO. 421
(Task I, Item 1)

H. Engel
6 May 1966

CLOCK ERRORS IN ORBIT DETERMINATION

Clock errors have been considered in the OEAP. We are now faced with the problem of how these clock errors may be estimated in an ODP, so that we can find radar residuals that can be subjected to statistical analyses.

We will consider the case of three-way Doppler first. The signal received by the slave station (s) at time t_s was transmitted by the master station (m) at time t_m, and relayed by the spacecraft at time t_v.

We select an arbitrary origin (center of the Earth, if you wish) relative to which positions are described. Then, for instance, the position of the spacecraft at time t is $\vec{r}_v(t)$.

In the absence of clock errors - and there are to be no clock errors until we introduce them later - we know t_{s1} and t_{s2}, the beginning and end of the interval during which the Doppler cycles are counted. In order to find the estimated value of the measurable it is necessary to find t_{v2} by solving the relativistic version of the equation

$$t_{s2} - t_{v2} = \frac{\left|\vec{r}_s(t_{s2}) - \vec{r}_v(t_{v2})\right|}{c}$$

where $\bar{r}_s(t)$ and $\bar{r}_v(t)$ are the estimated positions of the slave station and spacecraft at time t, and c is the speed of light; this should be part of an ODP. A similar equation

$$t_{s1} - t_{v1} = \frac{\left|\vec{r}_s(t_{s1}) - \vec{r}_v(t_{v1})\right|}{c}$$

must be solved for t_{v1}.

Having t_{v2} and t_{v1}, two more, similar equations may be solved for t_{m2} and t_{m1}, the interval during which this signal was transmitted by the master station.

$$t_{m2} - t_{m2} = \frac{\left|\vec{r}_v(t_{v2}) - \vec{r}_m(t_{m2})\right|}{c}$$

$$t_v1 - t_{m1} \simeq \frac{\left|\vec{r}_v(t_{v1}) - \vec{r}_m(t_{m1})\right|}{c}$$

These four equations or their equivalent relativistic versions are non-linear but they may be solved by algorithms similar to

Step 1: $\Delta t_x = \begin{cases} \text{Previous value of } \Delta t_x, \text{ or 0 if} \\ \text{there is no previous value} \end{cases}$

Step 2: $t_x = t_s - \frac{\left|\vec{r}_v\ (t_s) - \vec{r}_s\ (t_s)\right|}{c}$

Step 3: $\vec{r}_v\ (t_v) = \vec{r}_v\ (t_x) + \dot{\vec{r}}(t_x)\,\Delta t_x$

Step 4: $\Delta t_x = \frac{\left|\vec{r}_v\ (t_s) - \vec{r}_s\ (t_s)\right| - \left|\vec{r}_v\ (t_v) - \vec{r}_s\ (t_s)\right|}{c}$

Step 5: $t_v = t_x + \Delta t_x$

Repeat Steps 3, 4 and 5 until the change Δt_x is sufficiently small.

Step 1: $\Delta t_y = \begin{cases} \text{Previous value of } \Delta t_y, \text{ or } \Delta t_x \\ \text{if there is no previous value} \end{cases}$

Step 2: $t_y = t_v - \dfrac{\left|\vec{r}_m(t_v) - \vec{r}_v(t_v)\right|}{c}$

Step 3: $\vec{r}_m(t_v) = \vec{r}_m(t_y) + \dot{\vec{r}}(t_y)\,\Delta t_y$

Step 4: $\Delta t_y = \dfrac{\left|\vec{r}_m(t_v) - \vec{r}_v(t_v)\right| - \left|\vec{r}_m(t_m) - \vec{r}_v(t_v)\right|}{c}$

Step 5: $t_m = t_y + \Delta t_y$

Repeat Steps 3, 4 and 5 until the change Δt_y is sufficiently small.

In the absence of clock errors the estimated Doppler count between t_{s1} and t_{s2} is

$$M_{est} = \frac{1}{2\pi}\left[\phi_s(t_{2s}) - \phi_m(t_{2m}) - \phi_s(t_{1s}) + \phi_m(t_{1m})\right]$$

$$= \frac{1}{2\pi}\left[\left\{\phi_s(t_{2s}) - \phi_s(t_{1s})\right\} - \left\{\phi_m(t_{2m}) - \phi_m(t_{1m})\right\}\right]$$

in which $\phi_s(t)$ is the phase of the slave clock at t and $\phi_m(t)$ is the phase of the master clock at t. We have

$$\phi_s(t_{2s}) - \phi_s(t_{1s}) = \omega_o(t_{2s} - t_{1s})$$

and

$$\phi_m(t_{2m}) - \phi_m(t_{1m}) = \omega_o(t_{2m} - t_{1m})$$

in which ω_o is the angular frequency of each station (ignoring the frequency offset of the slave station used to obtain a non-ambiguous Doppler count). Then

$$M_{est} = \frac{\omega_o}{2\pi}\left[(t_{2s} - t_{1s}) - (t_{2m} - t_{1m})\right]$$

The frequency offset is some multiple $\alpha\omega_o$ of ω_o, so that the measured number of Doppler cycles must be compared with

$$M_{est} = \frac{\omega_o}{2\pi}\left[(1+\alpha)(t_{2s} - t_{1s}) - (t_{2m} - t_{1m})\right]$$

We now introduce the clock errors. The time indicated by the slave station clock at ephemeris time (or UMT or whatever time is employed) t_s is called $\overline{t}_s$. The corresponding indicated time at the master station at ephemeris time (or other) t_m is called $\overline{t}_m$. We express t_s and t_m in terms of $\overline{t}_s$ and $\overline{t}_m$ as

$$t_s = \overline{t}_s + A_s + B_s\overline{t}_s + C_s\overline{t}_s^{\,2}$$

$$t_m = \overline{t}_m + A_m + B_m\overline{t}_m + C_m\overline{t}_m^{\,2}$$

in which A_s, B_s, C_s, A_m, B_m and C_m are all very small.

Then, the actual measurements are in the interval from $\bar{t}_{s1}$ to $\bar{t}_{s2}$. Using the estimated values of A_s, B_s and C_s the estimated values of t_{s2} and t_{s1} can be computed. Using the iteration algorithm presented previously, t_{v2}, t_{v1}, t_{m2} and t_{m1} can then be calculated. Having t_{m2} and t_{m1} it is possible to calculate $\bar{t}_{m2}$ and $\bar{t}_{m1}$, but this involves solution of quadratic equations. In order to avoid solution of these quadratic equations, we may write

$$t_m \overset{o}{=} \bar{t}_m + A_m + B_m \left[(\bar{t}_m - t_m) + t_m\right] + C_m \left[(\bar{t}_m - t_m) + t_m\right]^2$$

$$= \bar{t}_m + A_m + B_m t_m + C_m t_m^2 + (\bar{t}_m - t_m) \left[B_m + C_m (\bar{t}_m + t_m)\right]$$

Now $(\bar{t}_m - t_m) B_m$ and $C_m (\bar{t}_m - t_m)(\bar{t}_m + t_m)$ are small compared to the other terms in this last equation, so we may write

$$\bar{t}_m = t_m - A_m - B_m t_m - C_m t_m^2$$

and so solve for $\bar{t}_{m1}$ and $\bar{t}_{m2}$ using linear equations.

The estimated value of the measurable is then

$$M_{est} = \frac{1}{2\pi} \left[\left\{\phi_s(\bar{t}_{2s}) - \phi_s(\bar{t}_{1s})\right\} - \left\{\phi_m(\bar{t}_{2m}) - \phi_m(\bar{t}_{1m})\right\}\right]$$

Let us examine the relation between $\phi_m(\bar{t}_m)$ and $\bar{t}_m$. We have that

$$\phi_m(\bar{t}_{m2}) - \phi(\bar{t}_{m1}) = \int_{\bar{t}_{m1}}^{\bar{t}_{m2}} \omega_o \, d\bar{t}_m$$

in which ω_o is a <u>fixed number</u> built into the hardware and is not an estimate; so many cycles of the master oscillator means so large a change in apparent time. Since ω_o is a constant

$$\phi_m(\bar{t}_{m2}) - \phi_m(\bar{t}_{m1}) = \omega_o(\bar{t}_{m2} - \bar{t}_{m1})$$

In like fashion

$$\phi_s(\bar{t}_{s2}) - \phi_s(\bar{t}_{s1}) = (1 + \alpha)\,\omega_o(\bar{t}_{s2} - \bar{t}_{s1})$$

so that

$$M_{est} = \frac{\omega_o}{2\pi}\left[(1 + \alpha)(\bar{t}_{2s} - \bar{t}_{1s}) - (\bar{t}_{2m} - \bar{t}_{1m})\right]$$

and this is the quantity to be compared with the measured three-way Doppler count between $\bar{t}_{s1}$ and $\bar{t}_{s2}$.

For the estimated two-way Doppler measurable the computations are similar, except that the receiving station and transmitting station are one and the same. In this case the equation for M_{est} is of the same form as that in the three-way Doppler

$$M_{est} = \frac{\omega_o}{2\pi}\left[(1 + \alpha)(\bar{t}_{2r} - \bar{t}_{1r}) - (\bar{t}_{2t} - \bar{t}_{1t})\right]$$

but the times are times of reception by the master ($\bar{t}_r$) and times of transmission by the master ($\bar{t}_t$). The times $\bar{t}_r$ are given, the times $\bar{t}_t$ must be computed. The relationship between each of these terms and the "real" times t is

$$\bar{t} = t_m - A_m - B_m t_m - C_m t_m^2$$

The estimated range measurable as determined at receiving time $\bar{t}_r$ is the count

$$M_{est} = \frac{\omega_o}{2\pi} \left[\bar{t}_r - \bar{t}_t \right]$$

in which, once more,

$$\bar{t} = t_m - A_m - B_m t_m - C_m t_m^2$$

and $\bar{t}_t$ must be computed.

The partial derivatives of the measurables with respect to the clock parameters must be computed for use in orbit determination. Starting with the three-way Doppler, we have

$$\frac{\partial M_{est}}{\partial a_i} = \frac{\omega_o}{2\pi} \left[(1+\alpha) \left(\frac{\partial \bar{t}_{2s}}{\partial a_i} - \frac{\partial \bar{t}_{1s}}{\partial a_i} \right) - \left(\frac{\partial \bar{t}_{2m}}{\partial a_i} - \frac{\partial \bar{t}_{1m}}{\partial a_i} \right) \right]$$

in which a_i is any of the parameters A_s, B_s, C_s, A_m, B_m, or C_m.

Now for all these parameters $\partial \bar{t}_s / \partial a_i$ is zero. The computations for $\partial \bar{t}_m / \partial a_i$ are a little more complicated. We have that

$$\frac{dt_s}{d\bar{t}_s} = 1 + B_s + 2C_s \bar{t}_s$$

and dt_m / dt_s should be available from the ODP, since it is needed even in the absence of clock errors. We also have

$$\frac{d\bar{t}_m}{dt_m} = 1 - B_m - 2C_m t_m$$

so for a_i equal to A_s, B_s or C_s

$$\frac{\partial \bar{t}_m}{\partial a_i} = \frac{d\bar{t}_m}{dt_m} \frac{dt_m}{dt_s} \frac{\partial t_s}{\partial a_i}$$

where

$$\frac{\partial t_s}{\partial a_i} = \begin{cases} 1 \text{ for } a_i = A_s \\ \bar{t}_s \qquad B_s \\ \bar{t}^2 \qquad C_s \end{cases}$$

and

$$\frac{\partial \bar{t}_m}{\partial a_i} = \begin{cases} 1 \text{ for } a_i = A_m \\ -\bar{t}_m \qquad B_m \\ -\bar{t}_m^{\,2} \qquad C_m \end{cases}$$

Now, considering the case of two-way Doppler, we have

$$\frac{\partial M_{est}}{\partial a_i} = \frac{\omega_o}{2\pi} \left[(1+\alpha) \left(\frac{\partial \bar{t}_{2r}}{\partial a_i} - \frac{\partial \bar{t}_{1r}}{\partial a_i} \right) - \left(\frac{\partial \bar{t}_{2t}}{\partial a_i} - \frac{\partial \bar{t}_{1t}}{\partial a_i} \right) \right]$$

in which a_i is A_m, B_m, C_m of that station. We have that $\partial \bar{t}_2 / \partial a_i$ is zero, but recollecting that the transmitter is a master station

$$\frac{\partial \bar{t}_m}{\partial a_i} = \frac{d\bar{t}_m}{dt_m} \frac{dt_t}{dt_r} \frac{\partial t_r}{\partial a_i}$$

in which dt_t/dt_r should be available from the ODP, and

$$\frac{\partial t_r}{\partial a_i} = \begin{cases} 1 \text{ for } a_i = A_m \\ \bar{t}_r \qquad B_m \\ \bar{t}_r^{\,2} \qquad C_m \end{cases}$$

Let us digress for a while now to determine what clock parameters actually can be estimated.

Consider, first, the case in which several stations are employed. Each has a perfect clock, except that all clocks have the same time offset. Under these circumstances there is no practical way to determine from the radar data that such an offset exists; the estimate of the orbit is just determined according to the offset time. Actually, if the lunar ephemeris were perfect, the clock offset could be detected for a spacecraft in orbit about the Moon. The errors in the ephemeris make this impractical. The offset of one clock relative to another, however, can be estimated.

Next, consider the case in which several stations are employed. Each has a perfect clock, except that all clocks have the same rate error. Again, there is no practical way in which to estimate the clock error. One can visualize a way in which this could be done for a vehicle orbiting the Earth if the Earth's gravitation were known perfectly, but the errors in the estimates of the Earth gravitational potential result in far larger residuals than would the clock errors we are trying to estimate. (If, for a spherical Earth, μ were known perfectly, then the discrepancy between the actual orbit period of the spacecraft and that measured by the clock

$$\left[= 2\pi \sqrt{\frac{r^3}{\mu}} \right]$$

could be used to determine the clock rate error.)

In summary, absolute clock errors cannot be estimated (unless these clock errors are orders of magnitude larger than those in which we are interested) but the difference between clocks can be estimated. Therefore, in the ODP we must take one clock as being correct, and find the errors of other clocks relative to it. In this case the values of A, B and C associated with the station that is taken as correct are zero, and the values of A, B and C for other stations are considered as differences from the values for the station that is "correct."

The Bissett-Berman Corporation 2941 Nebraska Avenue, Santa Monica, California EXbrook 4-3270

APOLLO NOTE NO. 422
(Task I, Item I)

H. Epstein
1 June 1966

TECHNIQUES FOR ESTIMATION OF PARAMETERS ASSOCIATED WITH STATISTICAL TYPE ERROR SOURCES

PART III - Characteristics of Individual Noise Sources

INTRODUCTION

This Note will deal with the properties of several statistical type measurement error sources which have been encountered in DSIF residual data or test data on rubidium atomic standards. The presence of these types of error sources must be expected in USBS measurement data. Specifically, noise sources with certain properties, to be indicated in a later portion of this note, will be present in doppler tracking data with only the level of associated parameters differing between DSIF and USBS tracking stations.

It is important at this point to reiterate that a distinction should be placed between measurement errors and errors in desired end quantities (e.g., state vectors or dive angle). The processing performed on the measurement data to arrive at the desired end quantities as well as the measurement error characteristics determines the dominant error sources.

The purpose of the series of Apollo Notes (416, 419, this note, and a number to follow) is to establish high confidence estimates of measurement error sources which may prove to be important for Apollo applications. Somewhat repetitiously, analyses to be performed on measurement error data is specifically performed to achieve reliable estimates of the characteristics of dominant measurement error sources rather than attempt to ascertain "all" of the measurement errors. In summary, the measurement error model should possess the following characteristics.

1. Include all dominant error sources.
2. Obtain highly reliable estimates of the nature of pertinent noise characteristics.
3. Representation should be as simple as consistency with results will allow.
4. The model should be sufficiently complete that only the values of associated parameters need to be determined.

The characteristics of the noise sources have been determined and will continue to be determined primarily from equipment test data and spacecraft tracking data. Theoretical analyses are employed to aid in the identification of individual error components. Primary emphasis will be placed in this note on results applicable to the doppler mode of tracking by the USBS. However, the mathematical formulation will be suitable for use with range, angle or other types of measurement data. Evidence available to date indicate that the dominant statistical type sensor error source in the doppler model may be associated with the rubidium atomic standard and its associated frequency synthesizer. Other sensor noise sources which have been observed in tracking data may be associated with the doppler counter quantization error, and a small random phase error (probably associated with a phase-locked loop in the ground-based receiving station).

Non-stationary noise models are indicated as being appropriate on the measurable from either theoretical or analytical consideration at times. When this occurs, simple pre-whitening techniques will be employed to allow simple processing techniques to be employed to arrive at reliable estimates for associated parameters. Examples which will be treated are uncorrelated phase noise, white frequency noise, and flicker frequency noise. The terminology employed above will be explained in more detail in later sections of this note. Results will be indicated for both two-way and three-way doppler modes of operation. The pre-whitening technique to be employed will be indicated first.

I. PRE-WHITENING TECHNIQUE

No distinction other than scale factor needs to be made regarding useage of the terms range noise, phase noise, or accumulated count noise for present purposes. Range noise will be the term used at this time. The terms doppler and average range rate noise is obtained from the range noise by the subtraction of adjacent range intervals (first different) and dividing the quantity by the time elapsed between the range measurement.

If a stationary range noise component (n(t)) is present, then the spectral density $W_n(f)$ of the noise source and the autocorrelation function ($\phi_n(\tau)$) are Fourier cosine transforms of one another. These relationships may be written in the following fashion.

$$\phi_n(\tau) = \int_{-\infty}^{\infty} df\, W_n(f) \cos \omega\tau = 2 \int_{o}^{\infty} df\, W_n(f) \cos \omega\tau \qquad (1)$$

and $$W_n(f) = \int_{-\infty}^{\infty} d\tau\, \phi_n(\tau) \cos \omega\tau = 2 \int_{o}^{\infty} d\tau\, \phi_n(\tau) \cos \omega\tau \qquad (2)$$

where f = frequency (cps)
and $\omega = 2\pi f$ = angular frequency (radians per sec.)

These relationships are valid so long as the integrals expressed in equations (1) and (2) exist. The integral expressed by equation (1) will not exist for the simple noise models which will be presented shortly. The models which will be presented are simple in nature and account for effects both encountered in the analysis of spacecraft tracking data and the rubidium atomic standard data to date. The pre-whitening technique may be considered as a device to make the integrals exist or form stationary noise sources. The primary objective of pre-whitening is to allow simple processing techniques to be used to obtain estimates of parameters associated with noise sources. It is further desired that the pre-whitening function

employed result in a correlation function which by simple techniques lead to a covariance function for range or doppler.

The pre-whitening technique which will be employed is suitable for the class of noise sources with the following properties: one, the power spectral density is finite for all finite values of frequency (f) with the possible exception of f = 0; and two, the behaviour near f = 0 and f = $\pm\infty$ may be suitably approximated by a power of f. With these two restrictions, it is only necessary to examine the behaviour of the integral near zero and infinity to establish conditions for stationary behaviour after pre-whitening. The selected pre-whitening function ($W_{p-w}(f)$) is given below by the following formula.

$$W_{p-w}(f) = \frac{K_{p-w}\,(1 - \cos \omega T_1)^{M_1}}{\left[1 + (\omega T_2)^2\right]^{M_2}} \tag{3}$$

where K_{p-w} = a positive parameter selected for normalization purposes

T_1 = selected time interval which for doppler counters would be selected as the count time

T_2 = a smoothing time constant

M_1 = a selected positive integer or zero

M_2 = a selected positive integer or zero

$$\text{and } (\phi_n(\tau))_{p-w} = 2\int_0^\infty df\, W_n(f)\, W_{p-w}(f) \cos \omega\tau = \phi_m(\tau) \tag{4}$$

$$\text{Sufficiently near to zero frequency, } W_{p-w}(f) \propto f^{2M_1} \tag{5}$$

$$\text{Sufficiently near to infinite frequency, } W_{p-w}(f) \propto f^{-2M_2} \tag{6}$$

If we indicate the behaviour of $W_n(f)$ near zero frequency and near positive infinite frequency as the low frequency and high frequency behavious respectively, then the following forms are appropriate subject to $W_n(f)$ behaving as a power of f in these regions.

low frequency, $W_n(f) \sim f^{-p_1}$ (7)

high frequency, $W_n(f) \sim f^{-p_2}$ (8)

where p_1 and p_2 may take on any finite value.

The two conditions for stationary may then be shown from equations (1), (5), (6), (7), and (8) to be

$$p_1 - 2M_1 < 1 \tag{9}$$

$$p_2 - 2M_2 < 1 \tag{10}$$

Better forms for the selection of M_1 and M_2 which may be obtained from equation (9) and (10) are as follows.

$$M_1 > \frac{p_1 - 1}{2} \tag{11}$$

$$M_2 > \frac{1 - p_2}{2} \tag{12}$$

$M_1 = 0$ is satisfactory for $p_1 < 1$ which indicates that no low frequency filtering is necessary for this situation. $M_2 = 0$ is satisfactory for $p_2 > 1$ which indicates that no high frequency filtering is necessary for this situation. T_1 will not appear for $M_1 = 0$ and similarly T_2 does not appear for $M_2 = 0$. T_1 for most cases will be selected as the interval between successive measurements for uniform measurement intervals. This corresponds to the count time in doppler measurements. T_2 can frequently be obtained from the processing which has taken place in the equipment which processed the raw data to obtain the readings at selected time intervals. K_{p-w} as indicated earlier is simply a convenient numerical normalization factor.

Perhaps the rational for the factor $(1 - \cos \omega T_1)^{M_1}$ should be further explained. The R^{th} difference ($\Delta^R n$) of a noise source

with successive measurements at intervals of T_1 may be given by the following expression.

$$\Delta^R n(t) = \sum_{r=0}^{R} \frac{R!\,(-1)^r}{r!\,(R-r)!}\, n(t - rT_1) \tag{13}$$

Given that the LaPlace transform of n(t) is n(s), it can be shown that the LaPlace transform of Δ^R n(t) is given by the following formula.

$$L\left\{\Delta^R n(t)\right\} = n(s) \sum_{r=0}^{R} \frac{R!}{r!\,(R-r)!}\left(-e^{-srT_1}\right)^r = n(s)\left(1 - e^{-sT_1}\right)^R \tag{14}$$

The power spectral density is then obtained by replacing S by $j\omega$ and multiplying equation (14) by its complex conjugals. The final result is given below as:

$$W_\Delta(f) = W_n(f)\left[2(1 - \cos \omega T_1)\right]^R \tag{15}$$

where $W_\Delta(f)$ = spectral density of the R^{th} difference

$W_n(f)$ = spectral density of the original noise source.

The result obtained in equation (15) suggests that K_{p-w} should contain a factor of 2^R and R should be taken as M_1. Appropriate values of R will be shown as 0, 1, or 2 for the individual noise sources which will be considered in the following section.

II. MODELS FOR CORRELATION FUNCTIONS OF INDIVIDUAL NOISE SOURCES AFTER PRE-WHITENING

For stationary noise sources the functional form for the correlation function and spectral distribution need only be given for positive values of lag and frequency from the symmetry involved. Equation (4) will be indicated again for the sake of convenience in this section.

$$\phi_m(\tau) = 2 \int_o^\infty df\, W_n(f)\, W_{p\text{-}w}(f) \cos\omega\tau \tag{16}$$

The first noise model to be considered will be for n(t) a white frequency noise.

A. $W_n(f) = K$ (uncorrelated range noise)

$p_1 = p_2 = 0$ for this type noise.

We may then choose $M_1 = 0$ and $M_2 = 1$ for this noise source as being consistent with equations (11) and (12). Choosing $K_{p\text{-}w} = 1$, from equation (3) and (16) it can be shown that

$$\phi_m(\tau) = 2K \int_o^\infty \frac{df \cos\omega\tau}{1 + (\omega T_2)^2} = \frac{K}{2T_2}\, e^{-\left|\frac{\tau}{T_2}\right|} \tag{17}$$

and that the normalized autocorrelation function is given by

$$\rho_m(\tau) = \frac{\phi_m(\tau)}{\phi_m(o)} = e^{-\left|\frac{\tau}{T_2}\right|} \tag{18}$$

Now for $\left|\frac{\tau}{T_2}\right| >> 1$, $\rho_m(\tau) << 1$ and the noise may be considered as being uncorrelated. Two uncorrelated range noise sources have been found present in Ranger and Mariner Spacecraft tracking data. One is associated with the quantization error present in the doppler counting technique and the other probably with phase-locked loops in the ground-based receiving system.

The form of the measurable employed in the doppler mode for processing to determine such quantities as state vectors is the range difference divided by the associated time interval. Apollo spacecraft doppler tracking data is expected to be all of a continuous count (non-destructive count) nature. The doppler correlation function for this mode will be indicated below for an uncorrelated range noise source. The uncorrelated range noise source may be written in the following fashion.

$$E\left\{ m(t) \right\} = 0 \tag{19}$$

$$E\left\{ m(t)\, m(t - rT) \right\} = \phi_m \qquad r = 0 \tag{20a}$$

$$= 0 \qquad r \neq 0 \tag{20b}$$

Considering the doppler measurable as indicated below

$$e(t) = \frac{1}{T}\left[m(t) - m\,(t - T) \right] \tag{21}$$

Then $$E\left\{ e(t) \right\} = 0 \tag{22}$$

$$\phi_e\,(r) = E\left\{ e(t)\, e(t - rT) \right\} = \frac{2\phi_m}{T^2} \qquad r = 0 \tag{23a}$$

$$= -\frac{\phi_m}{T^2} \qquad |r| = 1 \tag{23b}$$

$$= 0 \qquad |r| \neq 0,\ 1 \tag{23c}$$

The normalized autocorrelation function is then given as

$$\rho_e(r) = \frac{\phi_e(r)}{\phi_e(o)} = 1 \qquad r = 0 \tag{24a}$$

$$= -\frac{1}{2} \qquad |r| = 1 \tag{24b}$$

$$= 0 \qquad |r| \neq 0,\ 1 \tag{24c}$$

This form may be recognized as one of the noise sources used for numerical analysis in Apollo Notes 416 and 419.

B. Three-Way Doppler Mode

The additional noise sources which will be considered for the three-way and two-way doppler modes may be associated with the combination of atomic frequency standard unit and frequency synthesizer. In the three-way mode, the critical frequencies are derived from separate atomic standards for transmitting and receiving purposes. All critical frequencies are derived from one frequency standard in the two-way mode. The best evidence available to date indicates that the rubidium atomic standards possess both a white frequency noise component and a flicker frequency noise component. A third noise component is also present which should only be significant for count intervals less than about .2 seconds. This third noise component will not be considered at this time.

Transmitting and receiving noise sources are considered as uncorrelated in the three-way doppler mode. As a consequence, the variance of each noise source of a given nature should be added to form the overall noise for a given type of noise (e.g., white frequency or flicker noise). The three-way analysis will treat the transmitting and receiving noise component separately. The white frequency noise will be treated first and then the flicker frequency noise both for the continuous count mode.

B-1. Three-Way White Frequency Noise ($W_n(f) = \frac{K}{\omega^2}$)

$p_1 = p_2 = 2$ for this type noise.

We may choose $M_1 = 1$ and $M_2 = 0$ for this noise source as being consistent with equations (11) and (12). The choice of $K_{p-w} = \frac{2}{T^2}$ and $T_1 = T$ = count time makes the processed noise directly

the "doppler" noise. Using the values and parameters selected above, it can be shown from equations (3) and (16) that

$$\phi_m(\tau) = \frac{4K}{T^2} \int_0^\infty \frac{df}{\omega^2} (1 - \cos \omega T) \cos \omega\tau \qquad (25)$$

After integration and simplification

$$\phi_m(\tau) = \frac{K}{T} \left[1 - \frac{|\tau|}{T} \right] \qquad |\tau| \leq 1 \qquad (26a)$$

$$= 0 \qquad |\tau| \geq 1 \qquad (27a)$$

Restricting ourselves to lag intervals an integral multiple (r) of the count interval, the following results may be directly obtained

$$\phi_m(o) = \frac{K}{T}$$

$$\rho_m(r) = \frac{\phi_m(r)}{\phi_m(o)} = 1 \qquad r = 0 \qquad (28a)$$

$$= 0 \qquad r \neq 0 \qquad (28b)$$

This is the other type noise source indicated in the examples contained in Apollo Notes 416 and 419. This noise component has been indicated in Ranger and Mariner tracking data.

B-2. Three-Way Flicker Frequency Noise ($W_n(f) = \frac{K}{|\omega|^3}$)

$p_1 = p_2 = 3$ for this type noise,

$M_1 = 2$ and $M_2 = 0$ are the values obtained by the choice of minimum values for these quantities which are either positive integers or zero. The choice of $K_{p\text{-}w} = \frac{4}{T^2}$ and $T_1 = T$ = count time makes this resultant processed noise the first difference of "doppler" residuals. (The doppler residuals themselves are not stationary.) Using the

values and parameters selected above, the substitution of equation (3) into equation (16) yields

$$\phi_m(\tau) = \frac{8K}{T^2} \int_0^\infty \frac{df}{\omega^3} (1 - \cos\omega T)^2 \cos\omega\tau \tag{29}$$

After integration by parts and simplication, the following result may be obtained.

$$\frac{2\pi\phi_m(a)}{K} = 6a^2 \ln|a| - 4(a+1)^2 \ln|a+1| - 4(a-1)^2 \ln|a-1| + (a+2)^2 \ln|a+2| + (a-2)^2 \ln|a-2| \tag{30}$$

where $a = \frac{\tau}{T}$

and $$\frac{2\pi\phi_m(a)}{K} = -4 \sum_{r=1}^{\infty} \frac{(4^r - 1)}{r(r+1)(2r+1)\, a^{2r}} \qquad \text{for } a > 2 \tag{31}$$

$$= -\frac{2}{a^2}\left(1 + \frac{1}{a^2} + \frac{3}{2a^4} + \frac{17}{6a^6} + \cdots\right)$$

The variance and a few values for the normalized autocorrelation function are given below.

$$\phi_m(0) = (8 \ln 2)\frac{K}{2\pi} = 5.54518\left(\frac{K}{2\pi}\right)$$

$$\rho_m(1) = -.2169$$

$$\rho_m(2) = -.1324$$

$$\rho_m(3) = -.0454$$

Additional values may be calculated as required with the aid of either equation (30) or equation (31). It may be noted that the correlation function is negative for lag values of one and greater. This might be

expected from the relationship between the correlation function and the spectral density with a zero value of the zero frequency spectral density.

C. Two-Way Doppler Mode

The results for the two-way doppler model of operation will be derived in a slightly different fashion for the sake of simplicity. The RF signal received via the spacecraft is a time delayed version of the signal at the receiver used for comparison purposes. This time delay is approximately the transit time from ground-based transmitter to the spacecraft and back to the ground-based receiver. Results will only be derived for the fixed period, continuous count mode of operation. Again both white frequency noise and flicker frequency noise will be considered. Both noise sources will be shown to be stationary doppler noise sources. No additional pre-whitening will be required. The doppler measurement noise (m(t)) for this case may be written in the following fashion.

$$T\, m(t) = n(t) - n(t - T) - \left[n(t - \tau_d) - n(t - \tau_d - T) \right] \tag{32}$$

After taking the LaPlace transform and multiplying by the complex conjugate with S replaced by $j\omega$, the following result may be obtained.

$$W_m(f) = \frac{4}{T^2} (1 - \cos \omega \tau_d)(1 - \cos \omega T)\, W_n(f) \tag{33}$$

where T = count time

τ_d = delay time

$$\text{as before } \phi_m(\tau) = 2 \int_0^\infty df\, W_m(f) \cos \omega \tau \tag{34}$$

Equations (33) and (34) are satisfactory as they stand for the two noise sources to be considered.

C-1. Two-Way White Frequency Noise. ($W_n(f) = \frac{K}{\omega^2}$)

$p_1 = -2$ and $p_2 = 2$ for this type noise with the inherent processing of the data.

$M_1 = M_2 = 0$ is then satisfactory and no additional pre-whitening is required. (K_{p-w} is taken as one.)

Using equations (33) and (34) and the assumed noise model, the following result may be obtained.

$$\phi_m(\tau) = 8K \int_0^\infty \frac{df\,(1 - \cos\omega T)}{(\omega T)^2} (1 - \cos\omega\tau_d) \cos\omega\tau \qquad (35)$$

After integration by parts and simplification the following result may be obtained.

$$\frac{2T\phi_m(a,b)}{K} = -4|a| + 2|a-1| + 2|a+1| + 2|a-b| + 2|a+b| - |a+b-1| - |a-b+1| - |a-b-1| - |a+b+1| \qquad (36)$$

where $a = \frac{\tau}{T}$ and $b = \frac{\tau_d}{T}$

Equation (36) is reasonably simple for numerical computational purposes. However, the physical picture is more difficult to extract. It can be shown from equation (36), $\phi_m(a,b) = 0$ for $a \geq 1 + b$. In addition, the zero lag value or variance is given by the following expressions.

$$\phi_m(0,b) = \frac{2Kb}{T} = \frac{2K\tau_d}{T^2} \qquad \frac{\tau_d}{T} = b \leq 1 \qquad (37a)$$

$$= \frac{2K}{T} \qquad \frac{\tau_d}{T} = b \geq 1 \qquad (37b)$$

Interest lies primarily with integer values for a. The one lag normalized auto-correlation has the following characteristics.

$$\rho_m(1,b) = \frac{\phi_m(1,b)}{\phi_m(0,b)} = -\frac{1}{2} \qquad b \leqslant 1 \tag{38a}$$

$$= -\frac{(2-b)}{4} \qquad 1 \leqslant b \leqslant 2 \tag{38b}$$

$$= 0 \qquad b \geqslant 2 \tag{38c}$$

Using equations (37a) and (38a) with the restriction of integer values for $a, b \leqslant 1$, and the property that $\phi_m(a,b) = 0$ for $a \geqslant 1 + b$

$$\rho_m(r) = 1 \qquad r = 0 \tag{39a}$$

$$= -\frac{1}{2} \qquad |r| = 1 \tag{39b}$$

$$= 0 \qquad |r| \neq 0, 1 \tag{39c}$$

This may be recognized as being the same result as for uncorrelated range noise. As a consequence, the techniques indicated in Apollo Notes 416 and 419 will not allow this noise component to be separated from uncorrelated range noise with $\tau_d < \tau$ and using only integer lag values for the correlation function. The minimum count time expected to be for Apollo purposes is one second. The delay time will be much less than one second for near earth phases. As a consequence, this type noise should be expected. In addition, for most transearth and translunar phases, the count time will be greater than 2-1/2 seconds which is the maximum delay time to be encountered on lunar mission (e.g., typically one minute or longer count time will be used). The principal exception will occur during tracking for LEM descent and LEM ascent for rendezvous. It might be expected for these cases that a count time of one second will be used with a delay time of about 2-1/2 seconds.

For simplicity, the results for the normalized autocorrelation function will be given for a and b integer and $b \geq 2$

$$\rho_m(r) = 1 \qquad r = 0 \tag{40a}$$

$$= -\frac{1}{2} \qquad |r| = b \tag{40b}$$

$$= 0 \qquad |r| \neq 0, b \tag{40c}$$

The $-\frac{1}{2}$ value for the normalized correlation function now occurs at a delay time equal to the transit time. This effect may be noted on Ranger 7, Mariner 4, and Pioneer residuals. For $b \geq 2$ and b not an integer the sum of the values of the normalized correlation function at the nearest integers above and below b will equal $-\frac{1}{2}$.

C-2 Two-Way Flicker Frequency Noise ($W_n(f) = \frac{K}{|\omega|^3}$)

$p_1 = -1$ and $p_2 = 3$ for this type noise with the inherent processing of the data.

M_1 and $M_2 = 0$ is then satisfactory and no additional pre-whitening is required (K_{p-w} is taken as one).

Using equations (33) and (34) and the assumed noise model, the following result may be obtained.

$$\phi_m(\tau) = 8K \int_0^\infty \frac{df\,(1 - \cos\omega T)(1 - \cos\omega\tau_d)\cos\omega\tau}{\omega^3 T^2} \tag{41}$$

After integration by parts and simplification, the following result may be obtained.

$$\begin{aligned}\frac{2\pi\phi_m(a,b)}{K} = {} & 4a^2 \ln|a| - 2(a-1)^2 \ln|a-1| - 2(a+1)^2 \ln|a+1| \\ & - 2(a-b)^2 \ln|a-b| - 2(a+b)^2 \ln|a+b| \\ & + (a+b+1)^2 \ln|a+b+1| + (a-b-1)^2 \ln|a-b-1| \\ & + (a+b-1)^2 \ln|a+b-1| + (a-b+1)^2 \ln|a-b+1|\end{aligned} \tag{42}$$

where $a = \frac{\tau}{T}$ and $b = \frac{\tau_d}{T} > 0$

Equation (42) is a rather cumbersome expression to interpret physically but is suitable for mathematical purposes. The result for $\tau_d = T$ (b = 1) corresponds to the results previously indicated relative to equation (30). Alternate expressions give better insight to the behaviour of the variance (a = 0) with respect to b.

$$\text{for } b \leqslant 1, \quad \frac{2\pi \phi_m(0,b)}{K} = 2(1+b)^2 \ell n (1+b) + 2(1-b)^2 \ell n (1-b) - 4b^2 \ell n b \qquad (43a)$$

$$= b^2 \left[4 \ell n \left(\frac{1}{b}\right) + 6 - 2 \sum_{r=1}^{\infty} \frac{b^{2r}}{r(r+1)(2r+1)} \right] \qquad (43b)$$

$$\text{for } b \geqslant 1, \quad \frac{2\pi \phi_m(0,b)}{K} = 2(b+1)^2 \ell n (b+1) + 2(b-1)^2 \ell n (b-1) - 4b^2 \ell n b \qquad (44a)$$

$$= 4 \ell n b + 6 - 2 \sum_{r=1}^{\infty} \frac{1}{r(r+1)(2r+1) b^{2r}} \qquad (44b)$$

Expressions (43b) and (44b) are particularly suitable for the purpose of physical understanding. It can be shown that the infinite series may be neglected for answers to within 10% accuracy. (1% accuracy for b > 2 or b < .5). Figure 1 is a graph of equations (43) and (44). The dashed region near b = 1 indicates the departure of equation (43b) and (44b) when the terms involved in the infinite series are neglected. It may be noted that b is a monotonically increasing function with b. Although the variance increases slowly with b for b > 1, the variance approaches infinity as b goes to infinity and the noise then no longer is stationary. This result should be expected. For infinite delay time, the correlation between the transmitting and receiving noise sources becomes unimportant and the results are similar to results one would obtain with two separate standards as in the three-

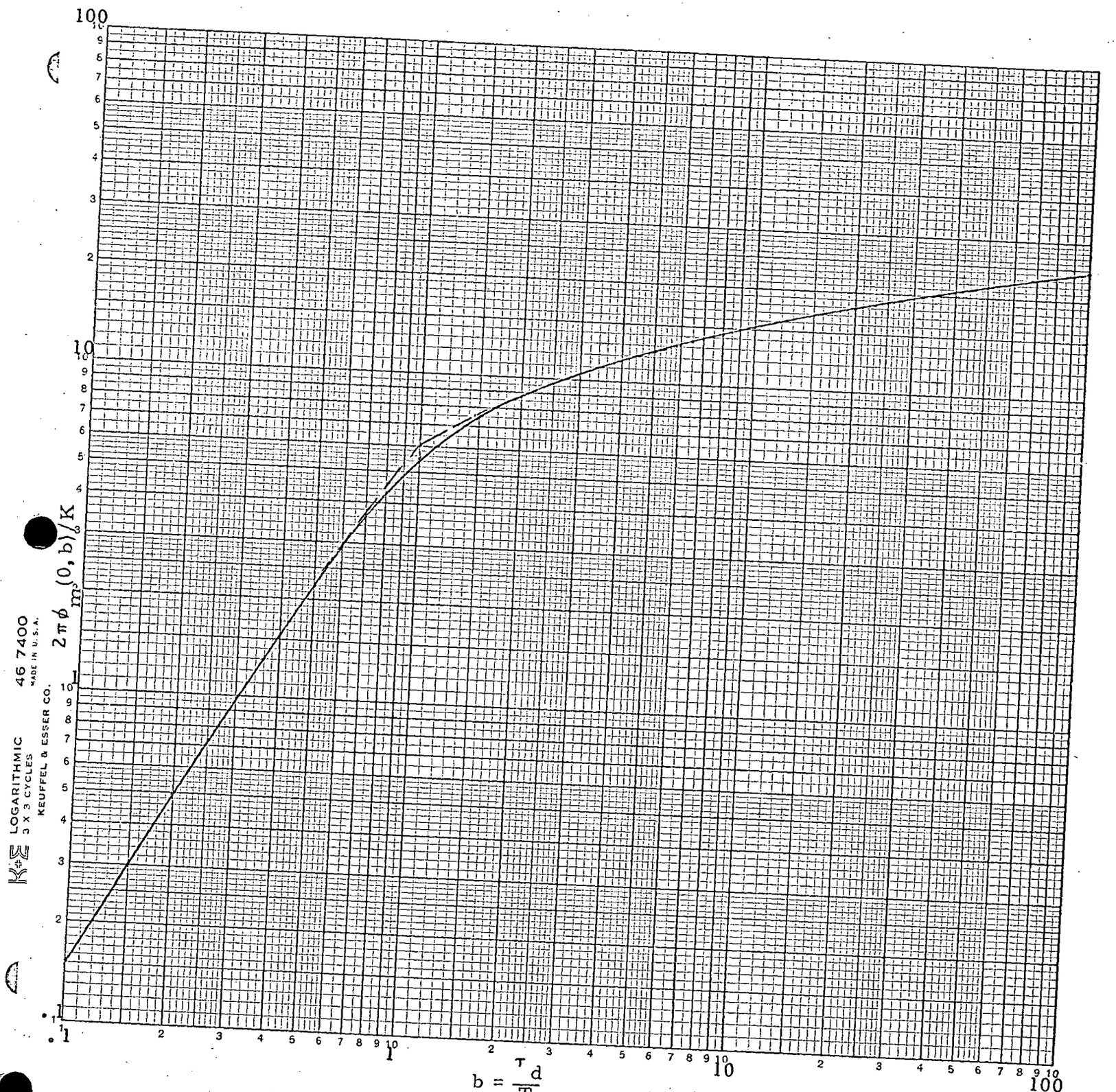

Figure 1. Variance of Flicker Frequency Noise vs. Normalized Delay Time.

way mode. (The results in Section B-2 indicated that three-way flicker frequency noise would be unstationary without additional pre-whitening.) Fortunately, this will be no problem for Apollo applications since b is less than about 2.5. The variance increases most rapidly for small values of b (variation approximately proportional to b^2) where the smallest variances occur.

An interesting result may be obtained for $a > b + 1$. The previous case of two-way white frequency noise indicated no correlation for $a > b+ 1$. After extensive manipulation, the following results may be obtained for the two-way flicker frequency noise.

for $a > b + 1$

$$\frac{2\pi \phi_m(a,b)}{K} = - \sum_{r=1}^{\infty} \frac{\left[(b+1)^{2r+2} + (b-1)^{2r+2} - 2b^{2r+2} - 2\right]}{r(r+1)(2r+1)\, a^{2r}} \qquad (45a)$$

$$= - \left[\frac{2b^2}{a^2} + \frac{b^4 + b^2}{a^4} + \frac{2b^6 + 5b^4 + 2b^2}{a^6} + - - - \right] \qquad (45b)$$

The result of equations (45a) and (45b) indicates that the correlation function will be negative and increase in a monotonic fashion to zero as a goes to infinity for $a > b + 1$.

Two further properties which can be obtained from equation (42) will be indicated. The one lag normalized correlation function will approach a value of $-\frac{1}{2}$ for $b << 1$ and a value of +1 for $b >> 1$. The normalized autocorrelation function at a lag value of b approaches $-\frac{1}{2}$ for $b >> 1$.

D. Summary of Properties of Individual Noise Sources

The noise sources analyzed in the previous section were uncorrelated range noise, two-way white frequency noise, two-way flicker frequency noise, three-way white frequency noise, and three-way flicker frequency noise. The results emphasized relationships appropriate to establish covariance matrices with continuous count

doppler (i.e., first difference of successive range count divided by time) as the form for the measurable to be employed for processing by the ODP.

The three-way flicker frequency noise was indicated as not being a stationary noise source with doppler as a measurable. In fact, this was the only non-stationary noise source considered. It was demonstrated that difference techniques could be employed to form a stationary noise source to simplify the estimation of the scale factor parameter associated with this type noise.

It was further shown that two-way white frequency noise with the delay time larger than the count time behaves similarly to uncorrelated range noise. This is rather important since this type noise should prove to be unimportant in the determination of state vector when the correct covariance noise matrix is used in place of the present simple noise covariance matrix which assumes no correlation on doppler noise.

Evidence available at this time indicates that a flicker frequency noise component will be present in the rubidium standards to be used by the USBS. No numerical estimate has been made regarding the magnitude of the scale factor parameter associated with this type noise to this date. A later Apollo note will attempt to establish an upper limit to this parameter. The three-way flicker noise component may prove to be the dominant noise source from the standpoint of accuracy of state vectors or other parameters of interest.

It is important to indicate a technique which will allow an estimate to be made of the degradation of accuracy due to non-stationary noises. This will be treated in a later Apollo note.

It has further been shown in this note that noise sources with considerable differences in nature of the spectral distribution may appear to have similar correlation functions. Under this situation,

the separation of noise components becomes much more difficult. As a consequence, care needs to be taken in how the data is taken to determine the noise characteristics.

The Bissett-Berman Corporation 2941 Nebraska Avenue, Santa Monica, California EXbrook 4-3270

APOLLO NOTE NO. 423
(Task 3)

Siska, C.
10 June 1966

MOON POSITION PARAMETER

The position vector of the Moon, $\vec{R}_{EM}(t)$, at time, t, is found by interpolating between values found on the lunar ephemeris tape. We introduce a Moon displacement parameter by considering that the Moon's position at true time t is actually that position found on the tape for time $t+\tau$, where τ is a constant time displacement. It is expected that the maximum value of τ will be about 1 second, corresponding to a displacement of the Moon along its path on the order of 1 kilometer.

Thus, the position vector of the Moon which is to be used in the ODP is defined as $\vec{R}^{1}_{EM}(t) = \vec{R}_{EM}(t+\tau)$. If the last term is expanded, we obtain,

$$\vec{R}^{1}_{EM}(t) = \vec{R}_{EM}(t) + \dot{\vec{R}}_{EM}(t)\tau + \ddot{\vec{R}}_{EM}(t)\frac{\tau^2}{2} + - - -$$

The maximum value of the acceleration term is on the order of 10^{-3} meters for τ equal to 1 second, so that the displacement vector of the Moon can be written

$$\vec{R}^{1}_{EM}(t) - \vec{R}_{EM}(t) \approx \dot{\vec{R}}_{EM}(t)\tau \qquad (1)$$

Since the dynamical equations for a lunar satellite will be solved in a selenocentric coordinate system, the Moon's displacement vector will cause the following two effects: (1) the position vector of the planets relative to the Moon will be slightly altered, and (2), the principal axis system of the Moon will be slightly displaced because librations are referenced to the Earth's relative position to the Moon.

The first effect will produce long period perturbation terms in the dynamical equations which lead to vehicle position changes on the order of 10^{-6} meters. Therefore, the planetary positions relative to the Moon can be computed without considering the Moon as being displaced.

With regard to the second effect, a 1 kilometer displacement of the Moon is equivalent to an angular displacement of the Earth about the Moon on the order of 0.25×10^{-5} radians. A displacement of the Moon's principal axis system of this order will have a negligible effect in calculating the Moon's gravitational potential forces upon vehicle. Therefore, in this case also, the displacement vector of the Moon's position can be ignored.

We must now find the partial derivatives of the measurable with respect to τ. We start with an artificial measurable, called the three-way range, and from it derive expressions for the desired partial derivatives.

The slant range vector from the Master station to the spacecraft can be written as

$$\vec{S}_1^{\,1} = -\vec{R}_M(t_M) + \vec{R}_{EM}^{\,1}(t_v) + \vec{r}_{MV}(t_v)$$

and the slant range vector from the spacecraft to the Slave station is

$$\vec{S}_2^{\,1} = \vec{R}_S(t_S) - \vec{R}_{EM}^{\,1}(t_v) - \vec{r}_{MV}(t_v)$$

where

t_M, t_v, t_S = time of transmission by the Master station, relay by the spacecraft, and receipt by the Slave station.

$\vec{R}_M(t_M), \vec{R}_S(t_S)$ = geocentric vectors to Master, Slave stations at the indicated times

$\vec{R}^1_{EM}(t_v)$ = geocentric vector to the displaced Moon at the time the signal is relayed by the spacecraft

$\vec{r}_{VM}(t_v)$ = selenocentric vector to spacecraft at time signal is relayed.

Using Equation (1), we can rewrite Equation (2) as

$$\vec{S}_1^{\,1} = \vec{S}_1 + \tau \dot{\vec{R}}_{EM}(t_v) \tag{3a}$$

$$\vec{S}_2^{\,1} = \vec{S}_2 + \tau \dot{\vec{R}}_{EM}(t_v) \tag{3b}$$

Now, $\vec{S}_1^{\,1}$ and $\vec{S}_2^{\,1}$ are related to the times t_M, t_v and t_S by

$$c(t_S - t_v) = \left|\vec{S}_2^{\,1}\right| \tag{4a}$$

$$c(t_v - t_M) = \left|\vec{S}_1^{\,1}\right| \tag{4b}$$

so the three-way range, which we will denote by m_3 is

$$m_3 = \left|\vec{S}_1^{\,1}\right| + \left|\vec{S}_2^{\,1}\right|$$

$$= c(t_v - t_M) + c(t_S - t_v)$$

$$= c(t_s - t_M)$$

The estimated value of the measurable is

$$\hat{m}_3 = c(\bar{t}_S - \hat{\bar{t}}_M). \tag{5}$$

The estimated values of $\hat{\bar{t}}_m$ and $\hat{m}$ are calculated from the measured time t_S, and the estimated parameters.

We have that

$$\frac{\partial \hat{m}_3}{\partial \tau} = \frac{\partial \hat{m}_3}{\partial \hat{\bar{t}}_m} \quad \frac{\partial \hat{\bar{t}}_m}{\partial \tau} = - c \frac{\partial \hat{\bar{t}}_m}{\partial t} \tag{6}$$

in which

$$\frac{\partial \hat{\bar{t}}_m}{\partial \tau} = \frac{\partial \hat{\bar{t}}_m}{\partial t_m} \left[\left(\frac{\partial t_m}{\partial t_v} \right)_\tau \frac{\partial t_v}{\partial \tau} + \left(\frac{\partial t_m}{\partial \tau} \right)_{t_v} \right]$$

In this analysis we can ignore the effect of clock errors, so $\partial \hat{\bar{t}}_m / \partial t_m = 1$, and

$$\frac{\partial \hat{m}_3}{\partial \tau} = - c \left[\left(\frac{\partial t_m}{\partial t_v} \right)_\tau \frac{\partial t_v}{\partial \tau} + \left(\frac{\partial t_m}{\partial \tau} \right)_{t_v} \right] \tag{7}$$

Using Equations (4b) and (3a), with t_v fixed, we find

$$\left(\frac{\partial t_m}{\partial \tau} \right)_{t_v} = \left\{ \frac{\vec{S}_1^1}{|\vec{S}_1^1|} \cdot \dot{R}_{EM}(t_v) \right\} \Big/ \left\{ c - \dot{\vec{R}}_m(t_v) \cdot \frac{\vec{S}_1^1}{|\vec{S}_1^1|} \right\}$$

$$\approx \frac{\vec{S}_1^1 \cdot \dot{\vec{R}}_{EM}(t_v)}{|\vec{S}_1^1| \, c} \left[1 + \frac{\vec{S}_1^1 \cdot \dot{\vec{R}}_M(t_v)}{|\vec{S}_1^1| \, c} + \cdots \right]$$

$$\approx \frac{\vec{S}_1^1 \cdot \dot{\vec{R}}_{EM}(t_v)}{|\vec{S}_1^1| \, c}$$

Using Equations (4a) and (3b), with t_S fixed, we find

$$\frac{\partial t_v}{\partial \tau} = \left\{ \frac{\vec{S}_2^1 \cdot \dot{\vec{R}}_{EM}(t_v)}{|\vec{S}_2^1|} \right\} \Bigg/ \left\{ c - \frac{\vec{S}_2^1}{|\vec{S}_2^1|} \cdot \left[\dot{\vec{R}}_{EM}(t_v) + \dot{\vec{r}}_{MV}(t_v) + \ddot{\vec{R}}_{EM}(t_v)\,\tau \right] \right\}$$

$$\approx \frac{\vec{S}_2 \cdot \dot{\vec{R}}_{EM}(t_v)}{|\vec{S}_2^1|\, c}$$

Using Equations (4b) and (3a), with τ fixed, yields

$$\left(\frac{\partial t_m}{\partial t_v} \right)_\tau = \frac{c - \dfrac{\vec{S}_1}{\vec{S}_1^1} \cdot \left[\dot{\vec{r}}_{MV}(t_v) + \dot{\vec{R}}_{EM}(t_v) - \ddot{\vec{R}}_{EM}(t_v)\tau \right]}{c - \dfrac{\vec{S}_1^1 \cdot \dot{\vec{R}}_M(t_M)}{|\vec{S}_1^1|}}$$

$$= 1 - \frac{\vec{S}_1^1 \cdot \dot{\vec{S}}_1}{|\vec{S}_1^1|\, c}$$

Inserting all these results into Equation (7), we find

$$\frac{\partial \hat{m}_S}{\partial \tau} \approx - \left[\frac{\vec{S}_2^1}{\vec{S}_2^1} - \frac{\vec{S}_1^1}{\vec{S}_1^1} \right] \cdot \vec{R}_{EM}(t_v) \qquad (8)$$

For the three-way Doppler measurable $\hat{m}_3$, which is the change in $\hat{m}_3$ in the interval from t_S to $t_S + \Delta t_S$, we find

$$\frac{\partial \hat{m}_3}{\partial \tau} = - \left[\frac{\vec{S}_2^{\,1}(t_S+\Delta t_S)}{\left|\vec{S}_2^{\,1}(t_S+\Delta t_S)\right|} - \frac{\vec{S}_2^{\,1}(t_S)}{\left|\vec{S}_2^{\,1}(t_S)\right|} \right] \cdot \vec{R}_{EM}(t_v+\Delta t_v)$$

$$+ \left[\frac{\vec{S}_1^{\,1}(t_S+\Delta t_S)}{\left|\vec{S}_1^{\,1}(t_S+\Delta t_S)\right|} - \frac{\vec{S}_1^{\,1}(t_S)}{\left|\vec{S}_1^{\,1}(t_S)\right|} \right] \cdot \vec{R}_{EM}(t_v) \qquad (9)$$

where Δt_S is the difference in estimated times between measurements of the Doppler count at the receiving station.

For a two-way range measurement and two-way Doppler, we change subscript S to m in Equations (8) and (9). Since, in this case, $\vec{S}_2^{\,1} = -\vec{S}_1^{\,1}$, from Equation (3), we have

$$\frac{\partial \hat{m}_2}{\partial \tau} = + 2 \frac{\vec{S}_1^{\,1}}{\left|\vec{S}_1^{\,1}\right|} \cdot \vec{R}_{EM}(t_v) \qquad (10)$$

$$\frac{\partial \hat{m}_2}{\partial \tau} = 2 \left[\frac{\vec{S}_1^{\,1}(t_M+\Delta t_M)}{\left|\vec{S}_1^{\,1}(t_M+\Delta t_M)\right|} - \frac{\vec{S}_1^{\,1}(t_m)}{\left|\vec{S}_1^{\,1}(t_m)\right|} \right] \cdot \left[\vec{R}_{EM}(t_v+\Delta t_v) - \vec{R}_{EM}(t_v) \right] \qquad (11)$$

APOLLO NOTE NO. 424
(Task II, Item II)

E. Pugh
20 June 1966

STEPWISE ESTIMATION

Let $[a, b]$ be a vector of parameters to be estimated from a given set of measurements $M_m(t_1), \ldots, M_m(t_N)$. Suppose that due to computer storage limitation the following stepwise procedure is adopted to obtain estimates of a and b. First, an a priori estimate b_o for b is assumed exact and an estimate $\hat{a}_1$ of a is computed. Then, the estimate $\hat{a}_1$ is assumed exact and an estimate $\hat{b}_1$ is computed for b. Next, $\hat{b}_1$ is assumed exact and an estimate $\hat{a}_2$ is computed for a. This process is repeated k times giving the estimates $\hat{a}_k$ and $\hat{b}_k$. How accurate are $\hat{a}_k$ and $\hat{b}_k$? It is true that $\hat{a}_k \to \hat{a}$ and $\hat{b}_k \to \hat{b}$ where $\hat{a}$ and $\hat{b}$ are the joint maximum likelihood estimates of a and b? These questions are answered in this paper for the straight line case. The conclusions should remain valid in the general orbit problem if the non-linearity is not too great.

Assume that N values of a measurable y_i are taken at times $t_1, \ldots, t_N$ where y_i may be written in the form:

$$y_i = a + bt_i + e_i \qquad i = 1, \ldots, N$$

The e_i are independent noise samples with zero mean and known variance σ_e^2. The maximum likelihood estimates of a and b are the values of a and b that minimize:

$$Q(a, b) = \sum_{i=1}^{N} (y_i - a - bt_i)^2$$

Setting $\partial Q(a, b)/\partial a = 0$ and $\partial Q(a, b)/\partial b = 0$ gives the two linear equations in a and b:

$$b = \left(-N/\sum t_i\right) a + \left(\sum y_i / \sum t_i\right) \qquad (1)$$

$$b = \left(-\sum t_i / \sum t_i^2\right) a + \left(\sum y_i t_i / \sum t_i^2\right) \tag{2}$$

The simultaneous solutions of these equations are the maximum likelihood estimates $\hat{a}$ and $\hat{b}$. Equation (1) has a larger absolute slope which can be proved from the inequality $\sum\left(t_i - \bar{t}\right)^2 > 0$ where $\bar{t} = (1/N)\sum t_i$. Thus, the situation is as illustrated below.

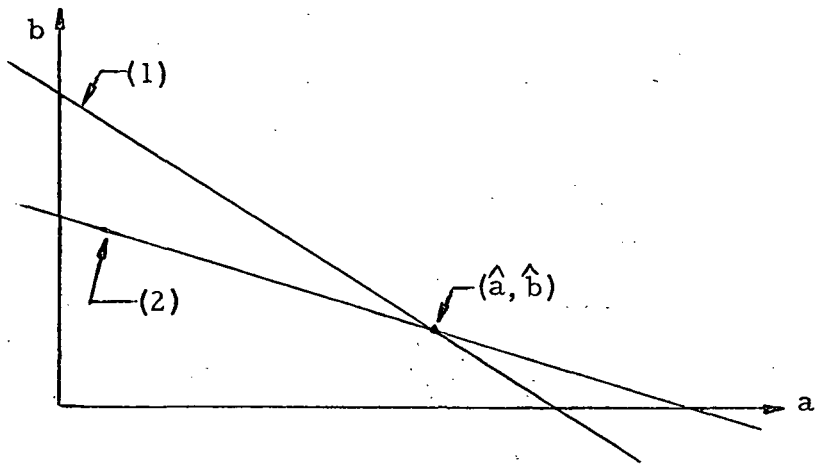

Now, if an a priori estimate b_o for b is assumed exact, the estimate of a is the value of a which minimizes:

$$Q(a, b_o) = \sum_{i=1}^{N} \left(y_i - a - b_o t_i\right)^2$$

This leads to the equation:

$$b_o = \left(-N / \sum t_i\right) a + \left(\sum y_i / \sum t_i\right) \tag{3}$$

which is Eq. (1) with b_o substituted for b. The solution of Eq. (3) is denoted $\hat{a}_1$. Now, if $\hat{a}_1$ is assumed exact, the estimate of b is the value which minimizes:

$$Q(\hat{a}_1, b) = \sum_{i=1}^{N} \left(y_i - \hat{a}_1 - b t_i\right)^2$$

which leads to Eq. (2) with $\hat{a}_1$ substituted for a. The solution is denoted $\hat{b}_1$. If we continue this iteration the situation is as illustrated below:

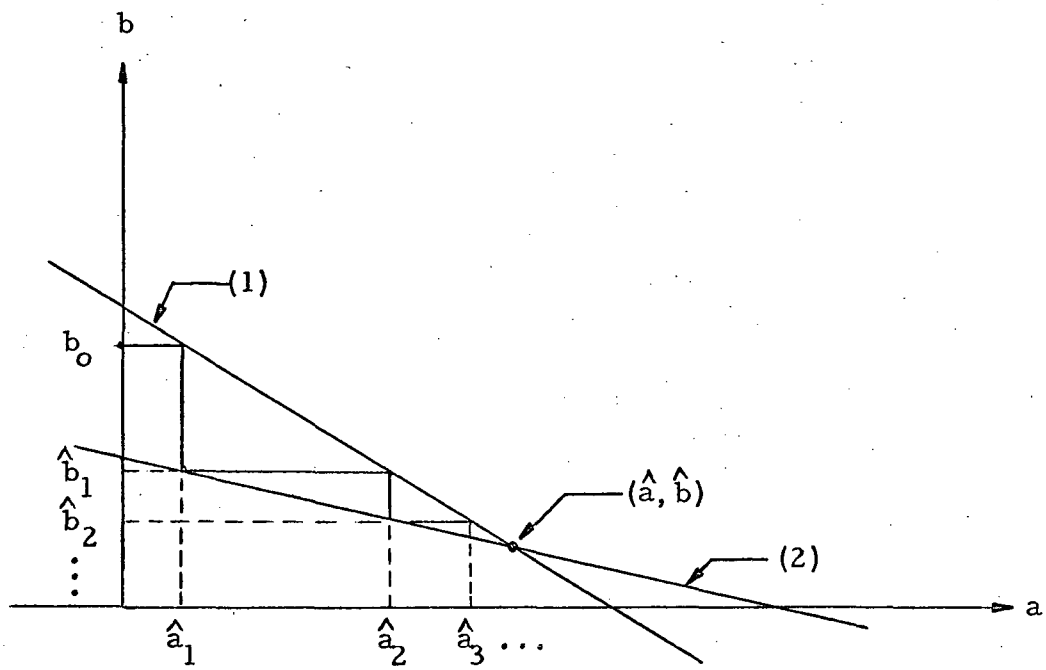

Thus, the estimates $\hat{a}_k$ and $\hat{b}_k$ converge to the joint maximum likelihood estimates $\hat{a}$ and $\hat{b}$.

The accuracy of the estimates $\hat{a}_k$ and $\hat{b}_k$ will now be investigated. Solving Eq. (3) gives:

$$\hat{a}_1 = \frac{1}{N} \sum_{i=1}^{N} \left(y_i - b_o t_i \right)$$

Substituting $y_i = a + bt_i + e_i$ gives $E\hat{a}_1 = a$ and:

$$(\hat{a}_1 - a)^2 = \left(\frac{1}{N} \sum_{i=1}^{N} \left[\left(b - b_o \right) t_i + e_i \right] \right)^2 = \left(1/N^2 \right) \left[\left(b - b_o \right) \sum_{i=1}^{N} t_i + \sum_{i=1}^{N} e_i \right]^2$$

Squaring and taking expectations gives:

$$\sigma^2_{\hat{a}_1} = \left(1/N^2\right)\left[\sigma^2_{b_o}\left(\sum_{i=1}^{N} t_i\right)^2 + N\sigma^2_e\right]$$

Note that this will be an <u>increasing function of tracking time</u> for sufficiently large tracking time, (see Apollo Note 395).

Substituting $\hat{a}_1$ into Eq. (2) and solving for b gives:

$$\hat{b}_1 = \sum_{i=1}^{N}\left(y_i - \hat{a}_1\right)t_i \Big/ \sum_{i=1}^{N} t_i^2$$

To find the variance of this expression we again substitute $y_i = a + bt_i + e_i$ to give $E\hat{b}_1 = b$ and:

$$\left(\hat{b}_1 - b\right)^2 = \left[\left(1/\sum t_i^2\right)\ \sum\left((a-\hat{a}) + bt_i + e_i\right)t_i \quad -b\right]^2$$

Squaring and taking expectations gives:

$$\sigma^2_{\hat{b}_1} = \left[\sigma^2_{\hat{a}_1}\left(\sum t_i\right)^2 + 2\left(\sum t_i\right)\sum t_i\ E(a-\hat{a})\ e_i + \sigma^2_e\ \sum t_i^2\right] \Big/ \left(\sum t_i^2\right)^2$$

Now,

$$e_i\hat{a} = \frac{1}{N}\sum_{j=1}^{N}\left(ae_i + e_i bt_j + e_i e_j - e_i b_o t_j\right)$$

$$Ee_i\hat{a} = \frac{1}{N}\sum_{j=1}^{N}\delta_{ij}\sigma^2_e = \sigma^2_e / N$$

Substituting this into the expression for $\sigma^2_{\hat{b}_1}$ gives, after simplification,

$$\sigma^2_{\hat{b}_1} = \frac{\left(\sum t_i\right)^2}{\left(\sum t_i^2\right)^2}\left[\frac{\sigma^2_{b_o}\left(\sum t_i\right)^2}{N^2} + \sigma_e^2\left(\frac{\sum t_i^2}{\left(\sum t_i\right)^2} - \frac{1}{N}\right)\right]$$

We now find an expression for $\sigma^2_{a_k}$ and $\sigma^2_{b_k}$. At the kth step we have:

$$a_k = \frac{1}{N}\sum_{i=1}^{N}\left(y_i - b_{k-1}\, t_i\right)$$

$$= \frac{1}{N}\sum_{i=1}^{N}\left(a + bt_i + e_i - b_{k-1}\, t_i\right)$$

Thus, $E a_k = a$ since $E b_{k-1} = b$. Also:

$$\left(a_k - a\right)^2 = \left[\frac{1}{N}\left(b - b_{k-1}\right)\left(\sum t_i\right) + \frac{1}{N}\sum e_i\right]^2$$

Squaring and taking expectations:

$$\sigma^2_{a_k} = \sigma^2_{b_{k-1}}(\bar{t})^2 - \frac{2\left(\sum t_i\right)}{N^2}\sum_{i=1}^{N} E\, e_i\, b_{k-1} + \frac{\sigma_e^2}{N}$$

where $\bar{t} = (1/N)\sum t_i$. The second term in the above equation turns out to be zero and so we have:

$$\sigma^2_{a_k} = \sigma^2_{b_{k-1}}(\bar{t})^2 + \frac{\sigma_e^2}{N} \qquad (4)$$

Also, at the kth step we have:

$$b_k = \frac{\sum (y_i - a_k) t_i}{\sum t_i^2}$$

Substituting $y_i = a + bt_i + e_i$, we find $E\, b_k = b$. Also, taking the expected value of $(b_k - b)^2$ gives:

$$\sigma_{b_k}^2 = \sigma_{a_k}^2 \frac{(\bar{t})^2}{(\overline{t^2})^2} - \frac{2}{N} \frac{(\bar{t})}{(\overline{t^2})^2} \sum t_i \, E\, e_i \, a_k + \frac{\sigma_e^2}{(N\overline{t^2})}$$

Substituting expression (4) for $\sigma_{a_k}^2$ gives, after simplification,

$$\boxed{\sigma_{b_k}^2 = \sigma_{b_{k-1}}^2 \delta^2 + \frac{\sigma_e^2}{N(\overline{t^2})} \left[1 + \delta - 2\delta^k\right]} \qquad (5)$$

where:

$$\delta = (\bar{t})^2 / (\overline{t^2}) \quad , \quad \bar{t} = \frac{1}{N} \sum_{i=1}^{N} t_i \quad , \quad \overline{t^2} = \frac{1}{N} \sum_{i=1}^{N} t_i^2$$

and $\delta < 1$ which can be proved from $\sum (t_i - \bar{t})^2 > 0$.

Consider the iterations in Eq. (5). The amount added each time changes with k, but:

$$\frac{\sigma_e^2}{N(\overline{t^2})} (1 - \delta) \leqslant \frac{\sigma_e^2}{N(\overline{t^2})} \left[1 + \delta - 2\delta^k\right] \leqslant \frac{\sigma_e^2}{N(\overline{t^2})} (1 + \delta)$$

Thus, we obtain the following bounds on $\sigma_{b_k}^2$ by adding the maximum and minimum amount each time:

$$\sigma_{b_o}^2 \delta^{2k} + \frac{\sigma_e^2}{N\overline{t^2}} \frac{\left(1-\delta^{2k}\right)}{(1+\delta)} \leq \sigma_{b_k}^2 \leq \sigma_{b_o}^2 \delta^{2k} + \frac{\sigma_e^2}{N\overline{t^2}} \frac{\left(1-\delta^{2k}\right)}{(1-\delta)}$$

Substituting these bounds into Eq. (4) gives bounds on $\sigma_{a_k}^2$ which are:

$$\sigma_{b_o}^2 \delta^{2(k-1)} (\overline{t})^2 + \frac{\sigma_e^2}{N} \delta \left(\frac{1-\delta^{2(k-1)}}{1+\delta} \right) + \frac{\sigma_e^2}{N} \leq \sigma_{a_k}^2$$

$$\leq \sigma_{b_o}^2 \delta^{2(k-1)} (\overline{t})^2 + \frac{\sigma_e^2}{N} \delta \left(\frac{1-\delta^{2(k-1)}}{1-\delta} \right) + \frac{\sigma_e^2}{N}$$

As $k \rightarrow \infty$ we have:

$$\sigma_{b_\infty}^2 \leq \frac{\sigma_e^2}{N\overline{t^2}} \left(\frac{1}{1-\delta} \right)$$

$$\sigma_{a_\infty}^2 \leq \frac{\sigma_e^2}{N} \left(\frac{1}{1-\delta} \right)$$

The righthand sides of the above equations are the variances for the joint maximum likelihood estimates of a and b.

The Bissett-Berman Corporation 2941 Nebraska Avenue, Santa Monica, California EXbrook 4-3270

H. Epstein/
C. H. Dale
27 June 1966

APOLLO NOTE NO. 425
(Task I, Item I)

THE EFFECT OF SAMPLING RATE ON THE UNCERTAINTY IN STATE VECTORS

A discussion took place at MSC during the ANWG meeting (June 7-8, 1966) regarding the effect of data sampling rate on ephemeris accuracy. The conversation was primarily addressed to the GO/NO-GO decision following S-1VB cutoff in the Earth ascent phase. C-band radars are the primary Earth-based sensors for this portion of the mission. The C-band radar errors were represented by a bias and an uncorrelated noise error. The noise error was considered to have a constant standard deviation for the range of data sampling rates of interest.

This note will indicate the asymptotic behavior for high sampling rates. The asymptotic variance of the parameters estimated will be shown to vary inversely with the data sampling rate, (linearly proportional to the interval between measurements) for a constant measurement period. The analytical and experimental results will be shown for an uncorrelated gaussian noise source with all state vectors and nuisance parameters updated.

The remainder of this note will be divided into three parts. The first part will treat the more general theoretical problem. The second part is an analytical result for the estimation of a straight line where simple results can be obtained in a closed analytical form. The third part will consist of a result obtained from the OEAP which is similar to the case considered by the ANWG.

Part I - Simplified Theoretical Analysis

This part will treat the case of estimation of a number of parameters in the presence of an uncorrelated gaussian error source in the measurable. No a priori information regarding the parameters to be estimated will be employed. Only one set of measurables will be considered.

Let

$$F = F(a_1, a_2, \ldots, a_i, \ldots, a_m; t) \tag{1}$$

where F = true value of the measurable as a function of time and the parameters involved.

a_i = true value of the ith parameter

m = number of parameters involved

$$\hat{F} = \hat{F}(\hat{a}_1, \ldots, \hat{a}_i, \ldots, \hat{a}_m; t) \tag{2}$$

where

$\hat{F}$ = estimated value of the measurable

$\hat{a}_i$ = estimated value of the ith parameter

$$F_m = F + n(t) \tag{3}$$

F_m = measured value of the data

$n(t)$ = uncorrelated noise error

Letting

$$e(t) = F_m - \hat{F} \tag{4}$$

assuming that a linear analysis is adequate

$$\hat{F} = F + \sum_{i=1}^{m} \frac{\partial F}{\partial a_i} \Delta a_i \tag{5}$$

and substituting Eqs. (3) and (5) into Eq. (4),

$$e(t) = n(t) - \sum_{i=1}^{m} \frac{\partial F}{\partial a_i} \Delta a_i \tag{6}$$

If n(t) is an uncorrelated gaussian noise source, then the minimum variance estimate of the parameter is the maximum likelihood estimate defining

$$e^2 = \frac{1}{N} \sum_{r=1}^{N} e^2(t_r) \tag{7}$$

It is simply necessary to solve the m set of linear equations obtaining, by setting, $\partial e^2 / \partial \Delta a_j = 0$ to obtain the estimates for Δa_i

$$\frac{\partial e^2}{\partial \Delta a_j} = 0 \text{ yields}$$

$$\frac{1}{N} \sum_{i=1}^{m} \Delta a_i \sum_{r=1}^{N} \frac{\partial F}{\partial a_i} \frac{\partial F}{\partial a_j} = \frac{1}{N} \sum_{r=1}^{N} \frac{\partial F}{\partial a_j} n(t_r) \tag{8}$$

It is convenient to employ matrix notation at this point. Letting,

$$C_{ij} = \frac{1}{N} \sum_{r=1}^{N} \frac{\partial F}{\partial a_i} \frac{\partial F}{\partial a_j}$$

be the elements of an m x m Matrix C

$$d_j = \frac{1}{N} \sum_{r=1}^{N} \frac{\partial F}{\partial a_j} n(t_r)$$

be the m elements of a column Matrix D,

and Δa_j be the m elements of a column matrix Δa.

Then Eq. (8) may be written as follows:

$$C\Delta a = D \tag{9}$$

and

$$\Delta a = C^{-1} D \tag{10}$$

Defining $n(t_r)$ as follows

$$E\left\{n(t_r)\right\} = 0$$

$$E\left\{n(t_r)\ n(t_r+\Delta t)\right\} = \phi_n \qquad \Delta t = 0$$

$$= 0 \qquad \Delta t \neq 0$$

Then,

$$E\left\{\Delta a\right\} = 0$$

$$E\left\{\Delta a\ \Delta a^T\right\} = C^{-1}\left\{E\left[D D^T\right]\right\} C^{-1} \tag{11}$$

but

$$E\left\{D D^T\right\} = \frac{\phi_n}{N} C \tag{12}$$

$$\therefore\ E\left\{\Delta a\ \Delta a^T\right\} = \frac{\phi_n}{N} C^{-1} \tag{13}$$

Since C^{-1} is determined from the values of C_{ij}, it is only necessary that C_{ij} becomes suitably independent of N for C^{-1} to be independent of N

$$C_{ij} = \frac{1}{N} \sum_{r=1}^{N} \left(\frac{\partial F}{\partial a_i}\right)\left(\frac{\partial F}{\partial a_j}\right) \tag{14}$$

is the quantity to be examined.

C_{ij} becomes substantially independent of N provided that the partial derivatives involved in Eq. (14) change very slowly over the interval between points. This is the same condition as the condition required to change the summation to an integral. By keeping the data interval a constant, the integral form for Eq. (14) will be a constant. As a consequence, for this case (constant tracking interval), the variance of the estimated parameters asymptotically varies inversely with N. N, in turn, is directly proportional to the data sampling rate.

Part II - Simple Analytical Example

The example selected for this portion of the note involves the calculation of the two parameters associated with a straight line. The measurement data will be assumed to be taken at equal time intervals. An odd number $(2M+1)$ of data points will be assumed for convenience. The time origin will be taken at the center of the data interval. In addition, no a priori knowledge of the parameters will be used. This is a standard type of example since the analytical results may be readily obtained in closed form. Again, the noise source will be assumed uncorrelated and of the same nature as indicated in the previous part.

The true value of the function (F) may be written in the following form:

$$F = a_1 + a_2 r\Delta t \qquad r = 0, \pm 1, \pm 2, \ldots, \pm M \qquad (15)$$

where a_1 and a_2 are parameters of the straight line, Δt = time interval between successive measurements.

Since there are $N = 2M+1$ points in the data set, one can write:

$$\Delta t = \frac{T}{2M} \qquad (16)$$

where T = tracking interval involved.

The substitution of Eq. (16) into Eq. (15) leads to the following equation.

$$F = a_1 + \frac{b_2 r}{2M} \tag{17}$$

with

$$b_2 = a_2 T \tag{18}$$

Equation (17) is of the desired form since the results are desired for a constant tracking interval.

In a similar fashion to Part I, one can, with

$$\hat{F} = \hat{a}_1 + \frac{\hat{b}_2 r}{2M} \tag{19}$$

$$F_m = F + n_r \tag{20}$$

$$e_r = F_m - F = n_r - \left(\Delta a_1 + \frac{\Delta b_2 r}{2M} \right) \tag{21}$$

where

$$\Delta a_1 = \hat{a}_1 - a_1 \tag{22}$$

$$\Delta b_2 = \hat{b}_2 - b_2 \tag{23}$$

$$\hat{e}^2 = \frac{1}{N} \sum_{r=-M}^{M} \left[n_r - \left(\Delta a_1 + \frac{\Delta b_2 r}{2M} \right) \right]^2 \tag{24}$$

Again, making use of the equivalence between the variance of minimum variance estimators and maximum likelihood estimators for uncorrelated noise sources,

$$\frac{\partial \hat{e}_2}{\partial \Delta a_1} = 0 \quad \text{yields,}$$

$$\frac{1}{N}\sum_{r=M}^{M} n_r = \frac{1}{N}\sum_{r=-M}^{M}\left(\Delta a_1 + \frac{\Delta b_2 r}{2M}\right) = \Delta a_1 \tag{25}$$

and

$$\frac{\partial \hat{e}_2}{\partial \Delta b_2} = 0 \quad \text{yields,}$$

$$\frac{1}{N(2M)}\sum_{r=M}^{M} r n_r = \frac{1}{N}\sum_{r=M}^{M}\frac{r}{2M}\left(\Delta a_1 + \frac{r\Delta b_2}{2M}\right) \tag{26}$$

$$= \frac{\Delta b_2}{N(2M)^2}\sum_{r=-M}^{M} r^2 = \frac{(M+1)\,\Delta b_2}{12M}$$

Since

$$\sum_{r=-M}^{M} r^2 = 2\sum_{r=1}^{M} r^2 = \frac{M(M+1)\,(2M+1)}{3} = \frac{M\,(M+1)\,(N)}{3} \tag{27}$$

From Eqs. (25), (26), and (27), it can readily be shown that,

$$E\left\{\Delta a_1^2\right\} = \frac{\phi_n}{N} \tag{28}$$

and

$$E\left\{\Delta b_2^2\right\} = \frac{12\phi_n}{N}\left(\frac{M}{M+1}\right) \sim \frac{12\phi_n}{N} \tag{29}$$

Equations (28) and (29) clearly indicate that the asymptotic variance is inversely proportional to the number of data samples for a constant tracking interval.

Part III - Numerical Example

The final part of this note treats a numerical example of the type of interest for Apollo purposes. The specific example is tracking by a single C-band radar of the Apollo spacecraft in the Earth ascent phase, subsequent to S-IVB cutoff for the GO/NO-GO decision (the hold phase). A nominal circular orbit at an altitude of 100 nautical miles was used. Cutoff of the powered flight phase was used at 1440 nautical miles down-range from the Cape Kennedy launch pad. The assumptions used in the study are summarized below.

1. Trajectory Parameters (circular orbit)

   Velocity: 25,568 fps
   Flight Path Angle: 0.0 degrees
   Altitude: 100 n.mi.
   Launch Azimuth: 108 degrees
   Down-range Cutoff: 1440 n.mi.

2. Data Type and Uncertainties, C-band Radar, 1 σ Values

	Noise	Bias
Range	30 feet	60 feet
Azimuth	0.4 m rad	0.8 m rad
Elevation	0.4 "	0.8 "

3. Station Location and Biases, 1 σ Values

   Latitude: $21^{\circ}15'$ North $\pm$ 0.3' or 0.3 n.mi. bias
   Longitude: $48^{\circ}45'$ West $\pm$ 0.3' or 0.3 n.mi. bias

The initial studies ignored the bias on the measurables and station location errors. Calcuations with the OEAP were made for tracking data intervals of 20, 40, 60, and 90 seconds. Initial values for the orbit parameters were calculated from the trajectory parameters indicated above. Program A data sheets and Program B data sheets were written to arrive at the required numerical results. An example of a Program A data sheet is given in Table I and an example of a Program B data sheet in Table II.

A summary sheet of this result for position and velocity errors is given in Table III. If desired, the results for speed, flight path angle, and altitude errors could also be given. The time interval between data points, rather than the data sampling rate, is used by the OEAP. Only a simple conversion is needed between the two quantities since one is the reciprocal of the other.

Figure 1 is a plot of the 3σ uncertainty in position as a function of the time interval between measurements for tracking intervals of 20, 40, 60, and 90 seconds. The initial measurement point for all cases was taken at the beginning of the tracking interval and the final data point as the end of the tracking interval. The uncertainties are indicated for the beginning of the tracking interval in all cases. These conditions permit a more consistent comparison of the effects of the data rate and tracking interval. The dashed curve indicates the asymptotic behavior suggested by the theoretical results of Part I, extrapolated from the numerical result for a 0.1 time interval between samples (ten samples/second). It may be noted from Figure 1 that 3σ uncertainty in position will be less than 0.1 n.mi. for tracking intervals greater than 20 seconds with a data rate of 10 samples per second.

The 3σ uncertainty in velocity is indicated in Figure 2, the asymptotic behavior extrapolated from the numerical value for a 0.1 second time interval between measurements is indicated by the dashed line. Again, it can be noted that the asymptotic behavior closely indicates the performance for the range of parameters of interest.

PROGRAM A

DATA INPUT SHEET

Keypunch: Punch a card for each row checked (✓)

xx; if 1st set on new tape; blank otherwise

✓	1 PROGRAM A 9	11 12	Station 15 26	Data Set 31 33
✓	PROGRAM A	XX	PO/HTGME	01/

| | | |

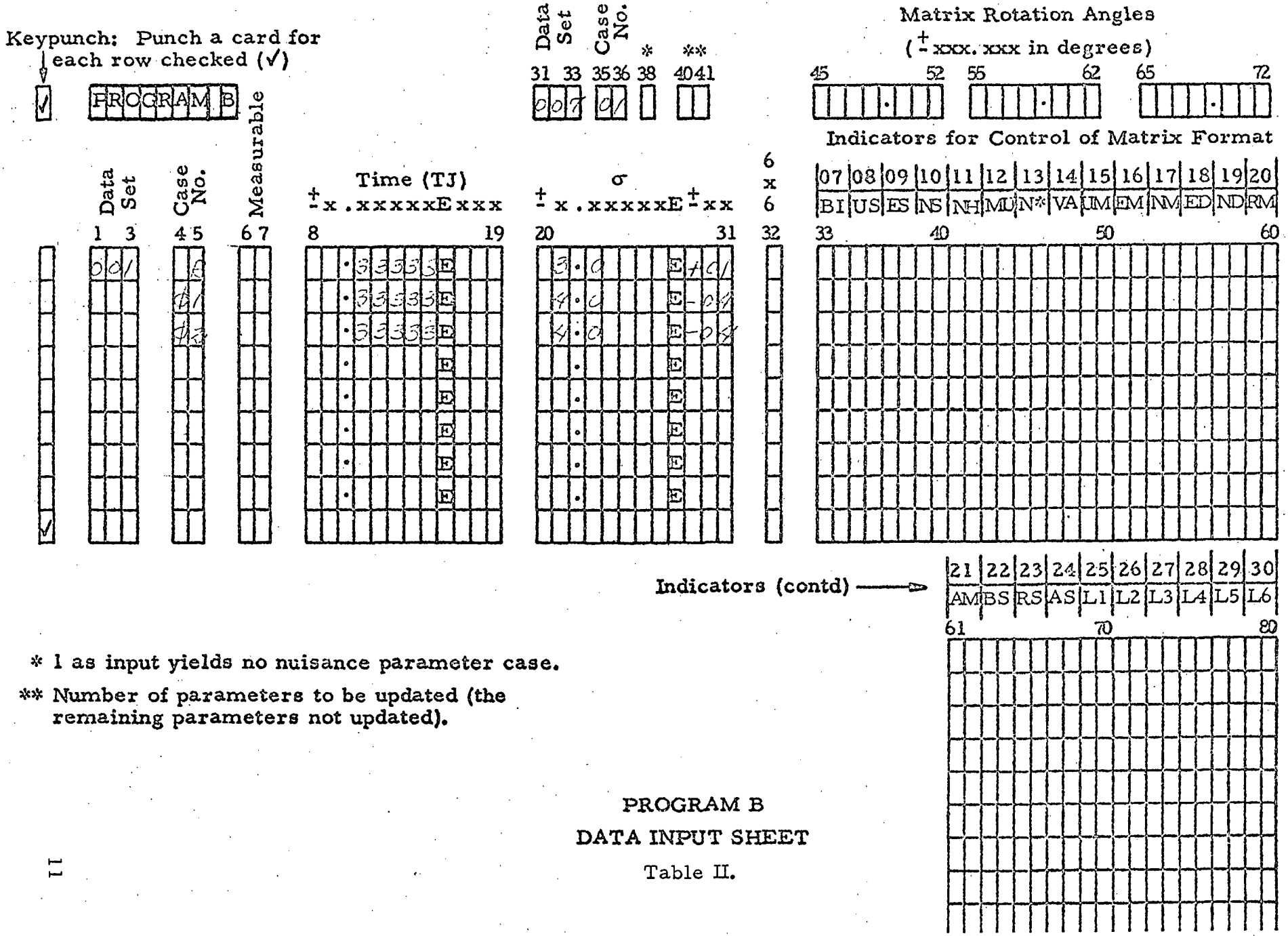

* 1 as input yields no nuisance parameter case.

** Number of parameters to be updated (the remaining parameters not updated).

PROGRAM B

DATA INPUT SHEET

Table II.

Time (seconds)	Position Error		Velocity Error	
	1 σ feet	3 σ n. mi.	1 σ fps	3 σ fps
ΔT = .1	195.0	.0962	15.49	46.47
.2	274.1	.1352	21.73	65.19
.5	425.8	.2101	33.55	100.65
1	585.2	.2887	45.64	136.92
2	785.2	.3874	60.05	180.15
T = 20 sec				
ΔT = .1	127.3	.0628	4.776	14.328
.2	179.5	.0886	6.728	20.184
.5	281.5	.1389	10.51	31.53
1	392.8	.1938	14.59	43.77
2	541.6	.2672	19.90	59.70
5	799.1	.3943	28.44	85.32
T = 40 sec				
ΔT = .1	100.3	.0495	2.456	7.368
.2	141.7	.0699	3.465	10.395
.5	222.9	.1100	5.438	16.314
1	312.5	.1542	7.598	22.794
2	434.8	.2145	10.49	31.47
5	656.7	.3240	15.51	46.53
T = 60 sec				
ΔT = .1	79.53	.0392	1.305	3.915
.2	112.3	.0554	1.842	5.526
.5	177.1	.0874	2.900	8.700
1	249.1	.1229	4.070	12.210
2	348.5	.1720	5.670	17.01
5	534.7	.2638	8.587	25.761
T = 90 sec				

Table III. Summary of Results

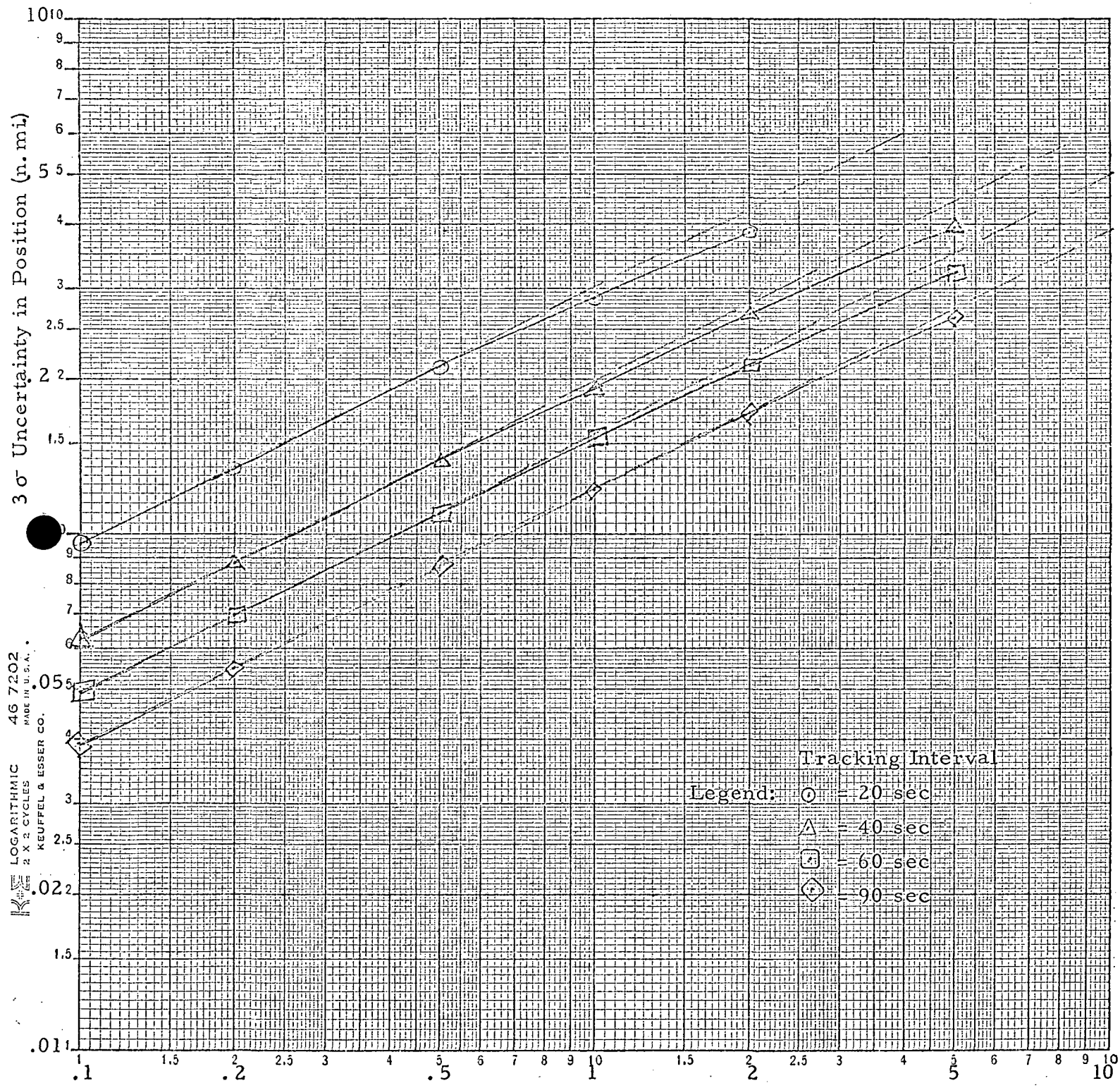
3σ Uncertainty in Position (n. mi)
Time Interval Between Measurements (seconds)
Tracking Interval
Legend: ⊙ = 20 sec
△ = 40 sec
□ = 60 sec
◇ = 90 sec
LOGARITHMIC
2 X 2 CYCLES
KEUFFEL & ESSER CO.
MADE IN U.S.A.
46 7202

Figure 1

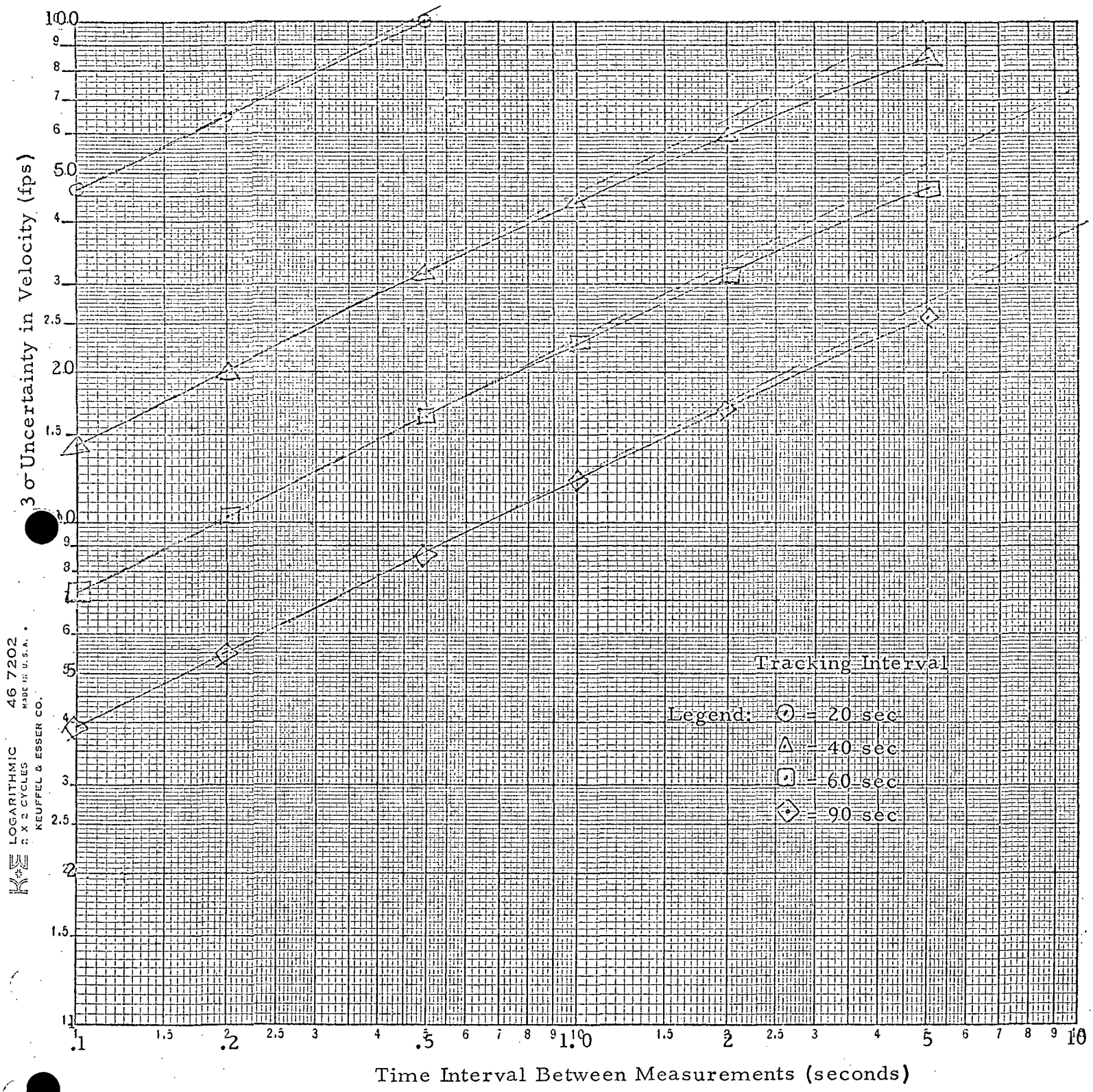
3 σ Uncertainty in Velocity (fps)
Time Interval Between Measurements (seconds)
Tracking Interval
Legend: ⊙ = 20 sec
△ = 40 sec
□ = 60 sec
◇ = 90 sec
LOGARITHMIC 46 7202
2 X 2 CYCLES
KEUFFEL & ESSER CO.
MADE IN U.S.A.

Figure 2

The results obtained demonstrate the value of high sampling rates for estimation purposes when no biases or systematic errors exist. The theoretical limitation to beneficial sample rates is limited by the correlation of the noise source.

The final portion of this study included the effects of the biases and station location uncertainties given on Page 8. A second set of computer runs using the OEAP gave the following results:

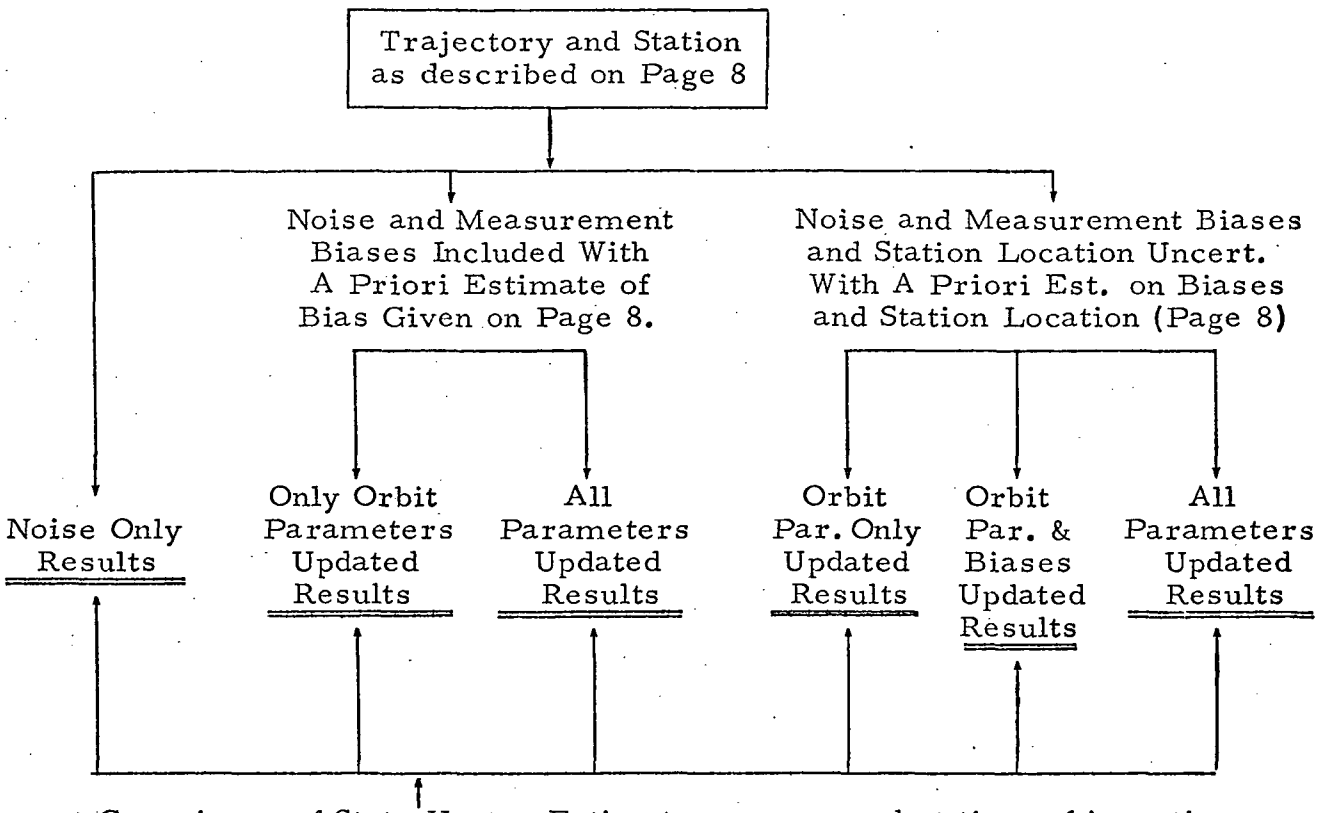

The data input sheets resemble those shown in Tables I and II, except that a priori inputs were included for biases and station locations and the proper "indicators for control of Matrix Format", (Table III), were used to allow updating and non-updating of the biases and station locations.

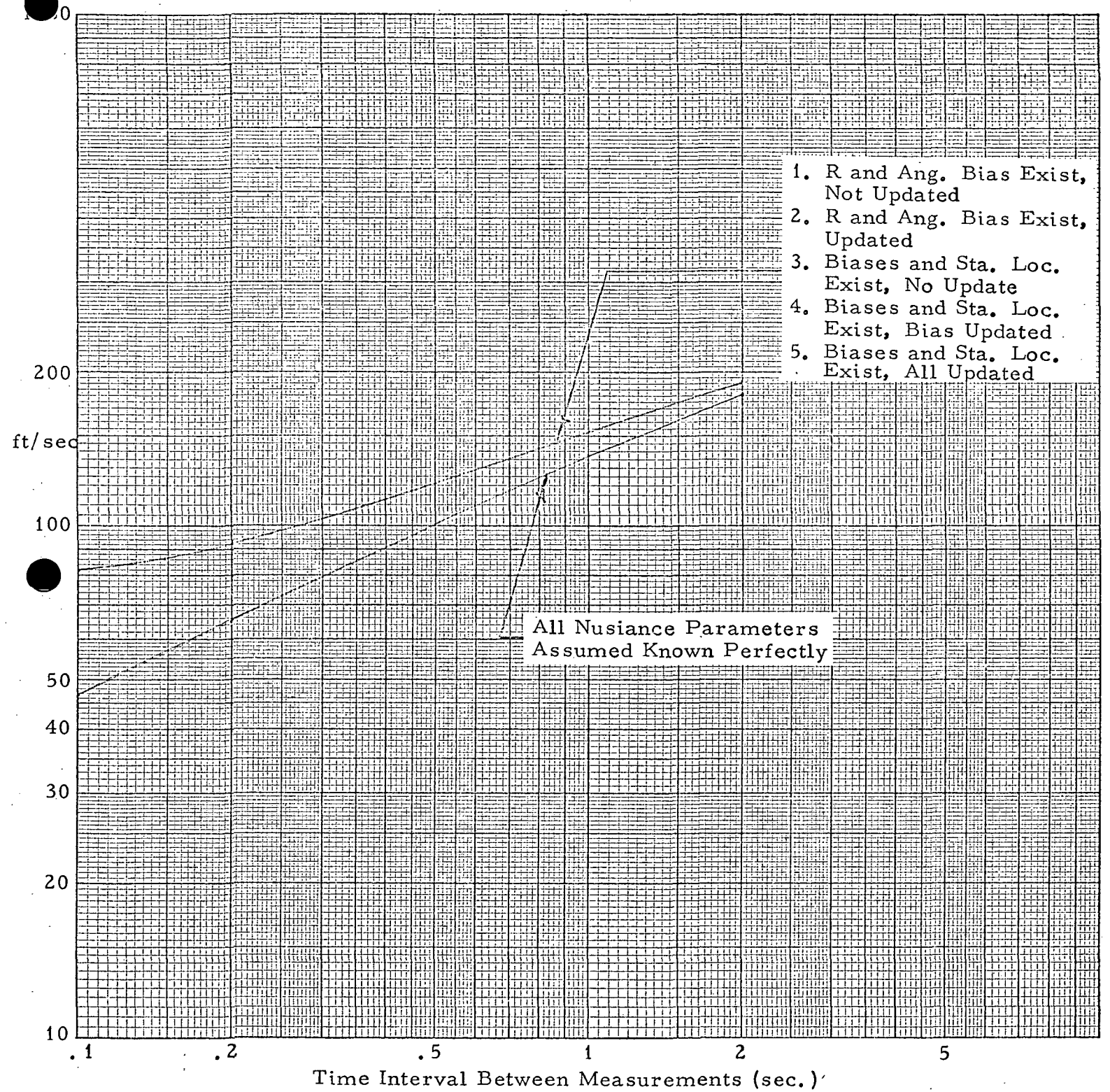

Figure 3. 3 σ Velocity Uncertainty - 20 Seconds Total Tracking

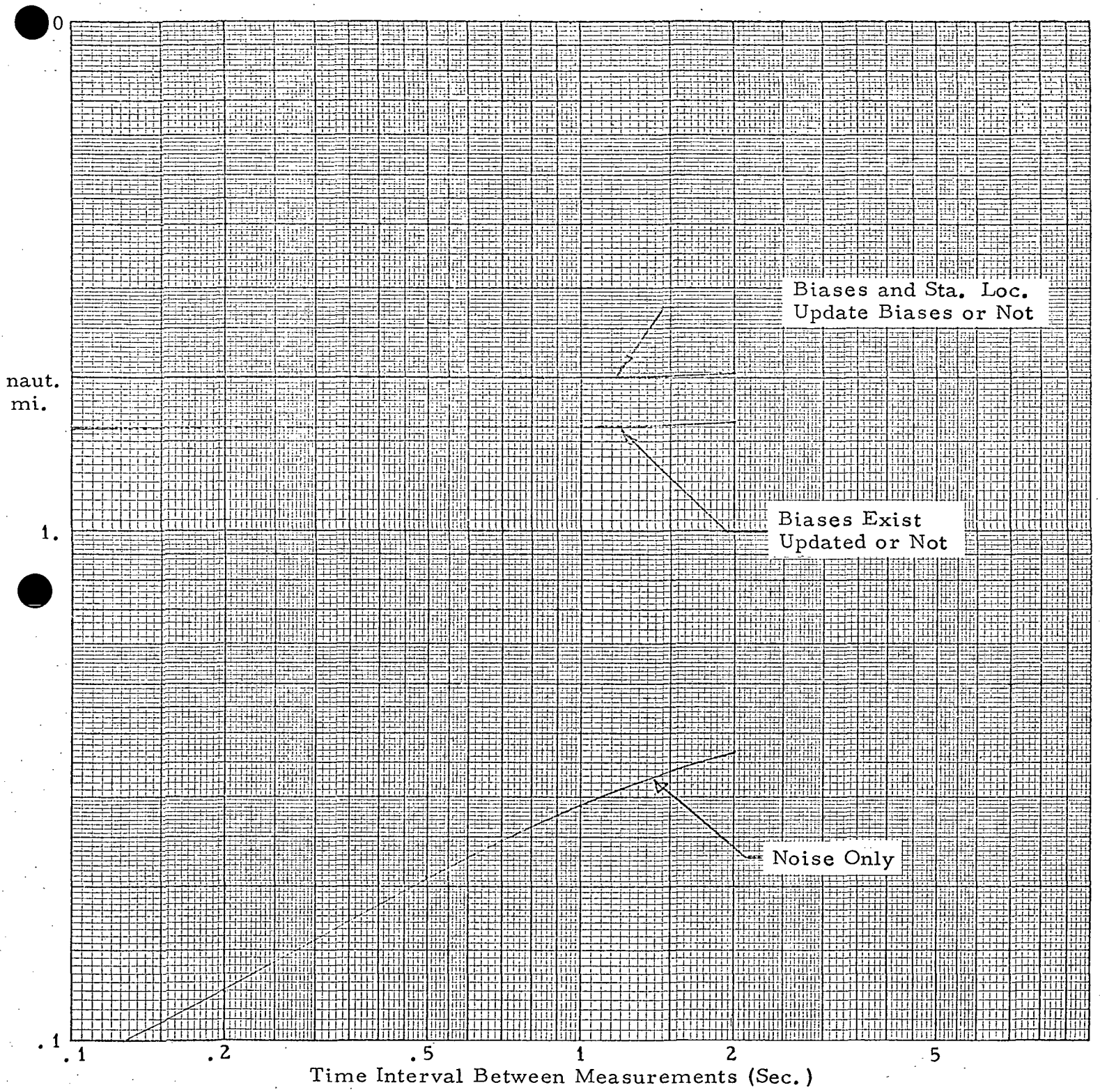

Figure 4. 3 σ Position Uncertainty - 20 Second Track

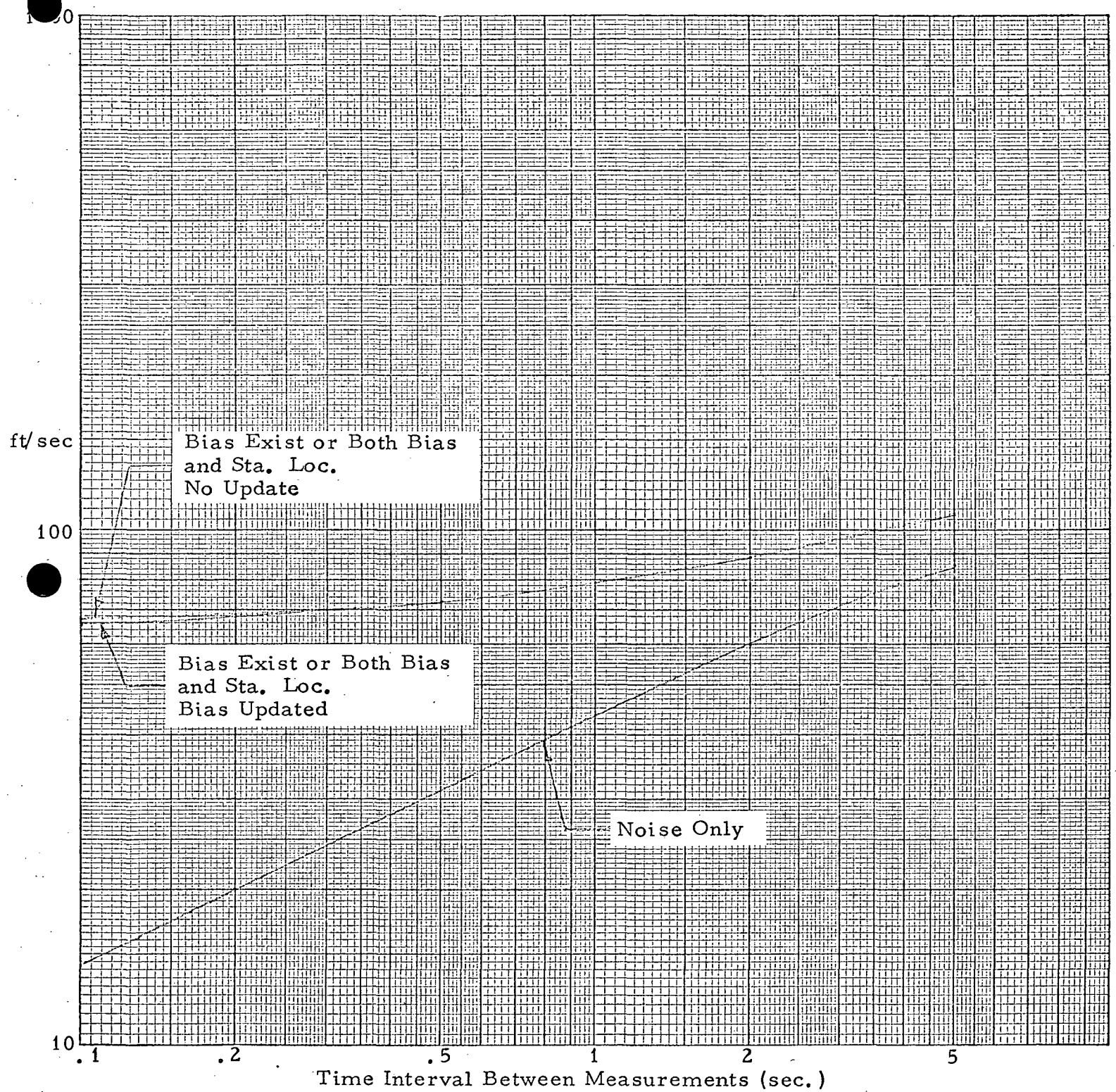

Figure 5. 3 σ Velocity Uncertainty - 40 Second Track

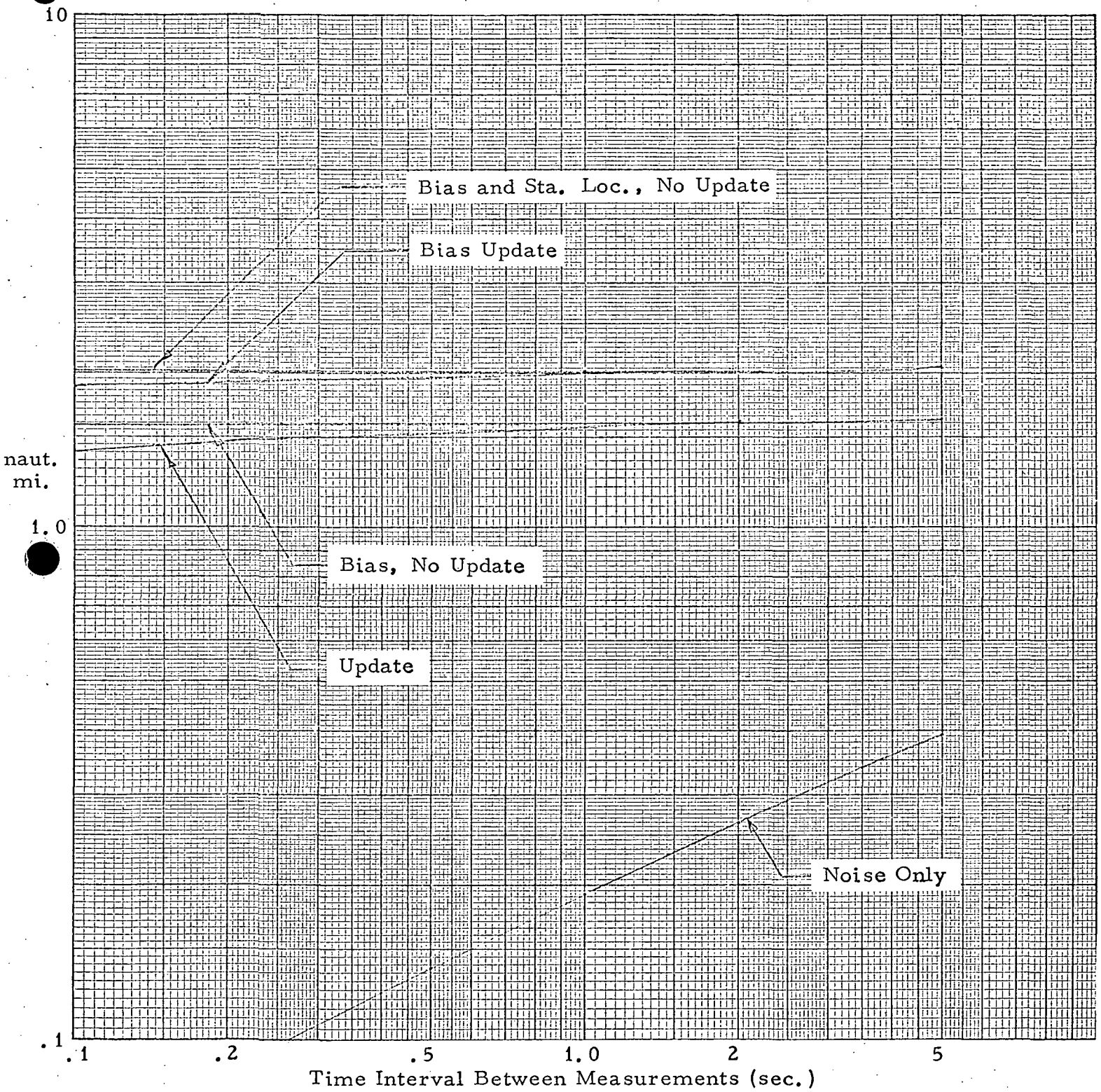

Figure 6. 3 σ Position Uncertainty - 40 Second Track

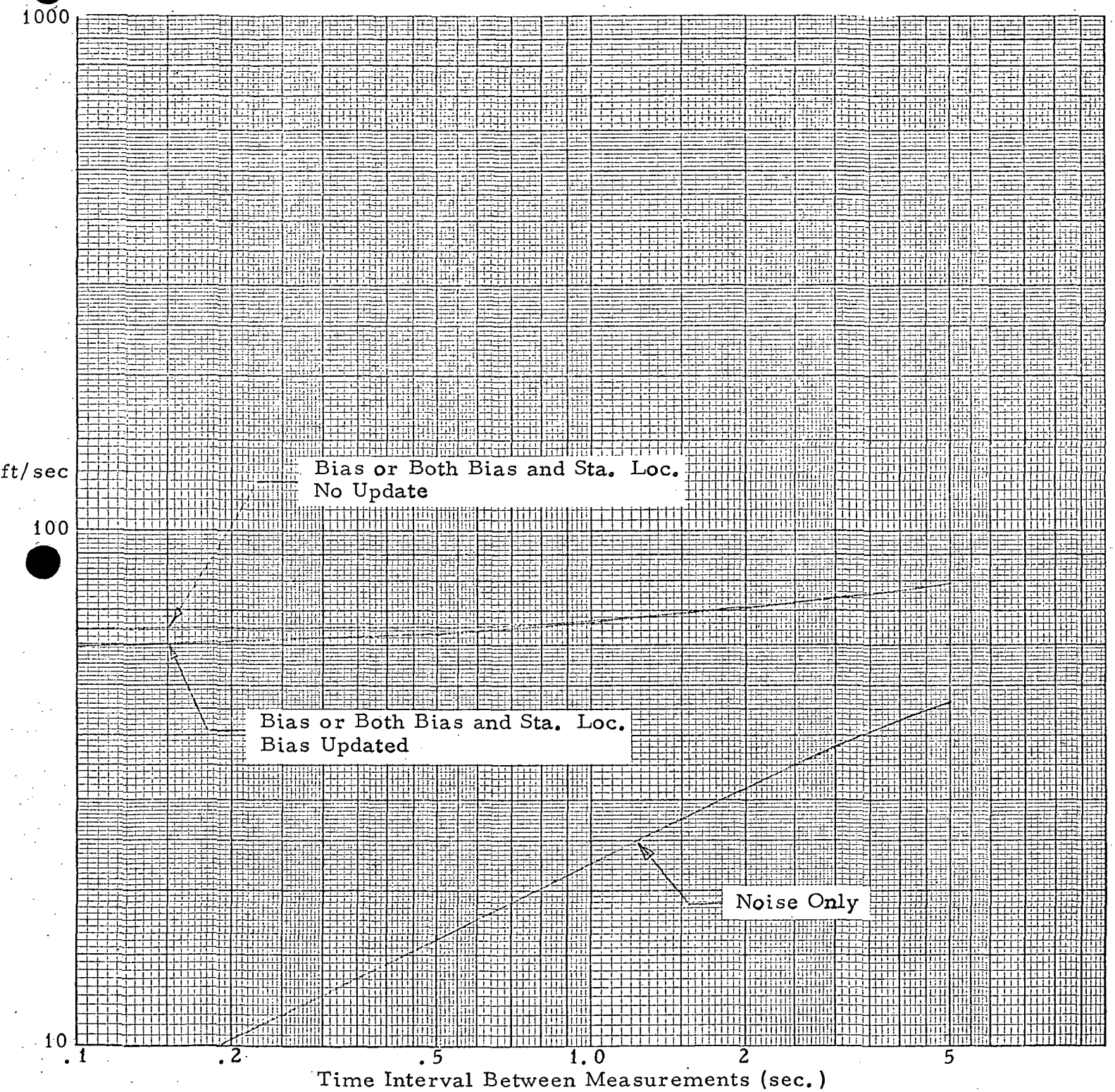

Figure 7. 3 σ Velocity Uncertainty - 60 Second Track

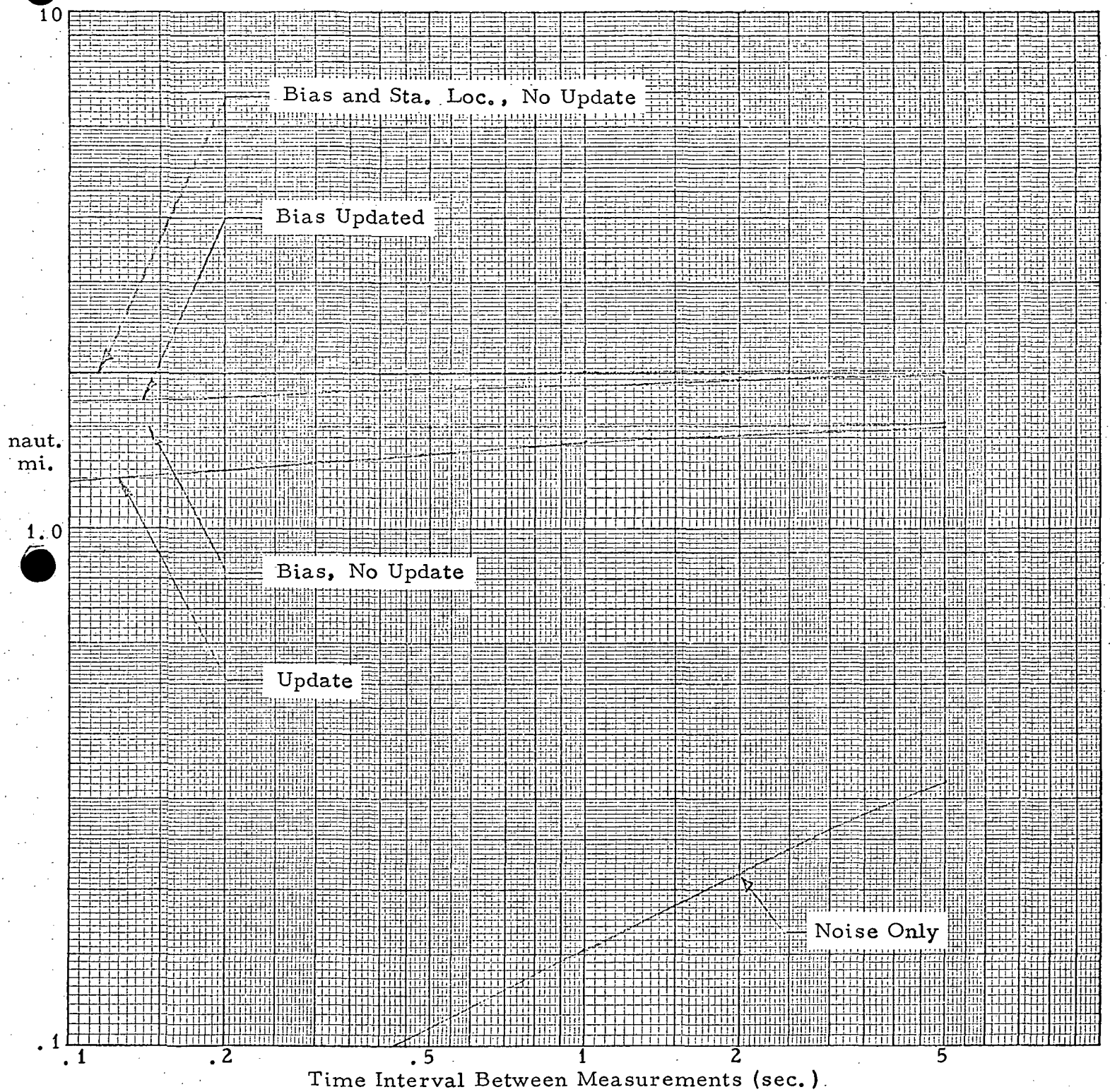

Figure 8. 3 σ Position Uncertainty - 60 Second Track

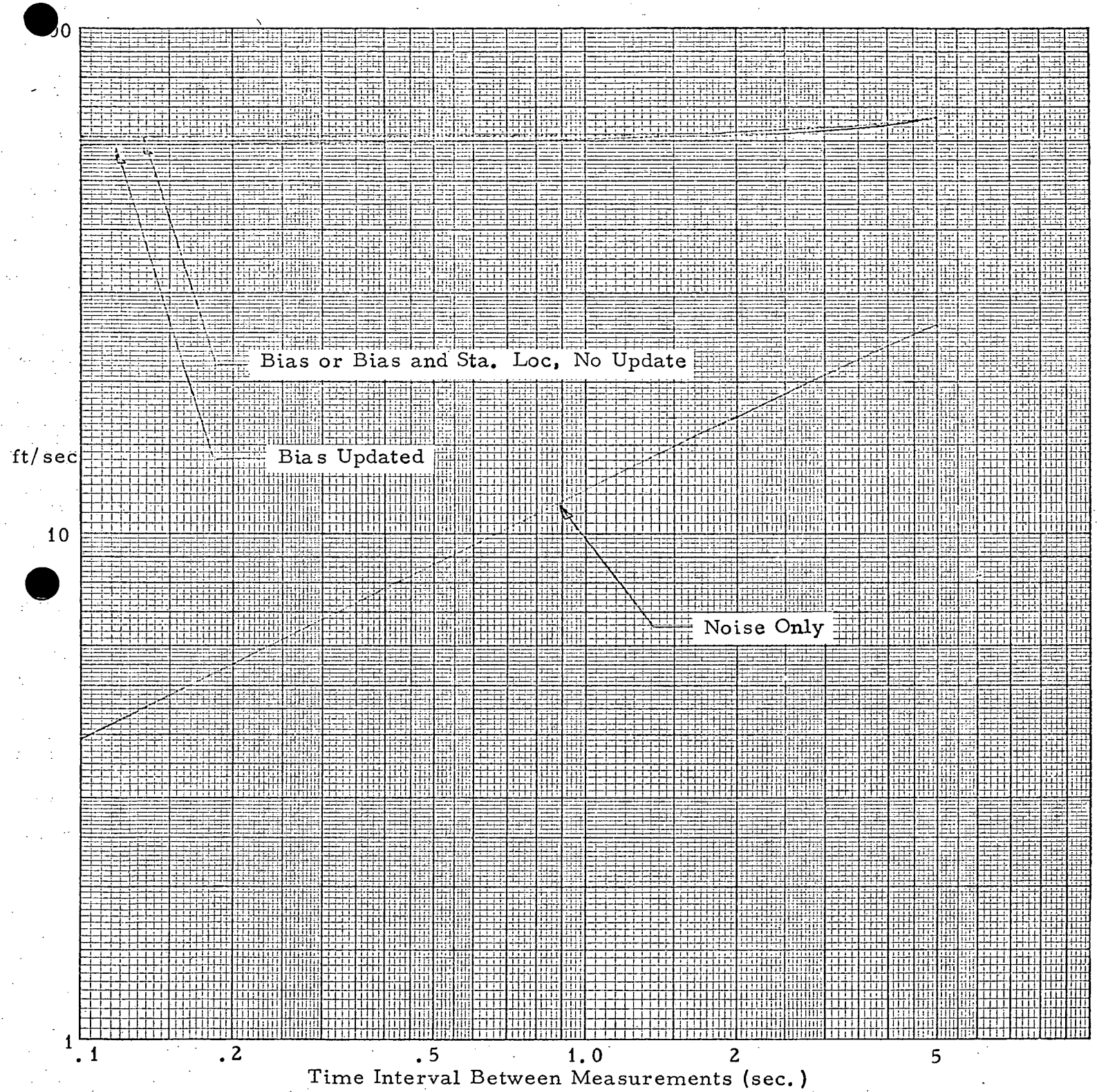

Figure 9. 3 σ Velocity Uncertainty - 90 Second Track

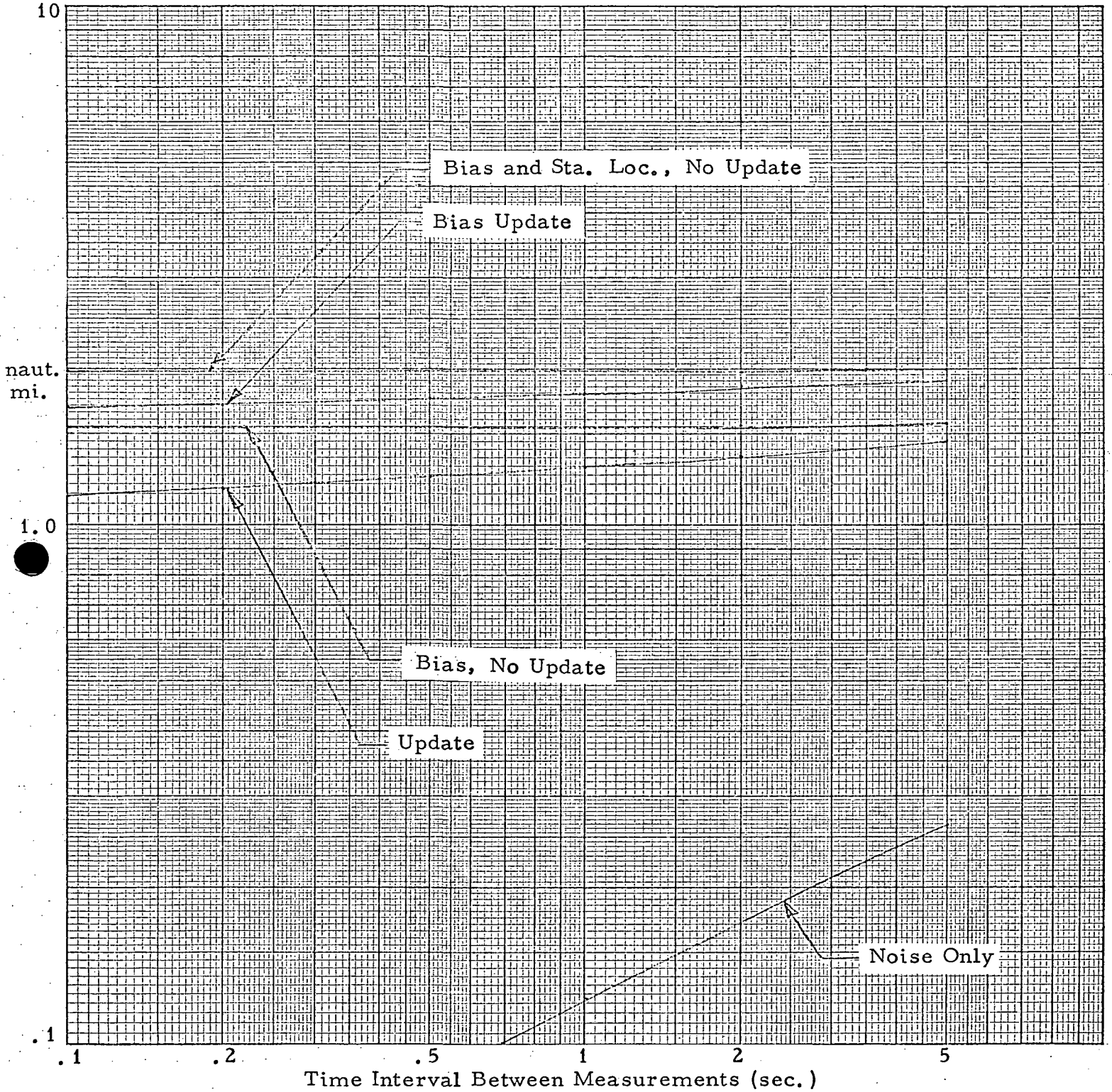

Figure 10. 3 σ Position Uncertainty - 90 Second Track

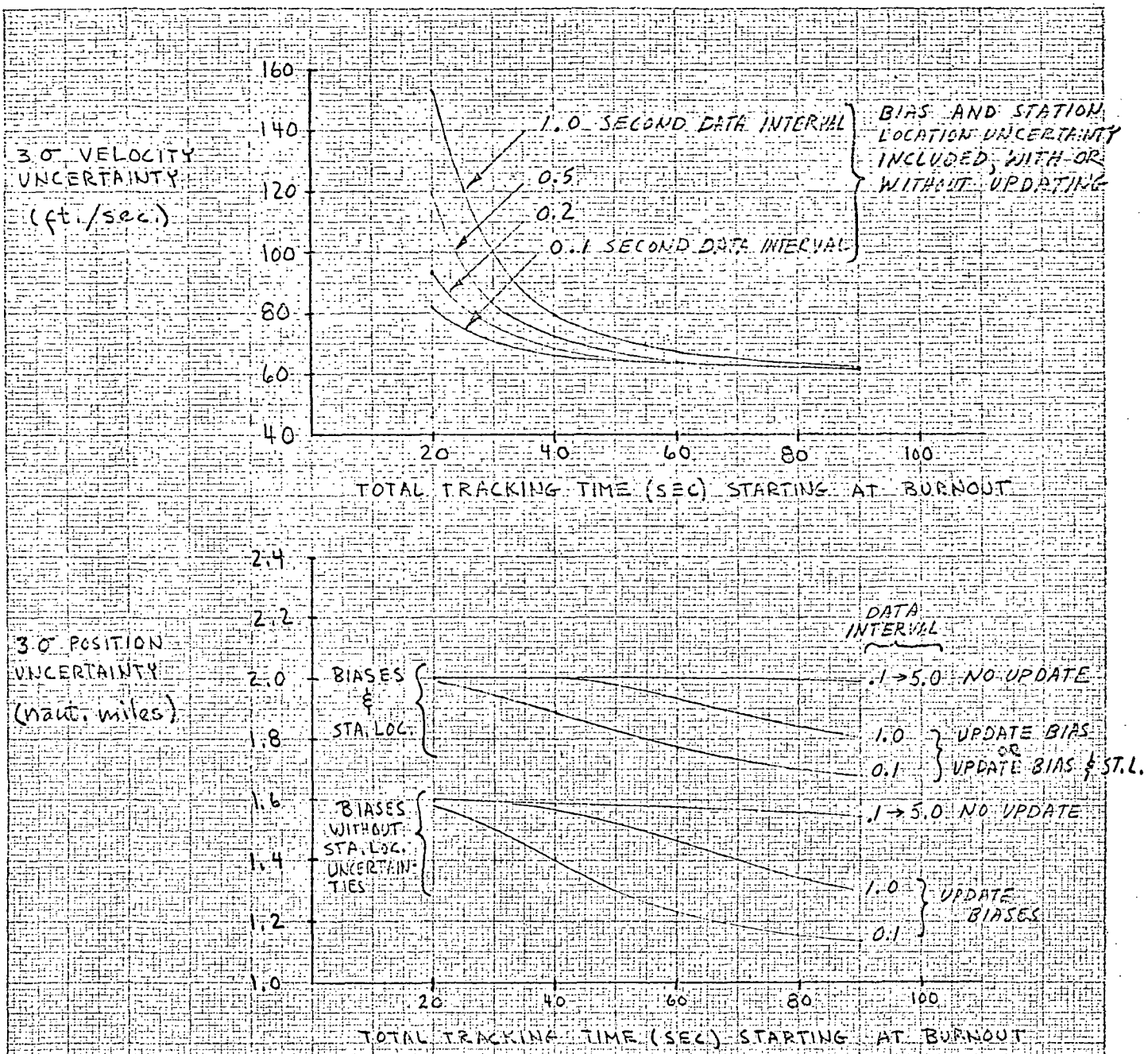

FIGURE 11

3σ POSITION AND VELOCITY UNCERTAINTIES, INCLUDING EFFECTS OF NOISE, BIASES, AND STATION LOCATION UNCERTAINTIES, FOR VARIOUS INTERVALS OF SAMPLING AND TOTAL TRACKING TIMES

CONCLUSIONS:

1.) VELOCITY UNCERTAINTY NOT IMPROVED BY UPDATING BIASES, OR BY HIGH DATA RATE WHEN TOTAL TRACKING PERIOD EXCEEDS ABOUT 50 SECONDS. ONLY WAY TO IMPROVE RESULTS, WITHOUT GREATLY INCREASED TRACKING IS TO LESSEN BIASES

2.) IF BETTER THAN 2 MILE POSITION UNCERTAINTY IS DESIRED, MUST ETHER REDUCE APRIORI BIAS AND STA. LOC. OR UPDATE BIASES USING HIGH DATA RATE AND LONG TRACKING TIME.

NOTE: POSITION AND VELOCITY VARIANCES DO NOT RELATE TO LIFETIME!

Figures 3 through 10 show the results; one figure for position and one figure for velocity uncertainty for each total tracking time. The position and velocity uncertainties are plotted for the results explained on Page 15, as a function of tracking interval between measurements.

Figure 11 is a cross-plot of position uncertainty against total tracking time and velocity uncertainty against total tracking time. The conclusions reached from Figure 11 may be misleading since position and velocity variance at cutoff do not describe orbital lifetime variance.

The three descriptors which are more appropriate are the square roots of the variances of radius, speed, and flight path angle. This is true for the example given for a very important reason: the radius of perigee, r_p, which in a way determines orbital lifetime, may be expressed in terms of the burnout radius, r, the burnout speed, V, and the burnout flight path angle above the horizontal, γ, :

$$r_p = \frac{1 - \sqrt{1 - \frac{V^2 r}{\mu}\left(2 - \frac{V^2 r}{\mu}\right)\cos^2\gamma}}{\left(\frac{2}{r} - \frac{V^2}{\mu}\right)}$$

Notice that the perigee radius is in no way a function of the out-of-plane initial position or the out-of-plane initial velocity. These out-of-plane uncertainties do appear, however, in the position and velocity uncertainties plotted in Figures 3 through 11. In fact, due to the tracking ship's location which is essentially "out-of-plane" from the vehicle, the out-of-plane vehicle uncertainties due to bias and station location error make up a good portion of position and velocity uncertainty. For instance, compare the following descriptors of the burnout uncertainty after 90 seconds of tracking using 0.1 second samples, all assuming bias and station location uncertainties exist:

90 Second Track, 0.1 Second Data,
Biases and Station Location Errors Exist

	Update Orbit Only	Update Orbit and Biases But Not Station Location
σx (up)	= 2087 ft	= 540
σy (along $\overline{V}$)	= 2457 "	= 2445
σz (out-of-plane)	= 2447 "	= 2392
$\sigma \dot{x}$	= 6.5 ft/sec	= 2.79
$\sigma \dot{y}$	= .93 "	= .711
$\sigma \dot{z}$	= 19.2 "	= 19.2
$\sqrt{(\sigma \dot{x})^2 + (\sigma \dot{y})^2 + (\sigma \dot{z})^2}$	= 19.48 "	= 19.48
$\sqrt{(\sigma x)^2 + (\sigma y)^2 + (\sigma z)^2}$	= 4048 ft	= 3463
σr (initial radius)	= 2087 "	= 540
σv (speed)	= .93 ft/sec	= .711
$\sigma \gamma$ (flight path)	= .24 mils	= .104 mils

The conclusions reached above are obvious, namely that σr, σv, and $\sigma \gamma$ are the proper descriptors and that while updating does not improve velocity and barely improves position; updating significantly improves radius (540/2087), and slightly improves speed (.71/.93) and does improve flight path angle (.104/.24).

Figure 12 is a plot of the burnout mean deviation in r, speed, and γ. Before firm conclusions can be drawn from Figure 12, one should reduce r, speed, and γ to some statistical criteria regarding the uncertainty in the perigee radius. This is being done and will be reported upon later. For other than circular nominal orbits the OEAP can presently handle the problem using a "QP" matrix operating upon the covariance at time zero. If one lightly glosses over the fact that uncertainties in r, speed, and γ are correlated, the following is true:

$\partial r_p / \partial r_o$ = 3 if Δr_o is positive, = 1 if Δr_o is negative

$\partial r_p / \partial$ speed = 0 if Δ speed is positive, = $-.55 \frac{\text{n. mi.}}{\text{ft/sec}}$ if Δ speed is negative

$\partial r_p / \partial \gamma$ = 4 n. miles/mil (but r_p occurs after 90^o of travel)

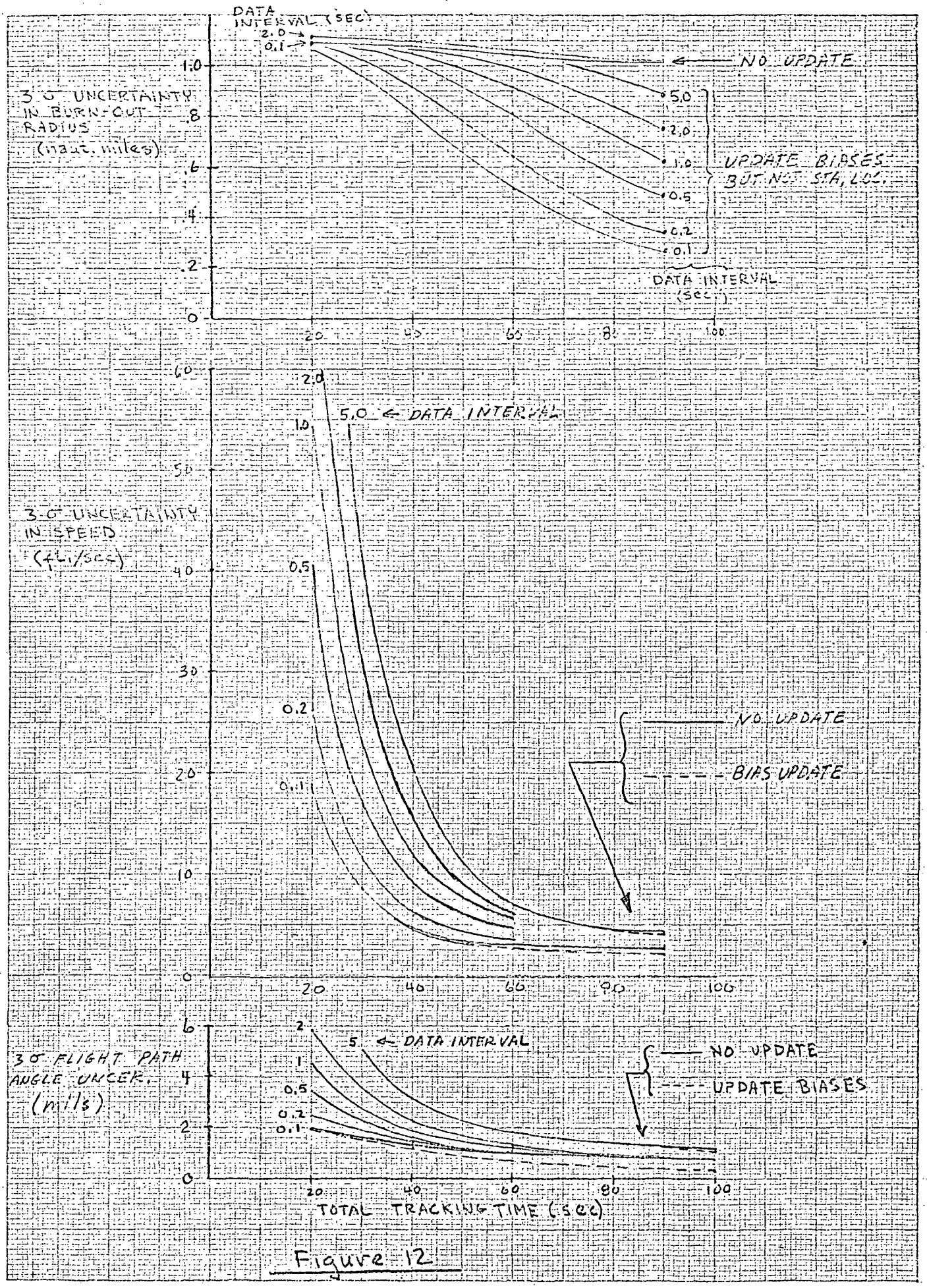
DATA INTERVAL (SEC)
2.0
0.1
NO UPDATE
5.0
2.0
1.0
0.5
0.2
0.1
UPDATE BIASES BUT NOT STA. LOC.
DATA INTERVAL (SEC)
3 σ UNCERTAINTY IN BURN-OUT RADIUS (naut. miles)
1.0
.8
.6
.4
.2
0
20
40
60
80
100
2.0
5.0 ← DATA INTERVAL
1.0
0.5
0.2
0.1
NO UPDATE
BIAS UPDATE
3-σ UNCERTAINTY IN SPEED (ft./sec)
60
50
40
30
20
10
0
20
40
60
80
100
2
5 ← DATA INTERVAL
1
0.5
0.2
0.1
NO UPDATE
UPDATE BIASES
3 σ FLIGHT PATH ANGLE UNCER. (mils)
6
4
2
0
20
40
60
80
100
TOTAL TRACKING TIME (sec)

Figure 12

The Bissett-Berman Corporation 2941 Nebraska Avenue, Santa Monica, California EXbrook 4-3270

APOLLO NOTE NO. 426
(Task I, Item I)

H. Epstein
28 June 1966

ERROR CHARACTERISTICS OF RUBIDIUM ATOMIC FREQUENCY STANDARDS

The purpose of this note is to indicate some error properties of Rubidium Atomic Frequency Standards. The properties of interest will pertain to the performance of the USBS in the Doppler mode of operation. The USBS is expected to be operated in the continuous count mode with counting intervals of one second or greater. In a broad sense, the frequency standard consists of a crystal oscillator whose long term characteristic is controlled by the Rubidium Atomic Frequency Standard. From this standpoint, it is convenient to categorize errors as being associated with the crystal oscillator and associated circuitry and to the atomic frequency standard and associated circuitry. Typically, the crystal oscillator errors are most important for time intervals substantially less than one second and the rubidium errors predominant for longer time intervals.

Neglecting environmental factors, oscillators are frequently assumed to possess white frequency type errors, flicker frequency type errors, and a linear frequency drift with time. The white frequency and flicker frequency type errors are of a statistical nature and the linear frequency drift of a systematic nature.

A first model for the error sources will be taken as follows for counting intervals greater than 1 second. The rubidium error will be considered as consisting of a white frequency error component, a flicker frequency error component, and a linear frequency drift. The crystal will be treated as only possessing a white frequency type error. Due to the nature of the interaction between the rubidium and crystal, the crystal white frequency error source will behave as a white phase error source. Each of these error components will be treated as being uncorrelated with all others. This model then presumes three statistical type error sources and one systematic error source. Difference Techniques will be employed in analysis to arrive at stationary quantities

compatible with simple estimation techniques to establish the desired parameters. Considering that the error data set consists of phase or time error measurements, no difference technique would be required for the white phase error component, a first difference would be required for the white frequency error component, and a second difference would be required for the flicker frequency error component. As a consequence, data with all three error sources present would require that the second difference (at least) of phase error measurement data be employed to arrive at stationary estimators. Presuming that second difference techniques are employed, the linear frequency drift error component may be calculated from the average value of the second difference error data.

Often, the measurement error data is expressed as the ratio of the frequency error to the average frequency. This form may be obtained by converting the phase error to a time error and dividing the time error by the count time. The situation becomes further complicated by data being taken both with continuous counting techniques and destruct counting techniques. Specific details of an analysis are then dependent on how the data is collected.

Some measurement error data on Rubidium Frequency Standards has been made available to BBC. The data was taken using two similar rubidium standards. As a consequence, the error estimated is a combination of the error of both frequency standards. Two sets of data on these frequency standards were analyzed; the first set of data involved 2004 points of approximately one second first difference data; and, the second set consisted of 1180 points of approximately 100 second first difference data. Both data sets were taken with a destruct type counter operation at a 50% duty cycle (e.g., one second of data every two seconds or 100 seconds of data every 200 seconds).

A simplified analysis was performed on these data sets. This allowed an earlier presentation of results. Furthermore, precise parameters of the error sources are required for USBS frequency

standards which will be used for Apollo rather than results on other similar standards. The noise measurable employed after processing is given below.

$$n_i(t) = \frac{1}{T_c}\left[m_i(t) - 2m_i(t-\Delta T) + m_i(t-2\Delta T)\right] \tag{1}$$

where $m_i(t)$ pertains to each individual time or phase error source,

$n_i(t)$ = processed error data

T_c = count time (seconds)

bT_c = ΔT = time interval between the initiation of successive measurements

For each noise source,

$$E\left\{n_i(t)\right\} = 0 \tag{2}$$

The following results may be simply obtained from results contained in Apollo Note 222.

For the white phase noise error component,

$$E\left\{n_1(t)\, n_1(t - r\Delta T)\right\} = \phi_{n_1}(r\Delta T) = \frac{6\phi_{m_1}}{T_c^2} \qquad r = 0 \tag{3a}$$

$$= \frac{-4\phi_{m_1}}{T_c^2} \qquad |r| = 1 \tag{3b}$$

$$= \frac{\phi_{m_1}}{T_c^2} \qquad |r| = 2 \tag{3c}$$

$$= 0 \qquad |r| \geqslant 3 \tag{3d}$$

and

$$\rho_{n_1}(r\Delta T) = \frac{\phi_{n_1}(r\Delta T)}{\phi_{n_1}(0)} = 1 \qquad |r| = 0 \tag{4a}$$

$$= -\frac{2}{3} \qquad |r| = 1 \tag{4b}$$

$$= \frac{1}{6} \qquad |r| = 2 \tag{4c}$$

$$= 0 \qquad |r| \geq 3 \tag{4d}$$

For the white frequency noise error component,

$$E\left\{n_2(t)\ n_2(t - r\Delta T)\right\} = \phi_{n_2}(r\Delta T) = \frac{2\phi_{m_2}}{T_c} \qquad |r| = 0 \tag{5a}$$

$$= \frac{-\phi_{m_2}}{T_c} \qquad |r| = 1 \tag{5b}$$

$$= 0 \qquad |r| \geq 2 \tag{5c}$$

$$\rho_{n_2}(r\Delta T) = \frac{\phi_{n_2}(r\Delta T)}{\phi_{n_2}(0)} = 1 \qquad |r| = 0 \tag{6a}$$

$$= -\frac{1}{2} \qquad |r| = 1 \tag{6b}$$

$$= 0 \qquad |r| \quad 2 \tag{6c}$$

$$\left(\frac{2\pi}{K}\right)\phi_{n_3}(a, b) = 4a^2 \ln|a| - 2(a-1)^2 \ln|a-1| - 2(a+1)^2 \ln|a+1|$$

$$-2(a-b)^2 \ln|a-b| - 2(a+b)^2 \ln|a+b|$$

$$+(a+b+1)^2 \ln|a+b+1| + (a-b-1)^2 \ln|a-b-1| \tag{7}$$

$$+(a+b-1)^2 \ln|a+b-1| + (a-b+1)^2 \ln|a-b+1|$$

$$b = \frac{\Delta T}{T_c} = 2 \tag{8}$$

and

$$a = \frac{\tau}{T_c} = \frac{r\Delta T}{T_c} = br = 2r \tag{9}$$

A few values for the correlation function for b = 2 are given in the table below.

r	$\frac{2\pi}{K}\phi_{n_3}(r)$	$\rho_{n_3}(r)$
0	8.68465	1
1	-2.92263	-.33653
2	-.60287	-.06942
3	-.23942	-.02757

Table I. Values for Processed Flicker Noise Correlation Function (b = 2, a = 2r)

An attempt was made to estimate the linear frequency drift (in addition to the parameters associated with the statistical type error source). The drift term was estimated from the average value of the processed data. The error at the drift coefficient (Δd) is given by:

$$\Delta d = \frac{1}{N}\sum_{r=1}^{N} n_r \tag{10}$$

For the noise sources considered,

$$E\{\Delta d\} = 0 \tag{11}$$

$$E\{\Delta d^2\} = \frac{1}{N^2} \sum_{i=1}^{N} \sum_{j=1}^{N} E\{n(i)\, n(j)\} \tag{12a}$$

$$= \frac{1}{N} \left[\phi_n(0) + 2 \sum_{r=1}^{N-1} \left(1 - \frac{r}{N}\right) \phi_n(r) \right] \tag{12b}$$

Using Eqs. (5a), (5b), and (5c) for the white frequency noise component, it can be shown that the associated variance in the drift component for this noise source is given by

$$E\{\Delta d^2\}_{n_2} = \frac{\phi_{n_2}(0)}{N^2} = \frac{2\phi_{m_2}}{N^2 T_c} \tag{13}$$

and

$$\sqrt{E\{\Delta d^2\}_{n_2}} = |\sigma_d|_{n_2} = \frac{1}{N} \sqrt{\frac{2\phi_{m_2}}{T_c}} = \frac{1}{N} \sqrt{\phi_{n_2}(0)} \tag{14}$$

is the desired expression for the standard deviation of the drift component due to white frequency noise.

The measurement data was treated as a fixed point number to eliminate machine round-off error. A scale factor of 1.72×10^{-14} then becomes associated with each count of the measurement data. The final results will be translated to frequency accuracy. Numerical results for the processed correlation function and drift coefficient in counts will be given in Table II for the two sets of data.

	Count Time (seconds)	
$\hat{\phi}_n(0)$ $(\text{counts})^2$	.985~1	98.5~100
	1.599×10^6	3.298×10^4
$\hat{\rho}_n(1)$	-.5020	-.4300
$\hat{\rho}_n(2)$	-.00023	-.0555
$\hat{d}$ (counts)	-.853	.0891
N	2004	1179

Table II. Estimates for Data Sets

A comparison of the values of the estimates of the normalized autocorrelation function with the values indicated for the three noise sources indicated previously, suggests that the white frequency noise is dominant in the first set. The number of data samples would not allow a good estimate of the other data error sources. One would surmise that the other noise sources must be about two orders of magnitude smaller than the white frequency noise component. The combined white frequency noise source from the two Rubidium Frequency Standards then has an expected value of 1.6×10^6 (counts^2) for a .985 second counting interval. Using the scale factor of 1.72×10^{-14} indicated previously, the relation frequency accuracy $(\Delta f / f)$ for .985 seconds count time is 2.28×10^{-11} $(1.72 \times 10^{-14} \sqrt{1.6 \times 10^6})$. A 1σ uncertainty of about 4% $(100 \sqrt{3/2004})$ would be expected due to the finite sample if only this noise source were present. This quantity is actually biased to a higher value due to the other noise sources.

The significance of $\hat{d}$ can be approximately estimated assuming the linear frequency trend is to be calculated in the presence of the white frequency noise estimated above using Eq. (14)

$$\left|\sigma_d\right|_{n_2} = \frac{1}{2004} \sqrt{1.6 \times 10^6} = .63 \text{ counts} \qquad (15)$$

The value of d = -.853 counts is then not a reliable estimate. Longer data sets with much larger count times are therefore desired to establish the linear trend. The white phase noise was insignificant for the .985 second count time. The variance of the white phase noise is reduced by a factor of 10,000 for the 98.5 second count time and is therefore expected to be a negligible effect.

Extrapolation of the .985 second variance of the white frequency noise of 1.6×10^6 (counts)^2 to the 98.5 second count time data, one would a priori expect a variance of 1.6×10^6 (.985/98.5) = 1.6×10^4(counts)^2, with a percentage 1 σ uncertainty of about 4%. The longer count time data involves fewer data points and the necessity to estimate one additional parameter – the flicker frequency noise parameter. For this situation, it should not be expected that a substantial improvement in the estimate of the white frequency noise component can be made. With this rationale, and for simplicity, the flicker noise parameter will be estimated from the variance of the 98.5 second data and the a priori estimate of the white frequency component as $3.3 \times 10^4 - 1.6 \times 10^4 = 1.7 \times 10^4$(counts)^2. With these two components approximately equal for a count time of 98.5 seconds, the flicker noise component would be about 1% of the white frequency component for a count time of .985 seconds which is small as compared to the 4% standard deviation and could be neglected.

The standard deviation of the error in the estimate of the flicker noise component is approximately equal to 7% ($\sim 100\sqrt{6/1179}$) due to the finite sampling even with perfect knowledge of the variance of the white frequency noise. The uncertainty in the white frequency noise (1 $\sigma \sim 4\%$) then does not have a large effect on the variance estimated in this fashion.

As an alternate approach, the variance of the white frequency and flicker frequency noise sources was calculated from Eqs. (86) and (87) of Apollo Note 416. The values were obtained as follows:

For the white frequency noise component,

$$\phi_{n_2} = \left|\frac{-.3365 + .4300}{-.3365 + .5000}\right| 3.298 \times 10^4 = 1.89 \times 10^4 (\text{counts})^2 \quad (16)$$

and for the flicker frequency noise component,

$$\phi_{n_3} = \left|\frac{-.4300 + .5}{.3365 + .5}\right| 3.298 \times 10^4 = 1.41 \times 10^4 (\text{counts})^2 \quad (17)$$

The results differ by about 18% from the better values using both data sets.

It is of interest whether a linear frequency trend can be reliably estimated from the 100 second data set. Using Eq. (14) and the numerical values indicated

$$\left|\sigma_d\right|_{n_2} = \frac{1}{1179}\sqrt{1.6 \times 10^4} = .107 \text{ counts} \quad (18)$$

This indicated that the white frequency noise component alone could account for the estimate of the linear trend. No reliable estimate of the linear frequency trend has been shown from the two data sets.

The flicker frequency noise component would behave as a non-stationary error source in the $\Delta f/f$ measurements which are made most frequently. As a consequence, considerable care must be made with interpretation of results obtained in this fashion.

The Bissett-Berman Corporation 2941 Nebraska Avenue, Santa Monica, California EXbrook 4-3270

APOLLO NOTE NO. 427
(Task II, Item II)

C. H. Dale
29 June 1966

CHECK OF THE BOOST AT T2 AND T3 IN THE LEM G AND N STUDY

Apollo Note No. 414 developed the covariance of the boost at t_2 using the Orbit Error Analysis Program. Since the writing of that Note, the LEM G and N Program output has been checked against these results.

Cov $(v_b(t_2))$ from Note 414

7.678×10^{-3}	1.989×10^{-2}	-4.116×10^{-6}
1.989×10^{-2}	5.610×10^{-2}	-1.016×10^{-5}
-4.116×10^{-6}	-1.016×10^{-5}	1.101×10^{-6}

LEM G and N Results (CVDLVB)

7.680×10^{-3}	1.990×10^{-2}	-4.122×10^{-6}
1.990×10^{-2}	5.612×10^{-2}	-1.017×10^{-5}
-4.122×10^{-6}	-1.017×10^{-5}	1.101×10^{-6}

The above check is quite good; minor differences are explained by the fact that the inputs to the two programs are not quite identical. In the G and N Program $\mathbb{K}$ and $\mathbb{L}$ matrices are used in place of the Euler angle inputs to the Orbit Error Analysis Program. In order to get the Euler angles, hand computation based upon the $\mathbb{K}$ and $\mathbb{L}$ matrices was performed which produced slightly differing results.

A boost of particular interest is the boost at t_3 since this circulatory boost does not have a target in the sense of most of the other boost. The $S_v(t_3)$ matrix used in the G and N Program thus differes in derivation from all other boosts. It was possible to check the boost covariance at t_3 under a few simplifying assumptions. First, that no boost errors were introduced. Second, that the small three intervals of tracking after $t_8 - \tau$, if omitted, would not sifnificantly change the results. And third, that

the position estimate at t_3 is zero because of a perfect boost at t_8. Points two and three are actually the same.

First we will analytically develop the estimate minus the reference state vector at t_3, and from this the boost covariance at t_3. The estimate of the state vector at t_3 less the reference or nominal state vector at t_3 is

$$\hat{x}(3) = Q\left(\frac{t_3}{t_8}\right) \left[\hat{x}(8) + v_b(8) \right] \tag{1}$$

where, since no further tracking after $t_8 - \tau$ is assumed, $\hat{x}(3)$ has only velocity components; the boost at t_8 removes position components of $\hat{x}(3)$. $v_b(8)$ is the boost at t_8 and is assumed to equal the command (this assumption is carried out in the LEM G and N program by setting $\sigma_{K4} = \sigma_{K7} = 0$). $\hat{x}(2)$ is, of course, the estimate less the reference state vector at t_8 before the boost and is based upon data prior to $t_8 - \tau$ for our case. The $Q(t_3/t_8)$ matrix may be partitioned giving.

$$Q(t_3/t_8) = \left[\begin{array}{c|c} Q_{11}(t_3/t_8) & Q_{12}(t_3/t_8) \\ \hline Q_{21}(t_3/t_8) & Q_{22}(t_3/t_8) \end{array}\right]$$

where $Q_{11}(t_3/t_8)$ is the first 3 x 3. Then since the purpose of the boost at t_8, $v_b(8)$, is to reduce the position error at t_3 to zero we may generate $v_b(8)$ in the following manner.

$$\hat{x}(3) \text{ position} = Q_{11}(t_3/t_8) \begin{bmatrix} \hat{x}_8 \\ \hat{y}_8 \\ \hat{z}_8 \end{bmatrix} + Q_{12}(t_3/t_8) \begin{bmatrix} \hat{\dot{x}}_8 \\ \hat{\dot{y}}_8 \\ \hat{\dot{z}}_8 \end{bmatrix}$$

expresses the estimated error that would exist at t_3 in position were no

boost at t_8 to be made. But the effect of the boost is to negate this estimated error.

$$\hat{x}(3) \text{ position} = -Q_{12}(t_3/t_8)\, v_b(t_8)$$

Thus

$$v_b(t_8) = -Q_{12}^{-1}(t_3/t_8)\, \hat{x}(3) \text{ position}$$

$$= -Q_{12}^{-1}(t_3/t_8) \left\{ Q_{11}(t_3/t_8) \begin{bmatrix} \hat{x}_8 \\ \hat{y}_8 \\ \hat{z}_8 \end{bmatrix} + Q_{12}(t_3/t_8) \begin{bmatrix} \hat{\dot{x}}_8 \\ \hat{\dot{y}}_8 \\ \hat{\dot{z}}_8 \end{bmatrix} \right\} \tag{2}$$

Now Equation (1) really only has velocity components since the boost at t_8 removed all position terms and no further tracking has occurred which would change our estimate of what the t_8 boost should have been. Thus, Equation (1) may be re-written as

$$\hat{x}(3) = \begin{bmatrix} \hat{\dot{x}}_3 \\ \hat{\dot{y}}_3 \\ \hat{\dot{z}}_3 \end{bmatrix} = Q_{21}(t_3/t_8) \begin{bmatrix} \hat{x}_8 \\ \hat{y}_8 \\ \hat{z}_8 \end{bmatrix} + Q_{22}(t_3/t_8) \begin{bmatrix} \hat{\dot{x}}_8 \\ \hat{\dot{y}}_8 \\ \hat{\dot{z}}_8 \end{bmatrix} + v_b \tag{3}$$

Using Equation (2) in Equation (1) yields the estimate less the reference at t_3 as

$$\hat{x}(3) \text{ velocity only} = Q_{21}(t_3/t_8) \begin{bmatrix} \hat{x}_8 \\ \hat{y}_8 \\ \hat{z}_8 \end{bmatrix} + Q_{22}(t_3/t_8) \begin{bmatrix} \hat{\dot{x}}_8 \\ \hat{\dot{y}}_8 \\ \hat{\dot{z}}_8 \end{bmatrix}$$

$$-Q_{22}(t_3/t_8) \left\{ Q_{12}^{-1}(t_3/t_8)\, Q_{11}(t_3/t_8) \begin{bmatrix} \hat{x}_8 \\ \hat{y}_8 \\ \hat{z}_8 \end{bmatrix} + \begin{bmatrix} \hat{\dot{x}}_8 \\ \hat{\dot{y}}_8 \\ \hat{\dot{z}}_8 \end{bmatrix} \right\}$$

which may be reduced to give

$$\hat{x}(3) = \left\{ Q_{21} - Q_{22} Q_{12}^{-1} Q_{11} \right\} \begin{bmatrix} \hat{x}_8 \\ \hat{y}_8 \\ \hat{z}_8 \end{bmatrix} \tag{4}$$

where the bracket (t_3/t_8) has been left off for clarity. Now a bit of manipulation will allow the simplification of the above bracket term. First note that

$$\begin{bmatrix} Q_{11} & Q_{12} \\ Q_{21} & Q_{22} \end{bmatrix}^{-1} = \begin{bmatrix} Q_{22}^T & -Q_{12}^T \\ -Q_{21}^T & Q_{11}^T \end{bmatrix}$$

which is a fact for Jacobian matrices of a potential function. Now by multiplication of Q by Q^{-1} in partitioned form we arrive at four equations

$$\begin{aligned} Q_{11} Q_{22}^T - Q_{12} Q_{21}^T &= I \\ -Q_{11} Q_{12}^T + Q_{22} Q_{11}^T &= 0 \\ Q_{21} Q_{22}^T - Q_{22} Q_{21}^T &= 0 \\ -Q_{21} Q_{12}^T + Q_{22} Q_{11}^T &= I \end{aligned} \tag{5}$$

We will now show that

$$\begin{bmatrix} Q_{21} & Q_{22} \\ Q_{11} & Q_{12} \end{bmatrix}^{-1} = \begin{bmatrix} -Q_{12}^T & Q_{22}^T \\ Q_{11}^T & -Q_{21}^T \end{bmatrix} \tag{6}$$

is true by assuming it and checking the results with Equation (5)

$$-Q_{21}Q_{12}^{T} + Q_{22}Q_{11}^{T} = I$$

$$Q_{21}Q_{22}^{T} + Q_{22}Q_{21}^{T} = 0$$

$$-Q_{11}Q_{12}^{T} + Q_{12}Q_{11}^{T} = 0$$

$$Q_{11}Q_{22}^{T} - Q_{12}Q_{21}^{T} = I$$

and these are identical to Equation (5). Now by the laws of partitionings, if

$$\begin{bmatrix} A & B \\ C & D \end{bmatrix}^{-1} = \begin{bmatrix} E & F \\ G & H \end{bmatrix}$$

then $E = (A-BD^{-1}C)^{-1}$. But then from Equation (6)

$$-Q_{12}^{T} = (Q_{21} - Q_{22}Q_{12}^{-1}Q_{11})^{-1}$$

the inverse of which is

$$-Q_{12}^{-T} = Q_{21} - Q_{22}Q_{12}^{-1}Q_{11} \tag{7}$$

thus we may substitute Equation (7) in Equation (4) giving

$$\hat{x}(3) = -Q_{12}^{-T} \begin{bmatrix} \hat{x}_8 \\ \hat{y}_8 \\ \hat{z}_8 \end{bmatrix} \tag{8}$$

From this equation we will now proceed to derive the boost covariance at t_3. First we define the nominal boost at t_3.

$$v_{bn}(t_3) = \begin{bmatrix} \sqrt{\frac{u}{r_a}} & 0 \\ 0 & -\sqrt{\frac{2\mu}{r_a + r_j}} \end{bmatrix} \quad \text{in } t'_3 \text{ coordinates}$$

Then the commanded boost at t_3 in t'_3 coordinates is

$$v_{bc}(t_3) = \begin{bmatrix} -\hat{\dot{x}}_3 - \sqrt{\frac{\mu}{r_a}} \left(\frac{\hat{y}_3}{r_a} \right) \\ \sqrt{\frac{\mu}{r_a + x}} - \sqrt{\frac{2\mu}{r_a + r_d}} - \hat{\dot{y}}_3 \\ 0 \end{bmatrix} \tag{9}$$

Or the commanded boost may be refererenced to the nominal boost by

$$v_{bc}(t_3) = v_{bn}(t_3) + \frac{\partial v_{bc}(t_3)}{\partial x(3)} \hat{x}(3) = v_{bn}(t_3) \Delta v_{bc}(t_3)$$

And from Equation (8)

$$\frac{\partial v_{bc}(t_3)}{\partial \hat{x}} = \left[\begin{array}{cccccc} 0 & \sqrt{\frac{\mu}{r_a^3}} & 0 & -1 & 0 & 0 \\ \hline \frac{-1}{2r_a}\sqrt{\frac{\mu}{r_a}} & 0 & 0 & 0 & -1 & 0 \\ \hline 0 & 0 & 0 & 0 & 0 & 0 \end{array}\right]$$

Now the term of interest is the covariance of the actual boost, which for our non-execution-error-case equals the covariance of the commanded boost, and is equal to

$$\overline{\Delta v_{bc}(t_3) \left[\Delta v_{bc}(t_3)\right]^T} = \frac{\partial v_{bc}}{\partial \hat{x}} \hat{x}(t_3) \hat{x}^T(t_3) \frac{\partial v_{bc}}{\partial \hat{x}}$$

or using Equation (7) in the above expression for $\hat{x}(t_3)$

$$\begin{aligned} \text{Cov}\,(v_b(3)) &= \frac{\partial v_{bc}}{\partial \hat{x}} \text{Cov}\,\hat{x}(t_3) \frac{\partial v_{bc}}{\partial \hat{x}} \\ &= \frac{\partial v_{bc}}{\partial \hat{x}} Q_{12}^{-T} \text{Cov}\,\hat{x}(t_8) Q_{12}^{-1} \frac{\partial v_{bc}}{\partial \hat{x}} \end{aligned} \qquad (10)$$

where by $\frac{\partial v_{bc}}{\partial \hat{x}}$ we mean the 3 x 3 terms

$$\begin{bmatrix} -1 & 0 & 0 \\ 0 & -1 & 0 \\ 0 & 0 & 0 \end{bmatrix}$$

Now to get Equation (10) by the OEAP is simple enough. We paraphrase Note No. 414 only we do not project to t_3 in our early runs. F_{ij} is thus defined at t_8 in t_8 coordinates and comprises only position components of the covariance of the estimate with respect to the reference trajectory. F_{ij} is thus Cov $\hat{x}(t_8)$. Using Q_{12} which is defined as $Q^1(t_3/t_8)$ in Note 414, and $\partial v_{bc}/\partial \hat{x}$ which are both entered as "Special Q" matrices we produce the Cov $(v_b(3))$ as defined in Equation (10). Euler angles are used to rotate this into t'_2 coordinates, the coordinates of ascent-burnout.

G and N Result Giving Cov $(v_b(3))$

1.22×10^{-2}	10.6×10^{-3}	0
10.6×10^{-3}	9.69×10^{-3}	0
0	0	0

Check of Cov $(v_b(3))$ Using OEAP and described above

1.06×10^{-2}	9.76×10^{-3}	0
9.76×10^{-3}	9.16×10^{-3}	0
0	0	0

The above check is reasonably good considering the fact that the G and N result uses three extra tracking intervals after $t_8 - \tau$.